'THE P21 PROTEIN AND DNA DAMAGE'

PROTEIN P21 UND DNA-SCHÄDEN

Von dem Fachbereich Biologie der Technischen Universität Darmstadt (D17) zur Erlangung des akademischen Grades eines Doctor rerum naturalium genehmigte Dissertation von

Dipl. Biol. Jeanette Heede Rudolph

aus Darmstadt.

1. Referent: Prof. Dr. G. Kraft
2. Referent: Prof. Dr. T. W. Holstein
3. Referent: Prof. Dr. P. G. Layer

Tag der Einreichung 30. August 2007
Tag der mündlichen Prüfung 01. February 2008

Darmstadt 2007

D17

THE P21 PROTEIN AND DNA DAMAGE

by

Dipl. Biol. Jeanette Heede Rudolph

from Darmstadt

A thesis submitted in partial fulfilment of the
requirements for the degree of

Doctor rerum naturalium

Technische Universität Darmstadt

Darmstadt 2007

Approved by

Prof. Dr. G. Kraft

Prof. Dr. T. W. Holstein

Prof. Dr. P. G. Layer

Date of submission 30. August 2007
Date of oral examination 01. February 2008

D17

TECHNISCHE UNIVERSITÄT DARMSTADT

THE P21 PROTEIN AND DNA DAMAGE

by Dipl. Biol. Jeanette Heede Rudolph

ABSTRACT

Radiation-induced DNA lesions lead to the activation of complex damage response pathways in mammalian cells. In one of these pathways the p21 protein, a well-characterized cyclin dependent kinase inhibitor, is induced by TP53 after DNA damage leading to cell cycle arrest in G1-phase. Independently of its transactivation by TP53, the p21 protein forms nuclear accumulations at heavy ion-induced DNA lesions [Jakob *et al.*, 2000]. As shown in this study, p21 foci also arise after exposure of cells to sparsely ionizing X-rays. In an attempt to elucidate the functional role of these p21 foci, their dependence on the proliferating cell nuclear antigen (PCNA) is demonstrated here. In particular, the requirement for a functional interaction between p21 and PCNA is revealed. In addition, the kinetics of the PCNA- and p21-accumulations at heavy ion-induced DNA lesions is shown to be very similar, and both proteins are part of the chromatin-bound protein fraction after DNA damage induction by X-rays. A possible involvement of p21 in the DNA double- and/or single-strand break repair pathways is discussed.

ZUSAMMENFASSUNG

Durch ionisierende Strahlung induzierte DNA Schäden aktivieren ein komplexes Netzwerk an Signalwegen zur Erkennung und Reparatur der hierdurch hervorgerufenen DNA Schäden. Das Protein p21 ist ein bekannter CDK (cyclin dependent kinase) Inhibitor, der nach DNA-Schäden TP53 abhängig induziert wird und den Zellzyklus arretiert. TP53 unabhängig akkumuliert p21 in Foci an Schwerionen-induzierten DNA Schäden [Jakob *et al.*, 2000]. In dieser Arbeit wird gezeigt dass p21 auch nach DNA Schadensinduktion durch Röntgenbestrahlung Foci bildet. Bei der Erforschung einer möglichen Funktion dieser p21 Akkumulationen an strahleninduzierten DNA Schadensstellen zeigte sich die Interaktion von p21 mit dem Proliferierenden Zellulären Nucleären Antigen (PCNA) als essentiell. Zudem erwies sich die Kinetik des Erscheinens und des Auflösens der p21 und PCNA Foci nach Schwerionenbestrahlung als sehr ähnlich, und beide Proteine konnten nach DNA Schadensinduktion durch Röntgenbestrahlung in der Chromatin-gebundenen Proteinfraktion nachgewiesen werden. Eine mögliche Rolle für p21 in der DNA Doppel- oder Einzel-Strangbruchreparatur wird diskutiert.

TABLE OF CONTENTS

LIST OF FIGURES

Number *Page*

LIST OF TABLES

Number *Page*

ACKNOWLEDGEMENTS

Firstly, I would like to thank Prof. Dr. Gerhard Kraft for the opportunity to carry out this project in his Biophysics group at the GSI. He encouraged me to continue and showed great understanding for my maternity leave during this thesis. Many thanks go to Prof. Dr. Thomas W. Holstein for giving me the possibility for an 'external' PhD. thesis. Furthermore, I thank Prof. Dr. Gerhard Kraft, Prof. Dr. Thomas W. Holstein and Prof. Dr. Paul G. Layer for taking their time approving this thesis.

I thank Dr. Gisela Taucher-Scholz to offer me the opportunity to work in her lab and for the supervision during this thesis. A warm thank-you also to Dr. Claudia Wiese to whom I am especially indebted. Her way of being motivated me to start this thesis. Unfortunately, she left our lab during this thesis, but even the long distance did not hinder her to assist me.

I am thankful to the members of the Biophysics group for the nice working atmosphere and their help when needed. Thanks also to the group supporting the heavy ion experiments used for this thesis.

My deepest gratitude is to my dear husband Andreas Rudolph for 'just being there' and for never losing trust in me. Luckily, our son Mark Heede Rudolph loved the child care he joined since his first birthday and our 'nr. 2' seems still happy 'inside', allowing me to finish this thesis. Thanks! I am grateful to my parents who somehow have led me to go this way in my life, without pressure at any time, leaving me free as a bird.

Finally, a special thanks to my fellow PhD. student Dipl. Biol. Yvonne Schweinfurth, with whom I have spend the days and nights during the experiments in the lab, for being such a good friend. Amazing, that we have never had a quarrel in all those years!

Thank you all!!!

ABBREVIATIONS

AG	Normal human foreskin fibroblast cell line AG1522C
ATM	Ataxia telangiectasia mutated
BER	Base excision repair
BIBA	'Biologischen Bestrahlungsanlage' (biological irradiation device)
BSA	Bovine serum albumin
CDK	Cyclin dependent kinase
CKI	Cyclin dependent kinase inhibitor
CPD	Cumulative population doublings
DNA	Desoxyribonucleic acid
DSB	DNA double-strand break
EDTA	Ethylendiamintetraacetate
ELISA	Enzyme-linked immunoabsorbance assay
F	Fluence [particles/cm^2]
FCS	Foetal calf serum
g	Gram or gravitation
Gy	Gray [J/kg]
h	Hour
HCT116	Human coloncarzinome cell line 116
HI	Heavy ion
hMre11	Human homologue of yeast meiotic recombination 11
HR	Homologous recombination
LET	Linear energy transfer
min	Minutes
MRE	Proteincomplex of hMre11, Rad50 und NBS1
N	Total cell number
N_0	Seeded (attached) cell number
NBS1	Protein expressed from *NBS1*, mutated in Nijmegen Breakage Syndrom
NER	Nucleotid excision repair
NHEJ	Non-homologous-end-joining
p21	Cyclin dependent kinase inhibitor 1A (CDKN1A)
PARP-1	Poly(ADP-ribose) polymerase-1
PBS	Phosphate buffered saline
PCNA	Proliferating cell nuclear antigen
PD	Population doublings
PE	Plating efficiency
RBE	Relative biological effectiveness
rpm	Rotations per minute
RT	Room temperature
SDS	Sodium dodecylsulfate
SDS-PAGE	SDS-polyacrylamidgel-electrophoresis
SIS	'Schwerionensynchroton'
SSB	DNA single-strand break
TP53	Tumour supressor protein p53
U	Units
UNILAC	Universal ion linear accelerator
v/v	Volume per volume
w/v	Weight per volume
w/w	Weight per weight
wt	Wild-type
XRCC1	X-ray repair cross complementing 1 protein
53BP1	Tumour supressor p53 binding protein 1

1 INTRODUCTION

Cells have to cope with various kinds of DNA lesions, which lead to complex cellular reactions. Because of the importance of maintaining DNA integrity and genome stability, cells have evolved many pathways to detect damaged DNA sites and to repair the induced lesions. If a cell is not able to repair the DNA damage, it may undergo apoptosis or necrosis. In the worst case, the damage is misrepaired leading to mutations that may end in uncontrolled cell division, promoting carcinogenesis.

DNA damage activates highly organised interactions between many different proteins. Some proteins are responsible for the DNA lesion detection (DNA damage sensors). Other proteins function as transducers which in their turn activate effector proteins. In parallel to the initiation of DNA repair pathways, the cell cycle has to be arrested, to get the time needed for the DNA repair. Many of the proteins involved have more than one function and with this, are active in several different pathways.

Ionizing radiation induces severe DNA damages, which can lead to cell inactivation. In tumour therapy, this is the desired effect of the exposure of cancerous tissue to ionizing radiation. However, the line between cancerous cells and its surrounding healthy tissue is very narrow demanding highly precise radiotherapy. To better understand how ionizing radiation works on cellular level, experimental data are of great importance.

In this thesis, the protein p21, also known as $p21^{CIP1/WAF1}$ or CDKN1A, is the protein of interest. p21 participates in several cellular pathways. p21 was first described as a cyclin-dependent kinase inhibitor that interacts with the cell cycle cyclins to delay or arrest the cell cycle. After DNA damage detection, the protein TP53 (tumour suppressor protein 53) is stabilized by phosphorylation, leading to a higher concentration of this protein. TP53 can induce p21 directly on transcriptional level, leading to increased amounts of p21 within the cell. The protein p21 then forms a complex with the cyclin A or E, resulting in cell cycle arrest. This cell cycle delay gives the cell the opportunity to repair the DNA damage. This was the first described function of p21, experimental data have shown many additional functions of this protein, most of them briefly mentioned in this thesis. Here, I try to elucidate the behaviour of p21 towards DNA lesions, as p21 accumulates directly at heavy ion-induced DNA lesions. The question came up, whether p21 is actively involved in the cellular response to DNA damage. A main topic within this thesis is the interaction with the proliferating cell nuclear antigen (PCNA). PCNA is known to be of importance for DNA replication as well as DNA repair. The p21/PCNA interaction is elucidated in response to irradiation-induced DNA lesions. With this thesis, even if p21 is only one protein from a huge amount of the cellular proteins, an additional role of this key player of the cellular response to irradiation-induced DNA damage is further clarified.

1.1 Ionizing radiation

As unstable atoms decay, they release radiation in the form of electromagnetic waves and subatomic particles. If this radiation transfers enough energy to liberate electrons from target atoms and ionize the atoms as it passes through matter it is referred to as ionizing radiation. The basic unit for ionizing radiation is the dose, measured in Gray [*Gy*] and defined as the radiation energy absorbed per mass unit of the irradiated matter: 1 Gy = 1 J/kg [ICRU, 1970].

Depending on the energy deposition, ionizing radiation is either sparsely or densely ionizing with a low or high linear energy transfer (LET), respectively. The LET [$keV/\mu m$] gives the energy transfer of the radiation per unit distance as it traverses the matter. High-energy electromagnetic radiations such as X- and γ-rays release fast electrons having a low LET which makes them sparsely ionizing. Neutrons release low energy protons. Both low energy protons and heavy ions produce a dense track of secondary electrons that has a high LET and is therefore densely ionizing.

The dose delivered to the irradiated matter is given by:

$$D[Gy] = 1.602 \times 10^{-9} \times \frac{dE}{dx}\left[\frac{keV}{\mu m}\right] \times F\left[cm^{-2}\right] \times \frac{1}{\rho}\left[\frac{cm^3}{g}\right]$$

The energy loss of a particle is specified by $\frac{dE}{dx}$, which is equivalent to the LET. F stands for the particle fluence, meaning the number of particles traversing one cm^2 of the irradiated matter and ρ is the mass density of the target material.

DNA damage induced by exposure to radiation is induced by either the direct action or indirect action of the irradiation. With the direct action secondary electrons resulting from absorption of a photon interacts directly with the DNA, the dominant process for radiations with high LET. By the indirect action secondary electrons interact with another molecule, e.g. H_2O leading to free radicals who induce the DNA damage (mainly process for low LET radiation).

Ionizing radiation can create single damaged DNA sites and clustered damaged DNA sites, in which two or more lesions are formed within a few helical turns of the DNA, after the passage of a single radiation track. It has been estimated that low-LET radiation creates approximately 1000 single-strand breaks (SSBs), 40 double-strand breaks (DSBs) and 2700 base damages per Gray in a mammalian cell [J. F. Ward, 1985, 1988, 1995].

1.1.1 Sparsely ionizing radiation

Photon irradiation, such as X-ray radiation and γ-radiation, are sparsely ionizing radiation types with a low LET (Fig. 1 A). With this kind of radiation, a part of the photon energy interacts with the electrons of the irradiated material. Electrons are knocked out of the atom and interact with surrounding electrons that result in a homogeneous deposition of secondary electrons (Fig. 1 B). The local energy desposition by sparsely ionizing radiation is given by the dose applied. Because of the statistic interaction of photons with the target material the beam of photons decreases in its intensity when penetrating through matter.

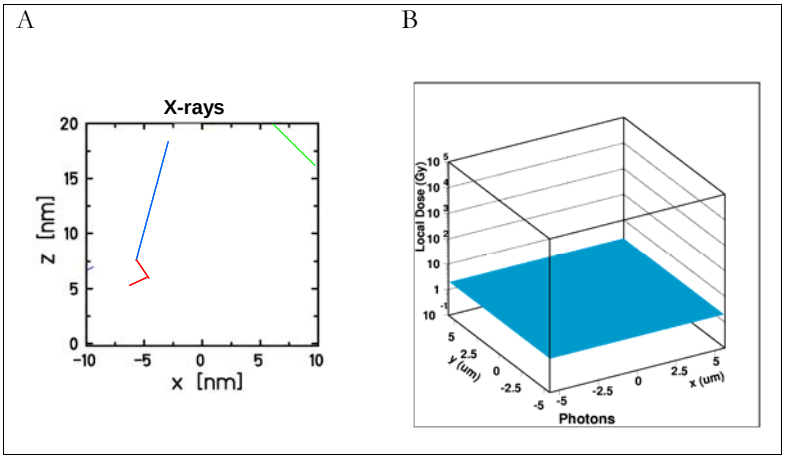

Fig. 1 **Sparsely ionizing radiation gives a random homogeneous deposition of secondary electrons, which results in a homogeneous dose distribution in the irradiated area** [Scholz, GSI].

1.1.2 Densely ionizing radiation

Particle radiation is densely ionizing radiation and has a high LET. Its interaction with matter generates secondary electrons with different energies along the particle track (Fig. 2 A). The energy deposition has a maximum in the centre of the particle track, decreasing quadratically with the distance from the track centre (Fig. 2 B).

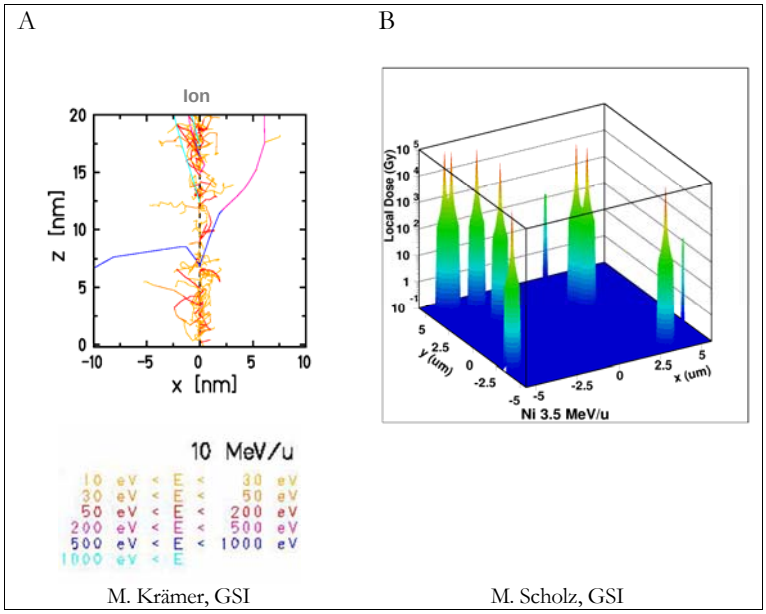

Fig. 2 **Densely ionizing radiation leave many ionisations within the particle track.** However, due to the particle track structure, it is very punctually localized and deposits a very high dose in the middle of the particle track.

The dose deposition as well as the maximum of the track diameter, depends on the kind and energy of the particle used. For particles the energy loss is inverse to the velocity: For high velocities, i.e. high energies, the interaction time is short and therefore the energy loss low but gets larger with decreasing energy. The deposited dose rises slowly with the penetration depth until the so-called Bragg-Peak is reached with a sharp increase in dose deposition at the end of the particle range [Bragg and Kleemann, 1905]. Just after the Bragg-Peak, the dose decreases rapidly within 1 mm. The depth of the Bragg-Peak can be modified by varying the particle energy. The dose of particle irradiation can be calculated based on the fluence and the LET [Taucher-Scholz und Kraft, 1999]. The feature of this inverted and adjustable dose deposition makes particle radiation to a powerful tool in cancer treatment. Because of the minor increase in dose deposition with the penetration depth prior to the Bragg-Peak and the extreme fast decrease just after this point, normal tissue in the entrance channel or surrounding the tumour can be spared during therapy. Furthermore, heavy charged particles have a very small lateral and longitudinal scattering effect which makes it possible to irradiate deep-seated tumours with high precision. These characteristics, and the fact that heavy ions have a higher relative biological efficiency compared to sparsely ionizing radiation as written below, led to the development of the successful tumour therapy with heavy ions at the GSI [Kraft, 2000].

1.1.3 Relative biological efficiency

The relative biological effectiveness (RBE) gives the effectiveness of densely ionizing radiation on living matter compared to sparsely ionizing radiation. It has been shown that densely ionizing radiation as carbon ions have an elevated RBE at the end of their range [Kraft, 1997]. This property allows a control of otherwise radioresistant tumourgenic tissue in tumour therapy. With the RBE it is possible to compare different radiation qualities in their biological efficiency. The RBE is defined as followed:

$$RBE = \frac{D_x}{D_{ion}}$$

D_x and D_{ion} are the X-ray and ion doses, respectively that are necessary to achieve the same biological effect. RBE is one if both types of radiation have the same effectiveness. If the test radiation is more effective, the RBE is larger than 1. As the RBE varies, the biologically effective dose [D_e] to living matter is given in Gray-equivalent [*Gyℓ*] as below:

$$D_e[Gy\ell] = D\,[Gy] \times RBE$$

With this knowledge, it is obvious, that it is very important to know the RBE for cell killing before any radiation is applied in therapy, to ensure that the desired level of radiation exposure is achieved. Furthermore, the maximum RBE value not only differs with the particle used, but also changes with the cell type and the absorbed dose [Kraft, 1997; Weyrather, 1999].

Fig. 3 shows a schematic dose effect curve for cell survival after irradiation with X-rays compared with particle irradiation. For a survival of 10 % of the irradiated cells a smaller dose of particle irradiation ($D_{part.}$) is required than for X-ray irradiation ($D_{X\text{-}ray}$). The high cell killing effect of particle irradiation is due to the difference in the level of induced DNA damage as written in the next chapter.

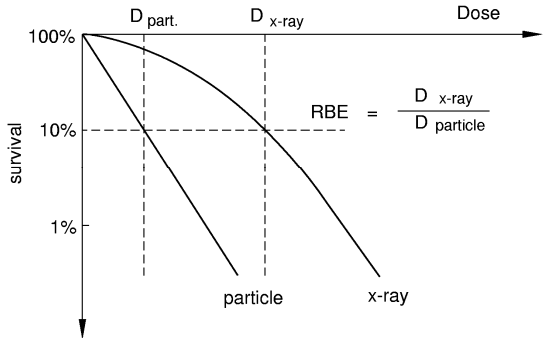

Fig. 3 **Schematic survival curve, demonstrating the RBE for cell killing.** The difference in effectiveness is seen in the higher X-ray dose compared to the particle dose required to achieve the same outcome for cell inactivation [Kraft, 2002].

1.2 DNA damage induced by ionizing radiation

The most critical part in living matter when exposed to ionizing radiation is the DNA [Munro, 1970]. Cells which are not able to repair the DNA correctly, cannot sustain the genomic stability and non-repaired or incorrectly repaired DNA lesions lead to mutation, transformation or apoptosis (programmed cell death). Ionizing irradiation induces various DNA lesions, such as base damages, DNA single-strand breaks (SSBs) or DNA double-strand breaks (DSBs), resulting from deoxyribose destruction or DNA-protein crosslinks (Fig. 4). Depending on the kind of irradiation, different types of DNA damages may occur. The DNA double-strand break is the more critical DNA damage than single strand breaks as the complementary DNA strand is broken too, which complicates the repair.

It has been shown that sparsely and densely ionizing irradiation does not significantly differ in the amount DSBs they induce [Heilmann *et al.*, 1995]. However, the quality of the induced DNA lesions has been shown to vary for these two types of radiation. The DSBs produced by high LET radiation are closer together ("clustered DNA damages") having a higher complexity of the lesions [Ward, 1994; Goodhead, 1994; Rydberg *et al.*, 1994]. The repair of these clustered DNA damaged sites is shown to be more difficult [Taucher-Scholz *et al.*, 1996]. Furthermore, DSBs induced by low energetic ions are repaired less complete than DSBs induced by X-rays or high energetic ions [Taucher-Scholz *et al.*, 1996]. The ability of the cells to repair the irradiation induced DSBs appear to depend on the proximity, distribution and number of the ionisation events in the nucleus.

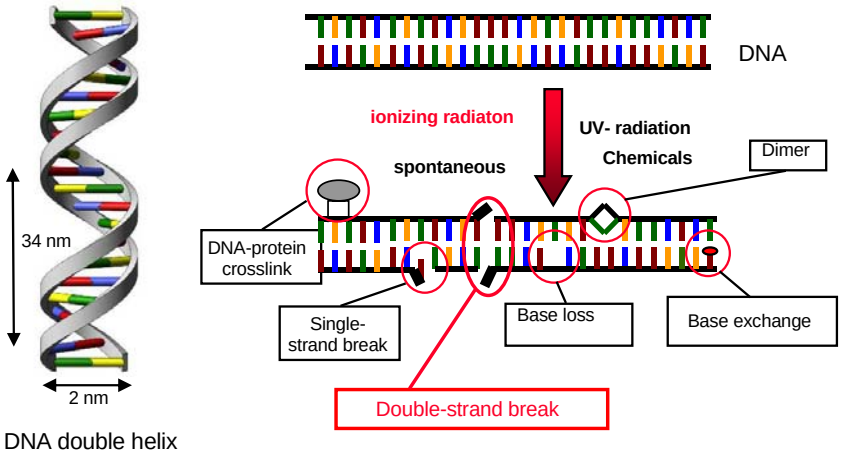

Fig. 4 **Schematic diagram of possible DNA lesions induced exogenously or spontaneously.** DNA damages are induced by ionizing radiation, UV radiation or chemicals, but also occur spontaneously. Possible DNA lesions are for example DNA single-strand breaks (SSBs), DNA double-strand breaks (DSBs), base loss, base exchange, dimerisation of bases or crosslinks between the DNA and proteins.

Not only the type of DNA damage influences a cell's ability to repair the lesion, but also the cell cycle stage in which the lesion is introduced plays a role for the ability to repair. A cell undergoes four different cell cycle phases, the G_1-, S-, G_2- and the M-phase (Fig. 5). In the G_1-phase (gap_1-phase) the cell is preparing for the DNA synthesis. At the end of the G_1-phase there is a G_1/S cell cycle checkpoint which controls whether the cell is ready to enter the following S-phase (synthesis-phase). During S-phase, which includes an intra-S-phase cell cycle control point, the DNA is synthesised. The S-phase is followed by the G_2-phase (gap_2-phase) which allow the cell time for the preparation of the cell division, the mitosis (M-phase). A G_2/M cell cycle checkpoint at the end of the G_2-phase controls if the entire DNA has been replicated correctly before cell division. Additionally, certain cell type's can reversibly or irreversibly leave the cell cycle and enter a resting state referred to as the G_0-phase.

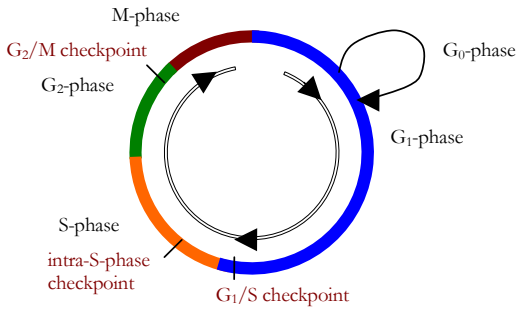

Fig. 5 **Model of the eukaryotic cell cycle.** The cell cycle is divided in four different phases; the G_1-, G_2-, S- and the M-phase. Additionally, certain cells can enter the G_0-phase. The cell cycle has three cell cycle control points controling whether the cell cycle can proceed or if the cell cycle has to be arrested: G_1/S, intra-S-phase and G_2/M checkpoint.

Depending on the cell cycle phase at time of DNA damage, different repair pathways are preferred. This mainly due to the DNA structure the cell has at the time-point the DNA has to be repaired. For example, for repair processes which use the homologous DNA strand for repair, the cell has to be in the S- or G_2-phase of the cell cycle where the sister chromatid is present. Controversially, the repair process non-homologous endjoining (NHEJ) was shown to operate throughout all cell cycle phases [Hinz *et al.* 2005]. The possible DNA repair pathways are briefly written in chapter 1.3 Mechanisms of DNA damage repair (page 9).

1.2.1 DNA damage induced by sparsely ionizing radiation

As mentioned in Sect. 1.1.1 (page 3) above, sparsely ionizing radiation generates mostly isolated secondary electrons and the local energy desposition is given by these electrons. On the cellular level, the nucleus encounters a wide spread of ionisations which produce isolated lesions in the DNA and its structure (Fig. 6). Because of this distribution of the damaged DNA sites, the cells seem to be able to have better possibilities of correct repair than the more clustered DNA damages induced by densely ionizing irradiation.

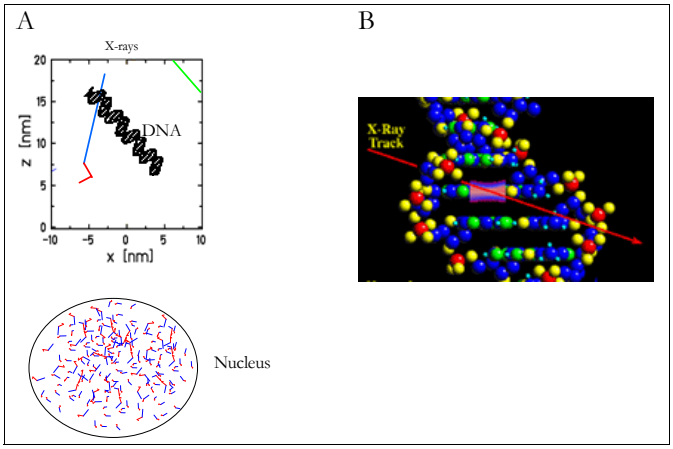

Fig. 6 **Sparsely ionizing irradiation generates a homogeneous deposition of secondary electrons.** Because of this, the DNA damages are distributed randomly in the genome; there are no highly clustered DNA lesions as with densely ionizing radiation as described below [Scholz, GSI].

1.2.2 DNA damage induced by densely ionizing radiation

DNA lesions induced by densely ionizing irradiation are more complex and with this appeared to be more difficult to repair. Many ionisations are produced along the particle trajectory, causing clustered DNA damage sites when passing the nucleus (Fig. 7). These clustered DNA lesions induced are the reason for the elevated RBE [Heilmann *et al.*, 1996; Kraft, 2002]. Furthermore, particle irradiation with high LET has been shown to induce a high fragmentation of the irradiated genomic DNA [Lobrich *et al.*, 1998], and the cell cycle is more extendedly delayed than after sparsely ionizing radiation [Fournier *et al.*, 2004].

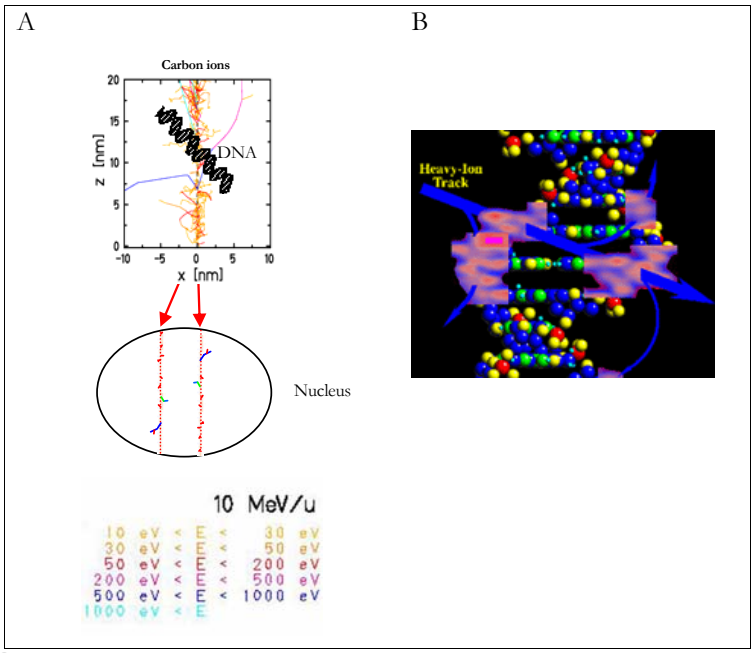

Fig. 7 **Densely ionizing irradiation such as carbon ions leaves massive ionisation events which results in clustered DNA damages as illustrated by the schematic DNA.** Along one track, many ionisations occur, which leaves a huge amount of DNA lesions in close proximity. Because of these clustered DNA damages, the repair of the damaged DNA is more difficult than with the isolated DNA lesions induced by sparsely ionizing irradiation [Krämer and Scholz, GSI].

1.3 Mechanisms of DNA damage repair

DNA repair is not only an issue after ionizing radiation, since cells also contain spontaneously induced DNA lesions due to radical attacks generated mainly by the oxidative energy metabolism. For example, a cell handles with about 10000 SSBs, 5000 base damages and 2 DSBs a day [Friedberg *et al.*, 1995]. Therefore, mammalian cells possess many pathways to repair the different DNA damages and preserve the genomic stability [Kohn, 1999; review: Sancar *et al.*, 2004]. Proteins detect the DNA damage (DNA damage sensors) and initiate pathways by activation or stabilisation of other proteins. The type of DNA lesion and the time of damage induction (e.g. cell cycle phase) determines which pathway is used. The DNA can be repaired, mis-repaired or not repaired. If the cell is not able to repair the DNA lesion correctly, the way of the programmed cell death (apoptosis) is preferred, as if the DNA is mis-repaired or no repair takes place, mutations occur which in worst case may lead to cancer (Fig. 8).

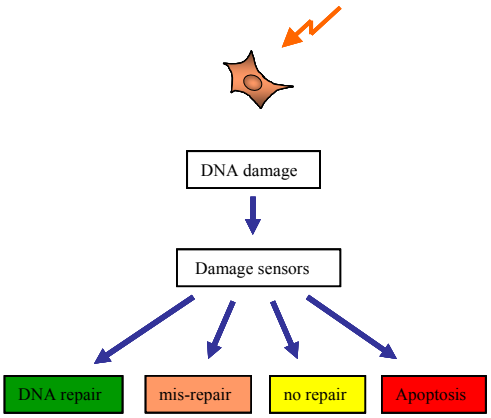

Fig. 8 **Schematic diagram of possible outcome of DNA damage, here induced by ionizing radiation.** The DNA lesion is detected by DNA damage sensors, which activate further pathways, depending on the DNA damage.

The DNA damages introduced can be repaired by the excision repair pathways (i.e. base-excision repair, nucleotide-excision repair or mismatch repair), or the DSB repair pathways (i.e. homologous recombination (HR) or non-homologous end-joining (NHEJ)) [review: Jeggo, 1998; Hoejmakers, 2001; Jackson, 2002]. Damaged bases are repaired by the base-excision repair (BER) or nucleotide-excision repair (NER) that involve excision and replacement of the individual damaged bases or larger nucleotide fragments, respectively. SSBs are repaired in a similar process [review: Caldecott, 2001]. DSBs potentially involve a number of repair processes. Which process is used, is mainly dependent on the cell cycle phase at time when DNA is damaged. DSBs that occur during or after chromosome duplication and before chromosome segregation (S- and G_2-phase of the cell cycle) are repaired by both NHEJ and HR. In HR the broken strand is repaired by non-crossover gene conversion events using the sister chromatid as a template, making it the main repair pathway in late S/G_1-phase of the cell cycle [Johnson and Jasin, 2000]. During all stages of the cell cycle, DSBs can be repaired by NHEJ, but it is of major importance when HR is minimal in G_0/G_1-phase [Lee *et al.*, 1997; Rothkamm *et al.*, 2003; Lobrich *et al.*, 2005; Hinz *et al.*, 2005].

The main DNA repair processes are described in brief below.

1.3.1 Excision repair

As the name implicates, the excision repair is a process whereby the damaged DNA is recognised and excised. The damaged DNA site, with either free bases or nucleotides, is removed and replaced by newly synthesized DNA, using the undamaged complementary DNA strand as a template. There are two types of excision repair, the base-excision repair (BER) and the nucleotide-excision repair (NER), both outlined in brief below (Fig. 9).

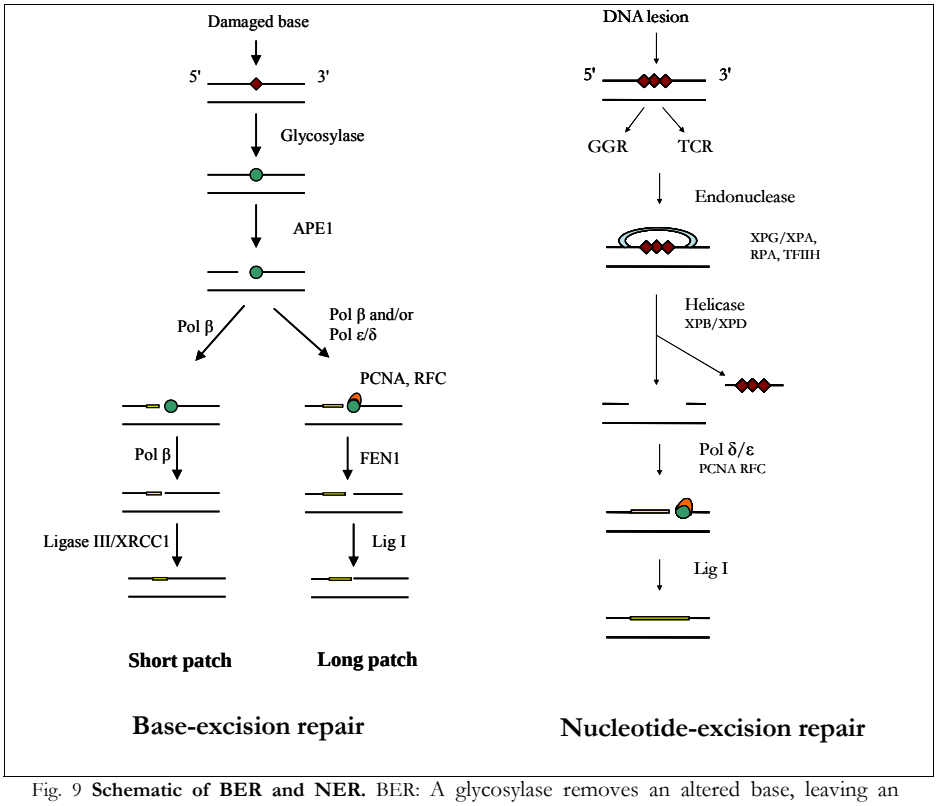

Fig. 9 **Schematic of BER and NER.** BER: A glycosylase removes an altered base, leaving an apyrimidinic site which is removed by the AP endonuclease APE1. The single-base gap is filled by sequential action of DNA polymerase and ligase (see text for more detail). Adapted and modified from Wilson *et al.*, 2006. NER: After DNA damage recognition by DNA damage sensing proteins, a nuclease cuts the DNA on each side of the lesion which is removed by a DNA helicase. By sequential action of DNA polymerase and ligase the removed fragment is filled in again.

1.3.1.1 Base excision repair

The BER repairs a single damaged nucleotide (short patch) or 2–10 nucleotides (long patch) around the damaged nucleotide caused by oxidation, alkylation, hydrolysation or deamination [Hoeijmakers, 2001]. The altered base is removed by a DNA glycosylase, which specifically recognizes the base modification and cleaves the N-glycosidic bond between the base and the deoxyribose of the DNA, leaving a so called AP site (apyrinic/apyrimidinic site) [Nash *et al.*, 1996; Krokan *et al.*, 1997; Pearl, 2000]. Bifunctional DNA glycosylases posses an AP lyase activity, making them capable to cleave the DNA at the 3'-side of deoxyribose, resulting in a single-strand break. Monofunctional glycosylases lack this lyase activity and the remaining ribose-phosphate group is excised by polymerase β [Matsumuto and Kim, 1995; Sobol *et al.*, 2000]. The AP site is recognised by an AP endonuclease, which recognises any deoxyribose sugar in the DNA with a missing base. The major mammalian AP endonuclease is termed APE1 [Demple *et al.*, 1991; Izumi *et al.*, 2003]. It removes the damaged DNA site by cutting the DNA upstream of the AP site. The resulting gap in the DNA helix is filled by sequential action of a DNA polymerase and DNA ligase (see schematic in Fig. 9).

In the case of short patch BER the excised lesion is filled by DNA polymerase β [Singhal *et al.*, 1995] and the nick sealed by DNA ligase I or DNA ligase III/XRCC1 (X-ray repair cross complementing 1 protein) complex [Wilson, 1998; Tomkinson and Mackey, 1998]. The long patch BER involves PCNA (proliferating cellular nuclear antigen) and the PCNA-dependent polymerases ε or δ together with the replication factor C (RFC) followed by excision activity of the flap endonuclease 1 (FEN1) [Dianova et al, 2001] and DNA ligation by DNA ligase I [Frosina *et al.*, 1996; Beard and Wilson, 2000]. Additionally, Pol β is described to be able to take part in this long patch pathway [Prasad *et al.*, 2000]. XRCC1 has been described to be a crucial factor for BER and single-strand break repair [review: Caldecott, 2003]. It has been shown to interact with several enzymes involved in these repair processes, such as pol β [Caldecott *et al.*, 1996], APE1 [Vidal *et al.*, 2001], PARP-1 [Masson *et al.*, 1998; Schreiber *et al.*, 2002] and DNA ligase III [Caldecott *et al.*, 1995].

1.3.1.2 Nucleotide excision repair

The nucleotide-excision repair (NER) repairs DNA damage affecting 2–30 nucleotides. It recognizes a wide range of DNA damages, including bulky distortions in the DNA helix, pyrimidine dimers and 6–4 photoproducts caused by UV light and single-strand breaks [Wood, 1996; Costa *et al.*, 2003]. Two different sub-pathways of NER are known; the global genomic NER (GGR) and the transcription coupled NER (TCR). The GGR pathway can repair DNA lesions at any location in the genome with efficiency depending on the type of the lesion [Tornaletti and Hanawalt, 1999] and genome condensation [Moggs and Almounzi, 1999]. The TCR pathway specifically removes lesions that block RNA polymerases on the transcribed strand of active genes [Bohr *et al.*, 1985; Mellon *et al.*, 1987]. These two repair processes vary in their way of recognising the helix-distorting DNA damage. After DNA damage recognition, the

damaged strand is excised by sequential action of helicases and nucleases, leaving a 2–30 nucleotide gap in the DNA helix. The resulting gap is restored by DNA polymerases δ and ε and ligase, using the intact strand as template (Fig. 9) [Nichols and Sancar, 1992; Shivji *et al.*, 1992].

In GGR the XPC-hHR23B complex has been shown to be the first component recruited at UV-induced DNA lesions and is required for the recruitment of subsequent NER factors [Volker *et al.*, 2001]. For the TCR, the first signal is the RNA polymerase II transcription arrest. If the RNA polymerase II detects a helix distorting structure during the transcription of a gene, it stalls the transcription and recruits NER proteins.

1.3.2 DNA double-strand break repair

As described above, most repair systems use the intact complementary DNA strand as template to fill in the resulted gap in the DNA. This makes the DSBs the most severe type DNA damage of the genome, as it leaves no intact template strand to use for the repair. If DSBs are not repaired correctly, chromosomal breakage, fragmentation and translocation may occur. DSBs can be caused exogenously by ionizing radiation and mutagenic chemicals but can also arise during replication or be induced by radicals from cellular metabolism. Two mechanisms have evolved to repair such DSBs, the non-homologous end-joining (NHEJ) and the homologous recombination (HR) [review: Kanaar *et al.*, 1998; van Gent *et al.*, 2001; Jackson, 2002; Lieber *et al.*, 2003; Bassing and Alt, 2004], both described in brief below (Fig. 10). Single-strand annealing (SSA) is considered a special form of HR involving sequence repeats [Pastink *et al.*, 2001]. Which of the pathway is used for the DSB repair appears to be largely influenced by the stage of the cell cycle at time of DNA damage induction [Jackson, 2002].

1.3.2.1 Non-homologous end-joining

With the NHEJ the two ends of the DSB are rejoined without the need of a homologous DNA strand as a repair template and by this can take place in all phases of the cell cycle [review: Critchlow and Jackson, 1998]. NHEJ is the predominant repair pathway in mammalian cells. The DNA termini are rejoined by a protein-DNA complex where DNA-PK and the ligase IV/XRCC4/XLF complex play a major role. DNA-PK binds to the DNA ends by the heterodimer Ku70/80 [Walker *et al.*, 2001] and the gap is closed by the activity of the ligase IV/XRCC4/XLF complex [Ahnesorg *et al.*, 2006]. See Fig. 10 for schematic model.

1.3.2.2 Homologous recombination

The homologous recombination (HR) is most efficient in the late S- and G_2-phase of the cell cycle, as it uses the sister chromatid as a repair template [Takata *et al.*, 1998; Johnson and Jasin, 2000]. A large number of proteins are involved in HR, such as RAD51, RAD52, RAD54, BRCA1, BRCA2, XRCC2, XRCC3 and the MRN complex [Karran, 2000; Thompson and Schild, 2001]. The DSB is recognised by ATM, ATR and DNA-PKcs [Durocher and Jackson, 2001]. The free DNA ends are processed by the MRN complex and after finding a homologous repair template and DNA synthesis the newly synthesised DNA strands are ligated by the action of ligase I. See Fig. 10 for schematic model. Single-strand annealing (SSA) is considered as a subpathway of HR. It is dependent on repeated sequences flanking the DSB and the non-homologous ends between these repeated sequences are lost during repair.

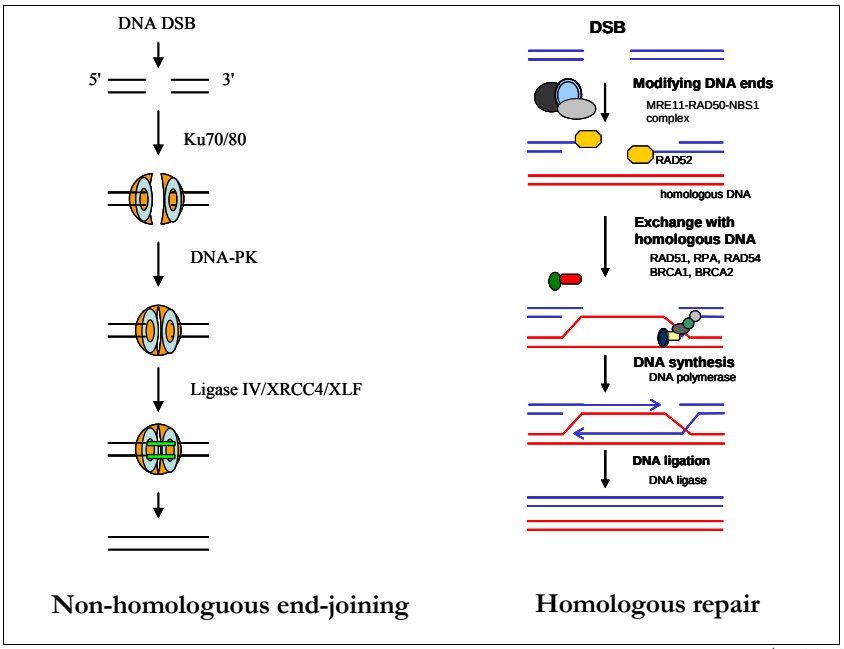

Fig. 10 **Schematic symplified model for DNA DSB repair by NHEJ and HR.** NHEJ: Ku70/80 binds to the DNA ends and recruits the DNA-PKcs, followed by the Ligase IV/XRCC4/XLF complex which seals the DNA ends. Adapted and modified from Helleday *et al.* (2007). HR: Schematic model of HR. A homologous DNA fragment is used as template. Free DNA ends are processed by the MRE11/Rad50/NBS1 complex. The single-stranded DNA interacts with RAD52, Rad 51, RPA and other proteins and searches for homologues DNA which is used as a template for DNA synthesis. Adapted from Sancar *et al.* (2004)

1.4 Accumulation of protein p21 at heavy ion induced DNA lesions

It was shown previously, that p21 accumulates at heavy ion (HI) induced DNA lesions. In studies performed by B. Jakob at the GSI [Jakob *et al.*, 2000] p21 accumulated along the heavy ion track through the nucleus of human fibroblasts shortly after irradiation (Fig. 11). Interestingly, these focal accumulations (foci) of p21 could not be detected after X-ray irradiation. In addition, it was reported that the persistence of the HI-induced p21 foci increased with the LET of the ion [Jakob *et al.*, 2002]. Furthermore, it was shown by Scholz *et al.* that the p21 foci correlate exactly with the heavy ion tracks, i.e. directly with the sites of severe DNA damage [Scholz *et al.*, 2001]. Colocalisation of p21 with hMre11 (human meiotic recombination 11) and PCNA (proliferating cell nuclear antigen) was detected at the heavy ion track [Jakob *et al.*, 2002]. hMre11 is part of the MRE complex (hMre11/Rad50/NBS) that has an important role in the DSBs repair and is involved in the NHEJ as well as HR [review: Jackson, 2002; Hopfner *et al.*, 2002]. PCNA, a subunit of DNA polymerase δ and ε, has been shown to take part in DNA replication, but is also active in the NER [Nichols and Sancar, 1992; Shivji *et al.*, 1995] and BER [Tom *et al.*, 2000; Tom *et al.*, 2001; review: Maga and Hübscher, 2003].

Furthermore has been stated that p21 foci formation induced by HI-irradiation occurred independently of NBS1 (Nijmegen breakage syndrome), ATM (Ataxia-telangiectasia mutated), XPA (Xeroderma pigmentosum group A) and TP53 [Jakob *et al.*, 2002]. NBS1 is described to be recruited to DSBs by binding to MRE11 in an ATM-dependent manner [for review see Kobayashi *et al.*, 2004]. The TP53 dependent p21 induction after IR induced DNA damage has been shown to be attenuated in NBS deficient cells but higher than the induction in AT cells [Matsuura *et al.*, 1998] which would be in line with this finding, suggesting that p21 is not involved in the DSB repair pathway downstream of NBS1 recruitment. The independency of ATM for the p21 foci formation shows that it takes place in absence of specific ATM phosphorylation. Even if protein phosphorylation can be done by several kinases, ATM has been shown to be the major activator of the cellular response to DSBs [Shiloh, 2003; Shiloh, 2006]. XPA plays an important role in the NER repair pathway as XPA deficient cells are not able to carry out NER [review: Vermeulen *et al.*, 1997]. This would suggest that p21 is not involved in XPA dependent NER. However, the involvement of p21 in NER has been studied by several groups, leading to contradictory results. It has been reported that p21 does not significantly inhibit or play an important role in NER [Shivji *et al.*, 1994; Sheikh *et al.*, 1997; Shivji *et al.*, 1998]. Opposite, studies with mutant forms of p21 showed that cells expressing p21 which is not able to interact with PCNA were deficient in NER, but wtp21 expressing cells could carry out NER [McDonald *et al.*, 1996].

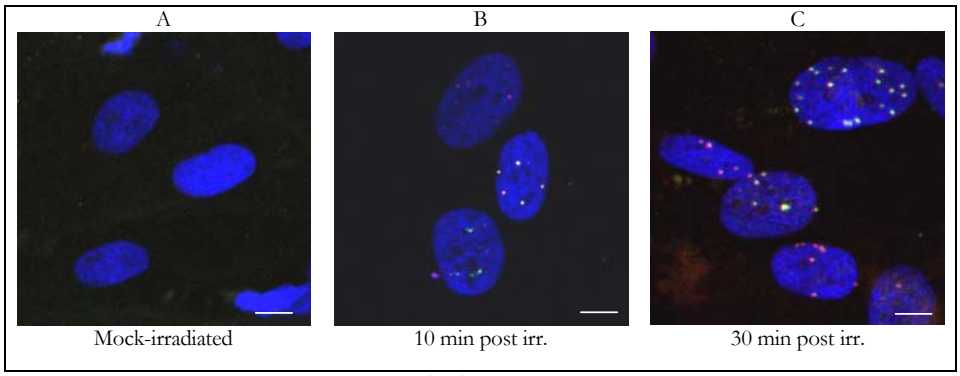

Fig. 11 **Foci formation of p21 and PCNA after exposure to chromium ions.** Human fibroblasts fixed and extracted according to the GSI modified Streck method at indicated times after irradiation with chromium ions (2×10^6 p/cm^2; 11.4 MeV/u; 2810 keV/µm). Immunostained proteins p21 (green) and PCNA (red); DNA visualised by ToPro-3 (blue). A: mock-irradiated. B: 10 min post irradiation. C: 30 min post irradiation. Bar: 10 µm.

As the p21 foci become visible almost immediately after heavy ion irradiation, this response appeared to be independent of p21's transcriptional induction through the TP53 pathway [Waldman *et al.*, 1995]. This assumption was supported by experiments carried out in HPV16 E6 cells that express the human papilloma virus 16 making them express only very small amounts of instable TP53. In spite of their non-detectable TP53 level (by Western Blot analysis), HPV16 E6 cells showed p21 foci shortly after HI irradiation [Jakob *et al.*, 2002].

In line with these observations, I was able to show in my Diploma Thesis that p21 foci formation was independent of protein synthesis [Heede, 2002]. I further demonstrated that both p21 protein synthesised before and after exposure to heavy ions was able to accumulate at the damaged DNA sites. In addition to these findings, I showed that if intracellular p21 levels were elevated artificially, p21 foci formation as well as their resolution was not altered. Additionally, the experimental studies in my Diploma Thesis indicated that the p21 focus most likely is a dynamic entity with p21 turnover.

1.5 Known functions of the p21 protein

The protein p21 has become a highly investigated protein, as it is involved in many different cellular events. The name p21 refers to its molecular weight, which is 18119 kDa and its running behaviour at 21 kDa in SDS-PAGE. p21 was first described by Harper *et al.* [1993] as a inhibitor of cyclin dependent kinases (CDKs) by its direct interaction and named CDK-interacting protein 1 (Cip1). Simultaneously, El-Deiry *et al.* [1993] identified this protein as a mediator of TP53-induced growth arrest, and named it wild-type p53-activated fragment (WAF1). Other

names for this protein are SDI1 (senescent cell-derived inhibitor 1), CAP20 (CDK2-associated protein 20), PIC1 or MDA6 (Melanoma Differentiation Associated protein 6). The p21 protein consists of 164 amino acids (aa.) and is primarily localized in the nucleus. Residues 140–143 comprise its nuclear localisation sequence (NLS, Fig. 12). Together with $p27^{Kip1}$ and $p57^{Kip2}$, p21 is member of the so called Cip/Kip family of cyclin dependent kinase inhibitors (CDKIs) whose actions affect the activities of cyclin D-, E-, and A-dependent kinases [Gu *et al.*, 1993; Harper *et al.*, 1993; El-Deiry *et al.*, 1993; Xiong *et al.*, 1993; Dulic *et al.*, 1994]. These CDKis share some sequence homology in their amino-terminal domains, through which they are able to bind both to cyclin and CDK subunits [Chen *et al.*, 1995, 1996; Nakanishi *et al.*, 1995; Lin *et al.*, 1996; Russo *et al.*, 1996; review: Sherr and Roberts, 1999]. At the carboxy-terminal domain, p21 has a PCNA (proliferating nuclear antigen; a subunit of DNA polymerase delta and epsilon) binding site (Fig. 12) [Xiong *et al.*, 1993; Kelman and Hurwitz, 1998; Ando *et al.*, 2001]. This site enables p21's direct interaction with PCNA, resulting in inhibition of PCNA's function in DNA replication [Waga *et al.*, 1994] and, with minor effects, in the NER [Pan *et al.*, 1995; Cooper *et al.*, 1999] and BER [Tom *et al.*, 2001] repair pathways. Recently, Perucca *et al.* [2006] showed that p21 is recruited to UV-C-induced DNA damaged sites and colocalizes with PCNA, Pol β, XPG and CAF-1, all proteins known to be involved in NER. Furthermore, these investigators showed a very fast recruitment of p21-GFP and RFP-PCNA to the regions of DNA damage induced by a 405 nm laser with RFP-PCNA showing slightly faster mobility than p21-GFP.

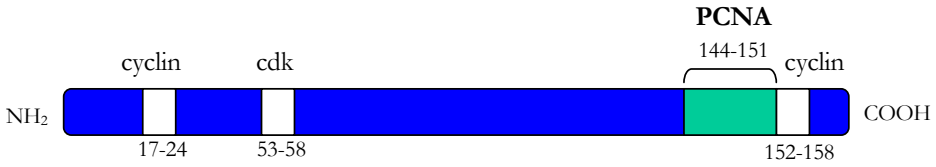

Fig. 12 **Cartoon to demonstrate the interaction sites of p21 with PCNA and cyclin/CDK complexes.**

In addition to the above mentioned binding sites, p21 has a number of additional direct protein-protein interactions [Dotto, 2000]. Depending on the protein partner p21 interacts with, different functions for p21 are described, such as cellular differentiation, DNA damage response, DNA repair, DNA replication or the mediation of TP53-dependent and -independent apoptosis (Fig. 13) [review: Gartel *et al.*, 1996; Gartel *et al.*, 2002]. Also, a possible role for p21 in the regulation of transcription has been described, as it interacts with proteins that regulate gene expression [Blagosklonny, 2002; Coqueret, 2003]. The function of p21 is mainly regulated by its expression level but also the subcellular localisation and the phosphorylation status of p21 have shown to be of importance [Child and Mann, 2006].

p21 has 2 phosphorylation sites at the carboxy-terminal domain through which different functions, such as PCNA binding ability or cyclin/CDK complex formation, of the protein can be mediated [Rossig *et al.*, 2001; Zhou *et al.*, 2001]. By specific phosphorylation of the protein its subcellular localisation can be influenced. Phosphorylation of Ser153 of p21 by PKC for example, contributes to its cytoplasmatic accumulation [Agell *et al.*, 2006]. Depending on its cellular localization, very different functions of p21 have been described [Conqueret, 2003]. Nucleolar p21 correlates with tumour suppressor functions, as PCNA binding inhibits DNA replication, p21's interaction with the CDK2/cyclin E complex induces cell cycle arrest, and, as

a transcriptional regulator, p21 induces cellular senescence and differentiation [Perkins, 2002]. Cytoplasmatic p21 however, shows proliferative influence by interacting with the CDK4/cyclin D1 complex which leads to the translocalisation of this complex into the nucleus and it inhibits apoptosis through binding to cytoplasmatic Ask1 and caspase 3 [Tanaka *et al.*, 2002; Asada *et al.*, 1999].

The carboxy-terminal domain furthermore includes a caspase cleavage site that is cleaved during apoptosis, leaving a protein unable to mediate growth arrest [Poon and Hunter, 1998; Zhang *et al.*, 1999].

The different functions, relevant for this thesis, of p21 that are known are described in more detail below.

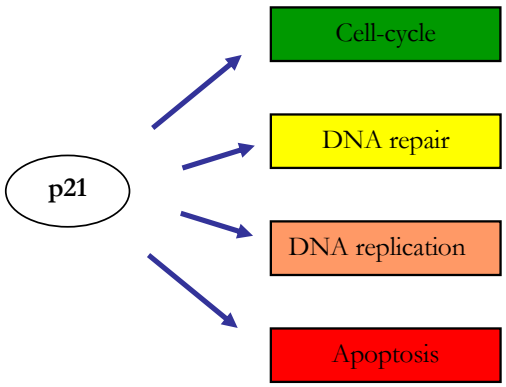

Fig. 13 **Schematic to represent the different cellular events in which p21 has a biological function.**

1.5.1 Role of p21 in the cell cycle regulation

As described in Sect. 1.2 (Page 6) the cell cycle consists of four phases, the G_1-, S-, G_2- and the M-phase (Fig. 5). The cell cycle is regulated and controlled by numerous proteins, ensuring that the DNA is fully replicated and distributed to the two resulting daughter cells. At different stages of the cell cycle, the cell cycle checkpoints, it is controlled whether the cell can continue cell cycle progression or not. If not, the cyclin dependent kinases (CDKs), which are needed for cell cycle progression, are inhibited. The protein p21 is one of the best described CDK inhibitors [Harper *et al.*, 1993; Sherr *et al.*, 1995; Gartel *et al.*, 1996; Niculescu *et al.*, 1998]. An elevated p21 level leads to G_1- and S-phase cell cycle arrest [Ogryzko *et al.*, 1997; Niculescu *et al.*, 1998; Radhakrishnan *et al.*, 2004]. Upon DNA damage induction, the protein ATM (ataxia telangiectasia mutated; a serine/threonine protein kinase) is recruited to DSBs by the hMre11/Rad50/Nbs1 (MRN) complex [Falck *et al.*, 2005; Lee and Paull, 2005]. The activated

ATM phosphorylates other proteins, such as TP53, which leads to the stabilisation of TP53 [review: Appella and Anderson, 2000; Kurz *et al.*, 2004]. TP53 induces p21 directly on the transcriptional level, resulting in an increase of the p21 protein [review: Vogelstein *et al.*, 2000] and leading to G_1- and S-phase cell cycle arrest [Ogryzko *et al.*, 1997; Niculescu *et al.*, 1998] by inhibiting cyclin/CDK2 complexes [Brugarolas *et al.*, 1999; Sherr *et al.*, 1999]. It has been shown by Waldman *et al.* [1995] that p21-null cells fail to undergo cell cycle G_1-arrest in response to DNA damage-induced TP53 stabilization, and both p21 and TP53 have been described to be essential to sustain the G_2-phase cell cycle checkpoint after DNA damage in human cells as well [Bunz *et al.*, 1998]. For an optimal inhibition of the cyclin/CDK complex, direct binding of both a cyclin and a CDK to p21 (aa. 17–24 and 53–58, respectively) is required [Chen *et al.*, 1996].

Interestingly, cytosolic phosphomimetic p21, which is not able to interact with PCNA, has no inhibitory effect on the cell cycle function [Zhou *et al.*, 2001]. Cytosolic localized p21, induced by the usage of a NLS-deficient construct however, was shown to lead to cell cycle progression [Dong *et al.*, 2003]. This suggests that not only the subcellular localization (i.e. nuclear) of p21 results in an inhibitory effect on the cell cycle, but also its interaction with PCNA is required to elicit G_1-arrest.

Different proteins can share sequence homologies due to which they compete in binding to the protein of interest. Protein p21 shares a sequence homology in its amino terminal domain (part of the cyclin binding site; aa. 17–24) with proteins such as p27, p57, positive regulators of cyclin/CDK complexes (for example Cdc25 phosphatase) and cyclin/CDK substrates (*e.g.* p107, p130 and E2F) [Saha *et al.*, 1997]. It does not only compete with p107 and p130 for binding to cyclin/CDK complexes, as it has been shown by Shiyanov *et al.* [1996] that p21 is able to disrupt already formed complexes of p107 or p130 with cyclin/CDKs. By binding to other proteins, p21 furthermore seems to be able to lend its NLS that leads to the translocation of the bound complex from the cytoplasm to the nucleus, as is the case for the CDK4/cyclin D1 complex [Agell *et al.*, 2006].

In contrast to its inhibitory effect on cell cycle progression, it has been stated that p21 is required for G_1- to S-phase transition in some cell types and that p21 functions as an assembly factor for cyclin D1/CDK4 complexes [LaBaer *et al.*, 1997; Weiss *et al.*, 2000]. More recently studies also indicated a positive role for p21 toward cell proliferation [Dupont *et al.*, 2003; Dong *et al.*, 2004].

1.5.2 p21 and DNA repair

The role of p21 in DNA repair to date is unclear. *In vitro* studies by Pan *et al.* [1995] demonstrated that p21 negatively interferes with NER due to its interaction with PCNA and inhibiting DNA synthesis, which was supported by *in vitro* studies from Podust *et al.* [1995]. Cooper and colleagues [1999] showed by *in vitro* and *in vivo* studies, using purified N-terminal and C-terminal p21 fragments, that the C-terminus of p21 inhibits NER, while the N-terminus did not have any effect. Interestingly, addition of purified PCNA relieved the NER inhibition by the C-terminal fragment. Sheikh *et al.* [1997] found that p21 may modulate the NER process and

that the clonogenic survival after UV-irradiation was increased when the p21 expression was artificially induced a few hours before and after UV exposure of DLD1 colorectal carcinoma cells. Contrarily, Shivij *et al.* [1994] suggested that p21 had no effect in NER, as supported by former *in vitro* findings of Li *et al.* [1994]. HCT116p21$^{-/-}$ cells showed no decrease in GGR or TCR, nor was the clonogenic survival after UV-irradiation altered by the absence of p21, suggesting that TP53-dependent NER does not require p21 [Adimoolam *et al.*, 2001]. This was supported by experiments from Wani *et al.* [2002] who showed that p21-null HCT116 cells did not differ in their DNA repair response to UV-irradiation compared to wild type HCT116 cells. Also studies with MEF cells lacking p21 only showed a minor effect on UV-induced DNA repair [Smith *et al.*, 2000]. On the other hand, Bendjennat *et al.* [2003] has shown that ubiquitin-dependent proteolysis of p21 is required for PCNA recruitment at UV-induced DNA lesions.

Recently, O'reilly *et al.* [2005] showed that the expression of BER repair enzymes was not altered in p21-deficient mice cells after exposure to oxidative stress although p21-wildtype cells showed an increased p21 level. This is contrary to former studies, where p21 was shown to decrease the BER ability in MEFs [Jaiswal *et al.*, 2002]. Also, *in vitro* experiments by Tom *et al.* [2001] showed an inhibition of BER by p21, due to its interaction with PCNA.

For DSB repair pathways, a direct role for p21 has not been shown. The results obtained during my Diploma Thesis [2002] showed no influence of p21 for the clonogenic survival or rejoining of DSB in HCT116 cells. When described in literature, it is as a part of the TP53 pathway where p21 is induced by TP53 following DSBs and p21 itself is not directly connected with DNA repair, as for example by Mirzayans and colleages [2004].

Furthermore, DNA-(cytosine-5) methyltransferase (MCMT; methylates newly replicated DNA) was shown to bind directly to PCNA and this PCNA-MCMT association was disrupted in human lung fibroblasts (MRC5 cells) by a peptide corresponding to aa. 141–160 of p21 [Chuang *et al.*, 1997]. This suggests that p21 can control DNA methylation levels during replication as well as possibly DNA repair.

1.5.3 Protein p21 and its role in apoptosis

The function of p21 in apoptosis is also a main topic, as p21 can inhibit as well as induce apoptosis. It has been described that the anti- or pro-apoptotic character of p21 partly depends on its subcellular localization [Gartel and Tyner, 2002]. Nucleolar localized p21 was shown to be pro-apoptotic [Dotto, 2000; Gartel and Tyner, 2002], whereas cytosolic localized p21 has an anti-apoptotic character [Asada *et al.*, 1999]. The exact pro-apoptotic function still has to be clarified, but for the anti-apoptotic role several models have been proposed. Due to the possibility to interact with proteins, such as c-IAP (inhibitor of apoptosis protein C) and procaspase-3, p21 is able to inhibit apoptosis [Asada *et al.*, 1999]. Gartel and Tyner [2002] have described that by the translocation of p21 from the nucleus to the cytoplasm it interacts with the apoptosis signal-regulating kinase 1 (Ask1) through which cells are protected from apoptosis.

Furthermore, nuclear localize p21 permits DNA repair by arresting the cell cycle, whereby the cell does not undergo apoptosis as a result of DNA lesions [Raderschall *et al.*, 2002].

1.5.4 Interactions of p21 and PCNA

PCNA has been shown to be required for NER [Shivji *et al.*, 1994; Nichols and Sancar, 1992] and is involved in many other cellular DNA replication and repair activities [Prosperi, 2006; Maga and Hübscher, 2003; Warbrick, 2000]. PCNA encircles the DNA and functions as a sliding clamp, enhancing the processivity of replicative DNA polymerases. PCNA and p21 physically interact through a PCNA binding site on p21 (aa. 144–151; see schematic Fig. 12) [Xiong *et al.*, 1993; Kelman *et al.*, 1998; Ando *et al.*, 2001]. The p21 binding to PCNA was originally shown to suppress PCNA-dependent DNA replication, leaving NER unaffected [Li *et al.*, 1994; Shivji *et al.*, 1994; Waga *et al.*, 1994; Chen *et al.*, 1995; Luo *et al.*, 1995; Sherr *et al.*, 1999]. However, inhibition of PCNA-dependent NER by p21 has also been reported [Pan *et al.*, 1995]. The fraction of p21 that is bound to active cyclin/CDK complexes in proliferating normal cells is also bound to PCNA [Zhang *et al.*, 1994]. The binding of p21 to PCNA can be modulated by reversible phosphorylation of p21 at its C-terminal domain [Scott *et al.*, 2000]. Neither the loading of PCNA onto DNA, nor the ability to move along DNA is affected by the p21 binding [Podust *et al.*, 1995; Cazzalini *et al.*, 2003], suggesting that the effects of p21 in inhibiting PCNA-dependent DNA replication may depend on preventing interactions with other proteins. This has recently been proposed for the function of p21 in TLS, where the binding of p21 to PCNA causes release of polδ (the p21 bindingsite on PCNA overlaps the polδ bindingsite [Gulbis *et al.*, 1996; Zhang *et al.*, 1998]) from the DNA lesion and PCNA [Livneh, 2006]. That p21 influences TLS is also supported by the results obtained from Avkin *et al.* [2006] who showed that p21, as TP53, are required for UV-induced mono-ubiquitination of PCNA.

Fen 1 (Flap endonuclease 1) which is a 5'–3' exonuclease that is essential in DNA replication for the joining of Okazaki fragments and completion of the lagging strand DNA synthesis [Siegal *et al.*, 1992; Waga *et al.*, 1994] has been shown to bind to the same overlapping region of PCNA in competition with p21 [Warbrick *et al.*, 1997; Chuang *et al.*, 1997]. Through its interaction with PCNA its enzymatic activity is stimulated [Li *et al.*, 1995; Wu *et al.*, 1996].

2 RESULTS

2.1 p21 and other DNA repair proteins accumulate along the tracks of heavy charged particles

Several DNA repair-related proteins - in addition to p21 - have been shown to accumulate along the DNA lesions induced by the charged particle track throughout the nucleus. Due to the clustered nature of the DNA lesions produced by heavy charged particles, a strong and very distinct signal for the accumulating proteins is obtained. Particularly, with the conventional irradiation geometry where samples are irradiated perpendicular to the particle beam. With this set up, is has not been possible to discriminate the accumulations of SSB- from DSB-related proteins at the induced DNA lesions. Therefore, a different irradiation geometry was used to follow the accumulation of different proteins throughout the nucleus and along the particle trajectory. With this set-up, cells were irradiated while positioned at an angle of 5° or less towards the incoming particle beam. This idea and exposure unit was developed by Dr. B. Jakob (GSI) with the aim to discriminate between different proteins accumulating along the particle trajectory [Jakob *et al.*, 2003]. I have used this new irradiation set-up to determine whether a distinct distribution of the various DNA lesions, especially DSBs and SSBs, and with this a distinct distribution of p21 and other proteins could be detected.

The detection of DSBs was done by immunostaining for either γH2AX (γ-phosphorylated Histone 2AX) or 53BP1 (tumour suppressor p53 binding protein 1). Phosphorylation of the histone H2AX is induced in response to DSBs and has become a commonly used DSB marker [review: Fernandez-Capetillo *et al.*, 2004]. 53BP1 is hyper-phosphorylated in response to DNA damage [Rappold *et al.*, 2001] and is a more specific marker for two-ended DSBs (i.e. exogeneously induced DSBs) in most cell lines.

For the detection of SSBs I decided to use indirect immunostaining of the XRCC1 protein (X-ray repair cross complementing 1 protein). XRCC1 has been shown to be required for the repair of the SSB [Brem and Hall, 2005]. Furthermore, it interacts with several enzymes known to be involved in BER and SSB repair [Vidal *et al.*, 2001].

2.1.1 Detection of p21 and 53BP1 at the heavy ion induced DNA lesions

The response of both p21 and the DSB-related protein 53BP1 to heavy ion (HI) irradiation was investigated in confluent human fibroblasts (AG cells) by the detection of these proteins with the indirect immunostaining method. AG cells were irradiated with iron ions (6×10^6 p/cm^2; 200 MeV/u; 337 keV/µm) as described in Sect. 4.2.3 (page 95), fixed without extraction of the soluble proteins (Sect. 4.4.1, page 99) at the time-points indicated and immunostained for p21 and 53BP1 (Sect. 4.4.4, page 100). Microscopic analyses were done as described in Sect. 4.5 (page 101).

Fig. 14 shows human fibroblasts at different times after irradiation. Overall mock-irradiated cells show no accumulation of p21 protein (Fig. 14 A). For 53BP1 however, a minority of the mock-irradiated nuclei showed 1–3 53BP1 foci per nucleus. Also if the DSB marker protein γH2AX was visualized, as done in several experiments, this was observed. It must be noted, that the red fluorescence signal often is not very clear in the pictures shown below, however, during microscopic analysis, if not mentioned otherwise, a weak red signal is observed.

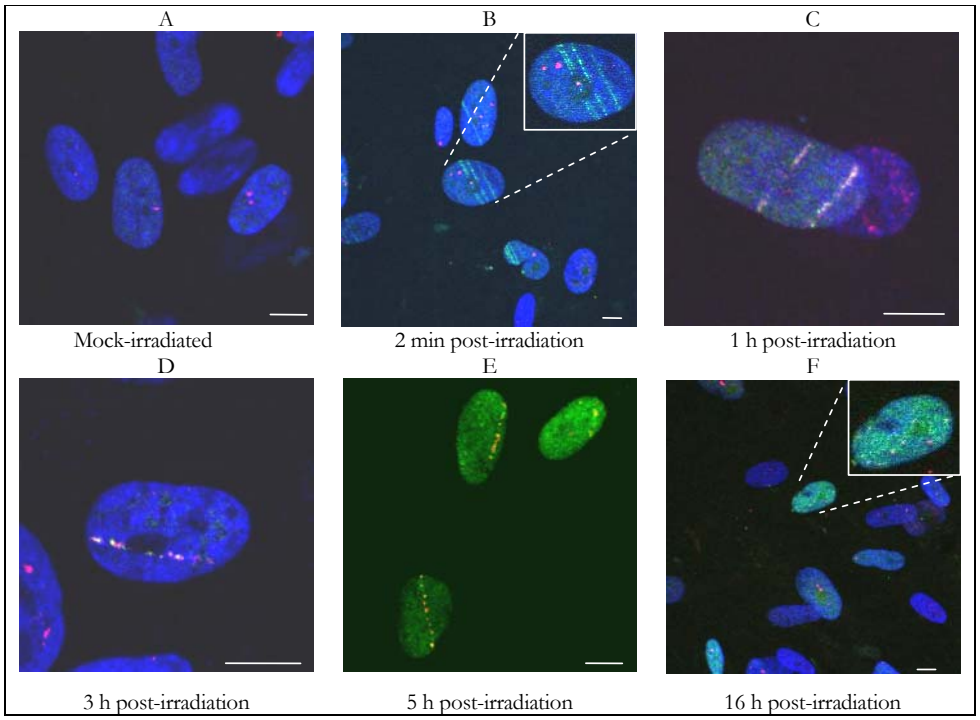

Fig. 14 **Indirect immunostaining to visualize p21 and 53BP1 along the particle trajectory throughout the nuclei of the irradiated AG cells.** Human fibroblasts were irradiated with the Fe ion beam (6×10^6 p/cm^2; 200 MeV/u; 337 keV/µm) at an angle of less than 5° (Sect. 4.2.3) at the UNILAC facility at GSI. Cells were fixed at the indicated times post-irradiation without extraction of soluble proteins. The cells were stained for p21 (green) and 53BP1 (red), the nucleus is visualized by DNA staining using ToPro-3 (blue). A: mock-irradiated nuclei; B–F irradiated with Fe ions. Note: Panel E is without ToPro-3 staining. Bar: 10 µm.

As shown in Fig. 14 p21 and 53BP1 form distinct protein tracks throughout the nuclei after irradiation with Fe ions. Both proteins became visible as early as 2 min after exposure to HI (Fig. 14 B). At 1, 2, 3 and 5 hours after exposure, protein tracks are detected (Fig. 14 C–F). 16 h after irradiation, only few of the nuclei display particle-induced streaks of p21 and 53BP1 (not shown), and the majority of the irradiated cells did not show any detectable protein accumulations (Fig. 14 F). The pattern of the protein accumulations appears to change with an increase in incubation time after irradiation, with the early distinct and streaky accumulations for p21 and 53BP1 becoming more dispersed at longer times after irradiation (see discussion 3.1.2). Nonetheless, both p21 and 53BP1 still appear to be colocalizing at later times after irradiation (5 h, Fig. 14 E). Note, that the protein tracks are discontinuous throughout the nucleus and appear to be localized in focal accumulations along the HI track.

2.1.1.1 Colocalisation analysis of p21 and 53BP by Scion Image analysis

To analyse whether two proteins, here p21 and 53BP1, colocalize the program Scion Image was used as outlined in Sect. 4.5.2. Employing Scion Image, it is possible to graphically display the intensity of the single channels from the microscopic analysis. Fig. 15 shows a representative graph obtained from the analysis by Scion Image.

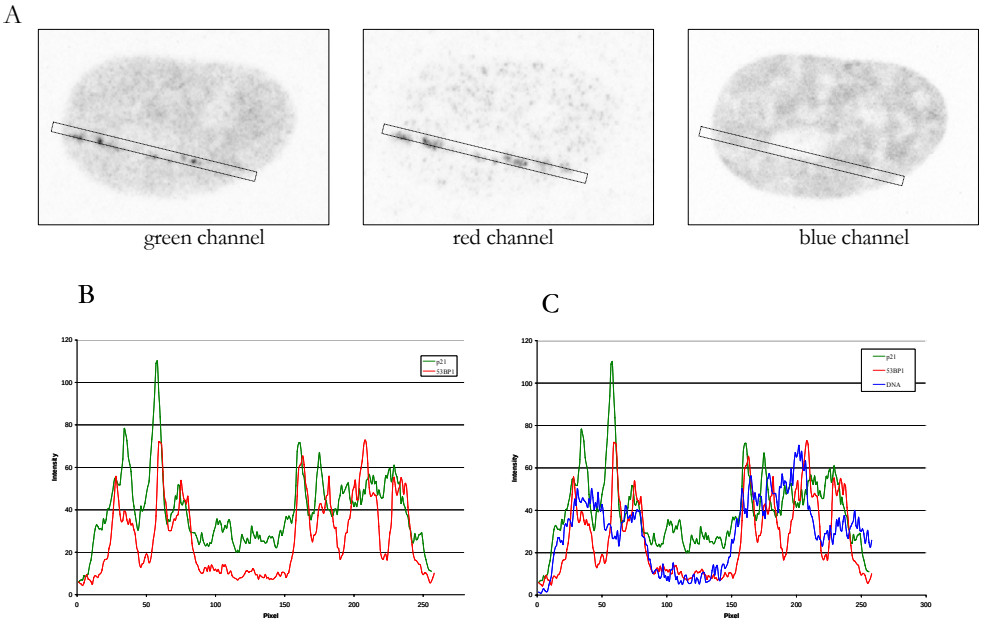

Fig. 15 **Representative analysis of the fluorescence intensities for p21 and 53BP1 accumulations along the particle trajectory.** Displayed is the analysis of the nuclei shown in Fig. 14 panel D. A: For each channel, fluorescence is converted into grey scale. The track is manually marked and the enclosed area is analysed for intensity levels. B: Graph of the given intensities for each of the two proteins detected by immunofluorescence. As described in the text, the intensity maxima of both fluorescent signals are localised very similar. C: The fluorescence intensities of the immunostained proteins plotted together with the intensity of the DNA staining ToPro-3, showing that the reduced detectable intensity for both proteins corresponds to a lower level of DNA staining.

The nuclei analyzed (12, $n = 31$) give overlapping positions for the intensity maxima of p21 and 53BP1, meaning that these proteins accumulate within the same region along the particle track. As obvious from Fig. 15, both the p21 and 53BP1 signals are reduced in some regions of the particle track. These discontinuous accumulations can not be explained by the physical distribution of ionisation events resulting from the HI track, as these shows a nearly continuous pattern along the ion trajectory (see Sect. 1.1.2 Fig. 2). It has been suggested that these 'gaps' in protein accumulation is due to the chromatin structure, i.e. the chromatin condensation [Jakob *et al.*, 2003]. Even if the DNA dye ToPro-3 is not appropriate to analyse the level of chromatin condensation, the nucleoli with low DNA density are distiguishable [Martin *et al.*, 2005]. The positions of low protein detection correlate with the area of reduced ToPro-3 staining, displaying the nucleoli (Fig. 15). The nucleoli were free of HI-induced accumulations of the immunostained proteins in all experiments done (data not shown). Only at the boundaries of the nucleoli, irradiation-induced focal accumulations of p21 and 53BP1 were detected in some cells (data not shown).

2.1.2 XRCC1 colocalises with p21 along the heavy ion trajectory

Due to the colocalization of p21 with the DSB-related protein 53BP1 along the HI tracks as shown above, I decided to study whether the structure of the detected foci results from a different distribution of the various DNA lesions. Here, p21 was immunostained (Sect. 4.4.4) in combination with the SSB-related protein XRCC1. Confluent fibroblasts were irradiated with iron ions (6×10^6 p/cm^2; 200 MeV/u; 337 keV/µm) and fixed without extraction of the soluble proteins (Sect. 4.4.1) at 2 min, 30 min, 1 h, 2 h, 3 h, 5 h and 16 h after irradiation.

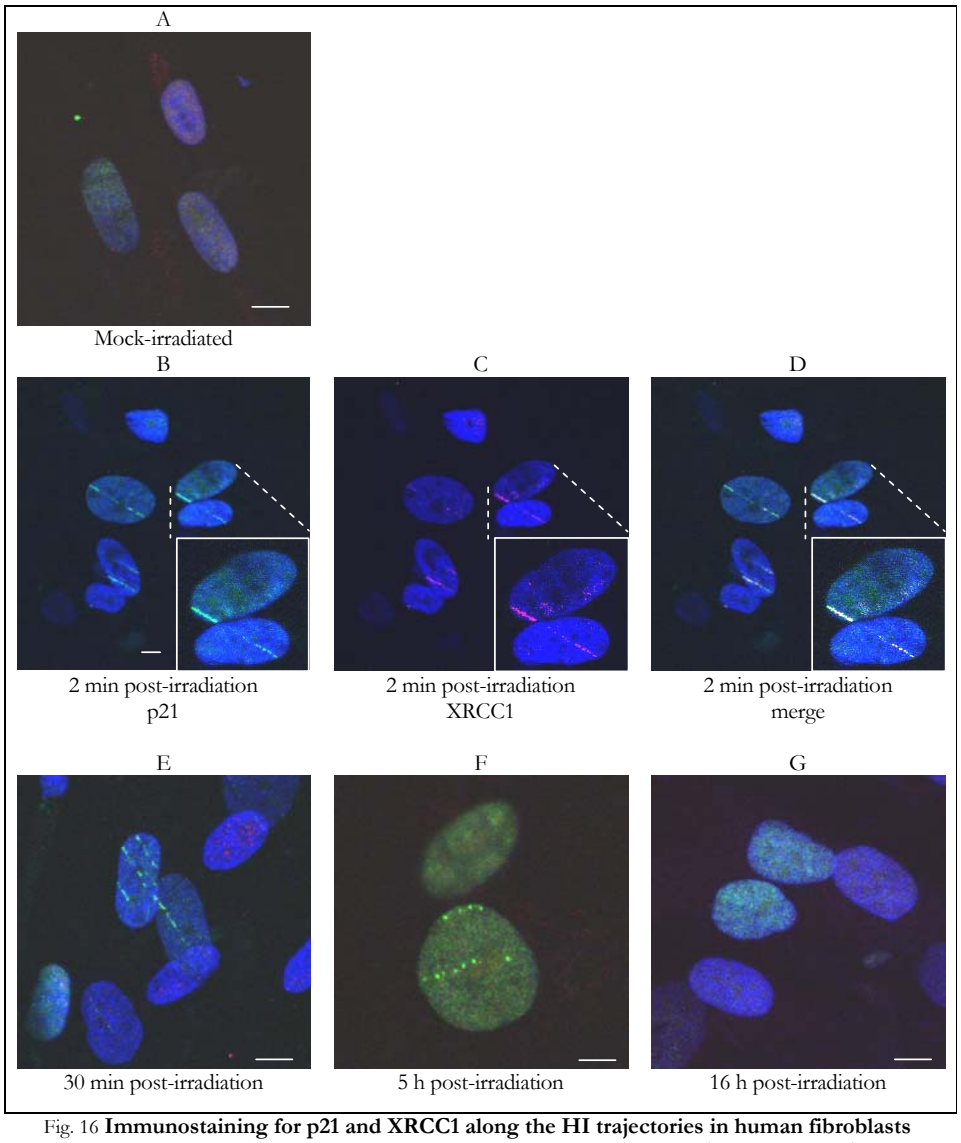

Fig. 16 **Immunostaining for p21 and XRCC1 along the HI trajectories in human fibroblasts after exposure to Fe ions.** Cells were irradiated with Fe ions (6×10^6 p/cm^2; 200 MeV/u; 337 keV/µm) and fixed at the times indicated without extraction of soluble proteins. p21 (green), XRCC1 (red), nucleus stained by ToPro-3 (blue). A: mock-irradiated AG cells; B–G: AG cells exposed to Fe ions. The accumulations of p21 mirror the particle trajectories. XRCC1 only show a weak signal, seen in panel C where the single channel is displayed. Note: Panel F no ToPro-3 staining. Bar: 10 µm.

Fig. 16 shows human fibroblasts nuclei and detection of p21 and XRCC1. The mock-irradiated cells (Fig. 16 A) do not show any protein accumulations, neither p21 nor XRCC1. Cells fixed 2 min after HI irradiation, show clear protein tracks of p21 as well as weak signals for XRCC1 at

the damaged DNA sites induced by particle traversal (Fig. 16 B–D). Furthermore, the XRCC1 accumulations show the same focal character as observed for p21 and 53BP1 (Fig. 14), giving colocalisation with the p21 accumulations. Five hours after irradiation, the protein tracks are still visible, but show a different pattern compared to earlier time-points (Fig. 16 F). The tracks become more dispersed with time, as also seen in the former experiment detecting p21 and 53BP1 (Sect. 2.1.1.). Cells fixed 16 h post-irradiation showed neither visible protein tracks nor focal accumulations of p21 or XRCC1 (Fig. 16 G). Note, that some tracks continue from one nucleus to a neighbouring nucleus, displaying an ion trajectory traversing two nuclei (Fig. 16 E).

2.1.3 Aprataxin accumulates at the HI-induced DNA lesions

The previous experiments did not show differential accumulations for p21 and 53BP1 or p21 and XRCC1, which made me study another protein called aprataxin. Aprataxin has recently been described to play a role in SSB repair and BER. Aprataxin deficient cells were shown to have an increased sensitivity to genotoxic agents but are not hypersensitive to IR [Gueven *et al.*, 2004]. However, neither IR, MMS, MMC nor H_2O_2 exposure induced detectable aprataxin foci in HeLa cells transfected with EGFP-aprataxin [Gueven *et al.*, 2004]. Due to the highly clustered DNA damage induction by HI irradiation, I investigated whether these clustered DNA lesions induced detectable aprataxin foci, maybe in a different pattern than the already studied proteins. For this, HeLa cells were transiently transfected with a plasmid encoding EGFP-aprataxin (transfected as described in Sect. 4.10.6) and irradiated with uranium ions (2×10^6 p/cm^2; 11.4 MeV/u; 14925 keV/μm) at a low angle (Sect. 4.2.3). The cells were fixed and stained for XRCC1 30 min after irradiation without extraction of the soluble proteins (Sect. 4.4.1).

The mock-irradiated cells show the successful ectopical expression of the transfected EGFP-aprataxin, with a high expression level in the nucleoli compared to the rest of the nucleus, but without any visible protein tracks (Fig. 17 upper panels, green fluorescence signal). In the irradiated cells, EGFP-aprataxin (green) as well as XRCC1 (red) form tracks across the nucleus, provoked by the HI traversals (Fig. 17 lower panels). Note that in this Fig. protein tracks are visible as if going through the nucleoli. This is obtained because the images shown represent the mean projection of the microscopically obtained stacks (12 planes). By displaying a single plane of the microscopically acquired stack, it is inferred that the protein tracks are either above or below the nucleolus (single planes not shown).

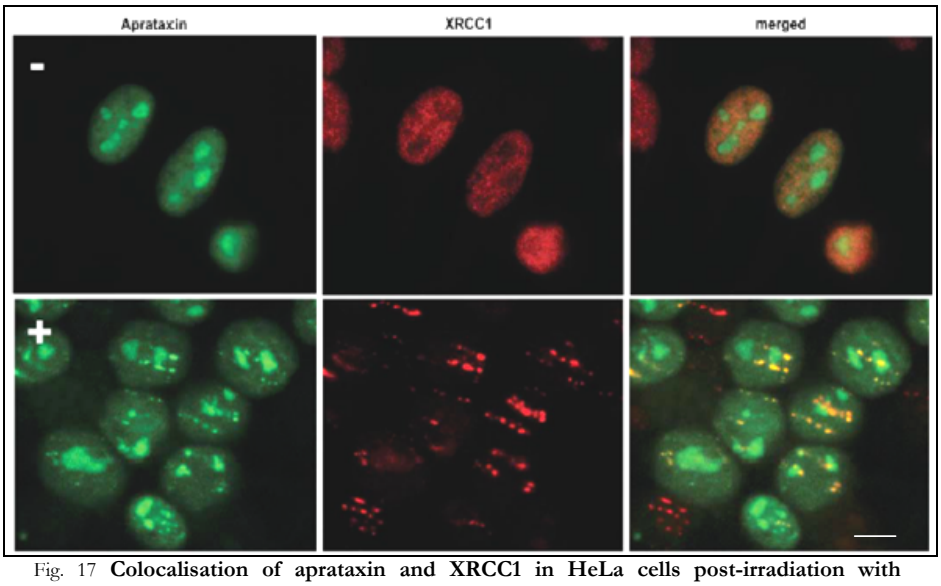

Fig. 17 **Colocalisation of aprataxin and XRCC1 in HeLa cells post-irradiation with uranium ions.** HeLa cells, ectopically expressing EGFP-aprataxin, 30 min post-irradiation (+) or mock-irradiated (-). XRCC1 visualized by red fluorescence (published: Gueven *et al.*, Human Molecular Genetics, 2004). Right panels: merged pictures to demonstrate partial colocalisation of aprataxin and XRCC1 (yellow) after uranium ions only. Bar: 10 µm.

2.1.4 DSBs and SSBs can not be differentiated by the new irradiation geometry.

In the former experiments, the accumulation pattern of p21 at the HI-induced DNA lesions was shown to be very similar to the observed XRCC1 and aprataxin accumulations, both described to be involved in BER and SSB repair. Furthermore, the detected p21 also colocalized with the used DSB markers 53BP1 and γH2AX accumulations along the HI trajectories (Sect. 2.1.1, page 23). This made me investigate, whether a differential distribution of γH2AX and XRCC1 can be visualized at the clustered HI-induced DNA lesions. However, the goal to differentiate between various DNA lesions induced by HI has not been obtained using an irradiation geometry that facilitates the analysis of the spatial distribution of the proteins accumulated at the DNA lesions along the particle trajectory, as written below.

Fig. 18 display AG cells after irradiation with Fe ions and detection of γH2AX and XRCC1. γH2AX show clear HI-induced tracks throughout the nuclei at the taken time-points. The microscopic analysis also gave weak HI-induced fluorescence tracks for the detected XRCC1 protein, the signal however is to low to be displayed in the figure. Very similar focal accumulations along the HI trajectory were obtained for both γH2AX and XRCC1 after Fe ions

exposure (6×10^6 p/cm^2; 200 MeV/u; 337 keV/µm; Fig. 18). Analysis with Scion Image was performed to verify that both proteins accumulate at the same positions along the HI track. An example of this analysis is shown in Fig. 19 with two tracks throughout one nucleus at 5 h after irradiation. Each track is analyzed separately, giving the data for the green and red channels of the fluorescence signal along the track. Both channels show the maxima at the same position. At 2 min and 1, 2, 3, and 5 hours after irradiation, γH2AX and XRCC1 tracks throughout the nuclei were detected and analysed (data not shown). Unlike for XRCC1, visible tracks for γH2AX were detected in some nuclei as late as 16 h post-irradiation (Fig. 18 D). Mock-irradiated cells did not show any protein accumulations (Fig. 18 A).

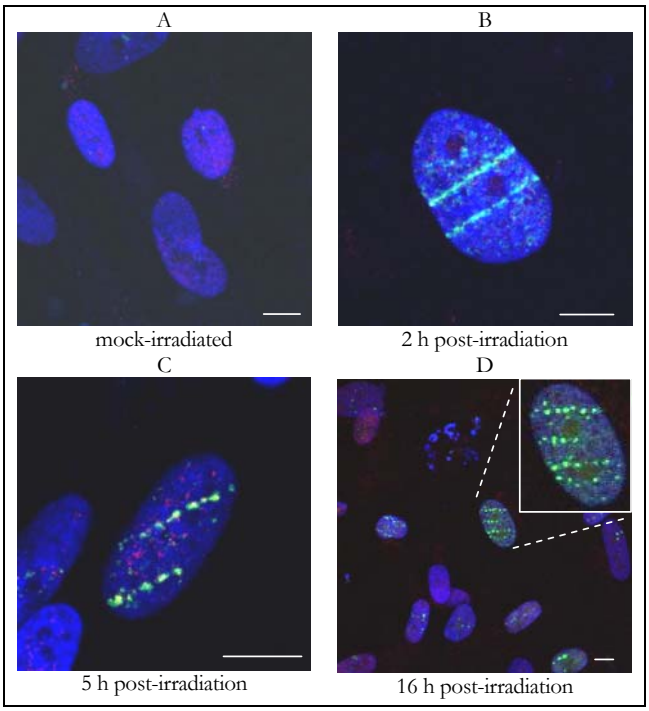

Fig. 18 **Indirect immunoflourescence to visualize γH2AX and XRCC1 in human fibroblasts after Fe ion irradiation.** γH2AX (green) and XRCC1 (red; detected by microscopic analysis, not clear visible in this figure), nucleus stained by ToPro-3 (blue). A: mock-irradiated AG cells. B–D irradiated with Fe ions. At early times post exposure the HI trajectory provokes streaky accumulations of both γH2AX and XRCC1. At 16 h post-irradiation only few nuclei show detectable protein tracks for γH2AX (D). Bar: 10 µm.

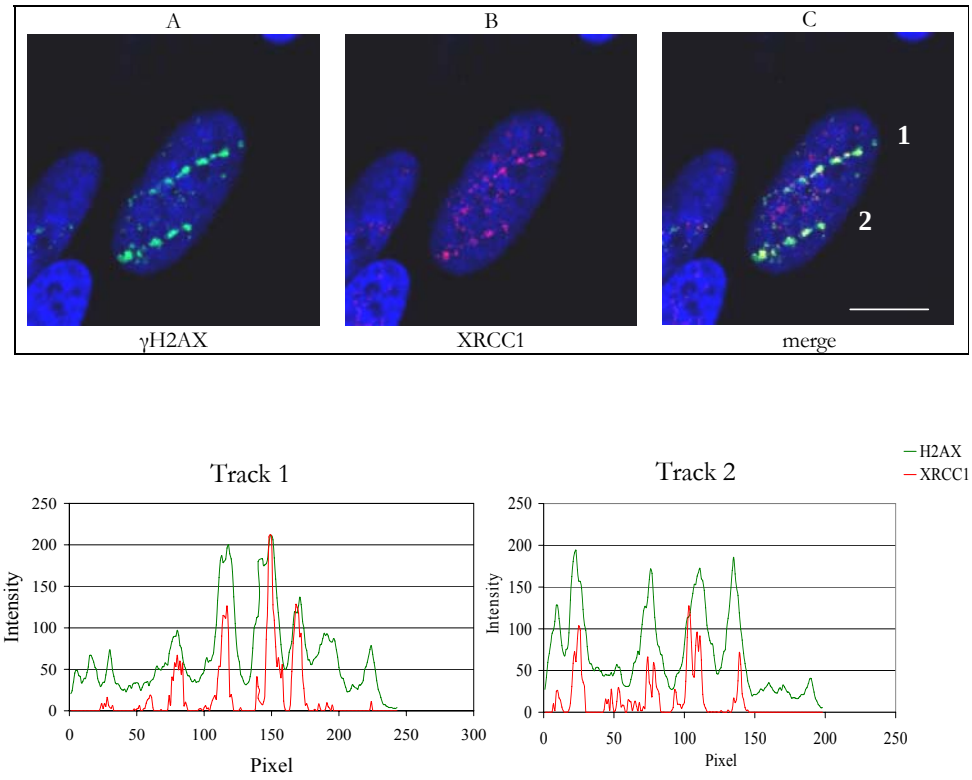

Fig. 19 **γH2AX and XRCC1 accumulate with a similar pattern along the HI trajectory**. Fluorescence intensities of γH2AX and XRCC1 are plotted for each track separately demonstrating colocalization of the intensity maxima within one track. Bar: 10 µm.

In summary, the results of these experiments show that p21 colocalises at the heavy ion tracks with γH2AX, 53BP1, XRCC1 and aprataxin. At the earliest time-point taken (2 min after irradiation) all proteins analyzed show detectable focal accumulations along the heavy ion tracks. In most experiments, the tracks of p21, 53BP1 and γH2AX are still visible in a few nuclei 16 h after DNA damage induction, XRCC1 however not. Here it must be noted though, that the obtained XRCC1 signal was weak compared to other stained proteins in all experiments done. Furthermore, I conclude that this experimental setup does not allow discriminating DSBs from SSBs after irradiation with heavy ions.

2.2 The accumulation of p21 at heavy ion-induced DNA damaged sites is dependent on its interaction with PCNA

Although p21 colocalises with PCNA at HI-induced DNA lesions and has a PCNA binding site, this does not prove an interaction of these two proteins at the DNA damaged site. To investigate whether one or both of the two proteins is dependent of the other for its foci formation at DNA lesions, the kinetics of p21 and PCNA accumulation was studied in more detail after HI irradiation. Furthermore, by the use of different p21 plasmids, I investigated whether p21 needs the intact PCNA binding site to accumulate at the HI-induced DNA lesions. Plasmids to elucidate this were kindly provided by Prof. Dr. S. Dimmeler (University of Frankfurt).

To visualise PCNA with the available antibody by immunostaining a special extraction method became necessary (see Sect. 4.4.3). Chromatin-associated PCNA protein was detected by a method modified from Streck *et al.* [Mirzoeva and Petrini, 2001] referred to as the 'GSI modified Streck method' in further context. However, as p21 could not be detected using this method, the modified Streck method was altered slightly, such that chromatin-bound p21 could be visualized paralell with PCNA by immunostaining ('GSI-modified Streck method' see Sect. 4.4.3). This adaptation led to both detectable PCNA and p21 foci after heavy ion irradiation. It should be mentioned though, that the PCNA as well as the p21 signal were proven to be fainter after extraction by the GSI-modified Streck method than after the original modified Streck method or the Hepes extraction method, respectively (data not shown).

2.2.1 Kinetics of p21/PCNA foci formation

To investigate the kinetics of the p21/PCNA foci formation after exposure to heavy ions, confluent human fibroblasts were irradiated as described in Sect. 4.2.3 followed by extraction and fixation according to the GSI-modified Streck method (Sect. 4.4.3) and staining for p21 and PCNA (Sect. 4.4.4). After irradiation, the cells were incubated at 37°C as indicated. To investigate whether the kinetics of the foci formation is influenced by the incubation temperature, cells were incubated at two different temperatures during the experiment with chromium ion irradiation. The sample holders used for the irradiation were cooled or pre-warmed at 4°C or 37°C, respectively and incubated at these temperatures for all samples fixed at 5 min and 10 min post-irradiation. These two early time-points were chosen, as it was likely that if there was a temperature dependent difference in the foci formation for p21 and PCNA, this would be shortly after irradiation. For radiation safety reasons, the shortest time-point possible to fix the samples after irradiation was 2 min. In parallel to this experiment, cells were irradiated in pre-warmed medium and incubated at 37°C for 15 min, 30 min and 7 h. Table 1 shows the different types of heavy ions which were used for the experiments to elucidate the kinetics of the p21 and PCNA foci formation.

Ion	Fluence [P/cm²]	Energy [MeV/u]	Energy on target [MeV/u]	LET [keV/µm]
Cr	2×10^6	11.4	5.6	281
Ni	2×10^6	11.4	4.5	3790
U	2×10^6	11.4	4.2	14925

Table 1 **Ions used to study the p21/PCNA kinetics.**

Immunostained nuclei to visualize the time-course of appearance for p21 (green) and PCNA (red) after exposure to Cr ions (2×10^6 p/cm^2; 11.4 MeV/u; 2810 keV/µm) are shown in Fig. 20 DNA is visualized by ToPro-3 staining (blue). At the first time-point taken, in this experiment 5 min post-irradiation, p21 and PCNA foci were readily detectable (Fig. 20 B). Focal accumulations of both proteins were clearly visible at 5, 10, 15 and 30 min post-irradiation (Fig. 20 B–E). However, 7 h after irradiation, hardly any p21 or PCNA foci could be detected (Fig. 20 F). Sporadically, an S-phase cell was observed, showing a high level of PCNA staining (data not shown).

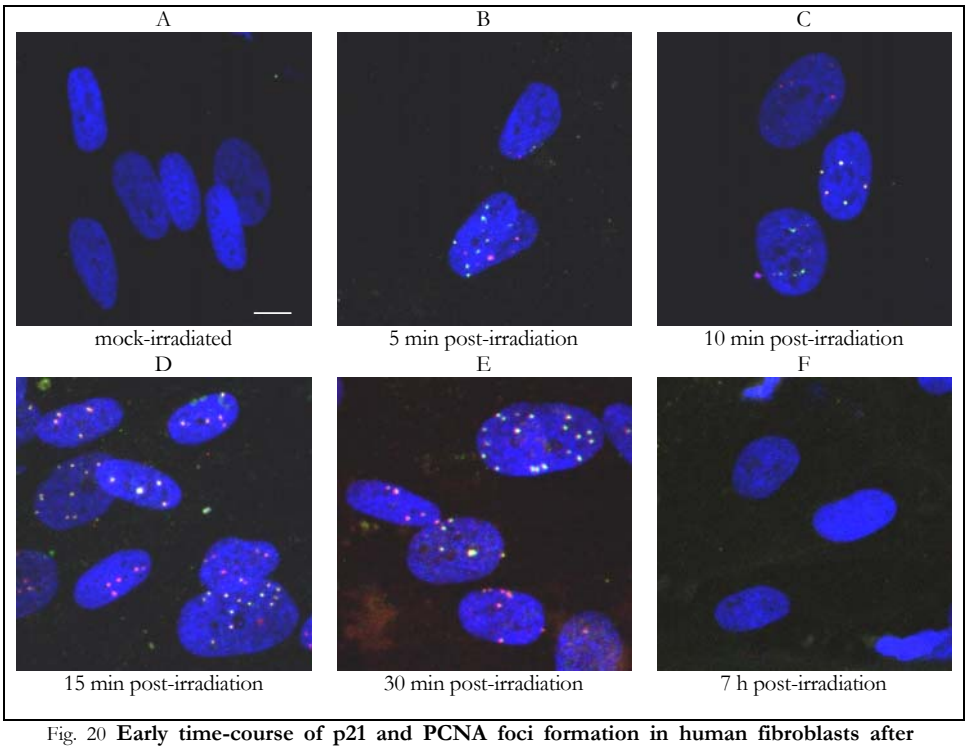

Fig. 20 **Early time-course of p21 and PCNA foci formation in human fibroblasts after irradiation with chromium ions.** A: mock-irradiated cells. Soluble proteins were extracted according to the GSI-modified Streck method and the cells fixed at the indicated times at 37°C after irradiation. Focal accumulations for p21 (green) and PCNA (red) are seen 5, 10, 15, and 30 min post-irradiation (B–E); 7 h after irradiation, only very few nuclei show focal protein accumulations (F). Mock-irradiated cells did not show any focal formation of either p21 or PCNA (A). DNA visualized by ToPro-3 staining (blue). Bar: 10 µm.

The influence of the temperature on the foci formation was analysed by manually counting visible p21 and PCNA foci in several nuclei. This was also done for the analysis of the kinetics of the focal formation of both proteins (Table 2).

Incubation time post-irradiation	**Incubation temperature**	**Cells with p21 foci**	**Cells with PCNA foci**	**Number of nuclei analyzed** (*n*)
5 min	4°C	41%	98%	41
5 min	37°C	54%	81%	81
10 min	4°C	33%	100%	39
10 min	37°C	69%	93%	67
15 min	37°C	47%	99%	67
30 min	37°C	79%	97%	78
7 h	37°C	2%	5%	41
Mock-irradiated	37°C	0%	0%	40

Table 2 **Analysis of early detectable p21/PCNA foci in human fibroblasts after irradiation with Cr.**

Independent of the temperature the majority of the cells showed PCNA foci at 5 min after exposure to chromium ions, while approximately half of the nuclei visualized p21 foci as summarized in Table 2 above. One third of the cells which were fixed 10 min post-irradiation showed p21 foci and all of the cells analyzed showed PCNA foci, if the medium was cooled compared to app. two third with p21 foci and almost all with PCNA foci in warm medium. After 15 min, app. half of the cells showed p21 foci and all of the cells were positive for PCNA foci when kept in 37°C medium. At 30 min post-irradiation, more of the cells irradiated in 37°C medium, had detectable p21 foci (79%) and nearly all cells showed PCNA foci. The cells that were fixed 7 hours after irradiation hardly showed any detectable foci formations for both proteins. Only in 2% of the cells p21 foci were seen and in 5% of the cells PCNA foci could be detected.

The temperature at which the cells were kept during the experiment had a slight influence on the number of nuclei with detectable p21 foci in this experiment, giving more detectable p21 foci at 37°C. With the PCNA foci however, the temperature did not seem to be of major importance. Also the early time-course of focal accumulations post HI exposure was not significantly changed. The same result was obtained in a second experiment (data not shown). Because of only the minor change in the detectable p21 foci, the following experiments were done in 37°C medium as the possibility of inducing cellular stress factors is assumed to be higher due to the cooling down to 4°C

The time-course of protein accumulation of p21 and PCNA was investigated after HI irradiation with the ions displayed in Table 1. After irradiation with uranium ions (2×10^6 p/cm^2; 11.4 MeV/u; 14925 keV/µm) already 2 min post-irradiation nearly all nuclei showed detectable p21 foci and all showed PCNA foci (supplement 6.1 Fig. 71 B). 15 min post-irradiation the majority of nuclei had visible p21 foci and all nuclei showed PCNA foci, compared to a slight reduction of p21 positive nuclei at 1 h after irradiation, where still all nuclei visualized PCNA foci (supplement 6.1 Fig. 71 D and E, respectively).

Incubation time	Cells with p21 foci	Cells with PCNA foci	Number of nuclei analyzed (*n*)
2 min	95%	100%	76
15 min	88%	100%	40
1 h	78%	100%	27
Mock-irradiated	0%	0%	40

Table 3 **Dectectable p21/PCNA foci after uranium ion irradiation in human fibroblasts.**

Both p21 and PCNA showed focal accumulations at the early times. Even if not all nuclei displayed p21 foci, approximately the half of them did after chromium ion irradiation and almost all after uranium ions irradiation. This shows that both proteins investigated are able to accumulate at the damaged DNA sites at a very early time-point after DNA damage induction by heavy ions. Furthermore, these results indicate a slightly slower recruitment of p21 at the HI-induced DNA lesions compared to the PCNA recruitment.

A possible role for p21 at DNA damaged sites following UV irradiation has been described discussing that p21 might loosen PCNA from the DNA damaged sites to help recycling the PCNA protein [Stivala *et al.*, 2001]. Because of these findings, I decided to investigate the vanishing of the p21 and PCNA accumulations at the heavy ion induced DNA lesions after irradiation with nickel ions, in spite of the known problem of protein detection after the extraction of the soluble proteins as described above (Sect. 2.2, page 31). For this, human fibroblasts were irradiated with Ni ions followed by fixation and extraction according to the GSI-modified Streck method. Because hardly any foci were detectable 7 h after irradiation with chromium ions, and nickel has a very similar LET, I decided to take samples with an incubation time below 7 h after irradiation.

Human fibroblasts irradiated with Ni ions and fixed 30 min, 1, 2, 3 or 5 h post-irradiation showed accumulations of p21 as well as PCNA (supplement 6.1 Fig. 72 B–F). Analysis showed, as summarized in Table 4 below, that within this chosen time frame, a maximum of cells showing p21 foci occurred 3 h post-irradiation (75%). However, 5 hours after irradiation, still many nuclei showed visible p21 foci (60%), with less nuclei displaying PCNA foci (40%). It must be noted that 5 h after irradiation the p21 level was quite high compared to the earlier taken time-points due to an induction of the p21 protein level and PCNA was hardly visible, making me analyze only 10 nuclei for a preliminary result.

Incubation time	Cells with p21 foci	Cells with PCNA foci	Number of nuclei analyzed (*n*)
30 min	63%	95%	41
1 h	31%	97%	29
2 h	66%	100%	29
3 h	75%	96%	28
5 h	60%	40%	10
Mock-irradiated	0%	0%	40

Table 4 **Analysis of the p21/PCNA dissolvement after nickel ion irradiation.**

Even if the analysis by further investigation may support the described role for p21 after UV irradiation to loosen PCNA from the DNA lesion, the method used here seemed too limited to clarify the accumulation and resolution of p21 and PCNA and I did not expand these experiments. Live analysis of tagged proteins would be needed to clarify the exact kinetics.

2.2.2 Transient expression of mutant forms of p21 in mammalian cells

The results presented above (Sect. 2.1) demonstrate that p21 and PCNA colocalize after heavy ion irradiation. Furthermore, both proteins appear to form foci similarly fast after exposure to heavy ions. This made me investigate whether the p21 foci formation after HI irradiation is affected by p21's direct interaction with PCNA.

It has been shown by Rossig *et al.* [2001] that the binding of p21 to PCNA is regulated by specific phosphorylation of the threonine 145 residue of p21 by the protein kinase Akt (Fig. 21). If this residue (Thr145) is phosphorylated, p21 can no longer interact with PCNA. I investigated whether ectopically expressed phospho-mimetic p21T145D abrogates p21 foci formation after HI irradiation. Prof. Dr. Dimmeler of the University of Frankfurt kindly provided three different expression plasmids for full-length human p21. The first plasmid carries the wild-type p21 (wtp21) open reading frame (ORF). Both of the other plasmids express p21 with a single-site mutation each at Thr145 to either abrogate p21's interaction with PCNA (p21T145D, phospho-mimetic) or to not inhibit p21's interaction with PCNA (non-phosphorylatable, p21T145A). All cDNAs were expressed from a CMV promoter as $(his)_6$- and c-myc-tagged C-terminal fusions (pcDNA3.1; Rossig *et al.*, 2001).

Fig. 21 **Cartoon to demonstrate the interaction sites of p21 with PCNA and cyclin-CDK complexes.** Arrow: Threonine[145], Akt phosphorylation site, which is replaced by aspartic acid (D) or alanine (A). Mutant p21T145D is not able to bind PCNA.

The three different plasmids were transfected individually into HCT116p21$^{-/-}$ cells or HeLa cells. HCT116p21$^{-/-}$ cells lack endogenous p21 due to targeted integrations at both p21 alleles [Waldman *et al.*, 1995] and HeLa cells express extremely low levels of their endogenous p21 protein because of their instable TP53. Endogenous p21 in HeLa cells could not be detected by Western Blot analysis or by immunofluorescence (IF) (Fig. 23 and Sect. 2.2.5 Fig. 29,

respectively). Thus, if a p21 signal is detected with a p21 specific antibody in these two cell lines, transfected with one of the p21 expression plasmids, it will be the ectopically expressed p21 protein.

To test whether a normal cell system gives the same results with the ectopically expressed p21 plasmids, I anticipated to transfect human fibroblasts, which I mainly use for other experiments in this thesis, as well. However, human fibroblasts are difficult to transfect, probably because of their extracellular matrix. Neither with Lipofectamine, nor with FuGene a positive signal for ectopic p21 could be detected by IF (data not shown). Only when a nucleofector (Amaxa, Köln, Germany) was used, transfection was possible, but the transfection efficiency for the human fibroblasts was below 10% (data not shown). For this reason, experiments with the p21 expression plasmids in human fibroblasts were carried out solely to check whether the ectopically expressed p21 protein retains its wild-type functions that are relevant to this thesis.

Ectopic expression and with this the successfully transfection of the plasmids was verified by Western Blot analysis (Sect. 4.9). Fig. 22 shows an example of the WB analysis of transfected HCT116p21$^{-/-}$ cells with the wtp21 or p21T145D plasmid by FuGene (Sect. 4.10.6). Twenty-four hours after transfection of the HCT116p21$^{-/-}$ cells Laemmli lysates were made as described in Sect. 4.7.1. The lysates were analysed by Western Blot analysis for p21 and α-tubulin (see Sect. 4.9). Tubulin detection verifies equal loading and transfer of the cell lysates across the gel (Fig. 22 upper bands in lane 2–5; not shown in further displayed WB). The non-transfected HCT116p21$^{-/-}$ cells do not express p21 as expected (Fig. 22 lane 2). Lanes 3 and 4 display the HCT116p21$^{-/-}$ cells transfected with wtp21 or p21T145D, respectively. Clear bands are seen for these two transfected cell lysates using an antibody to detect p21. Additionally, HCT116p21$^{+/+}$ cell lysate was loaded onto the SDS-PAGE, as a control for the WB analysis and to check the endogenous p21 expression of these cells (Fig. 22 lane 5). It is seen, that the endogenous p21 expression level is only a fraction of the amount of the exogenous p21 expression levels. Furthermore, the ectopically expressed p21 runs at a higher molecular weight because of its C-terminal tags (approximately 25 kDa versus 21 kDa).

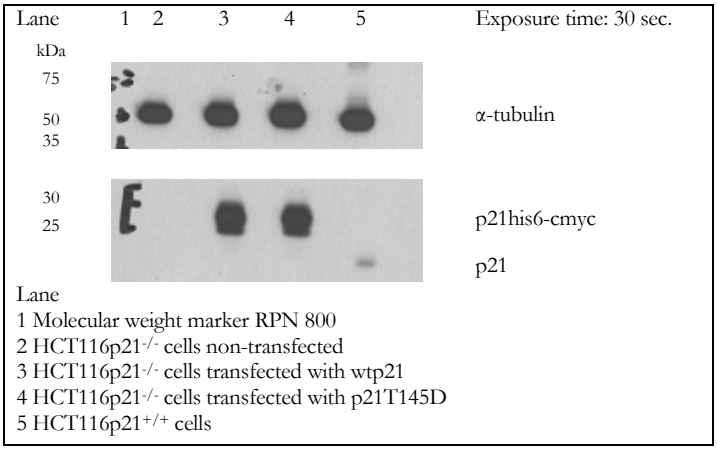

Fig. 22 **Representative example of the Western Blot analysis of the expression levels of transiently expressed wtp21 and p21T145D in HCT116p21$^{-/-}$ cells (lanes 3 and 4).** Lane 1: Molecular weight marker RPN 800. Lane 2: non-transfected HCT116p21$^{-/-}$ cells. Lane 5: non-transfected HCT116p21$^{+/+}$ cells. WB: α-tubulin and p21.

The Western Blot analysis in Fig. 23 displays the expression of the ectopically expressed p21 protein in HeLa cells. HeLa cells were transfected with the wtp21, p21T145A or p21T145D plasmid with Lipofectamine as described in Sect. 4.10.6. Twenty-four hours after transfection, protein lysates were prepared according to Laemmli (Sect. 4.7.1) and Western Blot analysis was done (Sect. 4.9). HeLa cells transfected with the p21T145A, p21T145D or wtp21 plasmid show a very high level of p21 (Fig. 23 lane 1, 2 and 4). At this exposure time (1 min), the p21 signal of the AG cells, used as a control for the Western Blot analysis and to show the position of endogenously expressed p21 protein, is not visible (Fig. 23 lane 6). After 5 min of exposure, the endogenous p21 of the AG cells was detected (Fig. 23 lane 6). Transfected HeLa cells show several bands in the Western Blot analysis, the main band running higher than the p21 band of the AG cells, because of the additional tag. The other detectable bands after the longer exposure time (5 min) are caused by degradation fractions and complexation with other proteins of the ectopically expressed p21 that are not fully denatured due to the very high expression level. Non-transfected HeLa cells do not express any detectable p21 (Fig. 23 lane 5). This verified the transfection and expression of the p21 expression plasmids in HeLa cells and showed that all three plasmids were expressed at very similar levels, meaning that the site-directed mutagenesis of T145 in p21 does not affect the protein expression level in HeLa cells (lanes 1, 2 and 4).

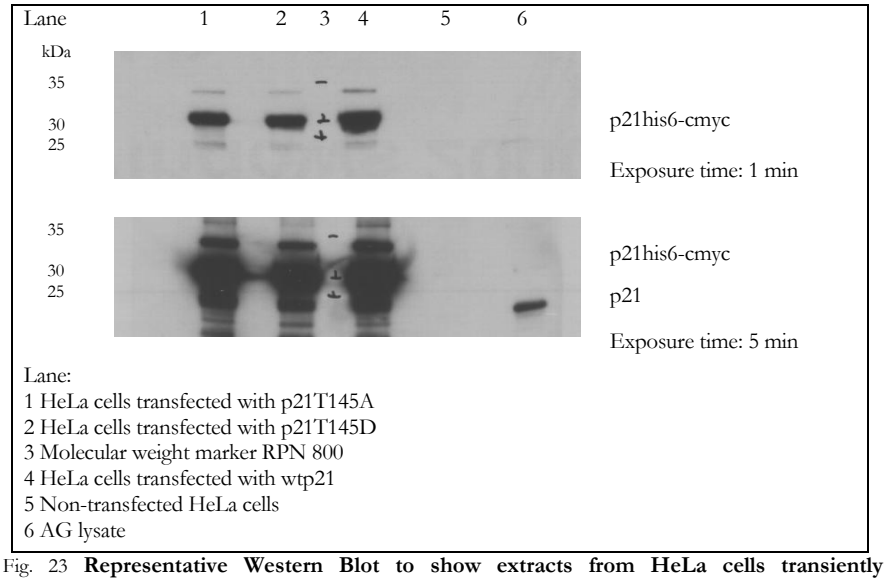

Fig. 23 **Representative Western Blot to show extracts from HeLa cells transiently transfected with three different plasmids to express p21T145A (lane 1), p21T145D (lane 2) or wtp21 (lane 4).** All plasmids show similarly high expression levels for p21. Lane 5: non-transfected HeLa cells. Lane 6: non-transfected human fibroblasts (AG1522C). WB: p21.

These results confirmed the successful transfection of plasmids and the ectopical expression of recombinant p21 in HCT116p21$^{-/-}$ cells and HeLa cells. Furthermore, ectopically expressed wild-type and mutant forms of p21 could be monitored by the same anti-p21 antibody (Cip1/Waf1 from Transduction Laboratories).

2.2.3 Recombinant wild-type p21 and p21T145A retain the interaction with both CDK and PCNA

After establishing a method to detect a p21/PCNA complex by specific p21 pulldown from cells expressing p21 compared to no immunoprecipitated complex from Hela cells as described in Sect. 2.8, the effect of three different ectopically expressed p21 constructs was studied. The expressed protein from the p21T145A plasmid is a p21 plasmid with a point-mutation at Thr145 to Ala145 which makes it non-phosphorylatable [Rossig *et al.*, 2001] and with this able to interact continuously with PCNA (see schematic Sect. 2.2.2, Fig. 21). Herewith, immunoprecipitation of ectopically expressed p21T145A from HeLa cells should result in co-precipitation of endogenous PCNA. To investigate this, HeLa cells were transfected with the wtp21 or p21T145A plasmid by the use of Lipofectamine (Sect. 4.10.6). Cell lysates were prepared 24 h after transfection according to Sect. 4.8.1, followed by anti-p21 immunoprecipitation as described in Sect. 4.8. To verify the immunocomplex of the ectopically expressed p21, immunoprecipitations were done both with an anti-p21 antibody and with an anti-myc antibody. The immunoprecipitated complex was separated by SDS-PAGE and detected for p21 and PCNA by Western Blot analysis (Sect. 4.9).

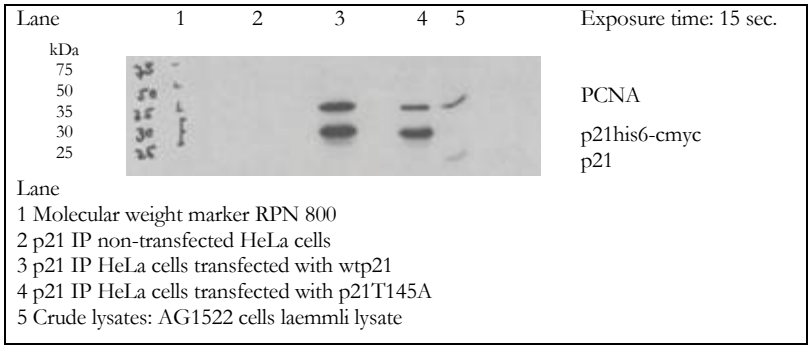

Fig. 24 **Western Blot analysis of anti-p21 immunoprecipitates from HeLa cell lysates.** The ectopically expressed wtp21 and p21T145A co-immunoprecipitate PCNA. WB: PCNA and p21.

The WB analysis displayed above shows that no p21 complex is immunoprecipitated from the non-transfected HeLa cells (Fig. 24 lane 2). The anti-p21 complex obtained from the HeLa cells transfected with the wtp21 plasmid, shows clear p21 and PCNA signals in this WB analysis (Fig. 24 lane 3). Importantly, the anti-p21 complex from the HeLa cells transfected with the p21T145A plasmid also contains PCNA (Fig. 24 lane 4). Lane 5 gives the signals for endogenous p21 and PCNA in crude lysates from AG cells, verifying the Western Blot analysis. Hela crude cell lysate is not loaded, as they were shown to have a non-detectable p21 level (Sect. 2.2.2, Fig. 23).

The WB analysis of the immunoprecipitated complex with the myc antibody resulted in a p21 and PCNA signal for the HeLa cells transfected with either wtp21 or p21T145A as shown in Fig. 25 (lanes 3 and 4, respectively). Anti-myc immunoprecipitation from non-transfected HeLa cells results in a slight background signal after PCNA detection, but does not show a clear p21 or PCNA band (Fig. 25 lane 2). This signal is not observed after p21 immunodetection as seen in the former Fig. 24. Crude lysate from AG cells displays a weak PCNA signal, but no p21 due to the small amount of total protein loaded where p21 is only a minor fraction because of the confluent grown cells (G_1-phase of the cell cycle) and the short exposure time (Fig. 25 lane 5). This verifies that the former immunoprecipitated p21 complex indeed is a result of specific immunoprecipitation of the ectopically expressed p21 as after the myc-pulldown the same result is obtained.

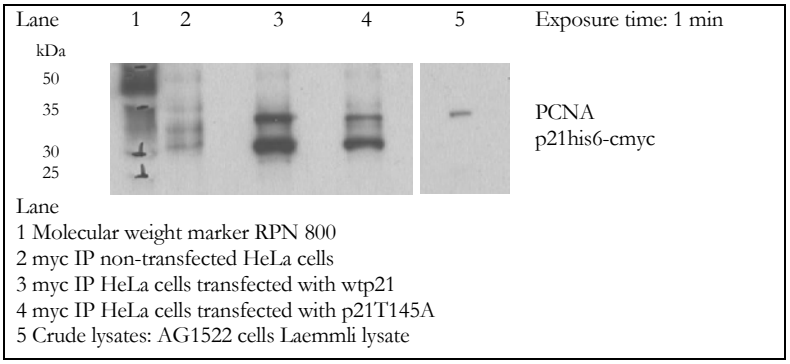

Fig. 25 **The anti-myc complex shows both precipitated exogenous p21 and co-precipitated PCNA in HeLa cells transfected with either the wtp21 or p21T145A plasmids.** WB: PCNA and p21.

The point-mutation at Thr145 should only affect the interaction of the expressed protein with PCNA, functional interactions with other proteins such as CDK2 which binding site is in the aa. 53–58 region should be retained (see Fig. 21). To investigate whether the ectopically expressed p21 protein retains its ability to complex with CDK2, the Western Blot was probed for the presence of CDK2 as shown below in Fig. 26.

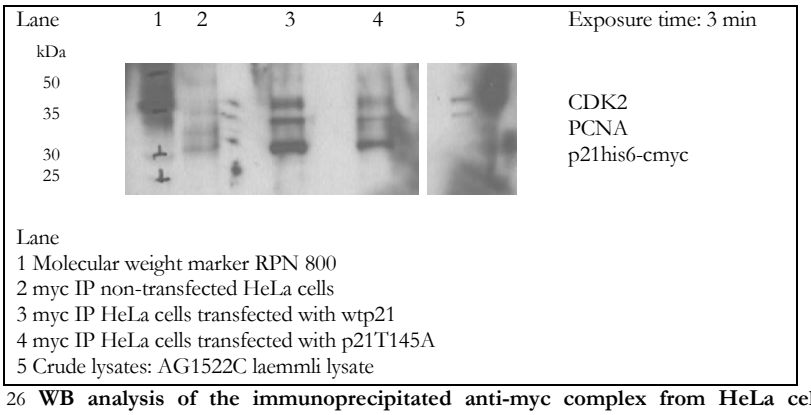

Fig. 26 **WB analysis of the immunoprecipitated anti-myc complex from HeLa cells transfected with the wtp21 or p21T145A plasmids results in a detectable CDK2 signal.** WB: CDK2, PCNA and p21.

As seen above, the wtp21 transfected HeLa cells show a detectable CDK2 signal on the Western Blot (Fig. 26 lane 3). A weak CDK2 signal is also obtained for the HeLa cells transfected with p21T145A which is in line with the weaker p21 signal obtained (Fig. 26 lane 4). The non-transfected HeLa cells have no detectable CDK2 signal (Fig. 26 lane 2). The additional loaded crude lysate from AG cells show a weak CDK2 band (Fig. 26 lane 5).

My results show that ectopically expressed wtp21 and p21T145A are able to form a complex with both PCNA and CDK2 in HeLa cells.

2.2.4 Recombinant p21T145D no longer interacts with PCNA

The p21T145D plasmid encodes a mutant p21 protein in which Thr145 was substituted by Asp, a phospho-mimetic residue. The protein expressed from this plasmid should not be able to interact with PCNA as described in Sect. 2.2.2 (page 35). To verify the lack of interaction, HeLa cells were transfected with the p21T145D plasmid as described in Sect. 4.10.6. Native cell lysates were prepared 24 h after transfection followed by specific anti-p21 or anti-myc pulldowns (Sect. 4.8). Western Blot analysis was done to analyze components of the p21T145D complex (Sect. 4.9).

In Western Blot analysis, precipitated p21 is visible in HeLa cells transfected with wtp21 or with p21T145D (Fig. 28 lanes 3 and 4, respectively). Non-transfected HeLa cells do not show any detectable p21 signal after anti-p21 immunodetection and Western Blot analysis (Fig. 28 lane 2). In crude lysates from AG cells weak p21 signal migrating slightly below the recombinant tagged version of p21 is detected (Fig. 28 lane 5). When the same Western Blot was probed to an anti-

PCNA antibody, a clear signal for HeLa cells expressing ectopic wtp21 and for crude lysates from AG cells is detected (Fig. 28 lanes 3 and 5, respectively), but no PCNA is detected in anti-p21 immunoprecipitations from non-transfected HeLa cells or from HeLa cells expressing p21T145D (Fig. 28 lanes 2 and 4 respectively). These results confirm the inability of p21T145D to bind to PCNA, similarly to what has been observed in umbilical cord cells [Rossig *et al.*, 2001].

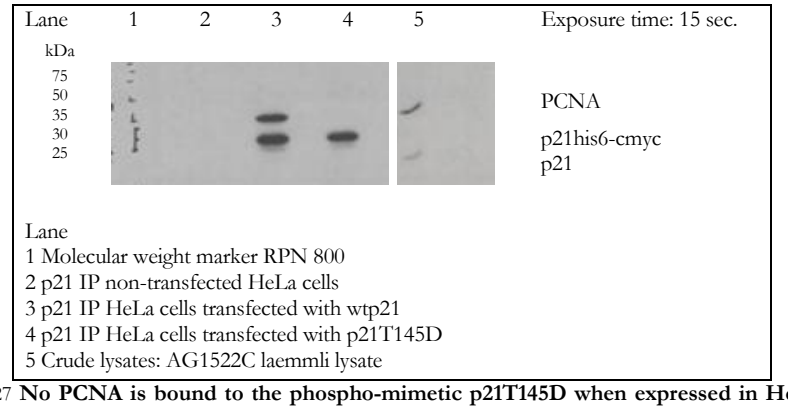

Fig. 27 **No PCNA is bound to the phospho-mimetic p21T145D when expressed in HeLa cells.** Western Blot analysis of the anti-p21 complexes from the HeLa cells. HeLa cells transfected with the wtp21 plasmid give a clear PCNA and p21 band (lane 3). HeLa cells transfected to express p21T145D do not show PCNA in anti-p21 complexes (lane 4). Negative control: non-transfected HeLa cells (lane 2). Lane 5: crude cell lysates from AG cells. WB: PCNA and p21.

Immunoprecipitations utilizing the anti-myc antibody were also carried out in order to only precipitate the tagged version of p21. The WB analysis for these immunoprecipitations is shown in Fig. 29. A weak non-specific signal is detected in the anti-myc complexes from non-transfected HeLa cells, as well as in HeLa cells transfected with the p21T145D plasmid after PCNA immunodetection of the WB (supplement 6.2 Fig. 73 lane 2 and lane 4, respectively). However, a specific band for PCNA, as in lane 3 containing the anti-myc protein complex of HeLa cells expressing recombinant wtp21 is not detected.

The same Western Blot was probed for anti-CDK2 to test whether p21T145D retains the ability to bind CDK2. As the p21T145D carries a single residue change within the PCNA binding site, the interaction of p21T145D with CDK2 should not be affected if the mutant form folds correctly (see Fig. 21). The WB analysis in Fig. 29 displays the result after CDK2 detection together with PCNA and p21. Crude lysates from AG cells show a signal for CDK2 and PCNA, p21 however is not visible (Fig. 28 lane 1). The anti-myc IP from the non-transfected cells shows background signal that results from the previous detected PCNA signal (supplement 6.2 Fig. 73) but no CDK2 or p21 signal (Fig. 28 lane 2). Clear CDK2 and p21 bands, as well as the formerly detected PCNA band, are seen in precipitates from HeLa cells expressing ectopic wtp21 (Fig. 28 lane 3). The HeLa cells expressing p21T145D also display a CDK2 and p21 band, without any detectable PCNA signal (Fig. 28 lane 4). This means, that the expressed p21T145D protein indeed is able to form a complex with other proteins such as CDK2 and is

likely to fold in wild-type conformation. However, its interaction specifically with PCNA is abrogated due to the amino acid substitution at Thr145.

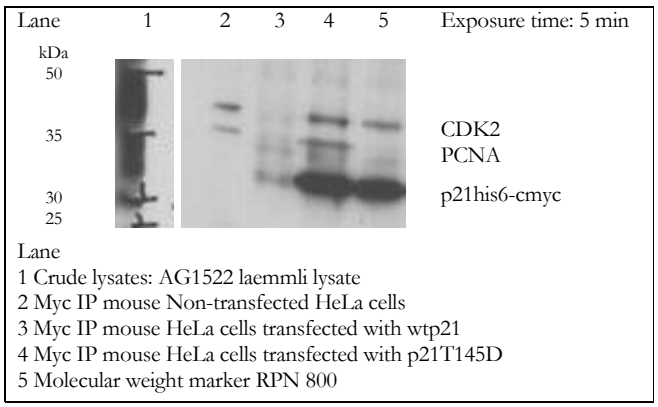

Fig. 28 **CDK2 is co-immunoprecipitated in anti-myc pulldowns from HeLa cells expressing p21T145D.** Western Blot analysis to show the components of the p21 complex in HeLa cells, either non-transfected (lane 2), transfected with the wtp21 plasmid (lane 3) or with the p21T145D plasmid (lane 4). WB: PCNA, CDK2 and p21. WB: CDK2, PCNA and p21.

Sequence analysis of the p21T145D plasmid was carried out and the single amino acid change from Thr to Asp at Thr145 was confirmed (see Sect. 4.10.5.4 page 122).

2.2.5 The non-phosphorylatable p21T145A accumulates at the sites of particle traversal

The non-phosphorylatable p21T145A protein was shown to interact with PCNA by immunoprecipitation experiments (Sect. 2.2.3, page 38). Whether the ectopically expressed p21T145A protein also is able to form HI-induced foci was investigated after irradiation with nickel and zinc ions. HeLa cells were transfected with the p21T145A or with the wtp21 plasmid as described in Sect. 4.10.6.2 (page 123). The cells were irradiated and fixed 30 min after irradiation without extraction of the soluble proteins to be able to detect the transfected cells (Sect. 4.4.1). Fig. 29 displays HeLa cells after immunostaining for p21 (green) in combination with 53BP1 (red) to visualise the sites of damaged DNA. Mock-irradiated cells show expression of p21 as seen by the green fluorescence throughout the nucleus, but no focal accumulations, as expected (Fig. 29 A and D). The 53BP1 protein accumulates to single foci in many of the mock-irradiated cells as it has been observed in previous experiments (Sect. 2.1.1, page 23). p21T145A accumulates to foci in the irradiated nuclei 30 min after exposure to Ni ions, as does 53BP1 (Fig. 29 B and C) and ectopically expressed wtp21 (Fig. 29 E and F). The experiments were repeated with both zinc and gold ion irradiations, leading to the same results (data not shown).

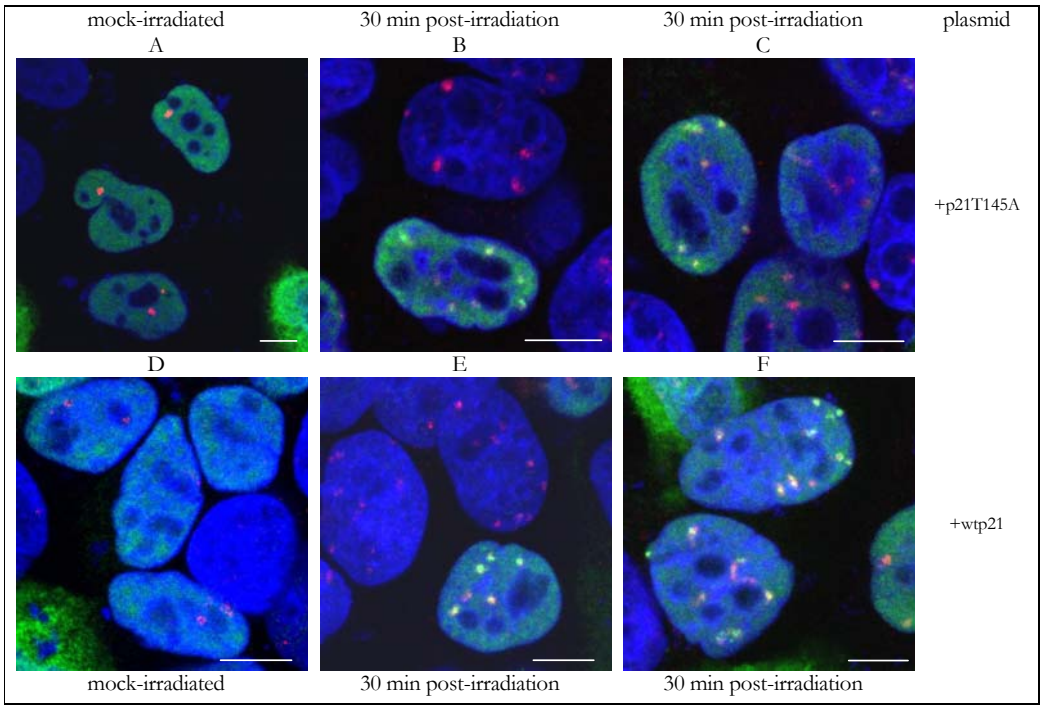

Fig. 29 **Ectopically expressed p21T145A and wtp21 accumulate at HI-induced DNA lesions.** HeLa cells transfected with the p21T145A (A–C) or wtp21 (D–F) plasmid. A and D: mock-irradiated cells. B, C, E and D: 30 min post-irradiation with Ni ions (2×10^6 p/cm^2; 11.4 MeV/u; 3790 keV/µm); Immunostained for p21 (green) and 53BP1 (red), DNA counterstained by ToPro-3 (blue). Mock-irradiated cells show single 53BP1 foci. Bar: 10 µm.

To make sure that only the ectopically expressed p21 proteins and not endogenous p21 is detected, HeLa cells transfected with wtp21 or p21T145A were immunostained for the myc-tag of the ectopically expressed protein. As seen in Fig. 30 focal structures of the myc-tagged p21 forms and of 53BP1 are visible 30 min after irradiation with zinc ions (3×10^6 p/cm^2; 11.4 MeV/u; 4120 keV/µm; panels B, C, E and F). Mock-irradiated cells show expression of the ectopically expressed p21 in some of the nuclei, but no p21 accumulations (green fluorescence signal in panels A and D).

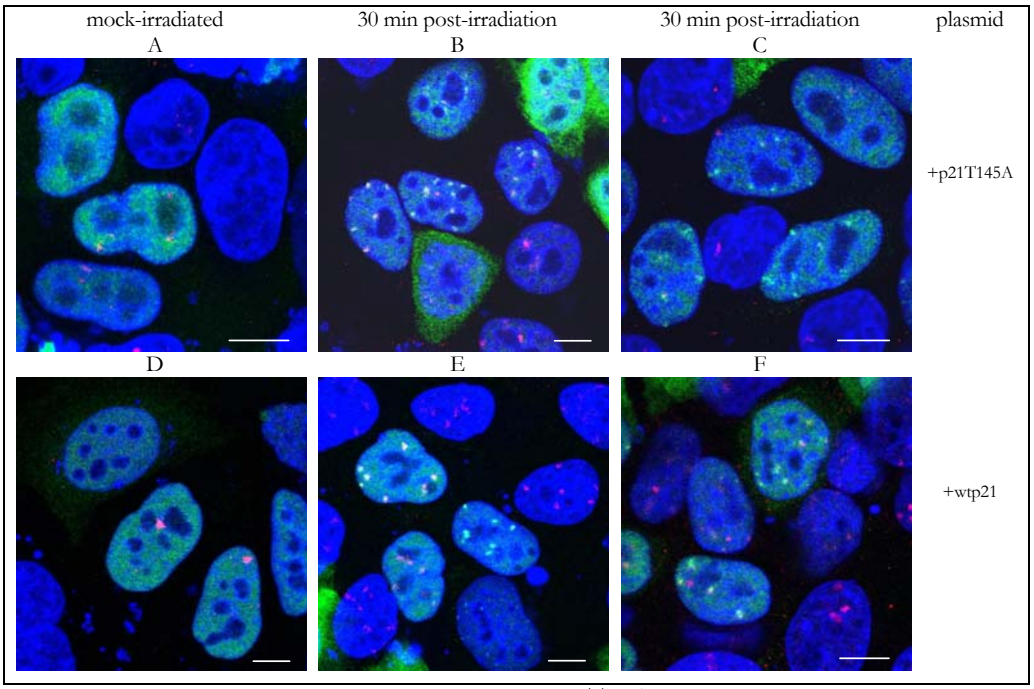

Fig. 30 **Ectopically expressed wtp21 and p21T145A is detectable by anti-myc immunostaining.** HeLa cells transfected with p21T145A, irradiated with Zn ions (3×10^6 p/cm^2; 11.4 MeV/u; 4120 keV/µm) and fixed 30 min post-irradiation. Clear irradiation-induced protein accumulations of the myc-tagged versions of p21 are detectable after irradiation (B and C). A: mock-irradiated cells. Anti-myc antibody (green) and 53BP1 (red). DNA counterstained with ToPro-3 (blue). Note: some cells express the p21 cytoplasmatically (B). Bar: 10 µm.

Following detection of the myc tag by immunostaining, HeLa cells transfected with the wtp21 plasmid show the same results as obtained for the HeLa cells transfected with the p21T1145A plasmid (Fig. 30, lower panels). In sum, these results demonstrate that the amino acid exchange from Thr to Ala at residue 145 does not affect the ability of p21 to accumulate at the HI-induced damaged DNA sites. The same experimental results were gained after exposure to gold ions (data not shown).

To exclude false-positive results non-transfected HeLa cells irradiated with zinc ions (3×10^6 p/cm^2; 11.4 MeV/u; 4120 keV/µm) were immunostained for p21 in combination with 53BP1 (Sect. 4.4.4). Fig. 31 displays the non-transfected HeLa cells which were fixed without extraction of the soluble proteins 30 min after irradiation. No signal is detected for p21 in these cells, neither in the mock-irradiated, nor in the irradiated samples (Fig. 31) and in line with the results presented by Western Blot analysis (Sect. 2.2.2, Fig. 23). For 53BP1 however, irradiation-induced protein accumulations are obtained, as expected (Fig. 31 C).

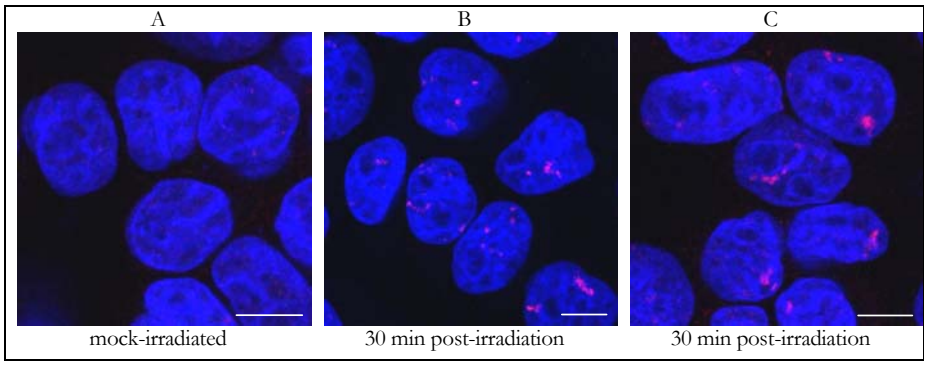

Fig. 31 **In non-transfected HeLa cells p21 cannot be detected by immunofluorescence.** Non-transfected HeLa cells irradiated with Zn ions (3×10^6 p/cm^2; 11.4 MeV/u; 4120 keV/µm; B and C) and fixed 30 min post-irradiation. A: mock-irradiated cells. p21 (green) and 53BP1 (red); ToPro-3 counterstained DNA: blue. Bar: 10 µm.

The response of ectopically expressed wtp21 was also investigated in a p21-null cell line (HCT116p21$^{-/-}$) which, in contrast to HeLa cells, should not express any endogenous p21 at all. The HCT116p21$^{-/-}$ cells were transfected to express wtp21 (Sect. 4.10.6) and fixed 30 min after irradiation with gold (3×10^6 p/cm^2; 11.4 MeV/u; 13030 keV/µm) or uranium ions (3×10^6 p/cm^2; 11.4 MeV/u; 14925 keV/µm) without extraction of the soluble proteins (Sect. 4.4.1). Immunostaining was done for p21 or myc in combination with γH2AX or 53BP1 (Sect. 4.4.4). The HCT116p21$^{-/-}$ cells, as shown in Fig. 32, display detectable accumulations of the ectopically expressed wtp21 protein in response to HI irradiation (panels B, C, E, F, H and I).

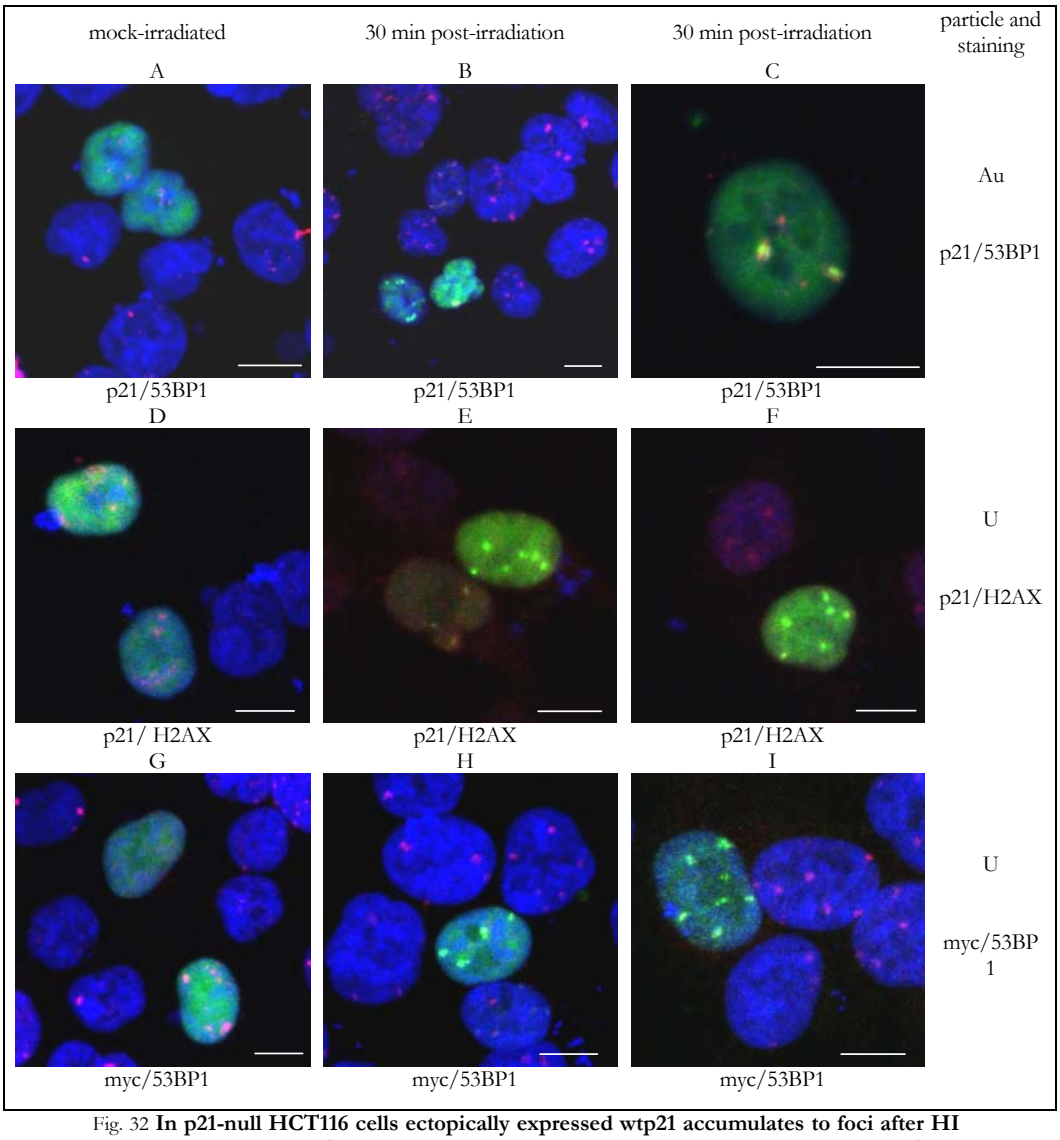

Fig. 32 **In p21-null HCT116 cells ectopically expressed wtp21 accumulates to foci after HI irradiation.** HCT116p21$^{-/-}$ cells were fixed and stained after irradiation with gold (3×10^6 p/cm^2; 11.4 MeV/u; 13030 keV/µm; B and C) or uranium ions (3×10^6 p/cm^2; 11.4 MeV/u; 14925 keV/µm; E, F, H and I). A, D and G: mock-irradiated cells. DNA: blue (ToPro-3). Bar: 10 µm.

To verify that the behaviour of the ectopically expressed protein is comparable with the endogenous p21, cells from the wtp21 sister cell line, HCT116p21$^{+/+}$ cells were immunostained for p21, γH2AX, 53BP1 or XRCC1 after irradiation with gold ions (3×10^6 p/cm^2; 11.4 MeV/u; 13030 keV/µm)). As seen in Fig. 33 (panel D and E) the HCT116p21$^{+/+}$ cells show similar HI-induced protein accumulations as do the HCT116p21$^{-/-}$ cells for ectopically expressed wtp21

and endogenously expressed γH2AX, 53BP1 and XRCC1 (Fig. 32). The anti-myc staining in HCT116p21$^{+/+}$ cells however, did not give any signal, as expected (Fig. 33 F).

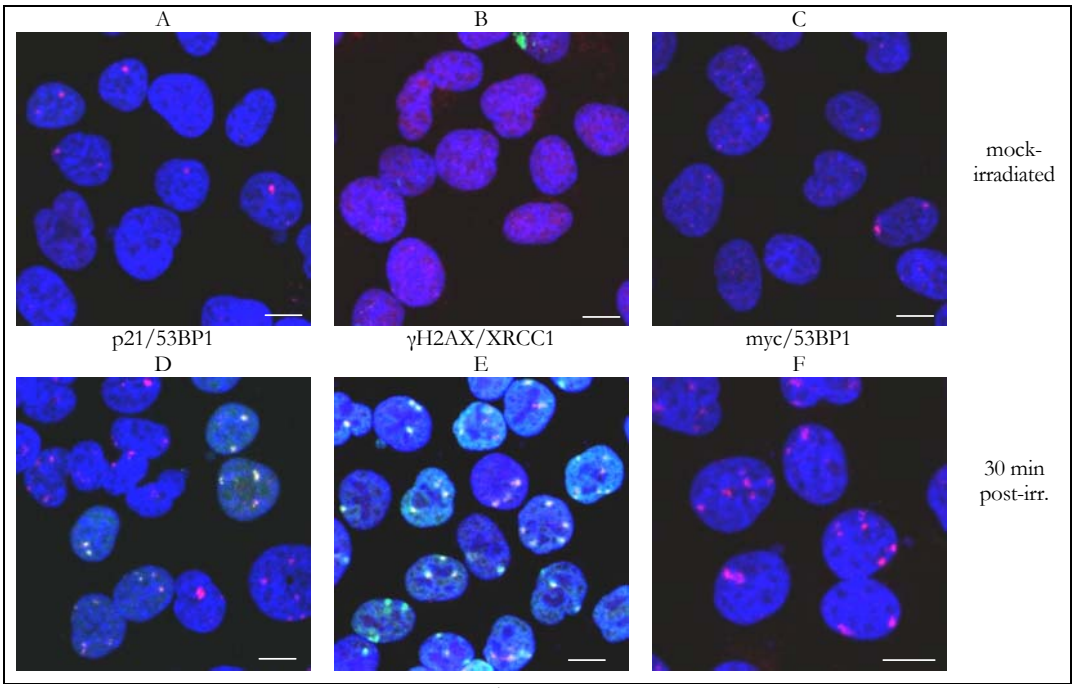

Fig. 33 **Endogenous p21 in HCT116p21$^{+/+}$ cells shows the similar focal accumulations as the ectopically expressed wtp21 in HCT116p21$^{-/-}$ cells (as seen in** Fig. 32**).** HCT116p21$^{+/+}$ cells irradiated with gold ions (3×10^6 p/cm^2; 11.4 MeV/u; 13030 keV/µm) and immunostained for p21, γH2AX, myc, 53BP1 or XRCC1. A–C mock-irradiated cells; D–F: 30 min post-irradiation. green: p21, γH2AX or myc. red: 53BP1 or XRCC1. DNA: blue (ToPro-3). Bar: 10 µm.

These results show that ectopically expressed wtp21 and p21T145A in HeLa cells and HCT116p21$^{-/-}$ cells act very similar to the endogenously expressed p21 in HCT116p21$^{+/+}$ cells and that the tagged versions of p21 are able to form HI-induced focal accumulations at the damaged DNA sites independently of endogenous p21.

2.2.6 The phospho-mimetic p21T145D does not accumulate at the sites of particle traversal

The previous section showed that ectopically expressed p21 protein, which is able to interact with PCNA forms foci at the HI-induced DNA lesions. If the accumulation of p21 at damaged

DNA sites is independent of its direct interaction with PCNA, the p21T145D protein should also be able to form irradiation-induced foci. The experiments described below elucidate the dependency of p21 on PCNA.

HeLa cells transfected 24 hours before irradiation to express p21T145D as described in Sect. 4.10.6 were irradiated with gold ions (2×10^6 p/cm^2; 11.4 MeV/u; 13030 keV/µm) and fixed without extraction 30 min after irradiation (Sect. 2.4.1). Following fixation, the cells were immunostained for p21 and 53BP1 with counterstaining of the DNA by ToPro-3 (Sect. 4.4.4).

Fig. 34 shows the successful expression of p21T145D in HeLa cells by immunostaining (green fluorescence). Mock-irradiated cells (Fig. 34 A and C) give a detectable p21 or myc signal dispersed throughout the nucleus. 53BP1 displays detectable foci in some of these non-irradiated nuclei. After DNA damage induction by irradiation with gold ions, still no accumulations of p21T145D were detected either by using the anti-p21 or the anti-myc antibody (Fig. 34 B and D). An elevated amount of visible 53BP1 foci verifies the induction of DNA damage by the gold ion irradiation. The same results were obtained after irradiation with Ni and Zn ions (data not shown).

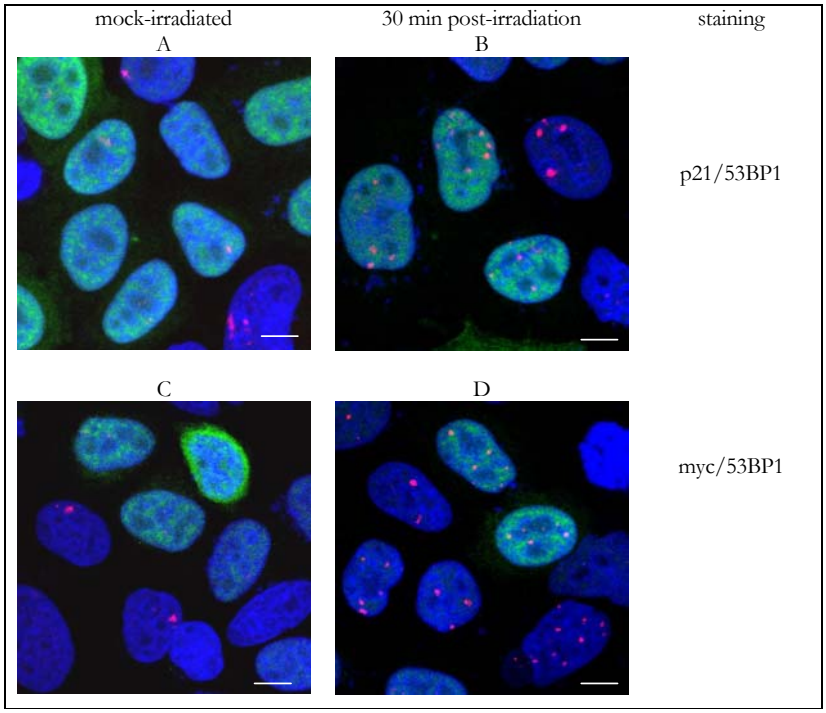

Fig. 34 **The phospho-mimetic p21T145D protein does not accumulate to foci at the HI-induced DNA lesions.** HeLa cells transfected with the plasmid p21T145D, fixed and immunostained for the indicated proteins after irradiation with gold ions (2×10^6 p/cm^2; 11.4 MeV/u; 13030 keV/µm)). A and C: mock-irradiated cells; B and D: 30 min post irradiation. DNA: blue (ToPro-3). Bar: 10 µm.

Additionally, HCT116p21$^{-/-}$ cells were transfected with the p21T145D plasmid and irradiated with gold (3×10^6 p/cm^2; 11.4 MeV/u; 13030 keV/µm)) or uranium ions (3×10^6 p/cm^2; 11.4 MeV/u; 14925 keV/µm). The immunostaining of p21 or myc and 53BP1 or γH2AX resulted in the same observations as described for the HeLa cells above. Also in this cell system, the phospho-mimetic p21T145D is not able to form foci at the HI-induced DNA lesions as seen in Fig. 35 below.

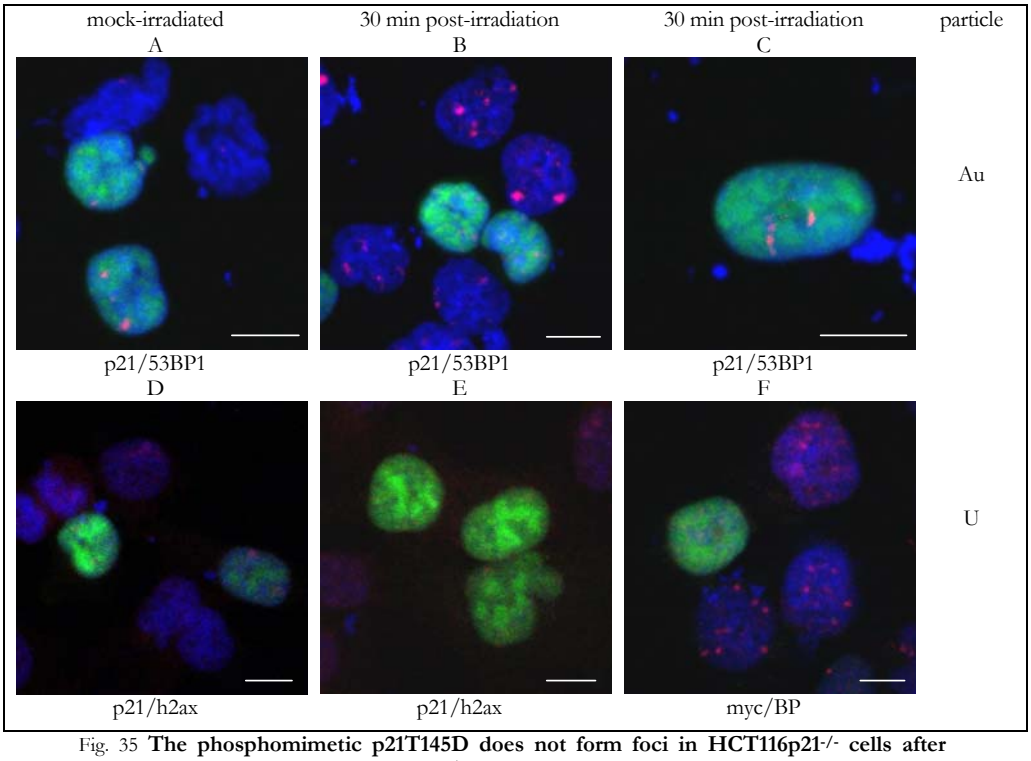

Fig. 35 **The phosphomimetic p21T145D does not form foci in HCT116p21$^{-/-}$ cells after exposure to heavy ions.** HCT116p21$^{-/-}$ cells transfected with the p21T145D plasmid and stained for p21 or myc (green) and 53BP1 or γH2AX (red). B and C: nuclei irradiated with gold ions; E and F: nuclei irradiated with uranium ions; A and D mock irradiated. DNA: blue (ToPro-3). Bar: 10 µm.

With these experiments, I have shown that the accumulation of p21 at HI-induced DNA lesions is affected by its direct interaction with PCNA. The protein p21T145D that is not able to bind to PCNA does not form HI-induced foci as illustrated above; suggesting that p21 only accumulates at the induced DNA damaged sites if it can interact with PCNA. Furthermore, this shows that p21 and PCNA interact at the induced DNA lesions. The association of this complex with the chromatin was investigated on biochemical level as described in the following section.

2.3 PCNA and p21 are part of the chromatin-bound protein fraction after DNA damage induction by X-ray irradiation

In the previous section, I have been able to show that the accumulation of p21 at heavy ion-induced DNA lesions is dependent on the interaction with PCNA. Here, I elucidate biochemically that the p21/PCNA complex associated with the induced DNA lesions after X-ray exposure is chromatin-associated.

The experiments described in Sect. 2.2 (page 31) were done with heavy ions to detect protein complexes at the induced DNA lesions by indirect immunostaining. To do so, single protein tracks throughout the irradiated nuclei were visualized along the damaged DNA sites induced by the heavy ion trajectories. The amount of accumulated protein to these distinct tracks is comparatively small and not expected to be detectable with the established protocols to assess the chromatin-associated protein fraction. Therefore, I decided to induce homogenously distributed DNA lesions by a high dose of X-ray irradiation, to gather as much DNA damage-induced chromatin-associated proteins as possible. To analyze chromatin-associated proteins, subcellular fractionation is carried out in which the soluble protein fraction is separated from the chromatin-bound protein fraction.

PCNA is mainly part of the soluble protein fraction, except during the S-phase of the cell cycle or during DNA repair. In confluent cultured cells the amount of chromatin-bound PCNA is very low, giving rise to the possibility to verify the efficiency of the subcellular fractionation method by comparing irradiated confluent cells with mock-irradiated confluent cells in their detectable chromatin-associated PCNA amounts. After establishing an appropriate method for subnuclear fractionation, immunodetection for p21 was carried out as well. For verification of an equal amount of total protein loaded actin was detected. Several methods were tested and modified until a reproducible result was achieved, as described below.

2.3.1 Establishment of a method to detect chromatin-bound PCNA

Subcellular fractionation studies according to a protocol of Balajee and Geard [2001] (see Sect. 4.7.3, page 105, for the exact protocol) led to high amounts of PCNA in the final pellet from both the mock-irradiated and the irradiated cells (data not shown). Using this method the pellet is discarded, as the supernatant is considered to contain the chromatin-bound protein fraction. In this approach, the protocol was modified according to Savio *et al.* [Savio *et al.*, 1996] where the chromatin-bound proteins are released by an additional incubation of the final pellet with DNase I. To assess the fraction of proteins possibly still remaining within the final pellet, the pellet was further incubated under denaturing conditions in Laemmli buffer (Sect. 4.7.1). However, even with the DNase I digest, a huge amount of PCNA was still detected in these Laemmli lysates obtained from the remaining pellet of mock-irradiated and irradiated cells (data not shown).

To minimize the amount of S-phase cells and exclude this as possible reason for the PCNA signal in the former experiment, AG cells were cultured for 3 days under serum starvation, a common used method to induce cellular quiescence. Three serum concentrations were used instead of the normally 20% v/v serum concentration in the culture medium, to see if a difference could be achieved: 0.2%, 0.4% and 10% v/v serum. The analysis was done by microscopically detecting the S-phase cells after immunostaining for PCNA (Sect. 4.4.4, page 100). This resulted in 2.7% (n = 113), 3.2% (n = 217) and 4.4% (n = 270) S-phase cells for 0.2%, 0.4% and 10% serum, respectively (data not shown). Additional flow cytrometric analysis was done for cells kept under 0.4% serum starvation, measuring 5% of all analyzed cells in S-phase (data not shown). I conclude that the low fraction of cells in S-phase should not interfere with the nuclear fractionation experiments. For this reason, another method described by Xu and Stern [2002] was tested.

According to Xu and Stern [2002] the subcellular fractions (e.g. cytosolic, nuclear and chromatin-bound protein fractions) are mainly separated by centrifugation after sequent lyses of the cell and nuclear membranes. The chromatin-bound protein fraction is then released by resuspension of the pellet, containing the chromatin-bound protein fraction in Laemmli buffer. With this method, hardly any chromatin-bound PCNA could be detected for the mock-irradiated or for irradiated G_1-phase cells at different times after irradiation (from 0.5 h up to 48 h after irradiation; data not shown).

A successful and reproducible subcellular fractionation procedure was finally achieved using the protocol from Stivala and Prosperi [2004]. Using this protocol, no PCNA signal for mock-irradiated AG cells and clearly detectable PCNA signals for AG cells at 3 h after irradiation with 8 Gy or 30 Gy X-rays were detected. A representative WB is shown in Fig. 36. The WB is probed for PCNA and β-actin. Detection of β-actin was used to asses the amount of total protein loaded (Fig. 36, upper bands). Lanes 2–3 and 12–14 display the soluble protein fractions. Here, a clear PCNA signal is observed for all samples: the mock-irradiated cells (lanes 2 and 12), the cells irradiated with 8 Gy (lanes 3 and 13) and the cells irradiated with 30 Gy X-rays (lanes 4 and 14). The chromatin-bound protein fractions are loaded in lanes 5–7. The mock-irradiated cells do not show a detectable level of chromatin-bound PCNA (lane 5). After X-ray irradiation though, a clear signal for the chromatin-bound PCNA is obtained for the cells irradiated with 8 Gy or 30 Gy X-rays (lanes 6 and 7, respectively). Interestingly, the detectable chromatin-bound PCNA fraction is higher for the cells irradiated with 30 Gy compared to the cells irradiated with 8 Gy (Fig. 36 lane 7 versus 6). Lanes 15–17 show the supernatant from the first wash of the pellet containing the nuclei with the chromatin-bound protein fraction. Lanes 18–20 display the supernatant from the second wash of the nuclei, before the chromatin-bound proteins are released from the DNA. It is seen, that after the first wash, still PCNA and actin are detectable on the WB (Fig. 36 lanes 15–17). In the supernatant obtained after the second wash however, no detectable PCNA and only a very weak signal for β-actin were observed (lanes 18–20). Taken together, I conclude that all the soluble proteins are removed using the wash and extraction procedure described above, leaving only the chromatin-bound protein fraction in the pellet. Chromatin-bound proteins can then be released from the DNA by digestion with DNase I (Fig. 36 lanes 5–7).

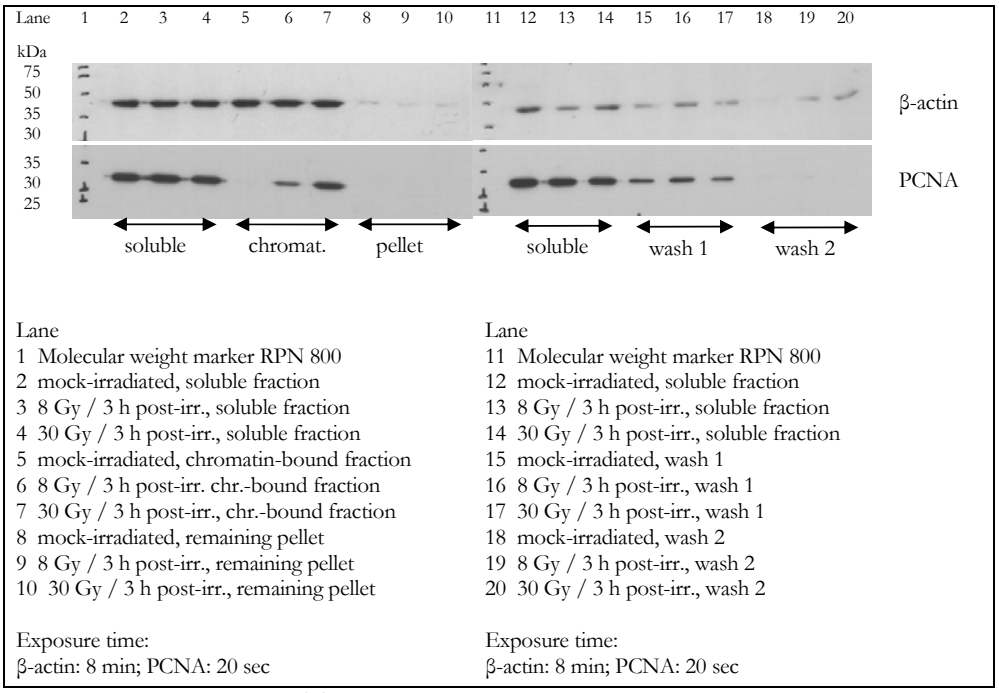

Lane	Lane
1 Molecular weight marker RPN 800	11 Molecular weight marker RPN 800
2 mock-irradiated, soluble fraction	12 mock-irradiated, soluble fraction
3 8 Gy / 3 h post-irr., soluble fraction	13 8 Gy / 3 h post-irr., soluble fraction
4 30 Gy / 3 h post-irr., soluble fraction	14 30 Gy / 3 h post-irr., soluble fraction
5 mock-irradiated, chromatin-bound fraction	15 mock-irradiated, wash 1
6 8 Gy / 3 h post-irr. chr.-bound fraction	16 8 Gy / 3 h post-irr., wash 1
7 30 Gy / 3 h post-irr., chr.-bound fraction	17 30 Gy / 3 h post-irr., wash 1
8 mock-irradiated, remaining pellet	18 mock-irradiated, wash 2
9 8 Gy / 3 h post-irr., remaining pellet	19 8 Gy / 3 h post-irr., wash 2
10 30 Gy / 3 h post-irr., remaining pellet	20 30 Gy / 3 h post-irr., wash 2
Exposure time:	Exposure time:
β-actin: 8 min; PCNA: 20 sec	β-actin: 8 min; PCNA: 20 sec

Fig. 36 **Mock-irradiated AG cells do not have a detectable amount of chromatin-bound PCNA.** Total protein loaded: soluble: 15 µg; wash 1: 10 µg; wash 2: 1.4 µg; chromatin-bound (chromat.): 5 µg; pellet: 2.5 µg. WB: β-actin and PCNA.

As with this method finally a clear irradiation-induced chromatin-bound fraction of PCNA was detected, the membrane was also probed for p21. Furthermore, as the sample irradiated with 30 Gy X-rays showed an elevated amount of chromatin-associated PCNA compared to the sample irradiated with 8 Gy X-rays cells were irradiated with 30 Gy X-rays in the following experiments.

2.3.2 The chromatin-bound p21 is degraded during subcellular fractionation

Human fibroblasts were irradiated with 30 Gy X-rays and subcellular fractionation according to the established protocol (Sect. 4.7.3) was carried out at 1 h or 3 h after exposure. A representative WB obtained after detection of PCNA and p21 is displayed in Fig. 37. The soluble protein fractions show clear signals for PCNA and p21 (Fig. 37 lanes 2–4 and 12–14). Also the first washes of all three samples contain detectable PCNA and p21 protein signals (Fig. 37 lanes 15–18). Wash 2 from the mock-irradiated and the irradiated sample at 1 h after

irradiation have hardly any visible protein-bands, the wash 2 from the cells incubated 3 h after irradiation gives a weak PCNA and a very weak p21 signal (Fig. 37 lane 20). The chromatin-bound fractions however, do not have a detectable p21 band at the normally expected position at 21 kDa, but instead show bands of lower molecular weight (i.e. ~ 15 kDa; Fig. 37 lanes 5–7). As this signal is detected by the specific p21 antibody and a slight increase is seen with incubation time after irradiation, I assume that it is degraded p21 protein. The remaining pellets do not show any signal for PCNA or p21 after WB analysis (Fig. 37 lanes 8–10).

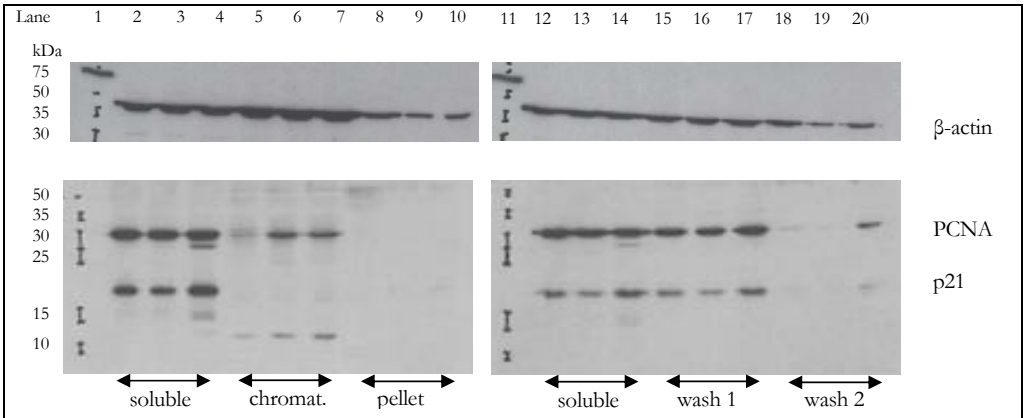

Lane	Lane
1 Molecular weight marker RPN 800	11 Molecular weight marker RPN 800
2 mock-irradiated, soluble fraction	12 mock-irradiated, soluble fraction
3 30 Gy X-ray 1 h post-irr., soluble fraction	13 30 Gy X-ray 1 h post-irr., soluble fraction
4 30 Gy X-ray 3 h post-irr., soluble fraction	14 30 Gy X-ray 3 h post-irr., soluble fraction
5 mock-irradiated, chromatin-bound fraction	15 mock-irradiated, wash 1
6 30 Gy X-ray 1 h post-irr. chr.-bound fraction	16 30 Gy X-ray 1 h post-irr., wash 1
7 30 Gy X-ray 3 h post-irr., chr.-bound fraction	17 30 Gy X-ray 3 h post-irr., wash 1
8 mock-irradiated, remaining pellet	18 mock-irradiated, wash 2
9 30 Gy X-ray 1 h post-irr., remaining pellet	19 30 Gy X-ray 1 h post-irr., wash 2
10 30 Gy X-ray 3 h post-irr., remaining pellet	20 30 Gy X-ray 3 h post-irr., wash 2
34 µg/lane AG1522C	17 µg/lane AG1522C

Fig. 37 **The chromatin-bound fraction of p21 appears to be degraded after subcellular fractionation studies according to Prosperi *et al.*** Exposure time: β-actin 20 sec; PCNA/p21 1 min. WB: β-actin, PCNA and p21.

2.3.3 Full-length p21 in the chromatin-bound fraction 3 h after 30 Gy X-rays

The degradation of the chromatin-bound p21 fraction obtained in the former experiment described above was assumed to be caused by the DNase I treatment, which was done at 37°C for 30 min. To release the chromatin-bound proteins however, a digestion of the DNA is required, as in previous experiments the chromatin-bound protein fraction to a big part remained in the pellet that is discarded. To solve this problem I digested the DNA by the use of Benzonase instead of DNase I, which does not need an incubation temperature of 37°C, but is active already at 4°C. With this modification, p21 was not degraded during the DNA digest. Fig. 38 shows an exemplary WB analysis with detection of β-actin, PCNA and p21. AG cells were exposed to 30 Gy X-rays and subjected to subcellular protein fractionation at 1 h or 3 h after exposure. The soluble protein fraction of all samples has a detectable quantity of PCNA and p21 (Fig. 38 lanes 2–4). PCNA is not detected in the chromatin-bound protein fraction of the mock-irradiated sample (Fig. 38 lane 5). Cells lysed 1 h or 3 h after X-ray exposure have a clear detectable chromatin-bound PCNA fraction as seen in lanes 6 and 7, respectively (Fig. 38). The PCNA is almost completely cleared out of the resulting pellet, as hardly any PCNA is detected following lysis by Laemmli buffer (Fig. 38 lanes 8–10). A weak signal for full-length p21 is detected in the soluble protein fractions of all samples (Fig. 38 lanes 2–4), showing a slight increase for the cells incubated 3 h after exposure (Fig. 38 lane 4). The chromatin-bound protein fraction has a detectable p21 signal in the lysate gained from the cells lysed 3 h after irradiation compared to a not detectable p21 signal for mock-irradiated cells (Fig. 38 lane 7 versus lane 5). Irradiated cells, which were lysed 1 h after irradiation, show a very weak p21 band (Fig. 38 lane 6). As seen in lanes 8–10 a little amount of p21 still remained in the resulting pellet, with an increase with the incubation time after exposure (Fig. 38 lane 10 compared to lane 9).

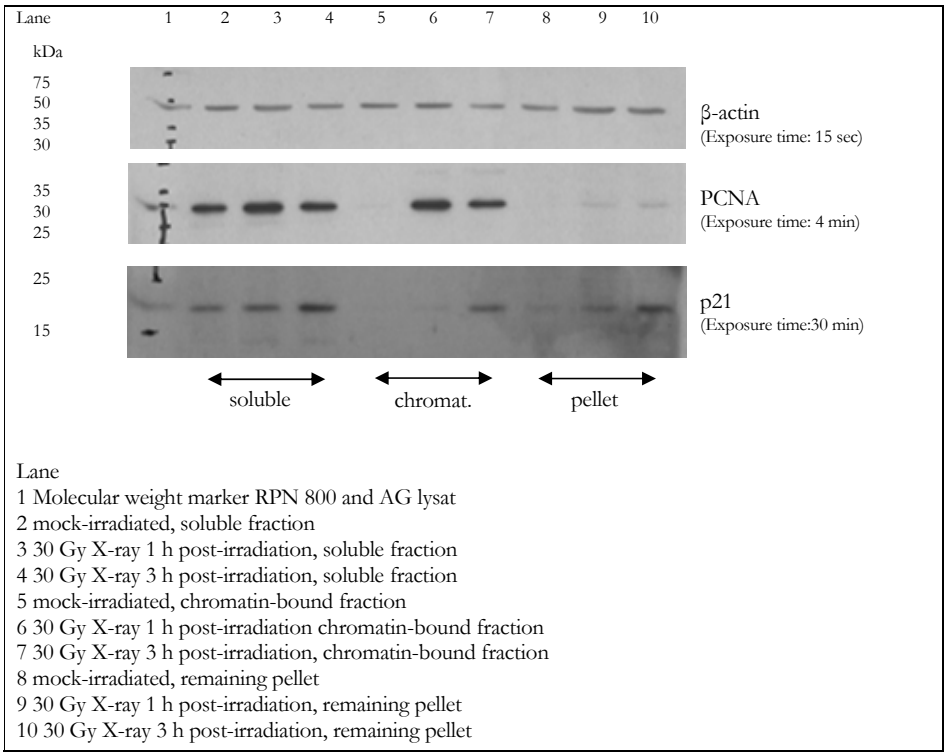

Lane
1 Molecular weight marker RPN 800 and AG lysat
2 mock-irradiated, soluble fraction
3 30 Gy X-ray 1 h post-irradiation, soluble fraction
4 30 Gy X-ray 3 h post-irradiation, soluble fraction
5 mock-irradiated, chromatin-bound fraction
6 30 Gy X-ray 1 h post-irradiation chromatin-bound fraction
7 30 Gy X-ray 3 h post-irradiation, chromatin-bound fraction
8 mock-irradiated, remaining pellet
9 30 Gy X-ray 1 h post-irradiation, remaining pellet
10 30 Gy X-ray 3 h post-irradiation, remaining pellet

Fig. 38 **p21 is part of the chromatin-bound protein fraction and can be detected 3 h after exposure to 30 Gy X-rays.** Representative WB analysis for the presence of p21, PCNA and β-actin after subcellular fractionation at 1 h and 3 h after exposure of human fibroblasts to 30 Gy X-rays. Note: Small amounts of PCNA remain within the pellet after Benzonase digest. The fraction of p21 that is not released by Benzonase treatment is approximately 50%. WB: β-actin, PCNA and p21.

These results show that a method has been established with which a chromatin-bound protein fraction containing p21 and PCNA can be detected by Western Blot analysis. PCNA and p21 are both shown to be detectable components of the DNA-associated protein fraction 3 h after DNA damage induction by exposure to 30 Gy X-rays. Interestingly, the PCNA level appears to be elevated at 1 h after irradiation compared to 3 h after irradiation, which was also seen in other experiments. The opposite is seen for p21, where the signal is elevated at 3 h after exposure.

2.4 p21 forms foci after low LET ionizing radiation

In the previous section, p21 and PCNA both are shown to be part of the chromatin-bound fraction after X-ray irradiation by biochemical analysis. Also, the accumulation of these proteins after high LET has been studied here by immunocytochemistry (Sect. 2.2, page 31). However, it was not possible to discriminate high LET-induced foci for proteins involved in different DNA repair processes and a change in irradiation geometry did not help to further elucidate the repair pathways in which p21 is involved after charged particle irradiation. With X-ray irradiation though, a more homogeneous distribution of the various DNA damaged sites is induced. As a consequence, a more dispersed distribution of different DNA lesions and focal protein accumulations may answer the question as to what DNA repair pathway requires the relocalization of p21 after radiation damage. Here, I tried to visualise p21 accumulations after DNA damage induction by X-ray irradiation. And indeed, in normal human fibroblasts p21 accumulates to small but discrete foci after irradiation with X-rays. Immunocytochemistry to detect p21 as well as other DNA repair proteins was carried out to investigate whether the focal accumulations of p21 after X-rays are associated with a specific DNA repair pathway.

2.4.1 p21 foci are detectable after exposure to X-rays

Human fibroblasts were first studied 3 h after exposure to X-rays as my previous experiments showed that at 3 h post 30 Gy X-rays a significant fraction of the p21 protein had associated with the chromatin. The samples were immunostained for p21 and γH2AX as described in Sect. 4.4.4 (page 100). Without extraction of the soluble proteins, the p21 level throughout the nucleus is very heterogeneous and the p21 level of the soluble p21 fraction possibly too high to discriminate radiation-induced focal p21 accumulations from background staining (data not shown). This problem was abolished here by the use of the Hepes extraction buffer.

Fig. 39 shows an example for p21 foci at 3 h after irradiation with 10 Gy X-ray irradiation. Soluble proteins were extracted with Hepes buffer (Sect. 4.4.2), followed by immunostaining of the fixed cells for p21 and γH2AX (Sect. 4.4.4). Focal accumulations of p21 (green) are visible in the irradiated AG cell nuclei (panel B). γH2AX foci (red) are also detected, but they are not as distinct as the p21 accumulations. Mock-irradiated cells do not show focal structures for p21 (panel A). However, some nuclei show 1–3 γH2AX foci (not seen in the Figure shown below). Note, that the two proteins do not seem to colocalize in contrast to the results obtained from previous experiments using heavy ions (Sect. 2.1 and 2.2).

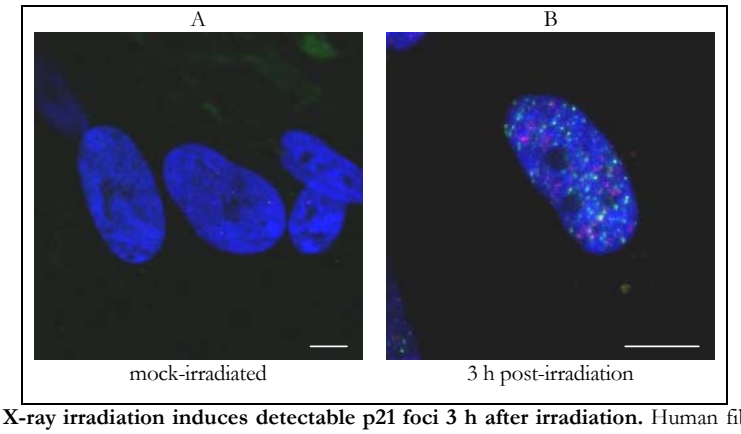

Fig. 39 **X-ray irradiation induces detectable p21 foci 3 h after irradiation.** Human fibroblasts fixed and extracted with Hepes buffer 3 h after irradiation with 10 Gy X-rays. Immunostaining was carried out for p21 (green) and γH2AX (red). A: mock-irradiated cells; B: 3 h post-irradiation; DNA: blue (ToPro-3). Bar: 10 μm.

2.4.2 Time-course for p21 foci formation after X-rays

To elucidate at which time after X-ray irradiation p21 foci accumulate, human fibroblasts were irradiated with 10 Gy X-rays and fixed at 1, 3, 5, and 22 h after irradiation. Prior to immunostaining for p21 and γH2AX (Sect. 4.4.4) the soluble proteins were extracted with Hepes buffer as described in Sect. 4.4.2 (page 99). Mock-irradiated fibroblasts hardly show any p21 signal (green) after extraction (Fig. 40). As a positive control for the irradiation and to display induced DSBs γH2AX was stained, leading to clearly detectable foci in all irradiated samples (Fig. 40 panels B–E). As stated above, mock-irradiated fibroblasts also show a few γH2AX foci in some nuclei. Focal accumulations for p21 are visible in a minority of the nuclei at 1 h after irradiation (Fig. 40 panel B) and 3 h post-irradiation most of the irradiated cells show p21 foci (Fig. 40 panel C). At 5 h post exposure to 10 Gy X-rays, the number of nuclei with p21 foci appears to be reduced and 22 h after irradiation no focal accumulations for p21 are detected (Fig. 40 panels D and E, respectively).

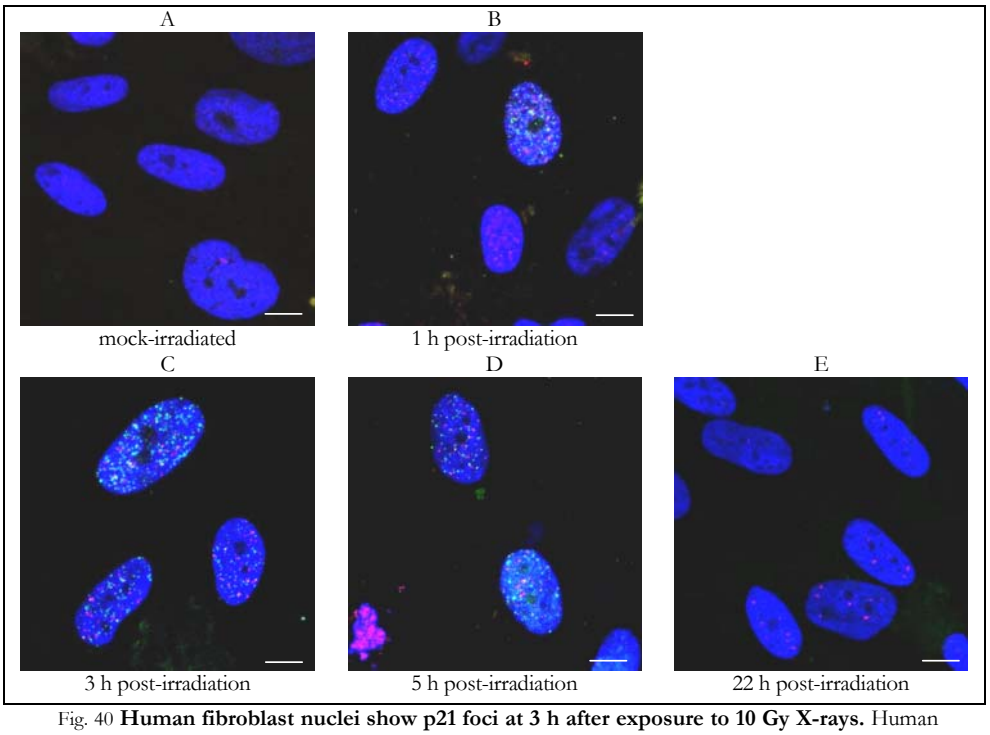

Fig. 40 **Human fibroblast nuclei show p21 foci at 3 h after exposure to 10 Gy X-rays.** Human fibroblasts were stained for p21 (green) and γH2AX (red) after extraction of the soluble proteins with Hepes buffer. A: mock-irradiated cells; B–E: irradiated cells fixed at the indicated times post-irradiation; DNA: blue (ToPro-3). Bar: 10 µm.

2.4.3 Dose dependency for p21 accumulations after X-irradiation

As described above (Sect. 2.4.2) p21 foci were visible in almost all of the irradiated nuclei at 3 h after X-irradiation. To elucidate whether p21 colocalizes with other proteins at these X-ray induced DNA lesions, an irradiation dose at which the foci both are visible and can be discriminated from focal accumulations of other DNA repair proteins is favorable to carry out colocalisation analysis with Scion Image (Sect. 4.5.2). For this, human fibroblasts were irradiated with 2, 4, 6, 8 or 10 Gy X-rays followed by fixation and extraction of the soluble proteins by Hepes buffer 3 h post-irradiation. Immunostaining was carried out for p21 and γH2AX.

Cells irradiated with 2 Gy X-rays show a slight irradiation-induced appearance of detectable p21 (green) and γH2AX (red) signals, however these foci are too weak to be analyzed (Fig. 41 panel B). 4 Gy X-rays induce more foci for both proteins dispearsed throughout the nuclei, and after 6 Gy the induced protein accumulations seem to be more easily distinguishable by eye (Fig. 41 panels C and D, respectively). 8 Gy X-rays induce very distinct p21 foci throughout the nuclei

that are clearly seen, where the γH2AX foci are more indistinct than the p21 foci (Fig. 41 panel E). After 10 Gy X-irradiation, focal structures can still be discriminated, but the total number of p21 foci per nucleus is very high (Fig. 41 panel F). Note that the number of p21 foci is noticeably higher than the accumulations for γH2AX (Fig. 41 panels E and F visualise this observation).

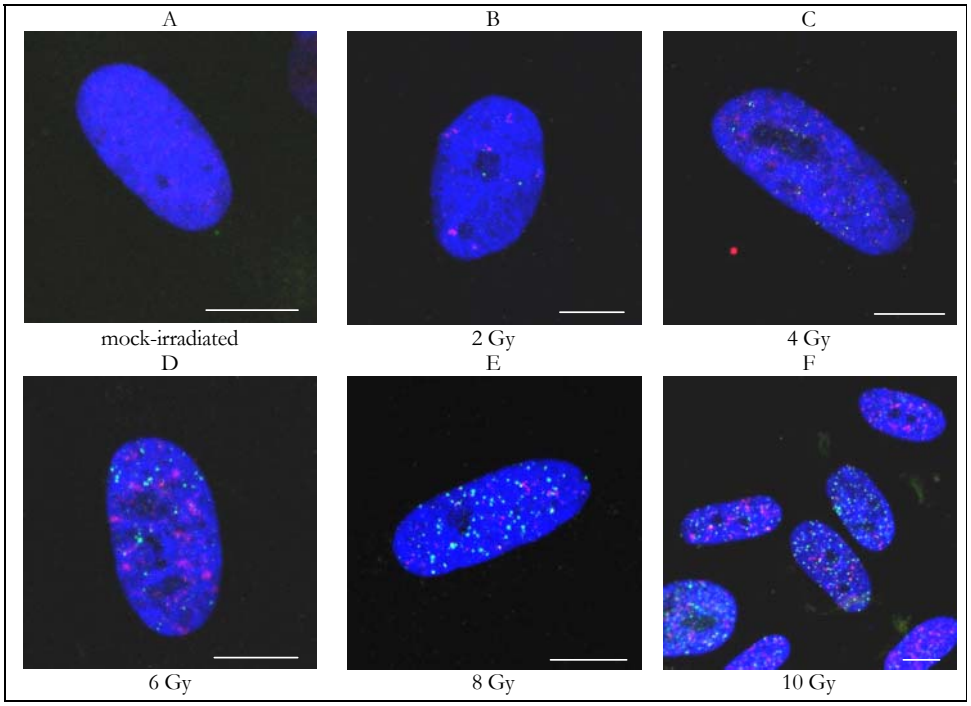

Fig. 41 **Increasing number of detectable p21 foci with X-ray dose in human fibroblasts.** Human fibroblasts irradiated with the indicated dose, fixed and extracted with Hepes buffer 3 h post-irradiation. Immunostained for p21 (green) and γH2AX (red). A: mock-irradiated cells; B–F: 3 h post irradiation with the indicated X-ray dose. DNA: blue (ToPro-3). Bar: 10 μm.

To confirm the lack of colocalisation I repeated the experiment with immunostaining carried out for p21 and 53BP1. As the amount of visible p21 foci after DNA damage induction by 10 Gy X-rays are possibly too high for analysis of colocalization, this X-ray dose was not used again. Fig. 42 displays the nuclei from AG cells at 3 h after X-ray irradiation with the indicated doses, followed by fixation and extraction with Hepes buffer and immunostaining for p21 (green) and 53BP1 (red). As in the former experiment, with an X-ray dose of 2 Gy already distinct p21 foci are detected (Fig. 42 B) and an increase in number of visible protein accumulations with the applied radiation dose is seen for both p21 and 53BP1 (Fig. 42 panels B–E). 53BP1 seems to show more foci than the γH2AX in the former experiment after 2 Gy X-rays (Fig. 42 panel B). The clearest and still distinguishable p21 foci are detected after an X-ray exposure with 8 Gy.

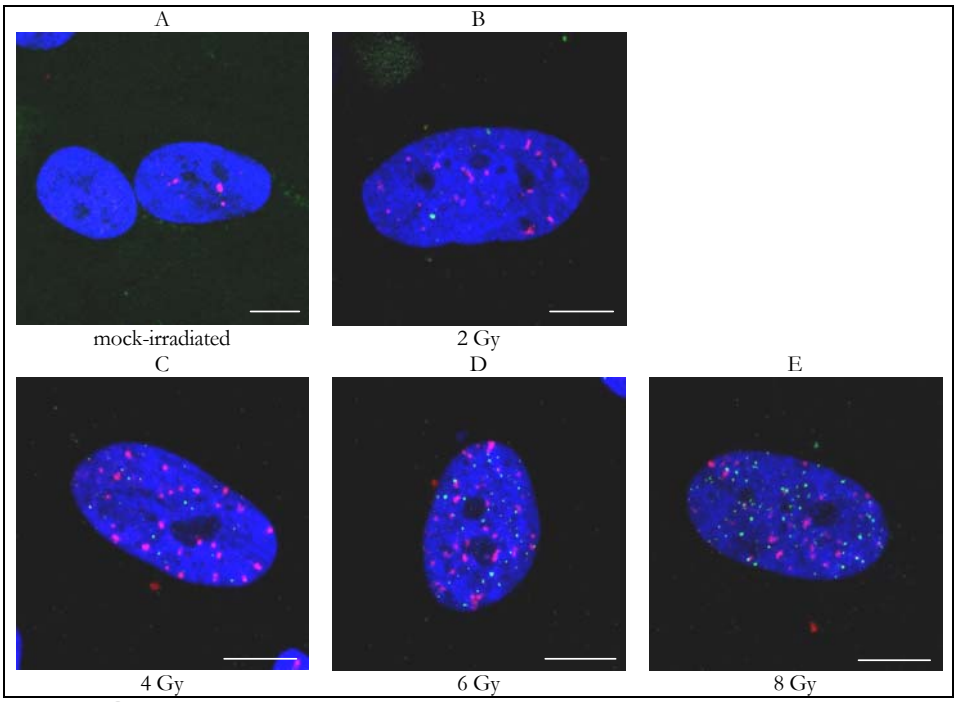

Fig. 42 **Dose dependency for p21 and 53BP1 foci in human fibroblasts 3 h after X-rays.** Human fibroblasts irradiated with the indicated dose, fixed and extracted with Hepes buffer 3 h post-irradiation. p21 (green) and 53BP1 (red). A: mock-irradiated cells; B–E: 3 h post-irradiation with the indicated X-ray dose. DNA: blue (ToPro-3). Bar: 10 µm.

2.4.4 Colocalisation analysis for p21 foci with DSB related proteins

In the previous section I have been able to show that p21 forms distinct focal accumulations after X-ray irradiation. Furthermore, p21 and the DSB markers γH2AX or 53BP1 do not seem to colocalise and differed in the number of detectable foci by visual observation. Here the colocalisation of p21 with DSB related proteins is elucidated by the use of Scion Image (Sect. 4.5.2).

Human fibroblasts were irradiated with 8 Gy X-rays and fixed with extraction of the soluble proteins (Hepes-extraction; Sect. 4.4.2) 3 h post-irradiation. Irradiated nuclei were stained for p21 in combination with γH2AX, 53BP1, TP53 or MDC1 (Sect. 4.4.4).

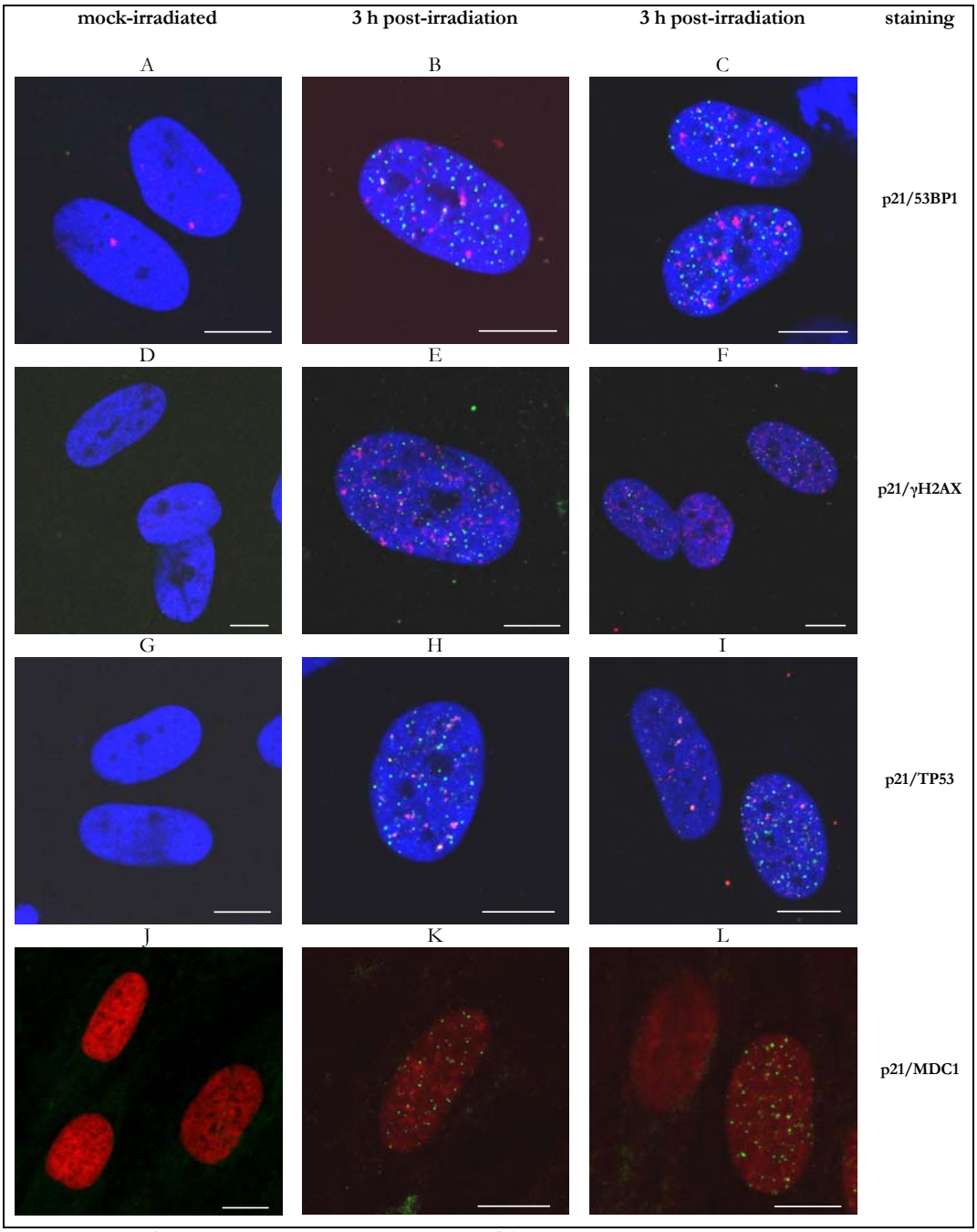

Fig. 43 **Colocalisation studies for p21 with DSB related proteins after X-rays.** Human fibroblasts irradiated with 8 Gy X-rays and fixed 3 h post-irradiation. Immunostaining was carried out after extraction by Hepes buffer for p21 (green) in combination with γH2AX, 53BP1, TP53 or MDC1 (red). A, D, G and J: mock-irradiated cells. B, C, E, F, H, I, K and L: 3 h post irradiation. DNA: blue (ToPro-3). Note: J, K and L no DNA staining. Bar: 10 μm.

As seen in Fig. 43 clear p21 foci are detected in all irradiated nuclei (panels B, C, E, F, H, I, K and L) and weak 53PB1 (panels B and C), γH2AX (panels E and F) and TP53 (panels H and I) foci can be seen. MDC1 however, is not detected in clear focal accumulations after irradiation; instead it appears to be localized homogeneously throughout the nucleus (Fig. 43, panels K and L). As a result, MDC1 was not evaluated for colocalisation with p21. Noticeably more p21 foci per nucleus are observed than for the DSB related proteins (see Fig. 43 panels B, E and H).

The colocalisation of p21 with 53PB1, γH2AX or TP53 was investigated by Scion Image with a program provided by B. Jakob (GSI) as described in Sect. 4.5.2 (page 103).

Staining	Chi20	*n*
p21/53BP1	2.26	37
p21/γH2AX	2.33	28
p21/TP53	5.75	44

Table 5 **Colocalisation analysis of p21 with 53PB1, γH2AX or TP53.** Def.: No colocalisation of the investigated proteins if Chi20 is below 8. Results are from two independent experiments.

As depicted in Table 5, colocalisation of p21 foci with either 53BP1, γH2AX or TP53 does not occur after X-rays. These results suggest that the p21 protein, albeit accumulated in focal structures after irradiation with X-rays, is not associated with DNA DSBs. As many more p21 foci per nucleus are seen than 53BP1, γH2AX or TP53 foci I speculate that the DNA lesions that p21 is associated with are more abundant than are DSBs and could represent SSBs as many more SSBs are induced after X-ray irradiation [Newman *et al.,* 2000]. The ratio of DSBs to SSBs after exposure to 1 Gy X-rays is estimated to be 1:25 [Ward, 1988].

2.4.5 Colocalisation analysis of p21 with the SSB protein XRCC1

To elucidate whether p21 accumulates at X-ray-induced SSBs, immunostaining was carried out for p21 in combination with the SSB-related protein XRCC1. Human fibroblasts were irradiated with 8 Gy X-rays and fixed after Hepes extraction of the soluble proteins (Sect. 4.4.2) 3 h post-irradiation. The cells were stained for p21 and XRCC1 (Sect. 4.4.4).

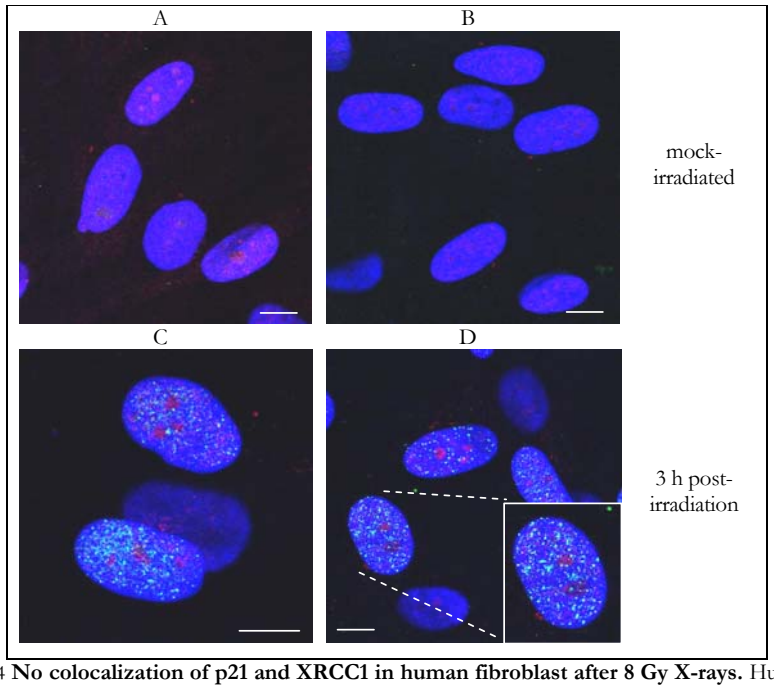

Fig. 44 **No colocalization of p21 and XRCC1 in human fibroblast after 8 Gy X-rays.** Human fibroblasts exposed to 8 Gy X-rays. Soluble proteins extracted by Hepes buffer after fixation, followed by staining for p21 (green) and XRCC1 (red). A and B: mock irradiated cells. C and D: 3 h post irradiation. DNA: blue (ToPro-3). Bar: 10 μm.

Fig. 44 displays the microscopic analysis of human fibroblast 3 h after irradiation with 8 Gy X-rays. Immunostaining for p21 (green) and XRCC1 (red), results in clear irradiation-induced p21 accumulations (Fig. 44 C and D). XRCC1, however, gives a punctuate background signal and a strong signal within the nucleoli, but no clear irradiation-induced foci formation for XRCC1 is seen compared to the mock-irradiated cells (Fig. 44 C and D versus A and B, respectively).

The absence of a clear X-ray induced XRCC1 signal precluded colocalisation studies for p21 and XRCC1 after DNA damage induction by X-ray exposure.

2.5 Camptothecin does not lead to distinct p21 foci

As XRCC1 did not appear to localize into distinct detectable foci after X-rays (Sect. 2.4.5), I tried to visualize XRCC1 after the induction of DNA SSBs using the topoisomerase I (Top I) inhibitor camptothecin (CPT). Top I normally cleaves, unwinds and religates DNA, however, when CPT binds to Top I, Top I is able to cleave but not to religate DNA. Thereby CPT induces SSBs in the DNA [Covey *et al.*, 1989]. In vicinity of the replication fork these SSBs can be converted to 1-ended DSBs in cycling cells [Furuta *et al.*, 2003].

Human fibroblasts (AG) were treated with 1 μM CPT for 1 h at 37°C as described in Sect. 4.3.1 (page 98). The soluble proteins were either not extracted or extracted by Hepes buffer as indicated (Sect. 4.4.1 and 4.4.2, respectively). Fixed nuclei were stained for p21 and XRCC1 (Sect. 4.4.4). In addition, immunostaining for 53BP1 was carried out to elucidate the levels of DSBs induced.

Unfortunately, neither p21 (green) nor XRCC1 (red) show clear focal accumulations after exposure to CPT. Cells which were not extracted show detectable p21 and weak XRCC1 staining, however, no difference in their appearance after incubation with CPT is seen (Fig. 45 A and B, respectively). The Hepes extraction reduced the p21 signal, the background signal for XRCC1 could still be detected (Fig. 45 C). After CPT treatment and following extraction of the soluble proteins, a slight increase in the overall signal for p21 (i.e. throughout the nucleus) is observed without any discernible focal accumulations (Fig. 45 D). This elevated signal shows that p21 is bound to some structure within the nucleus as it is not extracted. Furthermore, it is not due to an induction of p21 as an increase is not seen in the samples where the soluble proteins are not extracted (Fig. 45 panel A compared to panel B; panel E compared to panel F). XRCC1 does not show CPT-induced protein accumulations either, when compared to the non-treated cells (Fig. 45 C and D, respectively). Interestingly, less of the treated cells show a high XRCC1 expression level in the nucleoli as seen in panel D and compared to the stronger nucleoli-bound signal for XRCC1 in non-treated cells (Fig. 45 C). The combined staining for p21 and 53BP1 shows that additional DSB are induced by the CPT treatment compared to non-treated cells which also validates that the used CPT is active (Fig. 45 F and H compared to E and G, respectively). In these experiments, CPT does not induce visible p21 or XRCC1 accumulations even if DNA damage induction is achieved.

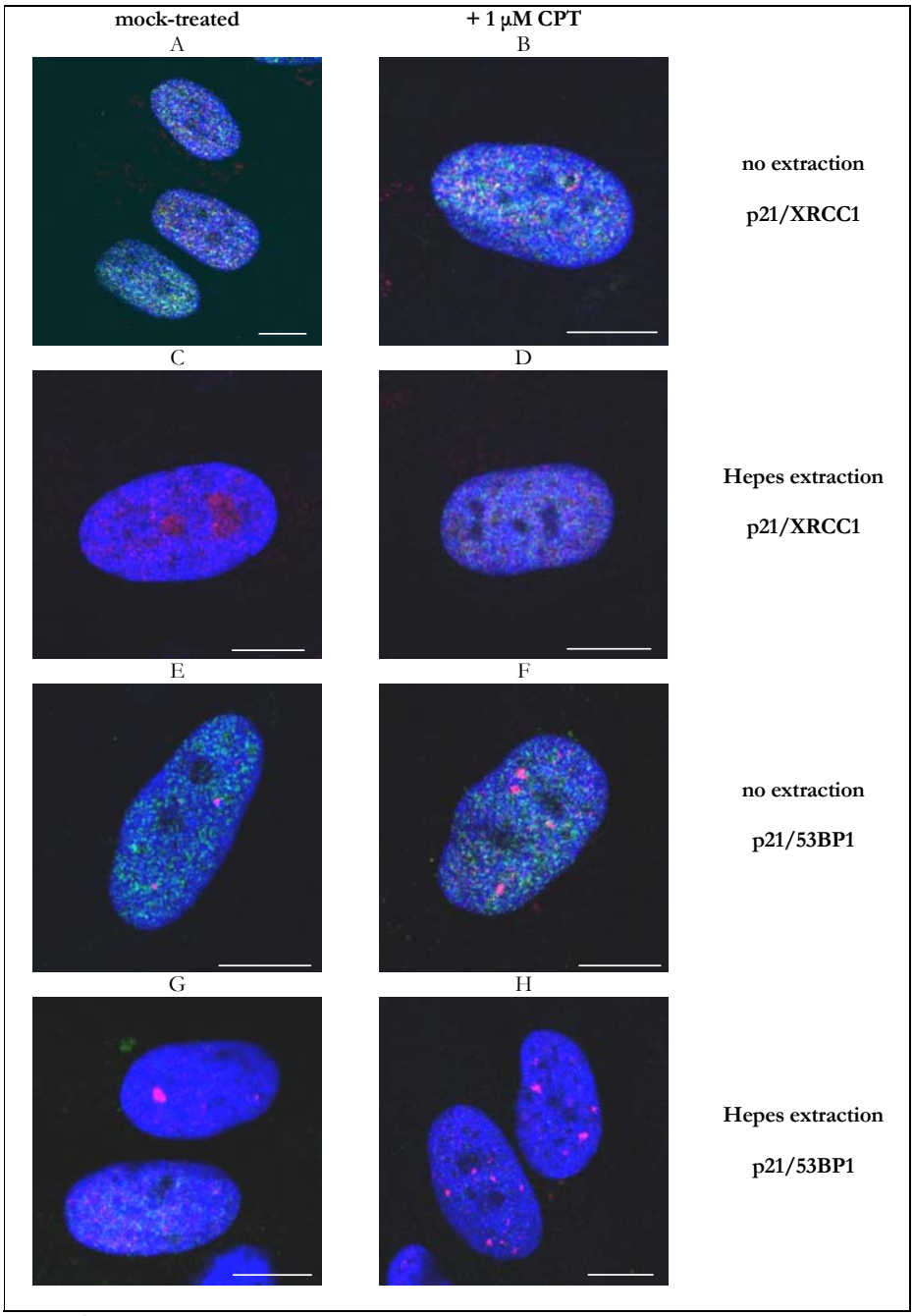

Fig. 45 **Camptothecin does not induce p21 accumulations in human fibroblast nuclei.** Human fibroblasts treated with 1 μM camptothecin for 1 h at 37°C (panels B, D, F and H); fixed without extraction (panels A, B, E and F) or with Hepes buffer extraction (panels C, D, G and H). Immunostaining was carried out for p21 (green) and XRCC1 (red; panels A–D) or 53BP1 (red; panels E–H). A, C, E and G: non-treated cells. DNA: blue (ToPro-3). Bar: 10 μm.

2.6 H_2O_2 leads to punctuate signal for p21

As camptothecin, which was used to induce mainly SSBs did not give any clear structural change of the detectable p21 or XRCC1 signals after immunostaining, DNA lesions were induced by hydrogen peroxide (H_2O_2). Treatment of cells with H_2O_2 produces specific DNA lesions including oxidized bases, SSBs and to a minor extends DSBs. The aim of these experiments is to elucidate whether p21 colocalises with BER/SSB-related proteins such as XRCC1 which has been shown to recruit to H_2O_2 induced DNA lesions [El-Khamisy *et al.*, 2003].

Human neonatal fibroblasts (NHDF) were incubated with different H_2O_2 concentrations in PBS for 20 min at RT as described in Sect. 4.3.2 (page 99) to acquire a concentration at which distinct protein accumulations are detected that can be differentiated. Following H_2O_2 exposure, the cells were briefly rinsed with PBS and incubated at 37°C for 15 min and fixed after extraction with Hepes buffer (Sect. 4.4.2) and immunostaining was carried out (Sect. 4.4.4).

With a H_2O_2 concentration of 10 mM or 5 mM the proteins p21 and XRCC1 were detected throughout the nuclei and did not show singularized foci (data not shown). After treatment with 0.5 mM H_2O_2 the detected p21 and XRCC1 signal became more dispersed, but could still not be discriminated (data not shown). With a concentration of 0.2 mM H_2O_2 granular structures for p21 and XRCC1 were detected, making me use this H_2O_2 concentration for the further experiments.

Immunostaining for XRCC1 and γH2AX was carried out to see whether a different distribution of the SSB related protein XRCC1 and the DSB related protein γH2AX after H_2O_2 treatment could be achieved. Fig. 46 displays representative images of NHDF cells treated with 0.2 mM H_2O_2 followed by immunostaining for XRCC1 and γH2AX. Many of the cells that are not treated with H_2O_2 show XRCC1 localized mainly in the nucleoli as seen in Fig. 46 panel B. For γH2AX 0–4 foci are seen in non-treated cells (Fig. 46 A). H_2O_2 treated cells show a higher level and granular structure throughout the nucleus for XRCC1 compared to the non-treated cells (Fig. 46 A–C compared to G and I, respectively). XRCC1 appears to change its position, as the high XRCC1 signal in the nucleoli as seen in many of the non-treated cells is reduced in cells exposed to H_2O_2. After treatment with H_2O_2, an elevated amount of γH2AX foci are detected within the nucleus (Fig. 46 D, E, H and I). It is clearly seen however, that the H_2O_2-induced XRCC1 and γH2AX foci are localized at different areas throughout the nucleus. Furthermore, many distinct punctuate signals are detected for XRCC1 whereas only a few γH2AX foci per nucleus are visible (Fig. 46 G and H, respectively). With this H_2O_2 treatment, a method is found to induce dispersed XRCC1 foci, with some additional DSBs that can be visualized and distinguished by the detection γH2AX.

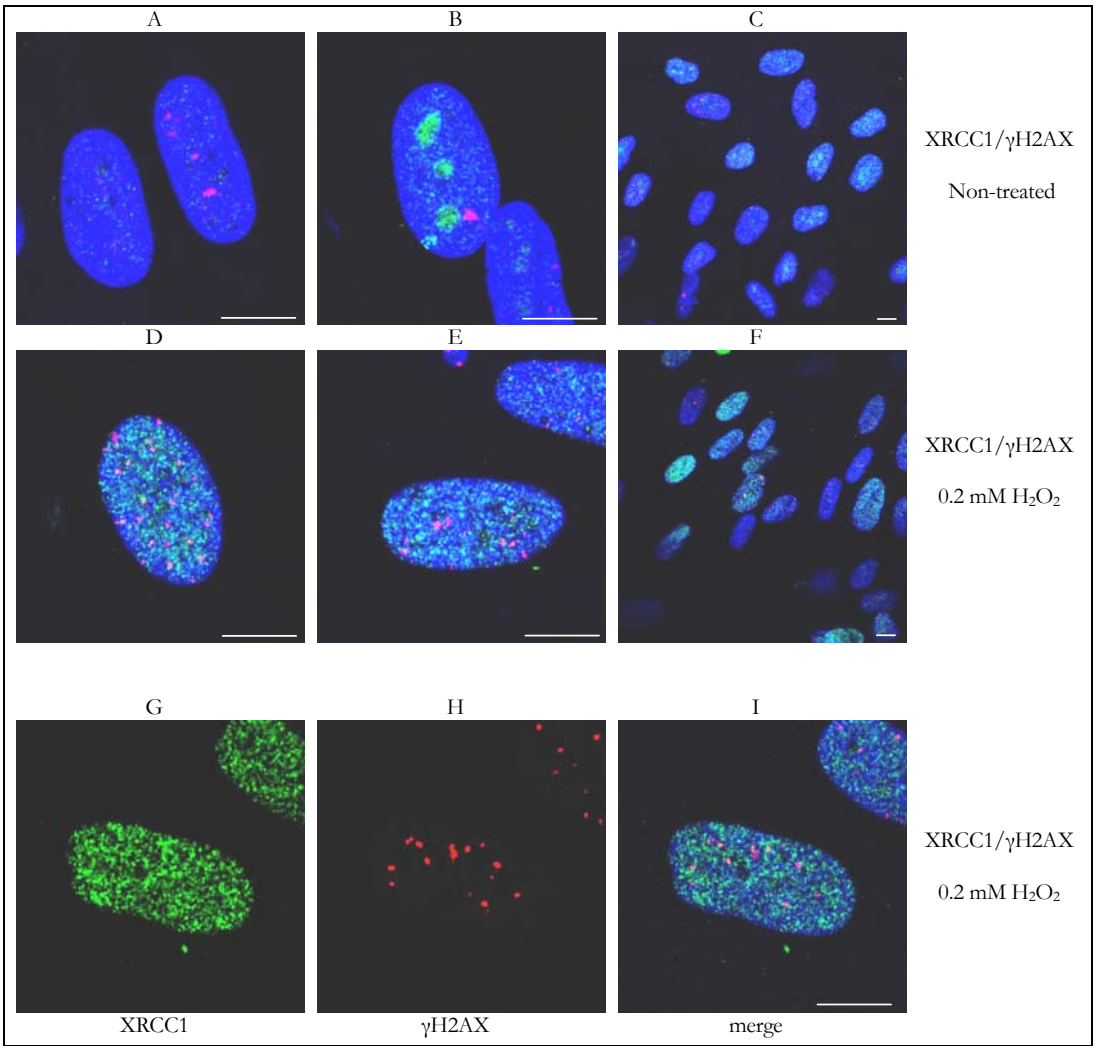

Fig. 46 **H_2O_2 induced SSBs and DSBs can be discriminated and visualized by immunostaining for XRCC1 and γH2AX.** NHDF cells 15 min after treatment with 0.2 mM H_2O_2 for 20 min, fixed and extracted with Hepes buffer; immunostained for XRCC1 (green) and γH2AX (red). A, B and C: non-treated cells. D–I: treated for 20 min with 0.2 mM H_2O_2. Blue: DNA (ToPro-3). Bar: 10 µm.

As a difference is visualized between the SSB-related protein XRCC1 and the DSB-related protein γH2AX after H_2O_2 treatment, p21 is detected in combination with XRCC1. NHDF cells, treated as above, were immunostained for p21 and XRCC1 and are displayed in Fig. 47 below.

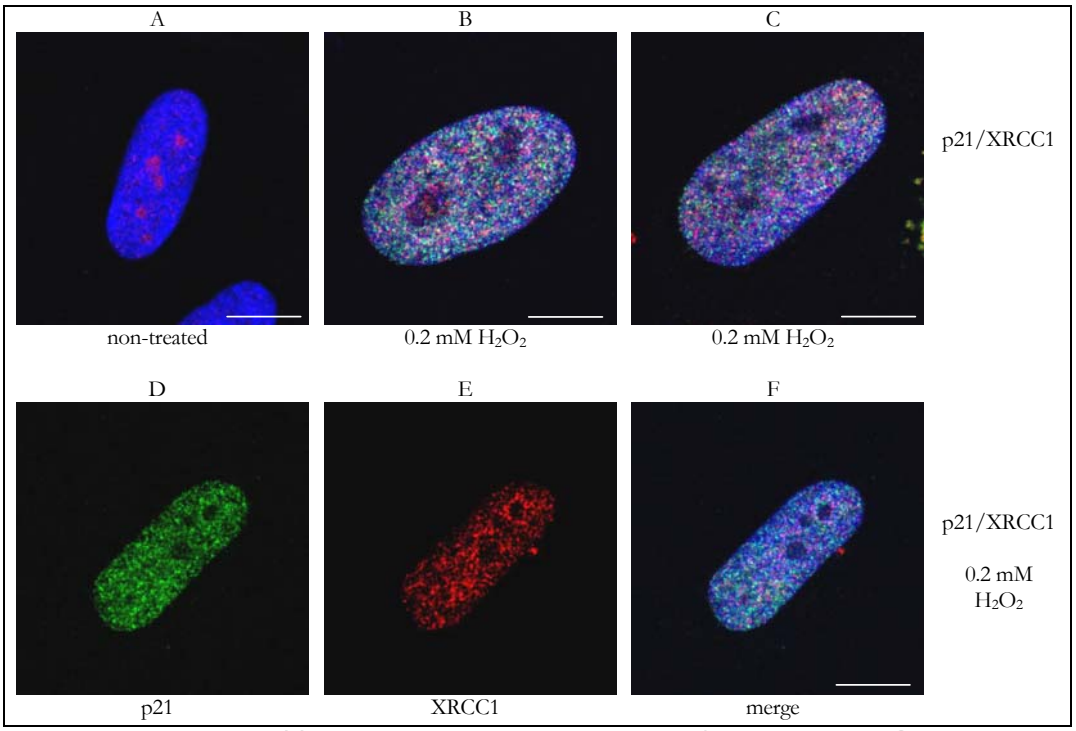

Fig. 47 **p21 and XRCC1 both form granular structures after H_2O_2 treatment of NHDF cells.** NHDF cells after oxidative DNA lesion induction by 0.2 mM H_2O_2 for 20 min at RT. Immunostained for p21 (green) and XRCC1 (red) after extraction by Hepes buffer and fixation 15 min after H_2O_2 treatment. A. non-treated. B–F: treated with 0.2 mM H_2O_2. The nuclei visualised by ToPro-3 DNA staining (blue). Bar: 10 μm.

Cells which are not exposed to H_2O_2 generally show XRCC1 in the nucleoli, p21 is not detectable (Fig. 47 panel A). The cells which are treated with 0.2 mM H_2O_2 show a granular structure for both p21 and XRCC1 (Fig. 47 panels B–E). These granular signals for p21 and XRCC1 were checked in individual nuclei for colocalisation as described in Sect. 4.5.2 (page 103). 22 nuclei were analysed giving a Chi20 of 2.4, suggesting, that p21 does not colocalize with the SSB-related protein XRCC1 after DNA damage induction by H_2O_2 in NHDF cells.

To exclude the possibility of some structural change caused by the H_2O_2 treatment leading to this result, additional experiments were done where cells were pre-treated with 0.2 mM H_2O_2 and irradiated with Ni ions. Here, weak XRCC1 foci and p21 foci were detected in some nuclei which colocalized (data not shown). This verified that H_2O_2 does not disturb the possibility of p21 and XRCC1 recruitment to the same site. These results indicate that p21 is not gathered at the here induced oxidative lesions that are recognized by XRCC1.

2.7 Ectopical expression of a GFP-p21 fusion protein

The possibility of making GFP fusion proteins gives the opportunity to detect proteins independently of staining methods. Furthermore, GFP fusion proteins can be observed in living cell systems, which has been shown to be very helpful to monitor the very early responses to induced DNA damage. To study the early kinetics of the p21 accumulations to heavy ion-induced DNA lesions, a GFP-p21 fusion protein was constructed.

The full-length p21 open reading frame (ORF) was obtained from the wtp21 plasmid kindly provided by Prof. Dr. S. Dimmeler (University of Frankfurt). The p21 ORF was amplified by PCR using the primers and the pEGFP-C2 plasmid as described in Sect. 4.10. With this vector the GFP is expressed at the N-terminal site of the expressed protein. The former experiments from showed that p21 needs the intact interaction with PCNA to accumulate at the DNA lesions (Sect. 2.2 page 31). The interaction with PCNA occurs at the C-terminal domain of p21 which is not altered by the use of the pEGFP-C2 plasmid. HCT116p21$^{-/-}$ cells and HeLa cells were transfected with the GFP-p21 plasmid (Sect. 4.10.6). 24 h after transfection, Laemmli lysates (Sect. 4.7.1) were prepared and the successful transfection and expression of the GFP-p21 fusion protein was verified by Western Blot analysis (Sect. 4.9) as shown in Fig. 48.

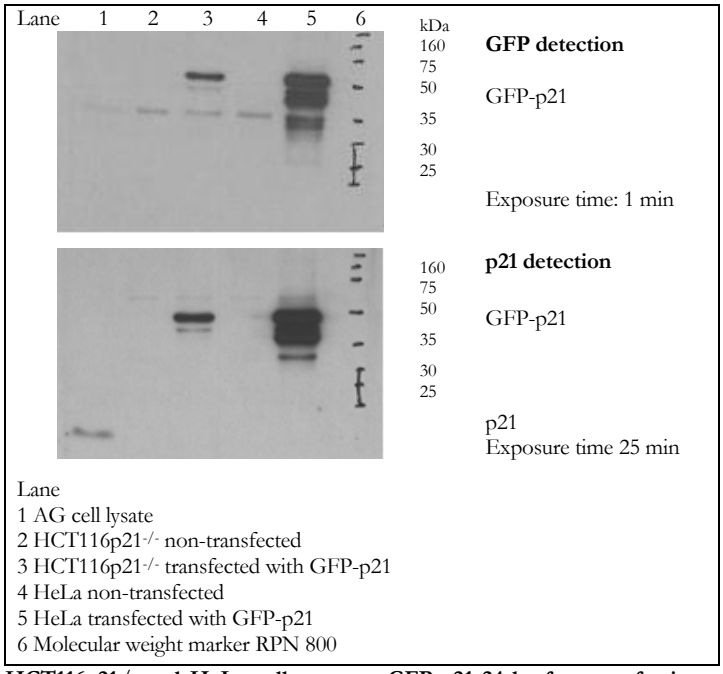

Fig. 48 **HCT116p21$^{-/-}$ and HeLa cells express GFP-p21 24 h after transfection with the GFP-p21 expression plasmid.** Western Blot analyses of the ectopically expressed GFP-p21 fusion protein shows clear bands for GFP-p21 in the transfected HCT116p21$^{-/-}$ and HeLa cells after GFP (upper WB) and p21 (lower WB) detection (lanes 3 and 5, respectively). Non-transfected cells show a weak non-specific signal after GFP detection and no signal after p21 detection (lanes 2 and 3).

Clear bands are seen after GFP detection for both cell lines transfected with the GFP-p21 plasmid; lane 3 displays the HCT116p21$^{-/-}$ cells, lane 5 the HeLa cells (Fig. 48 upper panel). The additional bands are possibly caused due to degradation of the extremely high expressed fusion protein. A weak non-specific signal is observed when anti-GFP antibody is used. Non-transfected HCT116p21$^{-/-}$ or HeLa cells and the AG cells do not show a specific GFP signal (Fig. 48 lanes 2, 4 and 1, respectively). The WB was stripped for the antibodies and the detection reagent (Sect. 4.9.5) after the GFP detection and probed to anti-p21 antibody (Fig. 48 lower panel). Endogenously expressed p21 is detected in AG cells (Fig. 48 lane 1), but not in non-transfected HCT116p21$^{-/-}$ cells, that do not express endogenous p21 , or in HeLa cells, that express only very small amounts of endogenous p21 (Fig. 48 lanes 2 and 4, respectively).

2.7.1 The GFP-p21 fusion protein localizes to the sites of particle traversals

After verification of the GFP-p21 expression in the used cell systems, GFP-p21 transfected cells were irradiated with particles to test whether the expressed fusion protein is able to accumulate at damaged DNA sites. HCT116p21$^{-/-}$ cells and HeLa cells were transfected with GFP-p21 as described in Sect. 4.10.6.2 (page 123) and irradiated with samarium (Sm; 3×10^6 p/cm^2; 11.4 MeV/u; 10290 V/μm) ions 24 h after transfection. The cells were fixed without extraction of the soluble proteins 30 min post-irradiation and immunostained for γH2AX (Sect. 4.4.4). To verify the irradiation induced signal of endogenously expressed p21, non-transfected HCT116p21$^{+/+}$ cells and non-transfected HeLa cells were irradiated additionally and immunostained for p21 and γH2AX.

Fig. 49 displays HCT116p21$^{-/-}$ cells transfected with GFP-p21. Mock-irradiated cells show heterogeneous GFP-p21 levels without any focal accumulations (green fluorescence signal), verifying the successful transfection and expression of the GFP-p21 plasmid (Fig. 49 A). Irradiated cells show distinct focal accumulations of GFP-p21 (green; Fig. 49 panel B) and γH2AX (red; Fig. 49 panel C) at 30 min after Sm irradiation. The same result was obtained for HeLa cells transfected with the GFP-p21 construct and irradiated with Sm ions (supplement 6.3 Fig. 74)

These results suggest that the ectopically expressed GFP-p21 protein is, at least in part, functional as it, similarly to the wild-type p21 protein, accumulates to foci that co-localize with γH2AX foci at heavy ion-induced DNA lesions. With this, a fluorescent signal of the GFP-p21 fusion protein and its response to heavy charged particle irradiation can be monitored in living human cells.

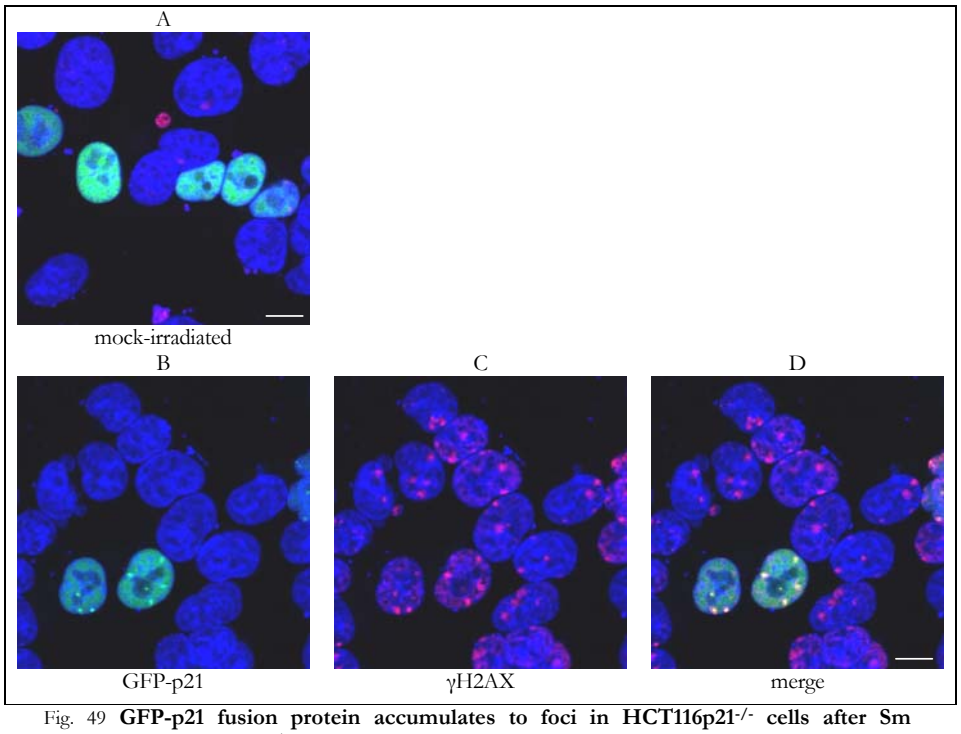

Fig. 49 **GFP-p21 fusion protein accumulates to foci in HCT116p21$^{-/-}$ cells after Sm irradiation.** HCT116p21$^{-/-}$ cells transfected with GFP-p21 plasmid and irradiated with Sm ions (3×10^6 p/cm^2; 11.4 MeV/u; 10290 V/µm) 24 h after transfection (B–D). Fixed without extraction and stained for γH2AX (red) 30 min post-irradiation. A: mock-irradiated. GFP-p21: green. DNA: blue (ToPro-3). Note: only approx. 20% of the transfected cells express the fusion protein to a level where it can be detected as foci. Bar: 10 µm.

2.7.2 Online observation of the formation of GFP-p21 foci

The very early accumulation of ectopically GFP-p21 was studied by live-cell imaging as the former experiment confirmed the functionality of the GFP-p21 in response to heavy ions. To do so, living cells expressing fluorescent proteins (here: p21) are observed on-line during the irradiation and for a desired time after irradiation. Here, live-cell imaging was kindly carried out by B. Jakob (GSI) using the GFP-p21 as described in Sect. 4.6 (page 103).

HeLa cells grown on polycarbonate dishes (Ø 18 mm) were transfected by Lipofectamine with the GFP-p21 construct 24 h before irradiation as described in Sect. 4.10.6. The polycarbonate dish with the transfected cell populations was mounted in a closed chamber and placed in the developed on-line microscopic system positioned directly at the beamline. After finding a

representative cell (i.e. a cell expressing GFP-p21), live-cell imaging was started remotely and the cells was then irradiated with krypton ions (4.8 MeV/u, LET 5265 keV/μm). An exemplary image series is shown in Fig. 50 below.

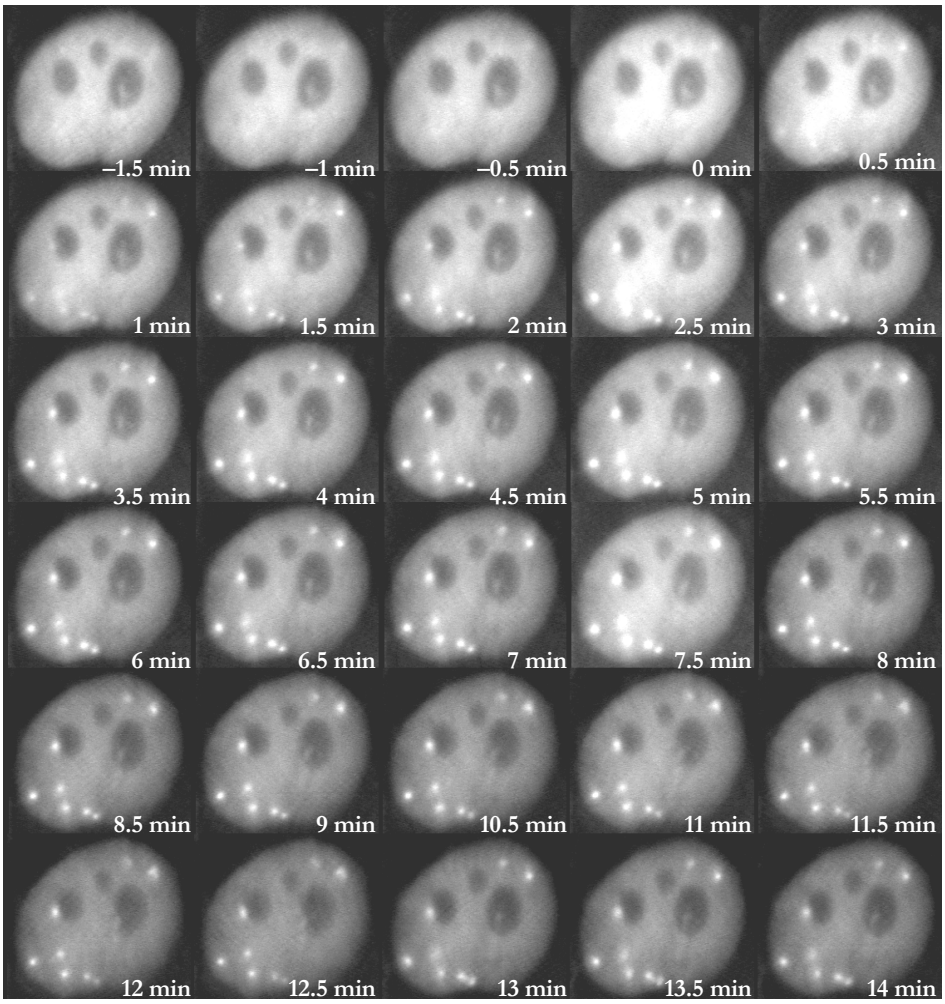

Fig. 50 **Live-cell imaging to show the recruitment of GFP-p21 in response to krypton ions.** Live-cell images were taken at the times indicated that are relative to the start of irradiation at 0 min. The very early accumulation of GFP-p21 is detectable at 0.5 min post-irradiation. Before irradiation and at 0 min, no distinct protein accumulations are detected. The darker spots in the nucleus represent the nucleoli.

The live-cell imaging shows a very fast appearance of the GFP-p21 foci at the ion-induced DNA lesions. The GFP-p21 foci are seen as early as 0.5 min after irradiation, and show greatest brightness at about 7.5 min post-irradiation. Foci did not show any further changes during the time-course of observation. Note: at later times (i.e. > 8.5 min) the foci appear weaker due to photo-bleaching, caused by the close frame-rate of 15 sec (every 30 sec is pictured in Fig. 50).

2.8 Focal accumulation of p21 at the DNA lesions is independent of PARP-1

Poly(ADP-ribose) polymerase-1 (PARP-1) is the founding family member of the PARP super family. PARP-1 plays a role in the detection and signalling of DNA strand interruptions. It has been described to be involved in early DNA damage recognition [Fernet *et al.*, 2000], base excision repair [Dantzer *et al.*, 1998; Masson *et al.*, 1998] and genome surveillance [for review see Shall and DeMurcia, 2000]. Due to its early involvement in the DNA damage response, I studied whether the focal accumulation of p21 was dependent of the interaction with PARP-1 as it has been shown that PARP-1 binds to p21 [Frouin *et al.*, 2003]. For this experiment Dr. G. DeMurcia (University of Strasbourg) kindly provided mouse embryonic fibroblasts (MEFs) derived from both wild-type (PARP-$1^{+/+}$) and PARP-1 deficient mice (PARP-$1^{-/-}$). The available antibodies against human p21 did not detect the endogenously expressed mouse p21 in these cells (data not shown). Therefore, the MEFs were transiently transfected with the formerly constructed GFP-p21 plasmid (Sect. 2.7) to be able to observe ectopically expressed human p21 protein in this cell system.

The transfection and expression of GFP-p21 in PARP-$1^{-/-}$ cells was verified by Western Blot analysis using anti-GFP antibody. The WB in Fig. 51 displays a clear GFP-p21 signal for PARP-$1^{-/-}$ cells transfected with GFP-p21 (lane 2). Non-transfected PARP-$1^{-/-}$ cells do not show any signal after GFP detection (Fig. 51 lane 3).

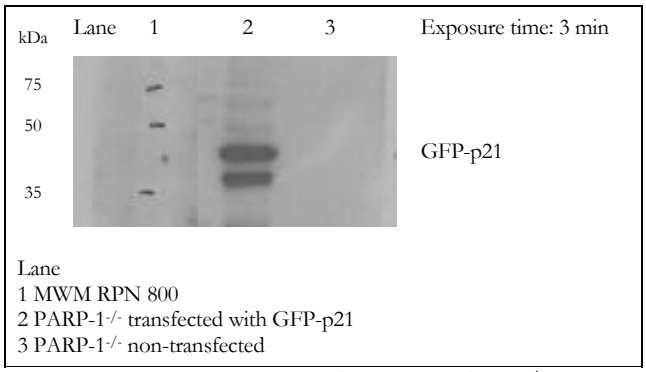

Fig. 51 **Western Blot to show the expression of GFP-p21 in PARP-$1^{-/-}$ cells.** Note: the bands of the used MWM runs higher with the here used NuPage SDS-PAGE than it should; with self-cast SDS-PAGE the GFP-p21 is detected at approx. 30 kDa MWM. WB: p21

Following verification of successful transfection and expression of the GFP-p21 plasmid as described above, transfected cells were irradiated with uranium ions 24 h after transfection. The cells were fixed 30 min post-irradiation without extraction of the soluble proteins (Sect. 4.4.1) and immunostained for γH2AX (Sect. 4.4.4). Mock-irradiated transfected PARP-$1^{-/-}$ cells show heterogeneous GFP-p21 levels as seen in Fig. 52 panel 1. After irradiation, clear green fluorescent foci are detectable, showing that GFP-p21 is able to form irradiation-induced foci in absence of PARP-1 (Fig. 52 panels B and C). Non-transfected PARP-$1^{-/-}$ cells do not show any

green fluorescence signal as expected (Fig. 52 D: mock-irradiated cells, E and F irradiated cells). The change in the γH2AX signals verifies the irradiation procedure. Unfortunately, γH2AX foci are only detectable in few nuclei (Fig. 52 F).

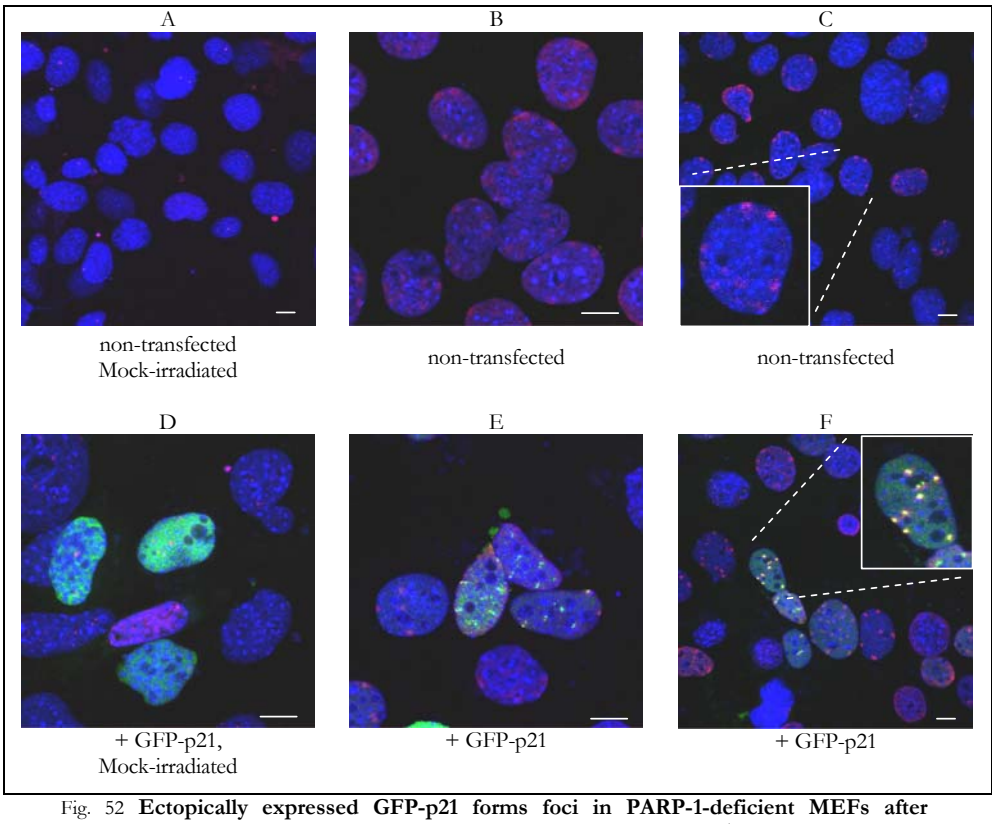

Fig. 52 **Ectopically expressed GFP-p21 forms foci in PARP-1-deficient MEFs after irradiation with uranium ions.** A, B and C non-transfected PARP-1$^{-/-}$ MEFs; D, E and F transiently transfected PARP-1$^{-/-}$ MEFs express GFP-p21 (green); A and D mock-irradiated; B–F 30 min post-irradiation with uranium ions (2×10^6 p/cm^2; 11.4 MeV/u; 14925 keV/µm). Stained for DNA (blue, ToPro-3) and γH2AX (red; unfortunately weak in this experiment). Non-transfected cells do not show any detectable green fluorescence, neither the mock-irradiated (A), nor the irradiated cells (B and C). Mock-irradiated cells transfected with GFP-p21 show a GFP-p21 expression (green) but no focal structures (D). Bar: 10 µm.

The mock-irradiated PARP-1$^{-/-}$ MEFs, transiently transfected to express GFP-p21, show ectopical expression of GFP-p21 in many nuclei, without any detectable focal accumulations (Fig. 52 D). Thirty min post-irradiation, clear focal accumulations of the GFP-p21 were detected in the PARP-1$^{-/-}$ MEFs cells transfected with the GFP-p21 plasmid (Fig. 52 E, F). Unfortunately, the γH2AX signal was very weak and distinct foci were only seen in few nuclei. Non-transfected PARP-1$^{-/-}$ MEFs cells did not have any green fluorescent signal 30 min post-irradiation (Fig. 52 D, E). These results demonstrate that the ectopically expressed GFP-p21 is able to form foci independently of PARP-1 in MEFs and in response to HI-induced DNA damage.

From these results I conclude that p21 foci formation at heavy ion-induced DNA lesions, at least at the time-points investigated and in this cell system, is not greatly dependent on the presence of PARP-1 expression.

2.9 p21 accumulates at DNA lesions in absence of XRCC1

The former experiment showed that p21 is able to recruit to foci independently of PARP-1. PARP-1 has been reported to detect and signal SSB and with this is involved in a very upstream step of the repair pathway. PARP-1 then recruits XRCC1 to the DNA lesion, which plays an important role in SSB repair and BER. El-Khamisy *et al.* showed that PARP-1 is required for the recruitment of XRCC1 at H_2O_2 induced DNA lesions [El-Khamisy *et al.*, 2003]. Here I elucidate whether XRCC1, which does not colocalise with p21 after H_2O_2 treatment as seen in Sect. 2.6 (page 66), is needed for the accumulation of p21 at HI-induced DNA lesions. For this, XRCC1 deficient hamster cells (EM9) and XRCC1 deficient hamster cells stably transfected with XRCC1-GFP were used. The cells were transiently transfected with the human wtp21 plasmid (Sect. 4.10.6), as the available p21 antibodies did not visualize the hamster p21 (data not shown). 24 h after transfection the cells were irradiated and fixed 30 min after exposure without extraction of the soluble proteins (Sect. 4.4.1). To confirm the successful transfection and expression of the human wtp21, non-transfected EM9 cells were investigated additionally.

Fig. 53 displays EM9 cells either transfected with wtp21 (Fig. 53 A and B) or non-transfected cells (Fig. 53 C and D). Mock-irradiated EM9 cells transfected with wtp21 clearly show expression of the human wtp21 protein (Fig. 53 A, red signal). Irradiated wtp21 transfected EM9 cells have irradiation induced accumulations of wtp21 (Fig. 53 B, red signal). Non-transfected EM9 cells do not have any detectable red fluorescence signal as expected, neither the mock-irradiated nor the irradiated samples (Fig. 53 C and D, respectively).

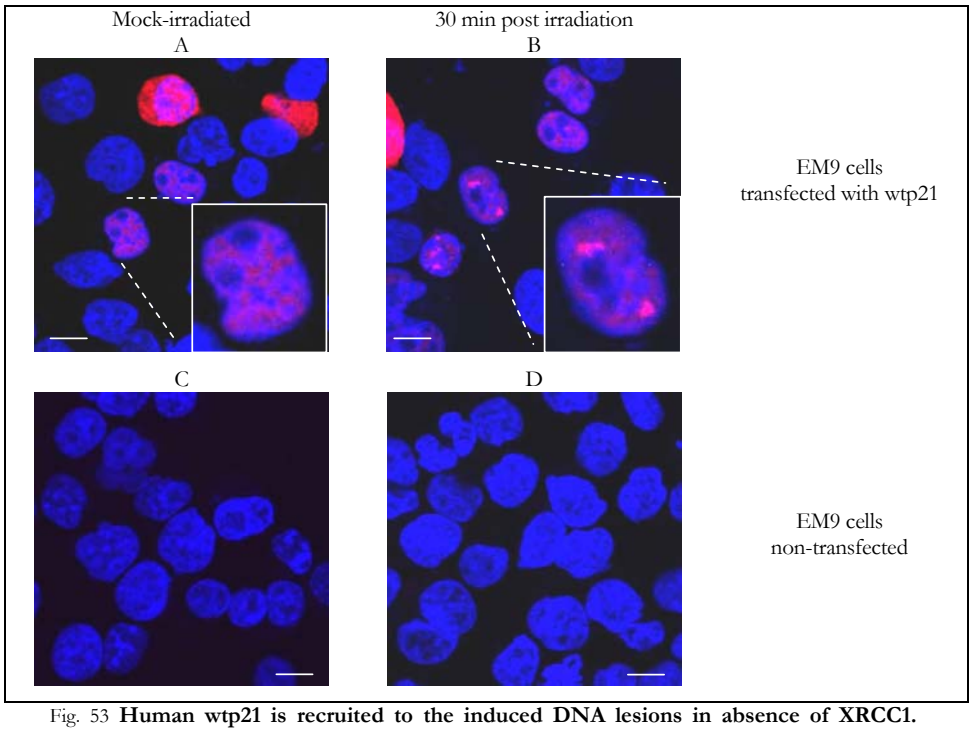

Fig. 53 **Human wtp21 is recruited to the induced DNA lesions in absence of XRCC1.** XRCC1 deficient hamster cells transiently transfected with human wtp21 show detectable wtp21 foci (red) after irradiation with Sm (3×10^6 p/cm^2; 11.4 MeV/u; 10290 V/µm) ions. A and B: EM9 cells transfected with wtp21. C and D: non-transfected EM9 cells. A and C: mock-irradiated. B and D: 30 min after exposure to Sm ions. DNA: blue (ToPro-3). Bar: 10 µm.

EM9 cells stably transfected with XRCC1GFP (EM9-XRCC1GFP) were treated as the EM9 cells above to confirm the obtained signal in the EM9 cells. Panel A (Fig. 54) shows mock-irradiated EM9-XRCC1GFP cells expressing the human wtp21 (red signal) without any wtp21 protein accumulations. 30 min after irradiation with Sm (3×10^6 p/cm^2; 11.4 MeV/u; 10290 V/µm) ions, XRCC1GFP (green) and wtp21 (red) foci are detected (Fig. 54 B and C, respectively).

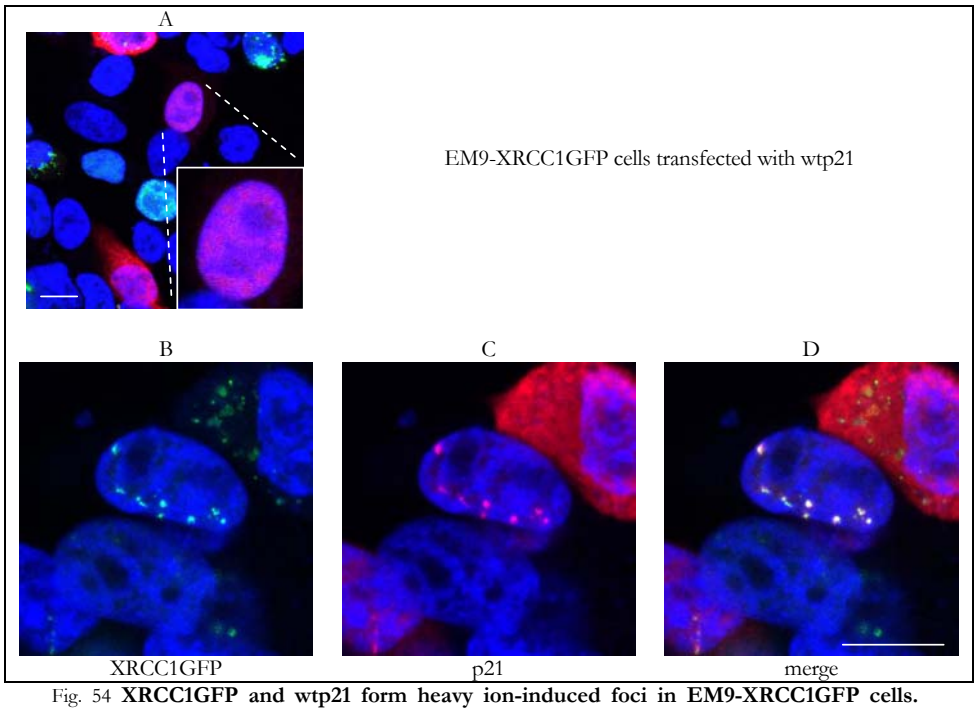

Fig. 54 **XRCC1GFP and wtp21 form heavy ion-induced foci in EM9-XRCC1GFP cells.** EM9 cells stably transfected with XRCC1GFP and transiently transfected with wtp21 show detectable Sm (3×10^6 p/cm²; 11.4 MeV/u; 10290 V/µm) ions-induced foci for both proteins (XRCC1: green, B and D; wtp21: red, C and D). A: mock-irradiated cells. B–C: 30 min after irradiation with Sm ions. DNA: blue (ToPro-3). Bar: 10 µm.

These results indicate that the ectopically expressed human wtp21 is able to accumulate at the heavy ions-induced DNA damaged sites in this cell system in absence of XRCC1.

2.10 Peptide mapping

As shown in Sect. 2.2 (page 31), p21 requires the intact interaction with PCNA to form irradiation-induced foci. This means that p21 is bound to PCNA at the DNA lesions as seen in Sect. 2.3 where both proteins were shown to be part of the chromatin associated protein fraction. For the p21-PCNA interaction p21 has to be dephosphorylated at threonine 145. Here, I aimed to show this irradiation-induced dephosphorylation of p21 by peptide mapping. With peptide mapping proteins are analyzed by separating and detecting the mixture of the peptides after enzymatic digestion of the protein of interest. With this method, a change in the phosphorylation status of a protein can be monitored. As the amount of protein assayed is very

small, the proteins are labelled with radioactive phosphor (^{32}P orthophosphate). Confluent NHDF cells and HeLa cells transfected with wtp21 to have a high p21 level were used for this experiment.

The cells were incubated overnight with phosphate-free culture medium at 37°C. The cells were exposed to 10 Gy γ-irradiation and labelled immediately with 2.5 mCi ^{32}P orthophosphate per plate as described in Sect. 4.11 (page 123) and incubated for 2.5 h at 37°C. The cells were lysed and p21 immunoprecipitation was carried out as described in Sect. 4.11. The immunoprecipitated complexes were separated by 12% SDS-PAGE which was dried and exposed to a hyperfilm (Amersham) film overnight. In Fig. 55 the autoradiograph is displayed, showing the 4 lanes of the prepared samples.

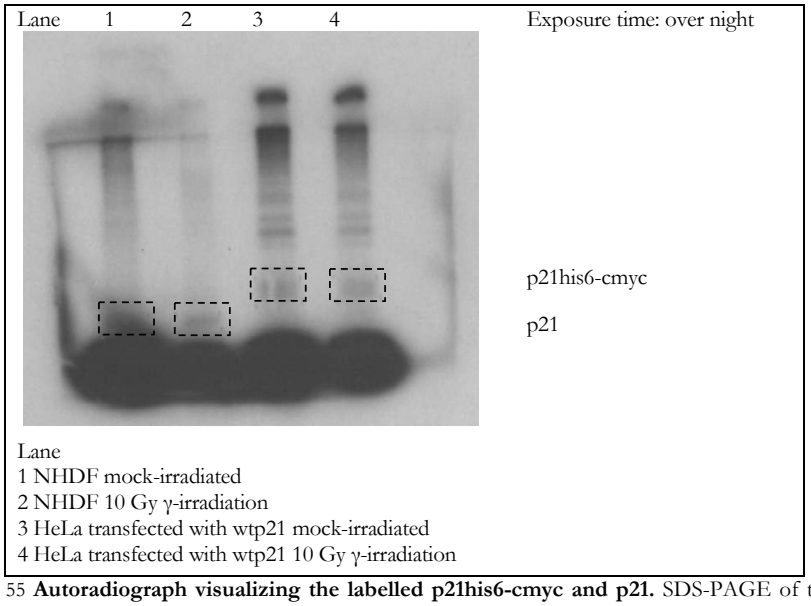

Fig. 55 **Autoradiograph visualizing the labelled p21his6-cmyc and p21.** SDS-PAGE of the immunoprecipitated complexes from the ^{32}P orthophosphate labelled samples. The rectangles show the areas of the gel which were excised from each lane, obtaining the ^{32}P orthophosphate labelled p21, and prepared for the 2-dimansional phosphopeptide mapping.

The areas of the gel where p21 or p21his6-cmyc were detected were excised and prepared for the 2-dimensional phosphopeptide mapping on thin-layer cellulose (TLC) plates as written in Sect. 4.11. This includes the digestion of the purified p21 with trypsin that specifically cuts after arginine (R) and lysine (K) leaving many small fragments (25 fragments with a length of 1–16 aa.). These peptides are then separated by 2-D electrophoresis on TCL plates. After the 2-dimensional electrophoresis, the TLC plates were exposed to a hyperfilm (Amersham) for 4 weeks and developed. Results are shown in Fig. 56 below.

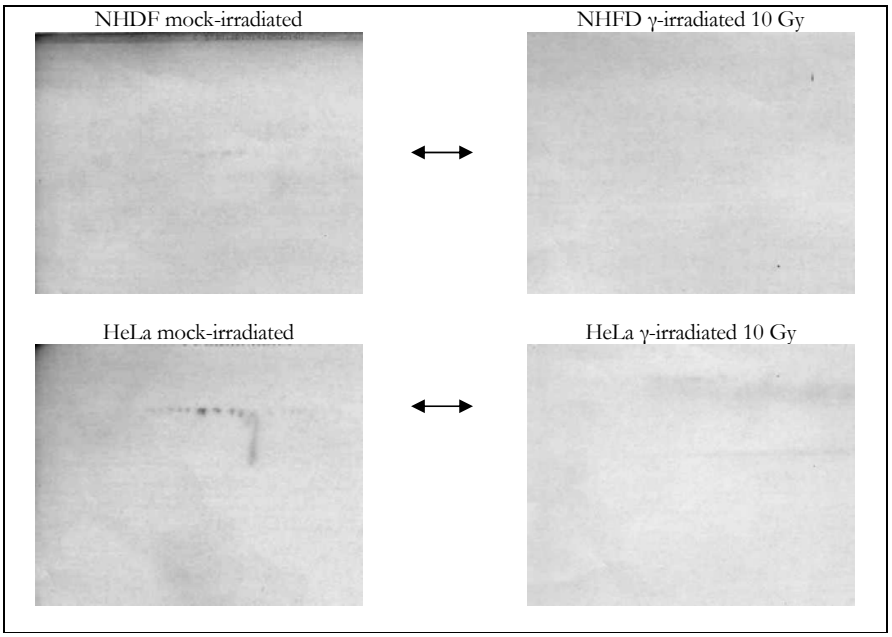

Fig. 56 **Autoradiographs of TLCs to demonstrate that p21 is dephosphorylated after 10 Gy γ-irradiation.** Mock-irradiated NHDF cells show hardly detectable spots on the film (upper left) which are not visible for the irradiated NHDF cells (upper right). The mock-irradiated HeLa cells transfected to express wtp21 show clear spots (lower left panel) whereas irradiated and transfected HeLa cells show no signal at all (lower right panel).

The mock-irradiated NHDF cells show a few faint spots as indicated by the arrow pointing to the left. However, at that exact same position no signal is obtained for irradiated NHDF cells (Fig. 56 upper two panels), indicating that dephosphorylation of p21 may have occurred in response to 10 Gy γ-rays. Nonetheless, the endogenously expressed p21 appears to be at very low levels in NHDFs precluding the definite detection of a clear dephosphorylation event. On the other hand, the higher amount of the ectopically expressed wtp21 in the HeLa cells clearly suggests that p21 is dephosphorylated in these cells in response to 10 Gy γ-rays (Fig. 56 lower two panels).

These results implicate the dephosphorylation of p21 after DNA damage-induction by γ-irradiation. This dephosphorylation is likely to enable the interaction between p21 and PCNA which has been shown to be a crucial factor for the ability to form p21 foci at HI-induced DNA lesions (Sect. 4.2).

3 DISCUSSION

Ionizing radiation induces DNA lesions that lead to the activation of complex damage response pathways in mammalian cells. In one of these pathways the p21 protein, which is one of the main cell cycle-depended kinase inhibitors, is induced via stabilisation of TP53 after DNA damage. TP53 regulates p21 on the transcriptional level, which in turn inhibits CDK and results in hyperphosphorylation of the Rb protein, leading to G1 arrest [El-Deiry *et al.*, 1993; Deng *et al.*, 1995; Brugarolas *et al.*, 1995]. However, recent studies suggest additional functions for p21 in diverse cellular processes such as DNA repair and apoptosis [review: Gartel *et al.*, 2002; Livneh, 2006; Janicke *et al.,* 2007].

In this thesis I aimed to elucidate a function for p21 at radiation-induced DNA lesions. PCNA, a well known interaction partner of p21, played an essential role in my investigations as it is known to be active in both DNA repair and replication [Tsurimoto, 1999; Warbrick, 2000; Maga and Hübscher, 2003]. Furthermore, I anticipated to correlate the formation of p21 foci after DNA damage to the occurrence of specific DNA lesions by investigating the co-localisation of DSB- and SSB-related proteins with p21.

3.1 Protein accumulations at charged particle-induced DNA lesions

Charged particle irradiation has been shown to be a powerful tool to investigate the response of certain proteins to the DNA lesions induced. In the past, our lab has shown that p21 forms distinct HI-induced foci [Jakob *et al.*, 2000] which colocalize with the sites of particle traversal [Scholz *et al.*, 2001] together with other DNA repair-related proteins such as hMre11, Rad50 or PCNA [Jakob *et al.*, 2002] and γH2AX [Jakob *et al.*, 2003]. Interestingly, the persistence of the HI-induced p21 foci increased with the LET of the ion [Jakob *et al.*, 2002]. These data suggested an involvement of p21 in DNA repair or damage recognition. In my Diploma Thesis [Heede, 2002], I was able to show that the presence of p21 status does not affect cell survival or DSB rejoining in HCT116 cells after exposure to X-rays. The p21 focus was shown to be a dynamic entity with p21 turnover at the HI-induced DNA lesion. Furthermore, the HI-induced p21 foci were independent of *de novo* protein synthesis.

3.1.1 p21 and PCNA show similar kinetics for heavy ion-induced foci formation

Both p21 and PCNA were detected as early as 2 min after exposure to uranium ions. Interestingly, the number of nuclei displaying PCNA foci appeared to be higher than the number of nuclei with p21 foci (51 versus 41 out of 69 analysed nuclei, respectively). However, both proteins formed foci in many nuclei (31 out of 69 analysed nuclei). Nonetheless, my

observation that PCNA foci are present in more nuclei than p21 foci needs to be interpreted with caution, as these proteins are likely to be extracted to different degrees which could result in a visualization problem as the number of protein molecules is a limiting factor for foci detectability (for example, it has been shown by Scheer *et al.* [1984] that 70–190 RPI molecules of an actively transcribing rRNA gene are needed to visualize individual transcription units by indirect immunofluorescence). This is also supported by my data showing that more nuclei show p21 foci after irradiation with uranium ions compared to irradiation with chromium ions. As early as 2 min after uranium irradiation, 95% of the nuclei showed detectable p21 foci and 100% PCNA foci (n = 76), compared to 54% of p21- and 81% of PCNA-positive nuclei after irradiation with chromium ions (n = 81). Uranium ions of 11.4 MeV/u have a much higher LET (14925 keV/µm versus 2810 keV/µm), resulting in a massive number of ionisation events along the trajectory, leaving far more DNA lesions of high complexity by passing the nucleus compared to the used chromium ions with lower LET (11.4 MeV/u; 2810 keV/µm). Due to the higher amount of total DNA lesions induced along the trajectory, more repair related proteins are accumulated, leading to a better detectability. That not all nuclei display clear p21 accumulations after HI-exposure could be caused by the heterogeneous expression level of this protein, as detected after p21 immunostaining [Fournier *et al.*, 2007]. Even if G_1-phase fibroblasts were used, which express a high level of p21 [Cai and Dynlacht, 1998], a heterogeneous nuclear expression level of p21 was observed if the soluble protein fraction was not extracted.

When live-cell imaging was used employing a GFP-p21 construct to examine very early times after HI irradiation, alterations in protein detection limits due to the indirect immunofluorescence method were avoided. As observed for endogenous p21, GFP-p21 accumulated at the HI-induced DNA lesions. The live-cell imaging experiments demonstrated that GFP-p21 accumulates at the HI-induced DNA lesions within 30 s after exposure to krypton ions (Sect. 2.7.2; page 71). Interestingly, using live-cell imaging Perucca *et al.* [2006] have recently shown that both p21 and PCNA are recruited very fast to laser-induced (405 nm) DNA lesions. Their results display that p21-GFP could be detected at 12 s after the laser irradiation, whereas RFP-PCNA already was visible as early as 4 s after exposure, suggesting that p21 recruitment follows the recruitment of PCNA at these laser-induced DNA lesions.

3.1.2 Heavy ion-induced DNA lesions are complex and individual SSBs and DSBs can not be identified by immunofluorescence

To obtain a more dispersed distribution of the DNA lesions and with this to be able to discriminate DNA lesions of different nature along the particle trajectory, the irradiation geometry was changed (Sect. 2.1; page 22) as described in Jakob *et al.* [2003]. With this method cells were irradiated with an angle of the beam towards the cell monolayer of less than 5°. To discriminate between the induced DSBs and SSBs, the DSB-related proteins γH2AX or 53BP1 and SSB-related protein XRCC1 were stained.

As described in Sect. 2.1 (page 22), streaks of p21 were found to co-localize with streaks of both 53BP1 and XRCC1 as early as 2 min after HI irradiation. These results are in line with former results obtained in our lab, where it was shown that p21 and γH2AX localize at the same sites

along the particle trajectory [Jakob *et al.*, 2003]. After immunodetection of γH2AX in combination with XRCC1, a very similar localization along the trajectory was detected. The XRCC1 signal however, was detected in smaller areas ('microfoci') within the larger streaks of γH2AX (Sect. 2.1.4; Fig. 19). That the area of detectable γH2AX signal is larger than the XRCC1 signal could be explained by the fact that the phosphorylation of H2AX in the vicinity of a DSB spreads over a region of ca. 50 kb surrounding the lesion [Shroff *et al.*, 2004]. Interestingly, Shroff *et al.* [2004] found that within 1–2 kb of the break only very little γH2AX could be detected, where other repair proteins were localized. Furthermore, Bekker-Jensen *et al.* (2006) have shown that single stranded DNA (ssDNA) can be visualized as microfoci within laser induced γH2AX streaks, displaying a similar picture to the here detected XRCC1 microfoci. This may suggest that the XRCC1 microfoci present ssDNA within the HI-induced protein streaks, in line with the described function for XRCC1 in SSB repair. Nonetheless, as the XRCC1 microfoci are localized within the γH2AX signal, I conclude that with the experimental setup used here, DNA lesions of different nature cannot clearly be distinguished after HI irradiation using immunofluorescence. Due to the fact that heavy ions produce a large spectrum of highly clustered DNA lesions, proteins from many different repair pathways (e.g. DSB repair, SSB repair, BER repair, NER repair) accumulate along the sites of particle traversal, such that the individual components of specific repair pathways cannot be distinguished from each other. The HI-induced protein streaks however, appeared to change with time as they became more dispersed with increasing time after exposure (p21/53BP1 and γH2AX/XRCC1 at 5 h after irradiation with Fe ions; Sect. 2.1.2 and 2.1.4, respectively), as if the protein tracks slowly dissolve, suggesting that DNA repair has taken place or chromatin domain movement during lesion procession as described by Aten *et al.* [2004]. The repair of the induced DNA lesion over time would be in line with the observation that the number of nuclei scored with p21, 53BP1 or γH2AX streaks was clearly reduced at 16 h after irradiation. The DNA repair after high-LET irradiation however is shown to be delayed and more difficult than low-LET irradiation, reflecting an unfaithful repair due to the high clustered DNA damages induced [Löbrich *et al.*, 1996; Equchi-Kasai *et al.*, 1996; Okayasu *et al.*, 2006].

The time after which the protein streaks were visible varied between the experiments (as seen for p21 in Sect. 2.1.1 versus Sect. 2.1.2 where p21 streaks were detected up to 16 h post Fe ions irradiation or not, respectively). These variations could be due to the experimental procedure that includes many steps before the final microscopic analysis limiting the conclusions that can be made regarding the kinetics and quantitative analysis.

Interestingly, the protein tracks (p21, γH2AX, 53BP1, aprataxin and XRCC1) did not display continuous tracks throughout the nucleus, but showed areas apparently free of protein. This discontinuous accumulation along the particle trajectory was detected for p21, γH2AX, 53BP1, aprataxin and XRCC1 and has been described also for PCNA and MRE11B in a previous study from our lab [Jakob *et al.*, 2003]. The nucleoli, visualized by the reduced DNA staining, were spared out of the detected protein tracks in all samples, leaving no detectable streaks. Particle trajectories displayed by protein staining could be detected at the nucleoli boundaries, but never throughout the nucleoli. Differences in the content, compaction and accessibility of the DNA have also been suggested to account for this observation [Bakkenist and Kastan, 2003; Jakob *et al.*, 2003; Kruhlak *et al.*, 2006]. Costes *et al.* [2007] recently showed that DNA damage-induced foci are detected more frequently in regions with low DNA density and especially at the boundaries between high and low DNA density. Furthermore, Kim *et al.* [2007] have shown that

H2AX is not efficiently modified in heterochromatin after DNA damage induction in yeast and mice embryonic fibroblast cells.

It must be noted, that 53BP1 and γH2AX showed focal accumulations in many of the mock-irradiated nuclei, likely to be localizing to spontaneously generated DSBs or at replication forks in S-phase cells as mentioned in literature before [Ward *et al.*, 2001; Sengupta *et al.*, 2004; Halicka *et al.*, 2005]. Costes *et al.* [2007] for example scored 1–5 DSB foci in 11% of nonirradiated human fibroblasts. Tumour cells seem to display overall more foci in more of the nonirradiated cells as Banath *et al.* [2004] described that 20–66% nuclei showed 1–54 foci, depending on the cell type.

3.1.3 Ectopically expressed GFP-p21 is recruited to the HI-induced DNA lesions independently of PARP-1 and XRCC1

PARP-1- (poly(ADP-ribose) polymerase-1) or XRCC1- (X-ray cross complementing factor 1) deficient cell lines were used to elucidate whether these two proteins are essential for the recruitment of p21 to the HI-induced DNA lesions and to investigate a possible role for p21 in BER or SSB repair. PARP-1 has been shown to play a key role in BER/SSB repair by its early binding to SSBs and subsequent activation modifying itself and other target proteins [for review see Amé *et al.*, 2004]. It has also been shown by El-Khamisy *et al.* [2003] that PARP-1 is required for the recruitment of XRCC1 at oxidative DNA damaged sites which are repaired by BER. My results from Sect. 2.8 (page 73) show that the accumulation of ectopically expressed GFP-p21 to the heavy ion-induced DNA lesions occurs independently of the presence of PARP-1. This means that after heavy ions, p21's recruitment is not dependent on the early PARP-1 signalling. XRCC1 has been shown to interact with PARP-1 [Masson *et al.*, 1998; Dantzer *et al.*, 2000; Schreiber *et al.*, 2002] and also plays an important role in both BER and SSB repair [for review see Caldecott, 2001]. It has been described to coordinate the assembly of repair complexes at the DNA damaged sites [Okano *et al.*, 2003; review: Caldecott, 2003] and XRCC1-deficient cells show a reduced rate of SSB repair [Thompson *et al.*, 1982]. In Sect. 2.9 (page 75) I show that the GFP-p21 foci formation occurs in absence of XRCC1 (EM9 cells), although the GFP-p21 accumulations are not as distinct as observed for the XRCC1 wild type cells. This may be caused due to the findings of Fan *et al.* [2004] where they propose that XRCC1 colocalizes and physically interacts with PCNA at replication foci in S-phase HeLa cells to facilitate the single-strand break repair. Also, Lan *et al.* [2004] have shown that PCNA recruits to DSBs but not to SSBs induced by laser irradiation in absence of XRCC1. Taken these findings together with my observation that p21 accumulates at the HI-induced damaged DNA sites independently of XRCC1 and PARP-1 and, that p21 is shown to be dependent of PCNA for its foci formation, as discussed below, suggests that PCNA is recruited to these lesions independently of these proteins as well. This leads to the assumption that the seen GFP-p21 foci display the induced DSBs after HI-irradiation where PCNA also is recruited independently of XRCC1. The difference in foci structure should be investigated further with better microscopic analysis. Nonetheless, the fact that the GFP-p21 fusion protein accumulates in an irradiation dependent manner in absence of PARP-1 or XRCC1 suggests that p21 has no major role downstream the PARP-1- and XRCC1-dependent DNA repair pathways.

3.2 p21 and PCNA interact at irradiation-induced DNA lesions

Very similar kinetics for PCNA and p21 accumulations at HI-induced DNA damaged sites was shown in Sect. 2.2.1 (page 31), leading me to elucidate whether the direct interaction of p21 with PCNA is required for p21 foci formation at these lesions. As the used immunofluorescence studies can not determine whether two proteins physically interact, immunoprecipitations were carried out to test the interaction of PCNA with mutant forms of p21 disrupting its interaction with PCNA. DNA lesions were provoked by HI to elucidate the necessity of an intact p21-PCNA interaction. I addition, the chromatin-association of p21 and PCNA was investigated after X-ray induced DNA lesions.

3.2.1 PCNA is required for the accumulation of p21 at heavy ion induced DNA lesions

Three forms of p21 were expressed in human cells to asses the necessity of an intact PCNA binding site for p21 foci formation: wtp21 plasmid containing the full-length p21 ORF, p21T145A and p21T145D [Rossig *et al.*, 2001]. As observed by Rossig *et al.* for human umbilical cord cells, the interaction of ectopically expressed wtp21 or p21T145A with PCNA was observed for HeLa and HCT116 cells in my study (Sect. 2.2.3, page 38). Furthermore, both proteins accumulated at HI-induced DNA damaged sites (Sect. 2.2.5, page 42). The phospho-mimetic p21 construct p21T145D was shown not to interact with PCNA (Sect. 2.2.4, page 40) similarly as described by Rossig *et al.* [2001]. Interestingly, it was not recruited to the HI-induced DNA lesions (Sect. 2.2.6, page 47). My results show that the accumulation of p21 at HI-induced DNA lesions requires the physical interaction between p21 and PCNA.

Former immunocytochemical results from our lab however, indicated that PCNA binding to particle-induced DNA lesions is not required for p21 to remain localized to foci [Jakob *et al.*, 2002]. One could argue that if PCNA acts as a loading dock for proteins, as suggested by Balajee and Geard [2001], p21 is able to stay at the lesion after it once is recruited. In my Diploma Thesis [Heede, 2002] though, I concluded that the p21 foci are a dynamic entity with p21 turnover, meaning that a quantity of PCNA is needed at the DNA lesion for p21 recruitment. That my results disagree with former findings from our lab is most probably due to the used method. As described above, the detection by indirect immunostaining has some difficulties and limits the outcome of kinetic studies. Possibly, a minor amount of PCNA which was not detectable with the immunohistochemical staining method used may be enough to recruit a detectable quantity of p21. The dependency of PCNA for the p21 recruitment at HI-induced DNA lesions shown in this thesis is sin accordance with the behaviour during NER repair revealed by the live-cell imaging recently done by Perucca *et al.* [2006] where the RFP-PCNA fusion protein appeared to be slightly faster visible at laser-induced DNA lesions than the p21-GFP fusion protein.

Interestingly, a delayed response of both p21 and PCNA to DNA damage induction by UVC light in XPA defecient cells (XPA cells) which are not able to carry out NER, compared to AG

cells that are proficient for NER was shown by D. Fink *et al.* [2006]. This indicates that also after UVC irradiation p21 and PCNA are both accumulated at an early timepoint at DNA lesions which are mainly repaired by NER, confirming a role for p21 in NER [Perucca *et al.*, 2006]. That p21 may play a role in NER through binding to PCNA supports findings of McDonald *et al.* [1996] who showed that cells with an intact p21-PCNA interaction were able to carry out NER, cells expressing a mutant p21 form, not able to interact with PCNA, however, were NER deficient. The delay of the accumulation in XPA deficient cells could implicate that as the NER pathway is inhibited other repairpathways, leading to p21 and PCNA recruitment, are activated. Paralell experiments with DNA lesion induction by HI revealed no difference in the appearance of p21 or PCNA foci in XPA and AG cells, which is in line with the fact that many different DNA lesions are induced due to the clustered nature of HI-induced DNA lesions and with this several repair pathways are activated.

The fact that p21 needs an intact PCNA binding site was also supported by the phosphorylation status studies performed in this thesis using p21 peptide-mapping. However, peptide-mapping was performed after exposure to high doses of γ-rays as the necessity to obtain large amounts of p21 existed. Following exposure to HI, presumable overall smaller amounts of p21 are recruited to the DNA damaged sites. Here, I was able to show that p21 indeed is dephosphorylated following DNA damage induction by γ-rays. This suggests that a part of p21 is dephosphorylated by which it becomes capable to interact with PCNA and possibly gather at the induced DNA lesions.

3.2.2 p21 and PCNA are both part of the chromatin-bound protein fraction after X-ray exposure

The similar kinetics of p21 and PCNA recruitment to the HI-induced DNA lesions and the PCNA dependency for p21 accumulation at these damaged DNA sites made me investigate a possible association of p21 and PCNA with the damaged DNA. The lesions induced by HI irradiation however, recruit only a small amount of the total protein to the charged particle-induced DNA lesion trajectories. To investigate a chromatin-associated protein fraction, a large amount of protein is needed. For this reason, homogenously distributed DNA lesions were induced by exposure of the cells to X-rays to provoke a large quantity of DNA lesions and with this recruitment of large amounts of p21 and PCNA to the DNA damaged sites.

The establishment of a successful and reproducible method to analyse an irradiation induced chromatin-bound protein fraction of human fibroblasts after DNA damage induction appeared to be a major problem. After several modifications I finally succeeded in separating the soluble protein fraction from the chromatin-associated protein fraction (Sect. 2.3.3, page 54). In this chromatin-associated protein fraction, both p21 and PCNA were detected after X-rays using Western Blot analysis, and no chromatin-associated p21 or PCNA was detected in mock-irradiated AG cells. At 3 h after exposure an increased fraction of PCNA was chromatin-associated compared to earlier times after X-irradiation. Similarly, when compared to lower X-ray doses (8 Gy) higher X-ray doses (30 Gy) lead to an increasee in the fraction of chromatin-associated PCNA. The amount of chromatin-associated p21 after 30 Gy X-rays appeared to be clearly lower than detected for PCNA, although likely variations in antibody affinities need to be

taken into account. Interestingly, a higher p21 level was detected at 3 h after exposure than at 1 h post irradiation and the contrary was seen for PCNA. The elevated p21 signal 3 h post exposure may be due to the fact that more p21 protein is available at later times post irradiation due to the irradiation-induced induction of p21 by TP53. The observed reduction of PCNA at later times post irradiation appears to be in line with suggestions by others who have postulated, that p21 releases PCNA from the DNA after UV irradiation [Savio *et al.*, 1996; Stivala *et al.*, 2001]. In the same line, former results from our lab showed that p21 is still detectable in foci at 4 h after exposure to carbon ions whereas PCNA is not [Jakob *et al.*, 2002].

The binding of p21 to PCNA has been shown to block the DNA synthesis [Waga *et al.*, 1994]. This has been supported by Cazzalini *et al.* [2003] who proposed that p21 does not interfere with the loading of PCNA at DNA replication sites, but inhibits the subsequent binding of DNA pol δ at the G1/S phase transition, suggesting that p21 can act as a switch between DNA repair and replication for the function of PCNA. By inhibiting DNA synthesis but not repair its cell cycle inhibitor function is supported as to gain time for the repair process without retarding the DNA repair efficiency. Furthermore, Frouin *et al.* [2003] have suggested that the association of chromatin-bound p21 with PARP-1 may avoid an interaction of p21 with PCNA, enabling PCNA to be recruited to DNA lesions. This finding is not supported by my results, as I have shown that p21 recruitment is dependent on PCNA (Sect. 2.2, page 31) and that the accumulation of p21 at the damaged DNA sites is independent of PARP-1 as described in Sect. 2.8 (page 73).

3.3 p21 accumulations can not clearly be correlated to either DSBs or SSBs

The accumulation of p21 at the HI-induced DNA damaged sites could not be related to a specific DNA lesion due to the highly clustered nature of the DNA damage induced as discussed in Sect. 3.1.2 (page 81). This made me try to visualise p21 after DNA damage induction by X-rays, CPT and H_2O_2 as they mainly provoke homogenously distributed SSBs with some additional DSBs.

3.3.1 X-rays induce distinct p21 foci that do not colocalize with DSB repair proteins.

The DNA damage induction by X-rays lead to distinct p21 foci in AG cells (Sect. 2.4, page 56). The X-ray-induced p21 accumulations appeared to be time dependent with good detectability at 3 h after exposure, mirroring the increase in the chromatin-associated p21 fraction at this time point as discussed in Sect. 3.2.2 above. Also, an increase in the number of p21 foci with an increase in X-ray dose (2 Gy to 10 Gy) was observed, underlining that p21 recruitment is induced in a dose (i.e. DNA damage) dependent manner.

Parallel immunostaining of p21 with the DSB-related proteins γH2AX, 53BP1 or TP53 clearly showed a higher fraction of p21 foci than γH2AX, 53BP1 or TP53 foci induced after exposure to 8 Gy X-rays (Sect. 2.4.4, page 60). Furthermore, colocalisation analyses by Scion Image resulted in no detectable colocalisation of p21 with any of the tested DSB repair proteins. My preferred view of these observations is that p21 does not accumulate at X-ray-induced DSBs but rather is gathered to X-ray-induced SSBs. However, I did not detect the SSB repair-related protein XRCC1 in foci after X-rays. Potentially, XRCC1 already have vanished at 3 h post exposure or the level of accumulated XRCC1 protein may have been too low for its detection by immunostaining. It has been described by Thompson *et al.* [1990] that XRCC1 deficient cells are 1.8-fold more sensitive to γ-irradiation, demonstrating a role for XRCC1 in the repair of radiation damage. Also, it has been reported that XRCC1 is recruited DNA SSBs by its BRCT1 domain shortly after DNA damage induction [Okano *et al.*, 2003; El-Khamisy *et al.*, 2003; Ame *et al.*, 2004]. Further studies should be performed to clarify a possible colocalization of p21 and XRCC1 at X-ray induced DNA lesions.

Interestingly, the X-ray irradiation-induced p21 foci were not detected in neonatal human fibroblasts (data not shown). I presume that these cells have a lower p21 level, preventing detectable p21 protein accumulations. Experiments to elucidate whether the low p21 expression level is the reason could be done by incubation of the cells with a proteasome inhibitor, such as lactacystine, by which the p21 levels are artificially elevated.

3.3.2 Hydrogen peroxide induces punctuate accumulations of p21 that do not colocalize with the SSB repair protein XRCC1.

Since, after X-rays, focal accumulations for XRCC1 could not be detected, camptothecin (CPT) and hydrogen peroxide (H_2O_2) were employed. However, treatment of AG cells with CPT did not result in visible p21 accumulations (Sect. 2.5, page 64). The overall nuclear p21 level was slightly elevated after treatment and following extraction, suggesting that p21 is bound to some intra-nuclear structure partially preventing its extraction from treated nuclei (note: this phenomenon was not observed for nuclei from non-treated cells). For XRCC1, no CPT-induced foci were detected, but it was observed, that the XRCC1 level within the nucleoli changed after CPT treatment. The XRCC1 level in the nucleoli was reduced after CPT treatment, suggestive for a translocation of XRCC1 from the nucleoli to the CPT-induced damaged DNA sites. That the protein accumulations at the CPT-induced DNA lesions could not be detected may be due to the amount of protein localised at the single lesions or be caused by a difference in accessibility of the DNA lesions due to the binding of Top I. Others have shown that cells lacking XRCC1 are about 3-fold more sensitive to CPT treatment than wild type cells [Caldecott *et al.*, 1991; Barrows *et al.*, 1998], proposing that XRCC1 is involved in the repair of CPT lesions.

The incubation with H_2O_2 resulted in homogenously distributed punctuate accumulations of both p21 and XRCC1 (Sect. 2.6, page 66). A role for XRCC1 in the repair of oxidative DNA damage was described earlier with XRCC1-deficient cells being about 2-fold more sensitive to hydrogen peroxide [Cantoni *et al.*, 1987] and H_2O_2 induced recruitment of XRCC1 in XRCC1 wild type cells [El-Khamisy *et al.*, 2003]. In my experiments, the H_2O_2-induced p21 and XRCC1

accumulations did not colocalise. Here it must be noted, that the concentration of H_2O_2 (0.2 mM) at which the punctuate protein pattern was observed lead to a considerable amount of DNA damages, inducing a high number of protein accumulations throughout the nucleus. This complicates colocalisation evaluation as foci may partially colocalize randomly. Further investigations should address this issue more carefully. It has recently been described by Levy *et al.* [2006] that XRCC1 may also be part of the DSB response after X-ray irradiation. They speculate that after replication fork stalling XRCC1 may direct the repair to the NHEJ repair pathway which is in line with others who have suggested an additional role for XRCC1 in DSB repair [Audebert *et al.*, 2004]. Taken together, one could speculate that the seen accumulations of XRCC1 after H_2O_2 treatment do not only display SSBs which was aimed. However, the H_2O_2-induced XRCC1 accumulations observed in my experiments do not colocalize with the visualized DSBs. Audebert *et al.* [2004] described a role for XRCC1 in an alternative route for DSB repair, meaning that if the normal DSB repair pathways are intact, XRCC1 may not be recruited at the induced DSB. This makes me assume that the H_2O_2-induced XRCC1 accumulations shown in this thesis do visualize SSBs, implicating that p21 is not part of the XRCC1-related SSB repair pathway.

Interestingly, Hwang *et al.* [2007] have shown that H_2O_2 at higher concentrations induces nucleocytoplasmatic translocation of p21 via two nucleolar export signals (NES) and degradation of the cytoplamatically localized p21. It is suggested, that depending on the oxidative stress cells are exposed to, proteins may be translocated and change function.

Immunostaining of γH2AX showed that DSBs were also induced by treatment with 0.2 mM H_2O_2 (Sect. 2.6, page 66). This observation is contradictive to former results described in literature, where no DSBs were formed with H_2O_2 concentrations of below 0.3 mM [Ismail *et al.* 2005]. These authors describe that ATM is not activated by H_2O_2 treatment below 3 mM and, using the FAR assay they conclude that no DSBs are induced after treatment with 0.3 mM H_2O_2. However, this assay is not very sensitive and can only detect DSBs down to 10 Gy, a dose expected to generate 200-500 DSBs per cell [Ismail *et al.* 2005]. With the immunohistochemical staining used in this thesis DSBs can be detected after an X-ray dose of 50 mGy, leading to approximately 3 DSB per cell as done in our lab by Y. Schweinfurth [PhD. Thesis, 2007]. Also, Rothkamm and Lobrich [2003] quantified DSBs by immunostaining after an X-ray dose down to 1 mGy. Ismail *et al.* [2005] estimated that < 0.1% of the total DNA strand breaks induced by 3 mM H_2O_2 are DSBs and describe that approximately 30000 SSBs per cell are induced at 0.2 mM H_2O_2. Taken their results together and assuming a linear dose-response relationship, less than 30 DSBs per cell would be induced by 0.2 mM H_2O_2, which explain my observations for γH2AX foci formation.

3.4 Conclusions

The results obtained during this thesis show that p21 accumulates at damaged DNA sites after HI-, X-ray- and H_2O_2-induced DNA lesions. The p21 recruitment at HI-induced lesions is dependent on an intact interaction of p21 with PCNA. Furthermore, p21 and PCNA are chromatin-associated after X-ray irradiation. Unfortunately, I was not able to directly connect p21 to either DSBs or SSBs, but the results suggest that p21 is not directly involved in the repair of DSBs induced by HI or X-ray irradiation. This supports the findings during my Diploma Thesis, where p21 was shown not to play a major role in DSB repair based on DSB rejoining and cell survival experiments [Heede, 2002].

My hypothesis is that p21 acts more as a switch on repair processes by occupying the binding site on PCNA than as a protein being itself directly active in the DNA repair. The results obtained by McDonald *et al.* [1996] indicated that the binding of p21 to PCNA modulates the ability for NER repair, as only cells capable of the p21-PCNA interaction were able to carry out NER. This could be caused by the fact that when the p21 binding site of PCNA was not occupied, other proteins had the chance to interact with PCNA and by this possibly inhibiting NER. Thus, due to its PCNA interaction, p21 can be recruited to damaged DNA sites, yet is not directly active in the DNA repair itself. This could also be the case here for lesions not related to NER. The p21 protein seems to have a function as regulator protein, guiding other proteins to specific pathways. A model supporting a regulatory function has previously been described by Livneh [2006] and Avkin *et al.* [2006] for a role of p21 in translesion DNA synthesis (TLS; see Prakash and Prakash, [2002]), where the authors postulate that the p21 binding to PCNA causes the release of pol δ from PCNA and the DNA, leading to synthesis arrest.

Perucca *et al.* [2006] stated that the p21 response seems to be independent of the type of DNA lesion, but related to PCNA dependent repair pathways. The independency of the type of DNA lesions is not supported by the results in this thesis, as it is clearly shown not to be DSB related after DNA damage induction by exposure to X-rays or H_2O_2 as seen in Sect. 2.2.4 and Sect. 2.6, respectively. The relation to PCNA however is in line with the shown chromatin association of both p21 and PCNA after X-ray exposure (Sect. 2.3.3) and the findings of D. Fink *et al.* [2006] in XPA cells where both p21 and PCNA are recruited with a similar delay after UVC irradiation in contrast to the immediate recruitment following exposure to heavy ions.

On the basis of the kinetic studies on p21 and PCNA accumulation to UV-laser-induced DNA lesions carried out by Perucca *et al.* [2006] further studies should be preformed aimed at investigating the early kinetics of p21 and PCNA at ionizing radiation-induced DNA lesions as produced by heavy ions. The use of differentially tagged constructs of these two proteins, allowing the live-cell imaging of both proteins in the same cell, will shed light on the hierarchy of PCNA and p21 associated to repair processes other than NER.

4 METHODS

4.1 Cell cultivation

All cell types were cultivated at 37°C with 5% CO_2 and 95% humidity. Depending on the experimental outline, the cells were grown either on Ø 30 mm cover slips (Menzel-Gläser, Braunschweig, Germany), in Ø 32 mm or Ø 150 mm petri dishes (Nunc, Roskilde, Denmark) or in 25 cm^2 or 75 cm^2 culture flasks (Falcon, BD Biosciences, CA, USA). The following cell types were used:

4.1.1 Finite lifespan normal human fibroblasts

Two different human fibroblast strains were used: normal human foreskin fibroblasts (AG1522C) and neonatal human dermal fibroblasts (NHDF).

AG1522C cells (in further context described as AG cells) were obtained from the Coriell Cell Repositories (Camden, NJ, USA) and were derived from a 3 day-old healthy infant. The AG cells that were utilized in the experiments described below were at 20–30 cumulated population doublings (CPD) and at passages 8–15.

The neonatal human dermal fibroblasts, referred to as NHDF in the following, were obtained from CellSystems Biotechnologie (St. Katharinen, Germany). As NHDF reach confluence faster than AG cells they were preferred in some of the experiments and were used at 11–20 CPD and passage number 6–12.

The CPD gives the total number of the population doublings (PD) of a cell population and is calculated as follows:

$$PD = \frac{\ln\left[\frac{N}{N_0 \times PE}\right]}{\ln 2}$$

$$CPD = \sum PD$$

PD: population doublings N: no. of cells harvested N_0: no. of cells seeded PE: plating efficiency
CPD: cumulative population doublings Σ PD: total no. of population doublings

Both cell strains were cultivated in EMEM medium (BioWhitaker/Cambrex), added 15% (v/v) foetal calf serum (Biochrom, Berlin, Germany), 2 mM L-glutamine (Biochrom), 100 U/ml penicillin and 100 µg/ml streptomycin (Biochrom). Unless stated otherwise, cells were grown 10–14 days with medium exchanges performed twice a week until they reached a monolayer, where the used fibroblasts reach confluence. Confluent fibroblasts are growth arrested due to contact inhibition and accumulate in G_0/G_1-phase. Cell cycle analysis was performed by flow cytometry to ensure that approximately 85–95% of growth arrested cells were in G_0/G_1.

Cell cultures were split by incubating the cell monolayer with a trypsine-EDTA solution (0.05 g/l trypsine, 1 g/l EDTA-solution in PBS without Mg^{2+} and Ca^{2+} obtained from PAN, Aidenbach, Germany) at 37°C for 5 min to detach the cells from the culture vessel. To obtain a single cell suspension the cells were mixed by pipetting up and down for several times. The trypsine solution was inactivated by addition of 3 × the volume of serum containing culture medium and an aliquot of this cell suspension was taken to assess the cell concentration using a cell counter (Z2 Coulter Counter, Beckman Coulter, Krefeld, Germany). The cells were reseeded at the appropriate density.

4.1.2 Human cancer cells

Due to accumulated genetic alterations within genes that control cell proliferation and/or cell death cancer cells divide in culture indefinitely. Thus, it is relatively easy to maintain large populations of cancer cells and it is much more difficult to maintain large populations of finite lifespan normal cells. In addition, human cancer cells are tolerant to genetic manipulations and it is much harder to genetically manipulate normal human fibroblasts. Therefore, in this thesis many of the transfection and transgene expression experiments were performed in human cancer cells.

4.1.2.1 Human colon cancer cells (HCT116)

To study the influence of p21, human colon cancer cells (HCT116) were used. HCT116 cells are TP53 wild-type (wt) and have a p21-deficient sister cell line (HCT116 $p21^{-/-}$) in which both genes for p21 were deleted by homologous recombination [Waldman *et al.*, 1995]. The HCT116 p21wt and the HCT116$p21^{-/-}$ cell lines were kindly provided by Bert Vogelstein (The Johns Hopkins Oncology Center, Baltimore, USA).

The HCT116 cells were cultivated in McCoy's 5A Medium (Sigma) with addition of 10% (v/v) foetal calf serum (Biochrom) and 2.8 mM L-glutamine (Biochrom). For routine passages, cells were split 1/8 twice a week as described under Sect. 4.1.1 (page 90) like human fibroblasts. The p21-defecient cells have a geniticin resistance and were kept under geniticin selection (0.4 mg/ml geniticin G418; Gibco BRL). The p21-defeciency was confirmed by Western Blot analysis (Sect. 4.9 page 112).

4.1.2.2 HeLa cells

HeLa cells are human cervical cancer cells that have been studied in culture extensively since 1951. HeLa cells were derived from a 31 year-old woman named Henrietta Lack and express the E6 protein due to transduction with the human papillomavirus The E6 protein promotes the degradation of endogenous TP53 via the ubiquitin pathway. This unstable TP53 protein in HeLa cells leads to the expression of very low levels of endogenous p21 that cannot be detected by Western Blot analysis. In some experiments derivates of HeLa cells were used which were stably transfected with *APTX-GFP* [Gueven *et al.*, 2004]

HeLa cells were kindly provided by Nuri Gueven (Queensland Institute of Medical Research, Brisbane, Australia) and were used in this study for experiments in which ectopically expressed mutant forms of p21 were investigated. HeLa cells were cultivated in RPMI medium with 10% (v/v) foetal calf serum (Biochrom) and 2.8 mM L-glutamine (Biochrom). The cells were split 1/8 twice a week as outlined in Sect. 4.1.1 for human fibroblasts.

4.1.3 Mouse embryonic fibroblasts

Mouse embryonic fibroblasts (MEFs) were used for experiments in which I investigated whether or not the formation of p21 foci was dependent on the presence of poly(ADP-ribose) polymerase-1 (PARP-1). Both PARP-1 wt and PARP-1 knockout MEFs were kindly provided by Dr. G. de Murcia (University of Strasbourg, France). These cells are immortalized MEFs derived from 13.5 days PARP-$1^{+/+}$ or PARP-$1^{-/-}$ embryos as described in DeMurcia *et al.* [1997]. The cells were cultivated in DMEM medium with 10% (v/v) foetal calf serum (Biochrom).

4.1.4 Chinese hamster ovary cells

Chinese hamster ovary cells (CHO) were used to test whether p21 foci formation is dependent on the presence of X-ray repair cross-complementing gene 1 (*XRCC1*). Parental CHO cells (AA.8) that express wild-type XRCC1 were used for comparison purposes and an AA.8 derivate (EM9 cells) expressing a truncated polypeptide lacking two-thirds of the normal hamster XRCC1 sequence was used as *XRCC1*-knockout. In some experiments derivates of EM9 cells were utilized that stably express recombinant APTX-GFP (EM-APTX-GFP cells) [Gueven *et al.*, 2004] or recombinant XRCC1-GFP (EM9-XRCC1-GFP cells). The *XRCC1-GFP* was generously donated by Dr. G. de Murcia (University of Strasbourg, France) and the EM9-XRCC1-GFP cells were generated as outlined for the EM-APTX-GFP cells in Gueven *et al.* (2004). The AA.8, EM-APTX-GFP and EM9-XRCC1-GFP cells were kindly provided by Dr. N. Gueven (Queensland Institute of Medical Research, Brisbane, Australia). The EM9 cells used were obtained from Dr. L.H. Thomson (LLNL, USA).

All CHO lines were cultivated in RPMI medium containing 10% (v/v) foetal calf serum (Biochrom) and 2.8 mM L-glutamine (Biochrom).

4.1.5 Cell stocking

For each cell line used, a frozen cell stock in multiple aliquots was prepared. For finite lifespan normal human fibroblasts this is particularly important as these cells differentiate and become senescent in culture. The p21 protein is involved in both processes and its expression level is affected and altered throughout the differentiation process. Therefore, it was necessary during the course of the work presented here to perform all experiments employing normal human fibroblasts with cells of similar differentiation status, e.g. similar CPD and passage number, which were frozen from expanded cell populations once.

For cell stocking, cells were trypsinized, counted with a cell counter (Z2 Coulter Counter, Beckman Coulter, Krefeld, Germany), centrifuged and resuspend at 1×10^6 cells/ml in the cell-specific freezing medium. To assure controlled and slow freezing, freezing vials with 2 ml cell suspension each were kept in an isopropanol container (Nalgene Cryo 1°C Freezing Container) at – 80°C, allowing for a temperature controlled freezing process (1°C/min). After 15–20 h at – 80°C, the freezing vials were transferred to a liquid nitrogen tank and kept there until further usage.

Human fibroblast (AG and NHDF) were frozen in EMEM medium (BioWhittaker) containing 15% (v/v) foetal calf serum (Biochrom), 2 mM L-glutamine (Biochrom), 100 U/ml penicillin and 100 µg/ml streptomycin (Biochrom) and 10% (v/v) glycerol. All other cell lines used were frozen in McCoy's 5A Medium (Sigma) with 10% (v/v) foetal calf serum (Biochrom) and 2.8 mM L-glutamine (Biochrom) and 10% (v/v) DMSO.

To taw the cells the vial was incubated briefly at 37°C. The cells were resuspended in 15 ml pre-warmed cell culture medium and this cell suspension was transferred to a 75 cm^2 culture flask. On the next day the culture medium was removed and replaced by fresh culture medium. For the human fibroblasts (AG and NHDF), the cell number in the removed medium was determined to assess the number of attached cells, giving the actually number of seeded cells (N_0) to determine the CPD (see Sect. 4.1.1).

4.1.6 Test for contamination of cell cultures with mycoplasma

Mycoplasma are the smallest free-living and self-replicating organisms (0.2–2 µm in diameter). They are very restricted in metabolic potential and closely associated to eukaryotic cells. Mycoplasma in cell cultures live as extracellular parasites, usually attached to the external surface of the cell membrane. Contamination of cell cultures with mycoplasma can alter DNA, RNA and protein synthesis and also initiate chromosomal aberrations. All cells used were checked regularly for contamination with mycoplasma using the ‚Mycoplasma Detection Kit' (Boehringer Mannheim) according to the manufacturer's protocol. When an infection with mycoplasma was detected, the cells were successfully treated with plasmocin from Amaxa according to the user's manual.

4.2 Irradiation of cells

For irradiation, cells were cultivated depending on the experimental outline either on glass cover slips (∅ 30 mm; Menzel-Gläser, Braunschweig, Germany), on petri dishes (∅ 32 mm or 150 mm; Nunc, Roskilde, Denmark) or in culture flasks (25 cm^2 or 75 cm^2; Falcon). The cells were irradiated with X-rays, γ-rays or heavy ions as described below.

4.2.1 X-ray irradiation

Artificially produced X-rays have a wide spectrum of energies resulting from the deceleration of electrons as they traverse high-atomic-number materials. Additional filtration selectively removes the less energetic photon component (i.e. the "soft" X-rays) and by this, hardens the X-rays. Here, the exposure to X-rays was performed using a industrial X-ray generator Isovolt DS1, type IV320-13, manufactured by Seifert (Germany). This X-ray tube is equipped with a 7 mm beryllium filter and one aluminium and one copper filter of 1 mm thickness each (Fig. 57). These additional filters are positioned below the tube and serve to eliminate the soft X-rays. The samples were irradiated with a voltage of 250 kV and a current of 16 mA. All samples were irradiated with a dose rate of 2–3.5 Gy/min. The dosimetry was done with a SN4 dosimeter (PTW Freiburg), calibrated according to Fricke [Fricke and Hart, 1966].

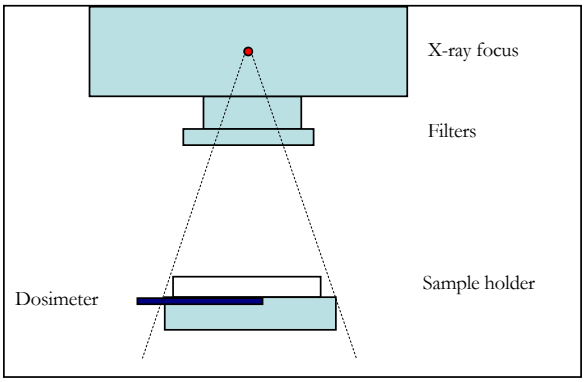

Fig. 57 **Experimental setup for the exposure of cell cultures to X-rays.**

4.2.2 γ-Irradiation

For experiments involving peptide mapping the cells were irradiated with γ-rays at the Forschungscentrum Karlsruhe. The γ-irradiation was performed at room temperature using a Gammacell 220 (A.E.C.L. Atomic energy of Canada limited, Ottawa, Canada) with a ^{60}Cobalt source. The cells were grown and irradiated in ∅ 150 mm petri dishes (Nunc, Roskilde, Denmark). The samples were irradiated with a dose of 10 Gy at a dose rate of 2 Gy/min.

4.2.3 Heavy ion irradiation

Two different facilities were used to expose cell cultures to heavy ions: the SIS ('***S***chwer***i***onen***s***ynchrotron': Heavy Ion Synchrotron) and the BIBA ('***Bi***ologische ***B***estrahlungs ***A***pparatur': biological irradiation device) of the UNILAC (***Uni***versal ***I***on ***L***inear ***Ac***celerator) facility [Kraft *et al.*, 1980; Haberer *et al.*, 1993] at the GSI (Fig. 58).

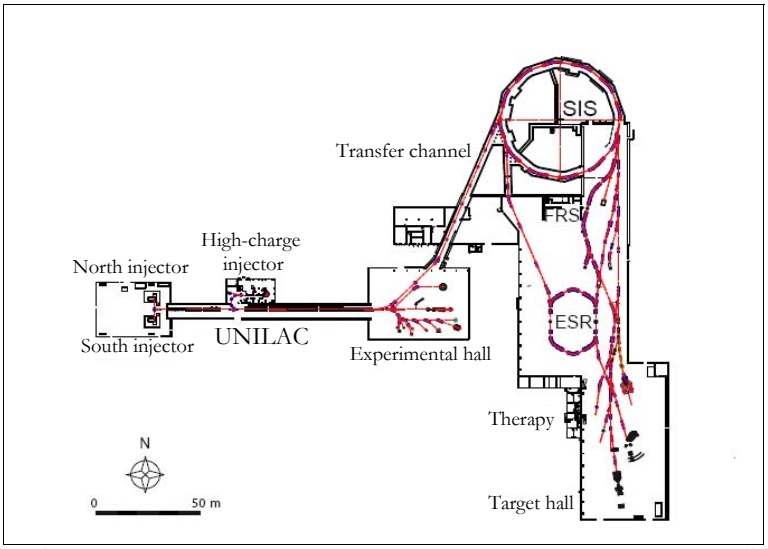

Fig. 58 **Schematic plan of the accelerator and experimentation facilities at the GSI.** Ions are injected by the North and South injectors and pass through the Wideröe structure or originate in the high-charge injector before being fired into the Alvarez structure. Part of the beam is diverted to the experimental hall for experiments, while the remainder is transferred to the SIS for further acceleration (GSI).

4.2.3.1 The UNILAC facility

The UNILAC is a 120 m long linear accelerator that accelerates ions to 20% of the speed of light. The ions, coming from a high current injector (HCI), are accelerated by a radiofrequency quadrupole (RFQ; up to 120 keV/u) plus interdigital H-structure up to 1.4 MEV/u. The collision of the ions with a N_2-jet stripper results in a partially stripping the ions of their electrons, giving the further acceleration higher efficiency. The UNILAC can accelerate ions to energies of 2–18 MeV/u.

For the detection of protein accumulations in form of foci after heavy ion irradiation, cells were cultivated and irradiated in petri dishes (∅ 32 mm; Nunc, Roskilde, Denmark). The petri dishes were placed vertically in a specially designed magazine, which can accommodate up to 20 petri dishes. The magazine was filled with the appropriate cell culture medium to avoid drying out of the cell monolayers during the irradiation procedure. The magazine then was placed into the BIBA device of the UNILAC facility. A computer controlled robot arm pulled out one petri dish after the other to expose the cell monolayers to the particle beam until the desired dose was applied. The irradiation procedure, including the transport to and from the BIBA device to the laboratory, took approximately 20 min. For experimental setup see Fig. 59.

A possible influence of the temperature during the irradiation was checked by cooling the used magazins (filled with medium) to a temperature of 4°C or by incubation of the magazins with medium at 37°C prior irradiation.

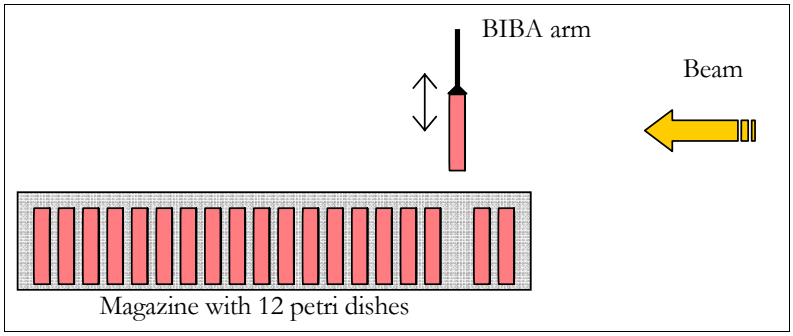

Fig. 59 **Schematic diagram of the sample holder for irradiation experiments at the UNILAC facility.**

For the experiments in which protein accumulations along the heavy ion tracks and horizontal to the culture surface were detected, cells were grown and irradiated on glass cover slips (∅ 30 mm; Menzel-Gläser, Braunschweig, Germany). Because of the short penetration depth of the ions accelerated with the UNILAC facility, the cells could not be irradiated on cover slips positioned horizontally to the particle beam. For exposures, the cover slips were fixed in the beam line at an angle of approximately 4° (see Fig. 60 for experimental setup) and the cells could not be covered with medium. To make sure that the cells did not suffer drying out, cells were kept without medium for less than 2 min during the irradiation procedure. With this setup, one cover slip at time could be irradiated.

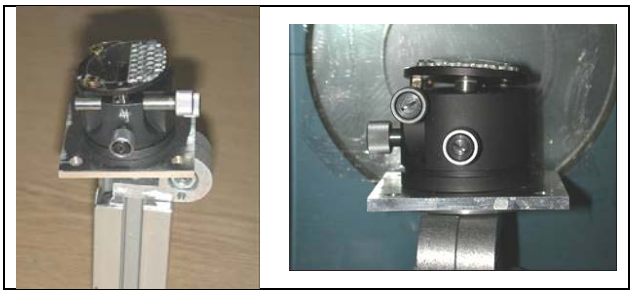

Fig. 60 **Sample holder for experiments where cells were irradiated at a low angle towards the beam-line.**

4.2.3.2 The SIS facility

The SIS is a heavy ion synchrotron with a diameter of 219 m that can accelerate the ion beam up to 90% of the speed of the light. After the acceleration at the UNILAC, ions can be led to the SIS. In the section between the UNILAC and the SIS facility, the ions pass a thin carbon foil, which ionizes the ions further. In the vacuum ring of the SIS, the ions are kept in a circular path by strong magnetic fields. Here, energies up to 2 GeV/u can be reached.

For the detection of protein tracks horizontal to the culture surface after irradiation at the SIS facility, cells were cultivated in petri dishes (∅ 32 mm; Nunc, Roskilde, Denmark) and irradiated horizontal to the particle beam. With the SIS facility, very high particle energies can be reached, which results in a high penetration depth, enough to penetrate the petri dish with medium. The petri dishes were placed in a plastic box filled with medium. For irradiation, a maximum of 4 petri dishes per box, in total 3 boxes, were irradiated. For experimental setup see Fig. 61.

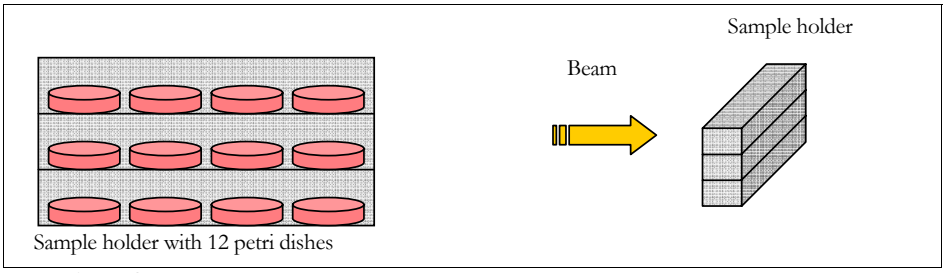

Fig. 61 **Sample holder for the petri dishes and experimental setup for the horizontal irradiation at the SIS facility at the GSI.**

The dosimetry of the heavy ion irradiation was done with an ionisation chamber, developed at the GSI and calibrated using the nuclear detector CR39. CR39 is a plastic that shows the ion tracks after it has been etched with 11 M NaOH [Scholz *et al.*, 2001].

The given dose was determined from the fluence as follows:

$$D[Gy] = \frac{1.602 \cdot 10^{-9} \times LET[keV/\mu m] \times F[1/cm^2]}{\rho[cm^3/g]}$$

Comment [j1]:

The charged particles used for experiments mentioned in this thesis involving heavy ions are summarized in Table 6 below.

Ion	**Fluence** [P/cm²]	**Energy** [MeV/u]	**Energy on target** [MeV/u]	**LET** [keV/µm]
Au	2×10^6; 3×10^6	11.4	4.0	13030
Cr	2×10^6	11.4	5.6	2810
Fe	6×10^6	200	175	337
Kr	3×10^6	11.4	4.8	5265
Ni	2×10^6; 3×10^6	11.4	4.5	3790
Sm	3×10^6	11.4	4.2	10290
U	2×10^6; 3×10^6; 1×10^7	11.4	4.2	14925
Zn	3×10^6	11.4	4.8	4120

Table 6 **Heavy ions used for the experiments described in this thesis.**

4.3 DNA damage induction by chemicals

4.3.1 CPT treatment

CPT was added to the medium of confluent NHDF cells on petri dishes to a final concentration of 1µM CPT. The cells were incubated at 37°C for 1 h. The medium was removed and the monolayer rinsed with PBS. The soluble proteins were either not extracted or extracted by Hepes buffer as indicated and described in Sect. 4.4 (page 99). Immunostaining for p21 and XRCC1 or 53BP1 was carried out (Sect. 4.4.4, page 100) and the cells analysed by confocal laser scanning microscopy (Sect. 4.5, page 101).

4.3.2 H_2O_2 treatment

The medium of NHDF cells was removed, the cell monolayer rinsed with PBS and incubated with 0.2 mM H_2O_2 in PBS for 20 min at RT. The H_2O_2 containing PBS was replaced by conditioned medium and the cells were incubated at 37°C for 15 min. The cells were washed with PBS and immunostained after fixation and extraction with Hepes buffer as described in Sect. 4.4 below.

4.4 Immunostaining

Protein accumulations within the nucleus were detected by indirect immunostaining. Specific primary antibodies were used to detect the proteins of interest. A secondary fluorochrome-labelled antibody was utilized to detect the primary antibody. Depending on the protein of interest, different cell extraction methods were used. For the detection of most proteins investigated in this thesis, either the no extraction prior to immunostaining or extraction of soluble proteins by Hepes-buffer was used. The detection of the PCNA protein required a special extraction method, as the PCNA could not be detected by the other methods used. Immunostaining to detect PCNA was done after extraction of the soluble proteins according to the modified Streck extraction protocol. The used protocols are described below.

4.4.1 Fixation and permeabilization of the cells without extraction of the soluble proteins

Following irradiation and a given incubation time, the culture medium was removed from the cells and the cells were washed with PBS. The cells were fixed with 2% paraformaldehyde (2% w/v) in PBS) for 20 min at RT prior to the permeabilization with 0.5% Triton X-100 (0.5% (v/v) in PBS) for 10 min. Cells were washed twice with PBS for 5 min and the non-specific antibody binding sites were blocked by incubation with a 0.5% BSA solution (0.5% (w/v) in PBS), either for 30 min at RT or over night at 4°C. Immunostaining for proteins of interest was carried out as described in Sect 4.4.4 (page 100).

4.4.2 Extraction of the soluble proteins by Hepes-extraction buffer

If the extraction of the soluble proteins was required, the method described by Pagano *et al.* [1994] with slight modifications was used. The medium was removed from the cells and the cells

were rinsed with PBS. Soluble proteins were extracted by a 10 min incubation on ice with Hepes-extraction buffer (10 mM Hepes-KOH, 10 mM KCl, 1.5 mM $MgCl_2$, 0.5 mM DTT, 0.1% (v/v) Triton X-100; pH 7.9), a hypotonic buffer containing the non-ionic detergent Triton X-100. Cells were fixed with 2% paraformaldehyde (2% (w/v) in PBS) for 20 min at RT, washed twice in PBS for 5 min each and the non-specific antibody binding sites were blocked with a 0.5% BSA solution (0.5% (w/v) in PBS), either for 30 min at RT or over night at 4°C. The specific proteins were immunostained as outlined in Sect. 4.4.4 (page 100).

4.4.3 Extraction of the soluble proteins by the GSI modified Streck method

Due to the nuclear abundance of the PCNA protein a specific signal for the irradiation-induced accumulated chromatin-associated fraction of the PCNA could not be obtained easily. For this reason, a special protein extraction and fixation method became necessary for the detection of the chromatin-associated PCNA fraction. Here, I have utilized the modified Streck method [Mirzoeva and Petrini, 2001] with slight modifications by B. Jakob (GSI) to visualize the chromatin-bound PCNA by indirect immunostaining. This method is referred to as the 'GSI modified Streck' method in the following.

The medium was removed from the cells, the cells were washed with PBS and the soluble proteins were extracted with cytoskeleton extraction buffer (10 mM pipes, 100 mM NaCl, 300 mM sucrose, 3 mM $MgCl_2$, 1 mM EGTA, 0.5% (v/v) Triton X-100, 4 mM Vanadyl-ribosyl complex, 1 mM AEBSF; pH 6.8) for 10 min on ice. Cells were then washed with PBS and fixed by incubation with 1% paraformaldehyde (1% (w/v) in PBS) for 5 min at RT, followed by incubation with the Streck fixative (150 mM 2-bromo-L-nitro-1.3-propandiol, 108 mM diazolidinyl urea, 10 mM sodium citrate, 50 mM EDTA, pH 5.7) for 30 min at RT. The cells were permeabilized with 0.5% Triton X-100 (0.5% (v/v) in PBS) for 10 min at RT, washed twice in PBS for 5 min each and the non-specific antibody binding sites blocked by incubation in 0.5% BSA solution (0.5% (w/v) in PBS) for 30 min at RT or over night at 4°C. Immunostaining for specific proteins was carried out as described below.

4.4.4 Indirect immunostaining

Following the incubation of cells in BSA blocking solution (0.5% (w/v) BSA in PBS), the proteins of interest were detected by the indirect immunohistochemical staining method. For this, specific primary antibodies are used to target the protein of interest and, in a second step, the primary antibody is targeted by a secondary antibody which is linked to a fluorochrome (Fig. 62).

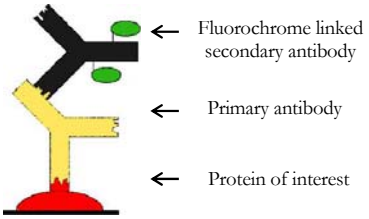

Fig. 62 **Schematic diagram of the indirect immunostaining.**

BSA blocked cell monolayers were incubated for 1 h at RT with the primary antibody (see Table 7), followed by three washes with PBS for 5 min each. Then cells were incubated with the fluorochrome-labelled secondary antibody (see Table 7) for 30 min at RT. All antibodies were diluted in 0.5% (w/v) BSA in PBS and used in concentrations as shown in Table 7 (page 116). To reduce the amount of antibody necessary for each antibody reaction and to prevent drying out of the samples, the cell monolayers were covered with Mylar foil during the incubation periods. To visualize the nucleus the DNA was stained for 20 min at RT with a 1 µM ToPro-3 in PBS (Molecular Probes, Leiden, Netherlands) with addition of 100 µg/ml RNase A from Boehringer Mannheim), followed by three washes for 5 min in PBS. The samples were air-dried and, to prevent a fading of the fluorescence signal, 'Vectashield Mounting Medium' (Vector Laboratories, Burlingame, CA, USA) was used to mount the cover slip (∅ 30 mm; Menzel-Gläser, Braunschweig). Until microscopic analysis the samples were kept protected from light at 4°C.

4.5 Confocal laser scanning microscopy (CLSM)

Microscopic analysis was carried out according to our standard procedures and as described in Jakob *et al.* [2000]. I used a Leica TCS confocal laser scanning system. This system is equipped with a DM IRBE inverted microscope (lens: PlanApo 63 × / 1.32 oil) and an argon/krypton laser (*l*ight *a*mplification by *s*timulated *e*mission of *r*adiation). The microscope was connected to a Märzhäuser computerised stage control SCAN 100 × 100. The used argon/krypton mixed gas laser gives three spectral lines for excitation at 488 nm (green), 568 nm (red) and 647 nm (dark red; displayed as blue on the monitor). The observed field was approximately 0.05 cm² large which in average showed 2000 cells.

4.5.1 Characteristics of CLSM

The CLSM uses a tiny laser spot, focused in a defined image plane, to excite fluorescence. This spot is scanned in lines across the field, resembling image formation by an electron beam on a monitor. The detection of fluorescence can be regulated by a photomultiplier with high sensitivity. The principal function and ray pathway of a CLSM is shown in Fig. 63 The laser, beam splitter and excitation filter wavelength are exemplified for FITC (488 nm; green) detection.

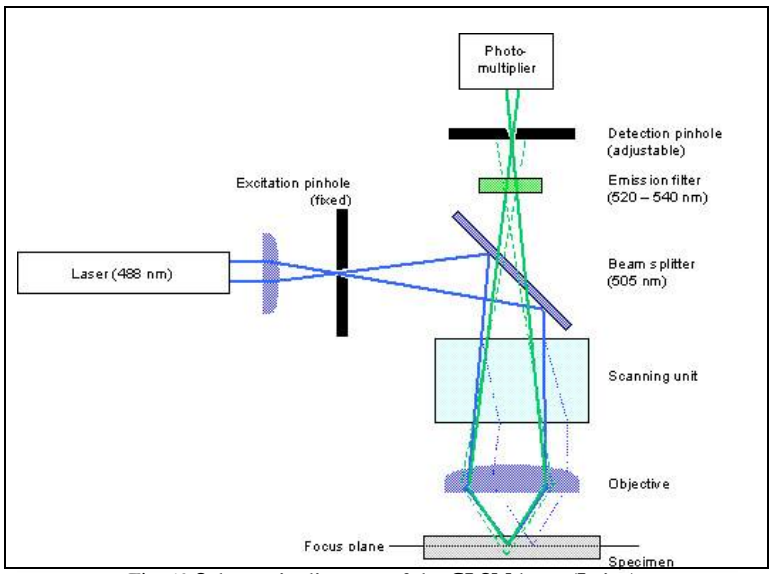

Fig. 63 **Schematic diagram of the CLSM laser (Leica).**

The laser produces high-intensity, coherent light of a defined wavelength. The principle of a laser is based on the fact that excited atoms or molecules radiate photons of a wavelength, which are perfectly coherent. Between laser and beam splitter, where the light is mirrored into the objective, the pinhole (an excitation aperture) produces a thin laser beam. The objective projects the laser beam into the focal plane within the sample. By fluorescence excitement, one image point (pixel) is formed out of a raster of 512 by 512 pixels. After straight transmission of the beam splitter, only this pixel is detected by the photomultiplier (PMT), as the emission pinhole is in a confocal position to the excitation pinhole. The different intensities recorded by the PMT are converted back into x/y information and depicted on the CLSM monitor. The intensity can be controlled by changing the voltage as well as the offset of the PMT.

Note that in some Fig. the protein tracks appear as if going through the nucleoli. This is obtained because the images shown represent the mean projection of the microscopically obtained 4–12 single planes. By displaying a single plane of the microscopically acquired stack, it

is inferred that the protein tracks are either above or below the nucleolus (single planes of the stacks are not shown in this thesis).

4.5.2 Evaluation of protein colocalisation

To verify whether the immunostained proteins colocalize after irradiation Scion Image (http://www.scioncorp.com) was used with a program provided by Dr. B. Jakob (GSI). Here, the median of the projections which were obtained with the CLSM were inverted in gray scala. The intensity of each channel was displayed separately and the colocalisation of the detected areas of each channel was calculated (see Fig. 64). If the resulting chi20 factor is above 8 the two channels are considered to show good colocalisation meaning two proteins colocalize. A random colocalisation is assumed with a chi20 factor of 1.

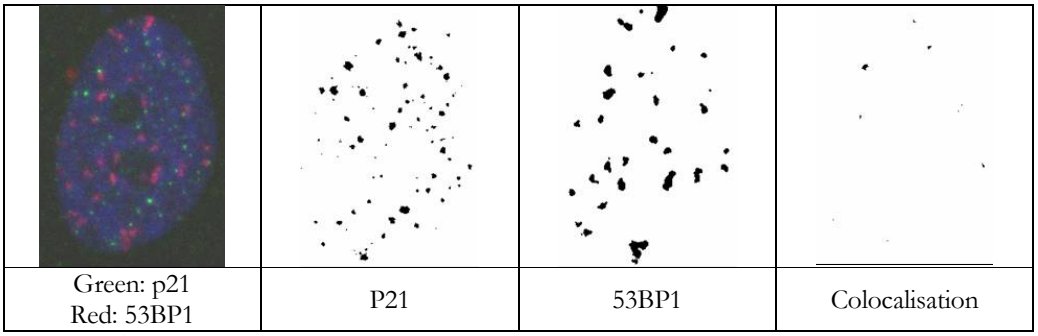

Fig. 64 **Example for the evaluation of colocalisation for p21 and 53BP1 following exposure to 6 Gy X-rays.**

4.6 Live-cell imaging by beam-line microscopy

This method was developed by Dr. B. Jakob at the GSI [Jakob *et al.*, 2005] who also kindly performed the live-cell imaging for the very early kinetics of the heavy ion-induced foci formation of the recombinant GFP-p21 for this thesis.

HeLa cells were seeded on approximately 2.4 × 2.4 cm ethanol-sterilized polycarbonate squares (40 µm thick) placed in petri dishes (∅ 32 mm; Nunc, Roskilde, Denmark) 3 days prior to the irradiation. To do so, 20000 cells were suspended in 1 ml of medium and centre-plated on the polycarbonate square. After adhesion of the cells, 2 ml of medium were added. One day prior to irradiation the cells were transfected with the GFP-p21 plasmid as described in Sect. 4.10.1. Just

before irradiation a silicon spacer with a thickness of 500 µm was placed on the polycarbonate square and covered with a cover slip. The spacer allowed for a medium layer on top of the cells to avoid drying out of the cells during imaging. The polycarbonate square with the spacer and cover slip was placed on an aluminium carrier and fixed on the microscopic setup as shown in Fig. 65

The irradiation was done with krypton ions (4.8 MeV/u; LET: 5265 keV/µm).

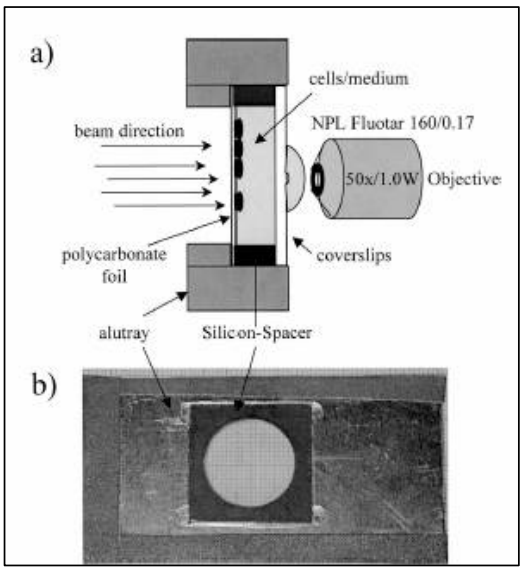

Fig. 65 **A: Schematic diagram of the radiation setup including polycarbonate square with spacer and coverslip on aluminium tray, microscope lens and ion beam.** For microscopy, a water immersion lens NPL Fluotar 50×/NA 1.0 was used. The fluorescence signal was detected through culture medium and a cover slip. **B: Top view (photo) of the cell container with silicon spacer.**

4.7 Preparation of cell lysates

Crude cell lysates were prepared under denaturing or native conditions. In addition, fractionated cell extracts were prepared according to several methods (see below).

4.7.1 Preparation of cell lysates under denaturing conditions

Whole cell lysates for Western Blot analysis were prepared according to Laemmli [Laemmli, 1970]. The medium was removed and the cell monolayer was rinsed with PBS. The cells were lysed by adding 2 × Laemmli buffer (100 mM Tris-HCl pH 6.8, 2% (w/v) SDS, 20% (v/v) glycerol) and removed from the culture vessel surface with a cell scraper. The lysates were heated for 10 min at 100°C and centrifuged at 13000 × g for 10 min at 15°C. The supernatant containing the proteins was transferred to a new tube and stored at – 20°C until further usage. The pellet containing the cell debris was discarded.

4.7.2 Preparation of native cell lysates

After some modifications, satisfying results were reached with the following method for the preparation of native cell lysates. The medium was removed and the cells were rinsed with PBS. The cells were incubated with the cell specific trypsine-EDTA solution (see Sect. 4.1 Cell cultivation, page 90) for 5 min on ice, detached from the culture surface with a cell scraper and singularized by pipetting several times up and down. The enzymatic activity of the trypsine was stopped by adding the 3-fold of culture medium. The cells were counted and centrifuged for 10 min (107 × g at 4°C), washed with PBS and centrifuged again (107 × g at 4°C, 10 min). The supernatant was discarded and the cells were resuspend at 3×10^7 cells per ml in RIPA buffer (1% (v/v) NP40, 50 mM Tris/HCl, 150 mM NaCl, 1 mM EDTA, 0.5% (v/v) sodium deoxycholate) with protease inhibitors (Complete, Roche). The cell suspension was homogenized by taking it 40 × through a 25 G cannula followed by a 30 min incubation on ice. The cell debris was separated by centrifugation (8000 × g for 30 min at 4°C) and the supernatant containing the proteins was kept at – 80°C.

4.7.3 Subnuclear fractionation studies

To analyze chromatin-associated proteins, subcellular fractionation is carried out in which the soluble protein fraction is separated from the chromatin-bound protein fraction. After this separation, the chromatin-bound proteins can be released from the DNA by several methods

and analyzed by the Western Blot analysis. For the subcellular fractionation of proteins many different protocols exist. However, depending on the protein of interest, only some of the protocols may give satisfying results. I tested several different protocols to investigate the presence of p21 and/or PCNA in subnuclear protein fractions to find the best suitable method. The different approaches are written below.

4.7.3.1 Subcellular protein fractionation by the use of Douncer pestles

Cells were harvested by trypsination as outlined in Sect. 4.1 (page 90), rinsed with PBS and pelleted by centrifugation (107 × g, 10 min, 4°C). The cells were resuspended in PBS and the exact cell number determined (Beckman Coulter Counter). The cells were spun down (230 × g, 10 min, 4°C), resuspended in Dignam buffer A (1.5 mM $MgCl_2$, 10 mM Hepes buffer pH 7.9, 10 mM KCl, 0.5 mM AEBSF, 0.5 mM DTT, protease inhibitors Complete from Roche; 5×10^7 cells/ml) and lysed by 40 strokes of a loose-pestle Dounce homogenizer (Wheaton, Millville, NJ, USA) on ice. The homogenate was centrifuged (8000 × g, 5 min, 4°C) to pellet the nuclei from the cytosolic proteins. The supernatant was transferred to a new tube and stored at – 20°C until further usage. The pelleted nuclei were resuspend in Dignam buffer C (1.5 mM $MgCl_2$, 20 mM Hepes buffer pH 7.9, 0.42 M NaCl, 0.2 mM EDTA, 25% (v/v) glycerol, 0.5 mM AEBSF, 0.5 mM DTT, protease inhibitors Complete from Roche; 5×10^7 cells/ml) by 40 strokes of tight-pestle Dounce homogenizer (on ice). After high speed centrifugation (19000 × g, 30 min, 4°C), the supernatant containing the nuclear protein fraction was transferred to a new tube and stored at – 80°C until further usage; the pellet discarded.

4.7.3.2 Cell fractionation according to Balajee and Geard [2001] and with modifications according to Savio et al. [1996]

Cell fractionation studies according to the protocol of Balajee and Geard [2001] led to high amounts of protein in the final pellet, which then is discarded using this method. The supernatant is considered to contain the chromatin-bound proteins. However, it became obvious that not all of the chromatin-bound proteins were released using a buffer with 0.5 M NaCl as requested according to Balajee and Geard. For this reason, the protocol was modified according to Savio *et al.* [1996] by releasing the chromatin-bound proteins by incubation with DNase I buffer as followed.

The medium was removed from the cells, the cells were washed with PBS and incubated with a trypsin-EDTA solution (0.05 g/l trypsine, 1 g/l EDTA-solution in PBS without Mg^{2+} and Ca^{2+} obtained from PAN) on ice for 2 min. The cells were scraped off, singularised and the trypsin was stopped by the addition of 3-fold culture medium. The cell concentration was determined with a cell counter (Beckman Coulter Counter) and cells were spun down (107 × g, 4°C, 10 min). The cell pellet was washed with PBS, centrifuged (107 × g, 4°C, 10 min) and the cells were resuspended at 10^7 cells/ml in Buffer I (10 mM Tris-HCl pH 7.4, 2.5 mM $MgCl_2$, 0.5% v/v) NP40, 1 mM AEBSF) with protease inhibitors (Complete) and incubated for 10 min on ice. The suspension was centrifuged with 735 × g at 4°C for 5 min, the supernatant containing the soluble cytosolic and nuclear proteins was transferred into a new tube and frozen

at − 80°C (lysate 1). The pellet was resuspended in Buffer I, incubated on ice for 10 min and spun down again. This was repeated to be sure that all soluble proteins were removed from the chromatin-bound protein fraction (lysate 2 and 3). Finally, the pellet was resuspended in DNase I buffer solution (200 u/10^7 cells DNase I in Buffer III: 10 mM Tris-HCl pH 7.4, 10 mM NaCl, 5 mM $MgCl_2$, 0.1 mM AEBSF) with protease inhibitors (Complete, Roche) at 10^7 cells/ml and incubated for 30 min at 37°C. The DNase I activity was stopped by adding EDTA (10 mM) and incubation on ice. After centrifugation (14000 × g, 4°C, 5 min), the supernatant containing most of the chromatin-bound proteins was transferred to a clean microfuge tube (lysate 4). The pellet was resuspended in a high salt concentration buffer (3 × 10^7 cells/ml Buffer II; 25 mM sodium phosphate buffer pH 7.4, 0.5 M NaCl, 1 mM EDTA, 0.5% (v/v) Triton X-100, 10% (v/v) glycerol, 5 mM $MgCl_2$) with protease inhibitor (Complete, Roche) to release the maintaining chromatin-bound proteins for 20 min on ice and centrifuged (14000 × g, 4°C, 5 min). This supernatant was combined with the previous supernatant obtained after DNase I digest (lysate 4). To assess the fraction of proteins remaining within the final pellet this pellet was lysed under denaturing conditions in 2 × Laemmli buffer (100 mM Tris-HCl pH 6.8, 2% (w/v) SDS, 20% (v/v) glycerol) as described previously (Sect. 4.7.1 page 105).

4.7.3.3 Cell fractionation as described by Xu and Stern [2002]

The medium was removed from the cells and cells were rinsed with PBS, trypsinized (0.05 g/l trypsine, 1 g/l EDTA-solution in PBS without Mg^{2+} and Ca^{2+} obtained from PAN) and scraped of the culture dish and singularised. The trypsin solution was inactivated by addition of culture medium and the cell concentration was determined using a cell counter followed by centrifugation (107 × g, 4°C, 10 min) and washing in PBS. The cell pellet was resuspended at 1.5 × 10^7 cells/ml buffer A (10 mM Hepes pH 7.9, 10 mM KCl, 1.5 mM $MgCl_2$, 0.34 M sucrose, 10% (v/v) glycerol, 1 mM DTT, 0.1% (v/v) Triton X-100) with protease inhibitors (Complete, Roche) and lysed on ice for 5 min. The nuclei were separated from the cytosolic proteins by centrifugation (1500 × g, 4°C, 5 min). The supernatant was transferred into a new tube and centrifuged (13000 × g, 4°C, 10 min) to clear the cytosolic proteins from the cell debris. This supernatant containing the cytosolic proteins was kept at − 80°C until further usage (lysate S2). Nuclei were washed in buffer A and repelleted (1500 × g, 4°C, 4 min). The supernatant was discarded. Then the nuclei were lysed on ice for 10 min in buffer B (1.5 × 10^7 cells/ml; 3 mM EDTA, 0.2 mM EGTA, 1 mM DTT) with protease inhibitors (Complete, Roche). Following centrifugation (2000 × g, 4°C, 4 min), the supernatant with the soluble nuclear proteins was transferred to a new tube and frozen at − 80°C (lysate S3). The pellet, containing the chromatin-bound nuclear proteins, was washed in buffer B and centrifuged (13000 × g, 4°C, 10 min) and the supernatant stored at − 80°C until further usage (lysate S4). The pellet with the remaining chromatin-bound proteins was resuspended in 2 × Laemmli buffer (100 mM Tris-HCl pH 6.8, 2% (w/v) SDS, 20% (v/v) glycerol), heated for 10 min at 100°C and centrifuged (13000 × g, 4°C, 10 min). The supernatant with the remaining chromatin-bound proteins was frozen at − 80°C (lysate P3).

4.7.3.4 *Cell fractionation according to Stivala and Prosperi et al. [2004]*

After medium removal, the cell monolayer was rinsed with PBS and the cells detached from the petri dish and singularized by a trypsin-EDTA solution (0.05 g/l trypsine, 1 g/l EDTA-solution in PBS without Mg^{2+} and Ca^{2+} obtained from PAN) incubation. The cell number was determined with a coulter counter and the cells pelleted by centrifugation (107 × g, 4°C, 10 min). Cells were resuspended with 10^7 cells/ml in a hypotonic lysis buffer (10 mM Tris-HCl pH 7.4, 2.5 mM $MgCl_2$, 0.5% (v/v) NP40, 1 mM DTT, 1 mM AEBSF, protease inhibitor cocktail Complete from Roche) and lysed for 10 min on ice. Centrifugation at 300 × g for 1 min (4°C) separated the soluble proteins (supernatant) from the chromatin-bound protein fraction (pellet). To be sure that all soluble proteins were separated from the chromatin-bound protein fraction, the pellet containing the chromatin-bound proteins and cell debris was washed twice by resuspending the pellet in washing buffer (10^7 cells/ml; 10 mM Tris-HCl pH 7.4, 150 mM NaCl, 1 mM AEBSF, protease inhibitor cocktail Complete from Roche) and centrifuge at 300 × g for 1 min (4°C). The pellet was resuspended in DNase I solution (10^8 cells/ml; 20 mM NaCl, 0.1 mM AEBSF, 200 DNase I units/10^7 cells) and 2 × digestion buffer was added (10^8 cells/ml; 20 mM Tris-HCl pH 7.4, 20 mM NaCl, 10 mM $MgCl_2$, protease inhibitor cocktail Complete from Roche) and incubated rotating for 30 min at 37°C. After centrifugation at 14000 × g for 1 min (4°C) the supernatant contained the chromatin-bound protein fraction - released by the DNase I digestion - and the pellet the cell debris. The remaining pellet was resuspended in 70 µl 2 × Laemmli buffer (100 mM Tris-HCl pH 6.8, 2% (w/v) SDS, 20% (v/v) glycerol) to assess potential remaining proteins.

As with this method the chromatin-associated p21 appeared to be degraded, the DNA digestion was done by 45 min incubation with Benzonase (200 units/10^7 cells) at 4°C instead of DNase I.

4.8 Immunoprecipitation of specific protein complexes

To detect whether proteins interact with each other in native cell extracts, protein complexes can be co-immunoprecipitated by specific antibodies. The precipitated protein complex can be separated under denaturing conditions and can be analysed by the Western Blot technique.

After establishing a successful method for p21 immunoprecipitation (see Sect. 4.8.1 below) the IPs were carried out as described in the following, if not stated otherwise:
An aliquot of the cell lysate corresponding to 1 mg of total protein was diluted in 1 ml Ripa buffer without SDS (2% (v/v) Igepal, 100 mM Tris/HCl, 300 mM NaCl, 2 mM EDTA 0.5% (v/v) sodium deoxycholate, protease inhibitors Complete from Roche). This lysate was precleared by addition of normal IgG (Amersham) for 2 h at 4°C (rotating). Ultralink Immobilized Protein A/G beads (10 µl; Pierce) were added and another 2 h of incubation at 4°C (rotating) was given. The lysate was cleared of the beads with the bound IgG and non-specific IgG binding proteins by centrifugation for 5 min with a speed of 1000 × g at 4°C. The supernatant was transferred to a new tube, the pellet containing the unspecific IgG binding

proteins discarded. The specific antibody was added (1 µg) and incubated over night at 4°C (rotating). Ultralink Protein A/G beads (10 µl) was added and incubated rotating for additional 2 h at 4°C. The samples were centrifuged (8000 rpm, 5 min, 4°C), the supernatant discarded and the beads with the bound protein complexes washed 4 times by resuspend with each 1 ml Babco buffer (50 mM Tris-HCl pH 7.5, 150 mM NaCl, 0.5% (v/v) NP40, 1 mM EDTA pH 8.0, 0.25% (v/v) gelatine) and centrifuge (4000 × g, 5 min, 4°C). The final pellets containing beads with the IP proteins were resuspended each in 30 µl 2 × Laemmli SDS-sample buffer (100 mM Tris-HCl (pH 6.8), 2% (w/v) SDS, 20% (v/v) glycerol, 0.02 mg/ml bromphenolblue, 2% (v/v) β-Mercaptoethanol) and denaturated for 10 min at 100°C. After centrifugation (13000 × g, 10 min, 10°C) the supernatant was transferred to a new tube and stored at – 80°C until Western Blot analysis was carried out; the pellet discarded.

4.8.1 Establishment of a method to immunoprecipitate a p21 complex

To establish a method for IP of a p21 complex, I used HCT116 cells, for which the isogenic p21 knockout cell line is available that can be used as a negative control. HCT116p21$^{+/+}$ and HCT116p21$^{-/-}$ cells were irradiated with 15 Gy X-rays as described in Sect. 4.2.1 (page 94) to induce DNA lesions and with this increase the amount of potentially available p21/PCNA complexes. Subnuclear protein fractionation was done with the Douncer pestles 16 h post irradiation as outlined in Sect. 4.7.3.1 (page 106). The immunoprecipitation was done with an anti-p21 polyclonal rabbit antibody (Ab5, Oncogene, Cambridge, USA) in Dignam A buffer (1.5 mM $MgCl_2$, 10 mM Hepes buffer pH 7.9, 10 mM KCl 0.5 mM PMFS, 0.5 mM DTT with protease inhibitors Complete from Roche) as described in Sect. 4.8 (page 108). Immunoprecipitated p21 complexes were analyzed by Western Blot analysis for the presence of p21 and PCNA.

The Western Blot analysis of the p21 IP's in Fig. 66 shows that the p21 pulldown from the chromatin-associated protein fraction from mock-irradiated HCT116p21$^{+/+}$ and HCT116p21$^{-/-}$ cells does not co-immunoprecipitate PCNA, as expected (Fig. 66 lanes 2 and 4, respectively). However, both irradiated samples show a weak PCNA signal (Fig. 66 lanes 3 and 5). Peculiarly, the HCT116p21$^{-/-}$ cells show even more co-immunoprecipitated PCNA than the wild-type p21 cells (Fig. 66 lane 5 versus lane 3). The p21 detection displays a clear induction of the immunoprecipitated p21 from the wild-type p21 cells (Fig. 66 lanes 2 and 3). Curiously, the HCT116p21$^{-/-}$ cells also show a detectable amount of p21 and a slight increase with irradiation (Fig. 66 lane 4 versus 5). Because of their p21 status however, they should not have a detectable p21 signal and with this, not be able to precipitate PCNA by specific p21 immunoprecipitation.

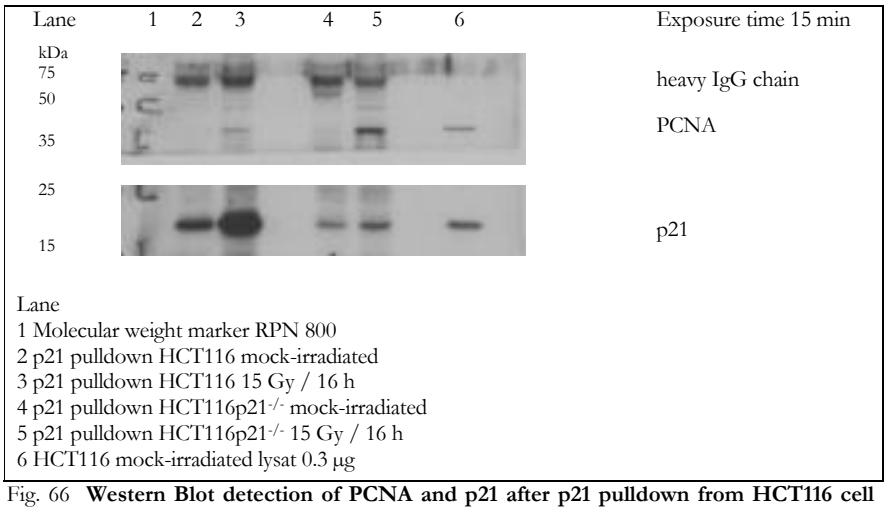

Fig. 66 **Western Blot detection of PCNA and p21 after p21 pulldown from HCT116 cell lysates.** Specific p21 pulldown from p21-deficient HCT116 cells result in a irradiation induced co-immunoprecipitated PCNA signal (lane 5).

The protocol for the IP was modified several times with the aim first to have no PCNA signal for the p21 IP from HCT116p21$^{-/-}$ cells. The first approach was to try another antibody that differed in the epitope for the p21 pulldown. I compared the p21 polyclonal rabbit antibody (Ab5, Oncogene, Cambridge, USA) with a potentially more specific p21 monoclonal mouse antibody (Ab3, Oncogene, Cambridge, USA). For these experiments, cells were not irradiated and whole cell lysate was used for the IP, as first I aimed a Western Blot analysis of the p21 pulldown of HCT116p21$^{-/-}$ cells with a non-detectable PCNA signal. A slight difference between the used antibody was seen, as the detectable PCNA band is elevated with the use of the p21 polyclonal rabbit antibody compared to the IP's done with the p21 monoclonal mouse antibody (supplement 6.4 Fig. 75 lanes 3 and 5 versus lanes 2 and 4). As the Ab5 p21 antibody gave the clearest detectable PCNA signal, this antibody was used for the further IP's.

My next approach was to check the non-specific binding of PCNA to the used IgG's. The pulldown with IgG mouse or IgG rabbit antibody in Dignam A buffer (1.5 mM $MgCl_2$, 10 mM Hepes buffer pH 7.9, 10 mM KCl 0.5 mM PMFS, 0.5 mM DTT with protease inhibitors Complete from Roche) both resulted in detectable PCNA signals for both HCT116 cell lines (supplement 6.4 Fig. 76, lanes 2 and 3 and lanes 5 and 6, respectively). This shows that with the used IgG's a non-specific binding of a PCNA complex is indeed reached. Before the specific p21 precipitation however, the lysates are precleared with the appropriate IgG antibody to make sure that this unspecific binding of PCNA does not interfere with the specific p21 pulldown results. Therefore, I assume that this is not the problem leading to the PCNA signal in the HCT116p21$^{-/-}$ cells. If the PCNA signal is caused by binding of a p21-like protein, possibly the binding affinity differ from the specific binding of p21. This made me try various protocols using different harsh buffers. It must be mentioned however, that the immunofluorescence analysis nor the WB analysis of HCT116p21$^{-/-}$ whole cell lysate did not give any positive p21 signal with the here used p21 antibodies.

Immunoprecipitations were carried out in RIPA buffer without SDS (2% (w/v) Igepal, 100 mM Tris/HCl, 300 mM NaCl, 2 mM EDTA 0.5% (v/v) sodium deoxycholate, protease inhibitors Complete from Roche) or Dignam A buffer (1.5 mM $MgCl_2$, 10 mM Hepes buffer pH 7.9, 10 mM KCl 0.5 mM PMFS, 0.5 mM DTT with protease inhibitors Complete from Roche) and the Babco waschbuffer (50 mM Tris-HCl pH 7.5, 150 mM NaCl, 0.1% (v/v) NP40, 1 mM EDTA pH 8.0, 0.25% (v/v) gelatine) was changed from 0.1% SDS Babco buffer to 0.5% SDS Babco buffer. The change of the buffer in which the IP was carried out from Dignam A to Ripa buffer made a severe difference in the unspecific IgG pulldown from the HCT116p21$^{-/-}$ cells. The IP in Dignam A buffer with the IgG rabbit from the HCT116p21$^{-/-}$ cell lysate resulted in a clear PCNA band after WB analysis (supplement Fig. 77 lane 3). However, if the RIPA buffer was used during this IP, a hardly detectable PCNA signal was observed (supplement 6.4 Fig. 77 lane 4). Also, the p21 pulldown with the p21 Ab5 antibody in HCT116p21$^{+/+}$ cells showed a difference in the PCNA signal, depending on the used buffer. The detectable PCNA is clearly reduced by the usage of the RIPA buffer in stead of Dignam A buffer throughout the IP (supplement 6.4 Fig. 77 lane 5 versus 6).

In spite of the done modifications, still a clear PCNA band was detected in the p21 pulldown lysate from the HCT116p21$^{-/-}$ cells. This finally made me test another cell system for these experiments. The HeLa cells seemed to be a useful cell line, as their instable TP53 status leaves them a non-detectable p21 level (see Sect. 2.2.2, page 35 for WB analysis and Sect. 2.2.5, page 42 for immunofluorescence staining).

RIPA cell lysates were prepared from mock-irradiated and with 30 Gy X-ray irradiated HeLa cells (Sect. 4.2.1, page 94) harvested 3 h after irradiation. IgG and specific p21 immunoprecipitation was carried out as described in described above (Sect. 4.8). The Western Blot analysis with immunodetection for PCNA is shown in Fig. 67. No PCNA signal is observed for the IgG or the p21 IP from the HeLa cell lysates after PCNA immunodetection of the WB, when exposed the normal exposure time to the X-ray film (2 min; data not shown). However, to see whether after a prolonged exposure still no PCNA signal is detected, the WB was exposed 30 min to the X-ray film (Fig. 67). Here, a slight PCNA signal is seen for the HeLa cells (Fig. 67 lanes 2–4). This signal however, is not elevated after irradiation and present in all HeLa samples, making me assume that it is a non-specific signal (Fig. 67 lanes 2 and 3 versus 4, respectively). The detected upper bands of the WB in Fig. 67 display the heavy chain of the IgG used for the immunoprecipitation (Fig. 67lanes 2–6). In addition, p21 IP was done with NHDF cells to verify the established protocol for cells expressing endogenous p21. The specific p21 IP in these cells resulted in a clear PCNA signal, verifying the established method (Fig. 67 lane 6). The additionally loaded AG lysate gives the position of endogenously expressed PCNA from AG whole cell lysate (Fig. 67 lane 7).

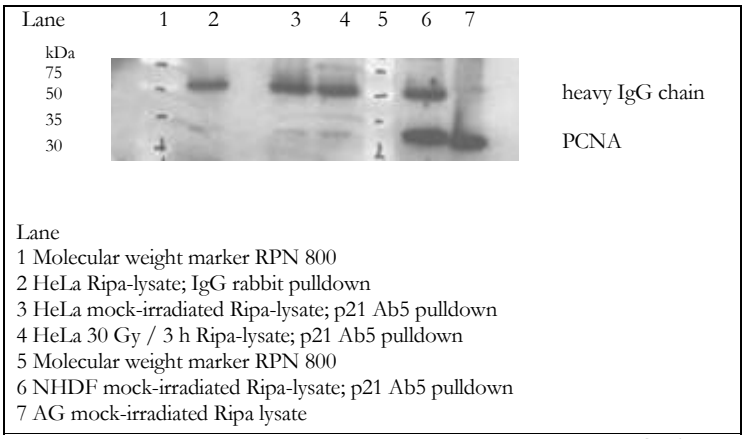

Fig. 67 **p21 pulldown in HeLa cells results in a non-detectable specific PCNA signal after WB analysis.**

This shows that finally a method was found to co-immunoprecipitate PCNA with a p21 antibody from p21 expressing cells with no PCNA signal after specific p21 pulldown in HeLa cells.

4.9 Western Blot analysis

Denatured proteins can be qualitatively and quantitatively assessed by the Western Blot technique. First, proteins are separated on denaturing sodium dodecyl sulphate (SDS) polyacrylamide gels (SDS-PAGE). Here, the anionic detergent SDS binds quantitatively to the proteins subjected to separation, giving them linearity and uniform negative charge. By this, the proteins are separated by the electrophoresis solely on the basis of their size. The separated proteins are then transferred (blotted) to a nylon membrane. The membrane is then exposed sequentially to the primary antibody directed against the protein of interest and the enzyme coupled secondary antibody that binds to the primary antibody. The enzyme, here horseradish peroxides (HRP), reacts with a particular substrate that is converted to an unstable intermediary product emitting chemiluminescence. By exposing the membrane to an X-ray film, the protein of interest can be detected.

4.9.1 Protein quantitation

Protein quantitation were performed according to Lowry [Lowry *et al.*, 1951] using the modified Lowry assay (D_C Protein Assay Bio-Rad) or according to Bradford [Bradford, 1976] using the Rotiquant system from Roth (Karlsruhe, Germany).

4.9.1.1 Lowry assay

The Lowry protein quantitation is based on the reduction of Cu^{2+} to Cu^{+} in an alkaline solution by forming a complex with the proteins of the lysate. Cu^{+} then reduces the Folin-Ciocalteau reagent, forming a blue complex. The light absorption of this solution gives the protein concentration of the samples as it is compared with a calibration curve of known protein concentration. The absorption was measured by an Elisa-*Reader* (EL_X 800, Bio-Tek Instruments) at 630 nm.

To produce a standard calibration curve a BSA stock solution of known protein concentration was used and serial dilutions of this stock solution were generated (0, 0.2, 0.4, 0.8 and 1 mg/ml).

4.9.1.2 Bradford assay

This assay is based on the light absorbance shift of coomassie brilliant blue from 465 nm to 595 nm when it binds to proteins in an acidic solution. The light absorption of the solution measured by an Elisa-*Reader* (EL_X 800, Bio-Tek Instruments) is compared to a calibration curve of known BSA concentration (0, 5, 10, 20 and 40 µg/ml).

4.9.2 SDS-PAGE

The proteins are separated solely according to their molecular weight by the SDS-PAGE. SDS is an anionic detergent, which denatures proteins by covering the polypeptide backbone of the proteins. SDS binds to proteins relative specifically in a mass ration of 1:4 (1.4 g SDS/g protein in a 1% (w/v) SDS-solution). By this, SDS confers a negative charge to the polypeptide in proportion to its length. The disulphide bridges in the proteins are reduced by the addition of β-Mercaptoethanol to the lysates. Polyacrylamide is used as support matrix as it inhibits a convective mixing of the samples and acts as a sieve for the means of separating molecules by size. In this thesis, proteins were separated by the discontinuous system according to Laemmli [Laemmli, 1970]. This means that a non-restrictive large pore stacking gel (Tris-glycine buffer, pH 6.8; 3–7% acrylamide/*bis*-acrylamide ratio 29:1) is layered on top of a separating gel, the resolving gel (Tris-glycine buffer, pH 8.8; and 5–8% acrylamide/*bis*-acrylamide ratio 29:1).

Protein separation was done either with the BioRad system as described below or with the NUPAGE system.

4.9.2.1 BioRad system

Protein separation with the BioRad system was done with the ‚Mini-Protean II' according to the user's manual. A 12% acrylamide/*bis*-acrylamide (ratio 29:1) separating gel with a size of 7 cm × 8 cm × 1 mm was used for the separation for proteins with a molecular weight of 10 to 100 kDa. The used stacking gel was a 3.2% acrylamide/*bis*-acrylamide (ratio 29:1) gel. The casted separating gel was topped off with H_2O to ensure a flat polymerisation surface and to exclude the contact with air, and was left to polymerize at RT for 1 h. After polymerisation, the H_2O was removed carefully and the stacking gel was casted on top of the separating gel. A comb with 15 or 10 wells holding 20 µl or 35 µl respectively was used. The separating gel was left at RT for 30 min to polymerize.

To the required amount of the samples an equal amount of 2 × SDS-sample buffer (100 mM Tris-HCl (pH 6.8), 2% (w/v) SDS, 20% (v/v) glycerol, 0.02 mg/ml bromphenolblue, 2% (v/v) β-Mercaptoethanol) was added and heated for 10 min at 80°C. The samples were centrifuged briefly (minifuge) and loaded into the wells. To verify the molecular weight of the separated proteins, a premixed protein molecular weight marker (RPN 800 ‚Full range rainbow protein molecular weight marker' 10 to 250 kDa; Amersham) was loaded once on each gel. Gelelectrophoresis in SDS-PAGE running buffer (50 mM Tris-base, 0.38 M glycine, 0.1% (w/v) SDS) was carried out for 2 or 3.5 h, for 1 or 2 gels respectively, at a constant currant of 16 mA and a voltage between 29 V and 85 V.

4.9.2.2 NuPAGE

For some Western Blot analysis the NuPAGE system was used, including precast 12% Bis/Tris SDS-PAGEs. The NuPAGEs were prepared and loaded according to the user's manual and run for 50 min with 200 V (110–70 mA; MOPs buffer).

4.9.3 Protein blotting from the SDS-gel to a polyvinyliden fluoride membrane

After protein separation by SDS-PAGE proteins were transferred to a polyvinylidene fluoride (PVDF) membrane. The proteins are transferred to the membrane by an electric field. In this field, the smaller SDS molecules are faster and so separated from the proteins during the transfer. The used transfer buffer contains methanol, which reduces the interaction of SDS with the proteins and facilitates the binding of the proteins to the membrane.

The transfer of the proteins from the gel to the membrane was done using the vertical tank-blotting system ‚Mini Trans-Blot' from Bio-Rad or the NuPAGE system as indicated. To do so, the membrane (Immobilon-P; MILLIPORE), filter paper and pads were pre-soaked in the transfer buffer (Bio-Rad: 20% (v/v) methanol, 0.02 M Tris-HCl (pH 8.3), 0.15 M glycine, 0.1% (w/v) SDS; NuPAGE: 20% (v/v) methanol, 0.025 M Bis-Tris-HCl (pH 8.3), 0.25 M Bicine, 1 mM EDTA; pH 7.2). The hydrophobic membrane was soaked in methanol and washed in water before it was soaked in the transfer buffer. The gel was positioned on the pre-soaked membrane with a pre-soaked filter paper and pad on either side. This sandwich was placed in the tank-blotting apparatus filled with transfer buffer. The transfer was done at constant voltage of 20 V and a current between 60 mA and 80 mA for 14 hours with the Bio-Rad system and 30 V (170–110 mA) for 1 h with the NuPAGE system. After the protein transfer, the membrane was subjected to the immunodetection (Sect. 4.9.4).

4.9.4 Immunodetection

Proteins that have been transferred to the nylon membrane can be identified and quantified by immunodetection using a protein specific primary and an enzyme-conjugated primary specific secondary antibody. The protein detection is based on the catalytic activity of the HRP linked to the secondary antibody. HRP – in the presence of H_2O – catalyses the oxidation of luminol generating an excited product that emits high intensity chemiluminescence which is detected on an X-ray film.

For the immunostaining, the membrane was briefly washed in 1 × TBST (10 mM Tris-HCl, 150 mM NaCl, 0.05% (v/v) Tween 20) directly after the protein transfer to remove remaining transfer buffer and SDS-gel fragments. First, the membrane was blocked by incubation in 5% blocking solution (5% (w/v) non-fat Nestlé milk powder in 1 × TBST) for 2 hours at RT with slight agitation. Then the membrane was incubated for 2 h at RT with the primary antibody, diluted in 5% blocking solution. Following this incubation the membrane was washed 3 × for 10 min wash in 1 × TBST to remove remaining primary antibody. Then the membrane was incubated with the HRP-linked secondary antibody, also diluted in 5% blocking solution, at RT for 1 h. The membrane was washed 6 × for 10 min each in 1 × TBST to remove remaining secondary antibody and incubated for 5 min at RT with the 'ECL Plus™ Western Blotting detection system' (Amersham) according to the user's manual. After incubation with the ECL Plus™, the membrane was exposed to an X-ray film (Hyperfilm ECL; Amersham) to detect the chemiluminescence signal. The exposure time depended on the antibodies used and took from 5 seconds to overnight. For the antibodies used and their working concentrations see Table 7.

Primary antibodies stock solutions	Produced in	Epitope (if known)	Dilution for WB	Dilution for IF
Cip1/WAF1 Transduction Laboratories 250 μg/ml	Mouse	full length	1:4000	1:80
WAF1 (Ab-5) Oncogene 100 μg/ml	Rabbit	15–61	1:1000	1:20
WAF1 (Ab-3) Oncogene 100 μg/ml	Mouse	58–77	1:100	-
p53 FL393 Santa Cruz 200 μg/ml	Goat	full length	1:1000	1:100
p53 (Ab-6) Oncogene 100 μg/ml	Mouse	21–25	1:2000	1:50
Myc Invitrogen 1.2 mg/ml	Mouse	-	1:4000	1:200
PCNA MAB424 PC10 Chemicon 1 mg/ml	Mouse	111–125	1:4000	1:50
PCNA (FL-261): sc-7907 Santa Cruz 200 μg/ml	Rabbit	1–261	1:2000	1:20
CDK2 PharMingen	Rabbit	C-terminal domain	1:1000	-
α-tubulin Sigma	Mouse	C-terminal domain	1:4000	-
β-actin Sigma	Rabbit	N-terminal domain	1:500	-
GFP Abcam	Rabbit	full length	1:2500	1:100
53BP1 Oncogene 2 mg/ml	Rabbit	full length	-	1:500
γH2AX (ser139) Upstate 1 mg/ml	Rabbit	134–142	-	1:200
γH2AX (ser139) clone JBW361 Upstate 1 mg/ml	Mouse	134–142	1:1000	1:500
Mouse-IgG Amersham Pharmacia	Sheep	-	1:10000	-
Rabbit-IgG Amersham Pharmacia	Sheep	-	1:10000	-
Alexa Fluor 488 labbeled goat-anti-mouse-F(ab')$_2$-IgG-fragments Molecular probes 2 mg/ml	Goat		1:400	-
Alexa Fluor 568 labbeled goat-anti-mouse-F(ab')$_2$-IgG-fragments Molecular probes 2 mg/ml	Goat		1:400	-
Alexa Fluor 488 labbeled goat-anti-rabbit-F(ab')$_2$-IgG-fragments Molecular probes 2 mg/ml	Goat		1:400	-
Alexa Fluor 568 labbeled goat-anti-rabbit-F(ab')$_2$-IgG-fragments Molecular probes 2 mg/ml	Goat		1:400	-

Table 7 **Antibodies used for Western Blot detection and Immunofluorescence staining.**

4.9.5 Stripping and reprobing of membranes

To be able to reprobe membranes after the first detection, the primary and secondary antibodies from the first detection reaction have to be removed. The membrane can be stripped of bound antibodies and reprobed several times if needed. For this, the membrane is rinsed with 1×TBST for 10 min and incubated for 30 min in stripping buffer (62.5 mM Tris-HCl pH 6.7, 2% (w/v) SDS, 100 mM β-Mercaptoethanol) at 50°C with slight movement. After washing the membrane 4 × 15 min in 1 × TBST the immunodetection can be carried out as described above (Sect. 4.9.5).

4.10 Expression of recombinant p21 protein in mammalian cells

To understand the function of proteins, the expression of recombinant proteins in mammalian cells can be helpful. With this it is possible to construct plasmids expressing a high level of the protein of interest. In this thesis I have used plasmids to express different p21 constructs and a GFP-p21 fusion protein. To gain the plasmid, the plasmid is transfected into *E. coli* from which it then is isolated. The mammalian cells are then transiently transfected with the plasmid, resulting in an expression of the encoded protein. The protocols and used vectors are described in brief below.

4.10.1 Cultivation and transformation of *E. coli*

All plasmids described in this thesis were replicated by the use of the *Escherichia coli* bacterium DH5α (Life Technologies, Gaithersburg, USA) or the dam^- GM2163 (Fermentas, St. Leon-Rot, Germany). Competent bacteria were transformed with the specific plasmid as described in the user's manual. 50 µl *E. coli* were transformed with 1-10 µg plasmid. The transformed cells were cultivated in LB medium (Lennox; Roth, Karlruhe, Germany) and plated on agar plates (Luria-Bertani Agar; Lennox; Roth, Karlruhe, Germany) with a specific selection antibiotic, either ampicillin (100 µg/ml; Applichem, Darmstadt, Germany) or kanamycin (50 µg/ml; Applichem, Darmstadt, Germany) depending on the used plasmid and incubated at 37°C over night until single colonies could be picked and used for the DNA purification as described for the used Qiagen kit.

4.10.2 Plasmids for the expression of recombinant p21 in mammalian cells

4.10.2.1 pcDNA3

The wtp21, p21T145A and p21T145D constructs used in this thesis were generously donated by Prof. S. Dimmeler (University of Frankfurt). These plasmids were constructed as described in Rossig *et al.* (2001) using a pcDNA3.1-Myc-His vector from Invitrogen (Fig. 68).

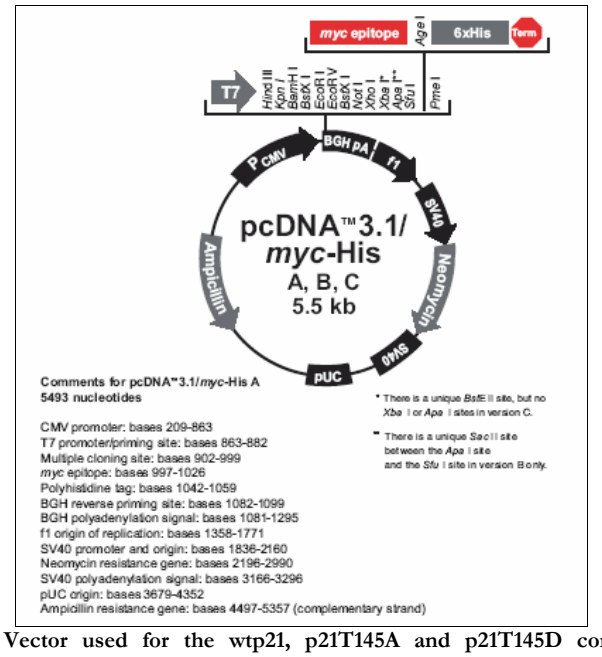

Fig. 68 **Vector used for the wtp21, p21T145A and p21T145D constructs (Invitrogen).**

4.10.2.2 pEGFP-C2

The vector used to make the GFP-p21 construct was the pEGFP-C2 vector from BD Biosciences Clontech (Fig. 69) which was kindly donated by Dr. C. Blattner (Institute of Toxicology and Genetics, Forschungszentrum Karlsruhe). With this vector, the EGFP is fused at the N-terminal site of the expressed protein. This vector was chosen, as the PCNA binding site, which has been proved to be of importance for the p21 foci formation at the damaged DNA sites, is on the C-terminal domain of p21 (see Fig. 12; page 17).

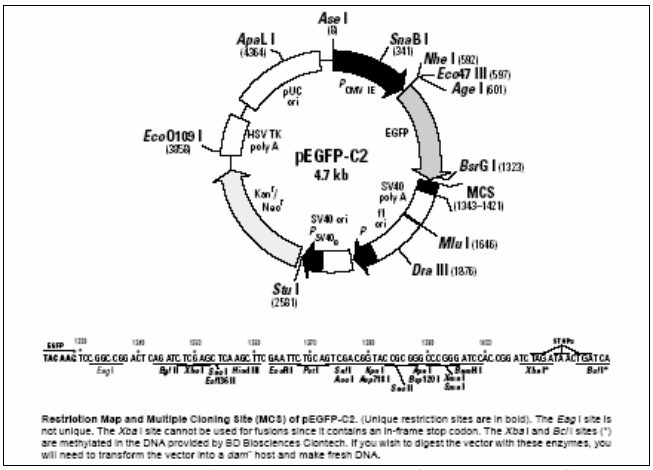

Fig. 69 **Vector used for the GFP-p21 construct (BD Biosciences Clontech).**

4.10.3 PCR

For the construction of the GFP-p21 fusion protein, the p21 cDNA was isolated from the wtp21 plasmid provided by Prof. S. Dimmeler (University of Frankfurt) by a PCR reaction using following primers (ordered at MWG-Biotech AG):

p21 primer forward:

HIND III
5‘ – ACT CAG ATC TCG AGC TCA AGC TTC ATG TCA GAA. CCG GCT GGG GAT GTC – 3’
multiple cloning site p21

p21 primer reverse:

Xba I
5‘ – TGA TCA GTT ATC TAG ATT TAG GGC TTC CTC TTG GAG AA.G ATC – 3’
multiple cloning site p21

The primers were resuspended in TE (10 mM Tris-Cl pH 7.4, 1 mM EDTA pH 8.0) to a concentration of 10 mg/ml and diluted with H_2O (as EDTA inhibits the polymerase) to a final concentration of 50 µg/ml. The p21 template was diluted with H_2O to a final concentration of 100 µg/ml.

5 µl	p21 forward primer (0.25 µg)
5 µl	p21 reverse primer (0.25 µg)
5 µl	10 × Pfu buffer (Promega)
5 µl	template DNA wtp21 (0.5 µg)
1 µl	dNTP mix (Promega)
1 µl	Pfu polymerase (Promega)
1 µl	50 mM $MgCl_2$
27 µl	H_2O

Time	5 min	30 sec	30 sec	1 min	5 min	∞
Temperature	94°C	94°C	55°C	72°C	72°C	4°C
Cycles			35 cycles			

Table 8 **PCR reaction.**

The PCR product was digested as described in Sect. 4.10.5.1 (page 121) and verified by gel electrophoresis as outlined in Sect. 4.10.5.2 (page 121).

4.10.4 Purification of plasmid DNA from *E. coli*

The plasmid preparation was done with the Qiagen kit (Qiagen, Hilden, Germany) according to the user's manual. Depending on the amount of cultures from which the plasmids were purified, either the miniprep or the maxiprep was carried out.

4.10.5 Plasmid analysis

To verify the plasmids enriched by *E. coli*, the plasmids were restricted with endonucleases to excise the insert and verified by gelelectrophoretical analysis.

For the GFP-p21 construct the restriction of the plasmid was not only for the verification of the plasmid. Here, the cDNA of p21 had to be isolated from the PCR product to be able to ligate the insert in the GFP vector. To be able to ligate the excised p21 insert with the GFP vector, the PCR product and GFP vector were digested with the same endonucleases. After digestion, the products were verified by gel electrophoresis.

4.10.5.1 Digestion of DNA with restriction endonucleases

The pEGFP-C2 vector and the wtp21 PCR product from Sect. 4.10.3 (page 119) were restricted with HIND III and Xba I from Promega (Mannheim, Germany). The restriction sites for these enzymes were encoded in the used primers for the p21 PCR. The use of two different enzymes ensured that the possibility of self ligation of the vector or the insert was minimized.

45 µl	**p21wt PCR product**
1 µl	HIND III
1 µl	Xba I
5 µl	10 × buffer B

3 µl	**pEGFP-C2 (5 µg)**
1 µl	HIND III
1 µl	Xba I
3 µl	10 × buffer B
22 µl	H_2O

Table 9 **Restriction mix**

The PCR product and vector were digested for 2 h at 37°C. The obtained DNA fragments were verified by agarose gel electrophoresis as described below.

4.10.5.2 Agarose gel electrophoresis

By gel electrophoresis the DNA fragments obtained after digestion are separated and allow purifying the p21 DNA and the linearized vector DNA. The gelelectrophoretic analysis was done with 1% agarose gels (1% (w/v) agarose in 1 × TAE buffer) with the gel electrophorese system from Renner (Dannstadt, Germany) with a constant voltage of 70 V and a current in the range of 65–85 mA for 1 h.

4.10.5.3 GFP-p21

After gel electrophoretic separation of the digested p21 PCR product and the pEGFP-C2 vector, the p21 DNA band (65 mg) and vector band (91 mg) were excised from the gel and purified using the DNA purification kit Easy pure (Biozym Diagnostik, Oldendorf, Germany) according to the user's manual. The purified p21 insert and linearized pEGFP-C2 were ligated for 1 h at room temperature giving the GFP-p21 plasmid used in the experiments.

2 µl	10 × ligase buffer T4 (Promega)
2 µl	pEGFP-C2 (linearized and purified)
6 µl	p21 insert
1 µl	DNA ligase T4 (Promega)
9 µl	H_2O

Table 10 **Ligation mix**

4.10.5.4 Sequence analysis

In Sect. 2.2 (page 31) different p21 plasmids, which were kindly donated by Prof. S Dimmeler (University of Frankfurt), were used: wtp21, p21T145A and p21T145D. The p21T145A and p21T145D have an aa. change at Thr145 that influences the PCNA binding possibility. To be sure that the results obtained in Sect. 2.2 was due to the single aa. change in p21T145D, making the protein expressed from this construct unable to interact with PCNA, this plasmid was sequenced by GATC Biotech (Konstanz, Germany). The single aa. change at Thr145 of p21 was confirmed.

p21 MSEPAGDVRQNPCGSKACRRLFGPVDSEQLSRDCDALMAGCIQEARERWNFDFVTETPLE
p21T145D MSEPAGDVRQNPCGSKACRRLFGPVDSEQLSRDCDALMAGCIQEARERWNFDFVTETPLE

p21 GDFAWERVRGLGLPKLYLPTGPRRGRDELGGGRRPGTSPALLQGTAEEDHVDLSLSCTLV
p21T145D GDFAWERVRGLGLPKLYLPTGPRRGRDELGGGRRPGTSPALLQGTAEEDHVDLSLSCTLV

p21 PRSGEQAEGSPGGPGDSQGRKRRQTSMTDFYHSKRRLIFSKRKPZ----------
p21T145D PRSGEQAEGSPGGPGDSQGRKRRQDSMTDFYHSKRRLIFSKRKPDIQHSGGRSSLEGPRF

p21 ----------
p21T145D EQKLISEEDLNMHTGHHHHHHHZVZTRZSASTVPSSCQPSVVCPSPVPSLTLEGATPT
c-myc tag **(his)6-tag**

4.10.6 Transfection of mammalian cells

The main problem of expressing ectopically proteins in mammalian cells is the transfection of these cells with the desired plasmid. Several methods are described; the efficiency however, depends on the used cell system and plasmid. In this thesis I have use two different systems to transfect mammalian cells. Electroporation was used for cell lines which were not or only with were little efficiency transfected by the otherwise used liposome mediated transfection. This was the case for AG and NHDF cells, probably due to their extracellular matrix. The two systems are briefly described below.

4.10.6.1 Electroporation

With the electroporation technique, the cell membrane is disrupted by a strong external electric field which leads to a diffusive permeability. By this, a DNA solution surrounding the cells can pass the membrane. For cells electrophorated in this thesis, the Nucleofector from Amaxa (Köln, Germany) was used. The cells and solutions were prepared according to the user's manual.

4.10.6.2 Liposome mediated transfection

The liposome mediated transfection was done either with Lipofectamine 2000 (Invitrogen, Carlsbad, CA, USA) or FuGENE 6 (Roche, Basel, Switzerland) according to the user's manual. HCT116 cells were transfected with FuGENE 6 and HeLa cells with Lipofectamine 2000 as experiments showed that the transfection efficiency for each cell line differed; making me chose the transfection reagent with the highest efficiency (data not shown).

4.11 Peptide mapping

Peptide mapping gives the possibility to detect the phosphorylation status of a protein by radiolabelling. In this thesis the phosphorylation status of p21 in NHDF and with wtp21 transfected HeLa cells was investigated after γ-irradiation and ^{32}P labelling. For this, the cells were grown on 15 cm Ø culture dishes. HeLa cells were transfected by Lipofectamine (Invitrogen, Karlsruhe, Germany) with wtp21 24 h prior to irradiation.

The cells were incubated overnight with phosphate-free culture medium containing 10% (v/v) dialyzed FCS (Biochrom, Berlin, Germany) at 37°C. After 10 Gy γ-irradiation (Sect. 4.2.2, page 95) the cells were labelled immediately with [^{32}P]orthophosphate by adding 2.5 mCi [^{32}P]orthophosphate per plate and incubate for 2.5 h at 37°C. The cells were lysed on ice for 1 h with NP40 lysis buffer (10 mM NaH_2PO_4 pH 7, 1% (v/v) NP40, 50 mM Tris pH 8, 5 mM EDTA, 150 mM NaCl, 1 mM AEBSF). The lysates were centrifuged for 10 min at 13000 × g at 4°C and the supernatants were collected. Immunoprecipitation for p21 from the supernatants was carried out as followed.

The p21 antibody (AB) was pre-linked to the beads (1 µg AB with 20 µl beads) by incubation for 1.5 h at 4°C (rotating). The lysates were added to this antibody complex and incubated for 2 h at 4°C (rotating). After incubation, the antibody complexes were subsequently washed 4 times with the NP40 lysis buffer. The supernatants were discarded and the pellets were added 20 µl 2 × SDS sample buffer (4% (w/v) SDS, 0.16 M Tris pH 6.8, 20% (v/v) glycerol, 10% (v/v) β-Mercaptoethanol, 0.002% (w/v) bromophenol blue). The immunoprecipitated complexes were denaturated by heating for 10 min at 100°C and protein separation was carried out on a 12% SDS-PAGE (see Sect. 4.9.2, page 113).

The 12% SDS-PAGE was dried and exposed to a hyperfilm (Amersham, Buckinghamshire, UK) overnight. The fragments of the gel containing the radiolabeled p21 from the NHDF cells or p21his6-cmyc from the HeLa cells were excised, rehydrated and fractionated with a douncer pestle in 500 µl ammonium bicarbonate solution (4 mg/ml). 500 µl ammonium bicarbonate solution (4 mg/ml), 0.2% (w/v) SDS and 2% (v/v) β-Mercaptoethanol were added and the samples heated for 5 min at 95°C followed by incubation at room temperature over night (rotating). After 2 times centrifugation for 10 min, the supernatants were added 20 µg RNase and 250 µl of ice cold 100% trichloroacetic acid to precipitate the proteins during 1 h incubation on ice. After centrifugation the pellets were washed with 1 ml 100% EtOH and centrifuged twice; the supernatant discarded. The pellets obtained after both centrifugation steps were resuspended in 50 µl performic acid (10% (v/v) H_2O_2 in formic acid) each to oxidize the proteins (performic acid converts Met to Met sulfone and Cys to cysteic acid) and unified. 300 µl H_2O was added and the samples were lyophilised.

The protein was digested over night at 37°C using trypsin (25 µg per sample) that specifically cuts after arginine (R) and lysine (K) residues leaving many small fragments (25 fragments with a length of 1–16 aa.). After adding another 25 µg trypsin and further incubation for 2 h at 37°C, 300 µl H_2O was added and the samples lyophilised. The samples were rehydrated 3 times with 300 µl H_2O and lyophilised. The final pellets were resuspended in 5 µl pH 1.9 buffer (7.8% (v/v) acetic acid, 2.5% (v/v) formic acid) and incubated over night at RT. The samples were centrifuged, the pellet discarded and the supernatants lyophilised. The lyophilised samples were resuspended in 50 µl pH 1.9 buffer and given drop wise on a thin-layer cellulose (TLC) plate each. The TLC plate was connected with the electrophoresis buffer (pH 1.9 buffer) by Whatman papers as displayed in Fig. 70 A. The 1st dimension was run at 500 V (8–10 mA) for 1.5 h.

The TLC plates were dried before the 2nd dimension was run, placed in phosphopeptide chromatography buffer (37.5% (v/v) n-butanol, 25% (v/v) pyridine, 0.75% (v/v) acetic acid) as displayed below in Fig. 70 B. After 6 h the TCL plates were dried and exposed to a Hyperfilm (Amersham) for 4 weeks.

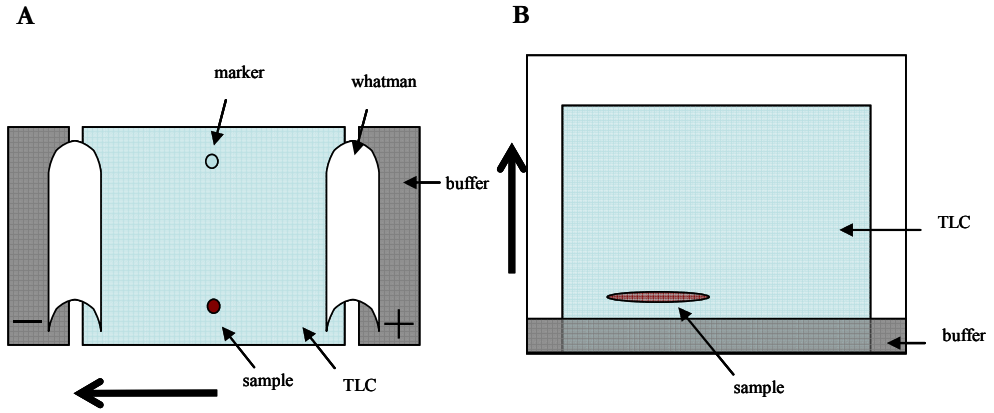

Fig. 70 **Schematic diagram of the 1st and 2nd Dimension of the phosphopeptide mapping.**

5 MATERIALS

5.1 Cell culture

AG medium
: EMEM (BioWhittaker, Walkersville, UK) with addition of 20% (v/v) foetal calfserum (Biochrom, Berlin, Germany), 2 mM L-glutamin (Biochrom), 100 U/ml penicillin (Biochrom) and 100 µg/ml streptomycin (Biochrom)

AG freezing medium
: AG medium with addition of 10% (v/v) glycerol

HCT medium
: McCoy's 5A Medium (Sigma) with addition of 10% (v/v) foetal calfserum (Biochrom, Berlin, Germany) and 2.8 mM L-glutamin (Biochrom)
HCT116 $p21^{-/-}$ additional 0.4 mg/ml geniticin G418 (Gibco BRL)

HCT freezing medium
: HCT medium with addition of 10% (v/v) DMSO

5.2 Solutions and buffers

Agarose gel loading buffer
: 5% glycerol, 0.025% bromphenolblue in 0.5 × TBE

Blocking solution 5% (w/v)
: 5% non-fat Nestlé-milkpowder in 1 × TBST

BSA solution
: 0.5% (w/v) in PBS

Dialyzed FCS (Biochrom, Berlin, Germany)

Ethidiumbromid staining solution
: 2 µg/ml EtBr in H_2O

Hepes extraction buffer
: 10 mM Hepes-KOH (hydroxyethylpiperazinethansulfosäure), 10 mM KCl, 1.5 mM $MgCl_2$, 0.5 mM dithiothreitol, 0.1% (v/v) triton X-100; pH 7.9, equilibrated with 1 M KOH

2 × Laemmli sample buffer
: 10 mM Tris-HCl pH 6.8, 2% (v/v)w, 20% (v/v) Glycerol

Paraformaldehyde solution
: 2% (w/v) paraformaldehyde in PBS

PBS
: Sigma w/o Ca^{2+} and Mg^{2+} (Dulbecco)

ToPro-3 solution with RNase A
: 1 µM ToPro-3 in PBS (Sigma) with addition of 100 µg/ml RNase A (Boehringer Mannheim)

SDS-PAGE laemmli running buffer
: 50 mM Tris-Base, 0.38 M Glycin, 0.1% (w/v) SDS

SDS-PAGE laemmli loading buffer
: 100 mM Tris-HCl pH 6.8, 2% (w/v) SDS, 20% (v/v) Glycerol, 0.02 mg/ml bromphenolblue, 2% (v/v) 2-mercaptoethanol

SDS-PAGE stacking gel (pH 6.8)
: 3.2% (v/v) acrylamid/*bis*-aAcrylamid (29:1), 0.125 M tris-HCl, 0.1% (w/v) SDS, 0.03% (w/v) ammoniumpersulfate, 0.05% (v/v) N,N,N',N'-tetramethylethylendiamin

SDS-PAGE seperating gel (pH 8.8)
: 12% (v/v) acrylamid/*bis*-acrylamid (29:1), 0.35 M tris-HCl, 0.1% (w/v) SDS, 0.03% (w/v) ammoniumpersulfate, 0.05% (v/v) N,N,N',N'-tetramethylethylendiamin

1 × TBST (pH 8.0)
: 10 mM Tris-HCl, 150 mM NaCl, 0.05% Tween 20

10 × TE (pH 8.0)
: 0.1 M tris-base, 0.01 M EDTA

SDS-PAGE transfer buffer
: 20% (v/v) methanol, 0.02 M Tris-HCl (pH 8.3), 0.15 M glycine, 0.1% (w/v) SDS

Trypsin-EDTA solution
: 0.05 g/l trypsin, 1 g/l EDTA in PBS without Mg^{2+} and Ca^{2+} (PAN, Aidenbach, Germany)

5.3 Materials and chemicals

Prestained protein weight marker
Premixed Protein Molecular Weight Marker (‚Full range rainbow protein molecular weight marker' 10 bis 250 kDa; Amersham, Buckinghamshire, UK)

Polyvinylidenfluorid membrane (Immobilon-P; MILLIPORE)

X-ray film (Hyperfilm ECL; Amersham, Buckinghamshire, UK)

Vectashield ‚Mounting Medium' (Vector Laboratories, Burlingame, CA, USA)

Glass cover slips (Menzel-Gläser, Braunschweig, Germany)

Perti dishes (Nunc, Roskilde, Denmark)

Culture flasks (Falcon, BD Biosciences, CA, USA)

Lipofectamine 2000 (Invitrogen, Carlsbad, CA, USA)

FuGENE 6 (Roche, Basel, Schwitzerland)

5.4 Used kits

Lowry Assay ‚D_C Protein Assay' (Bio-Rad, CA, USA)

‚ECL Plus™ Western blotting detection system' (Amersham, Buckinghamshire, UK)

‚Mykoplasma Detektion Kit' (Boehringer Mannheim, Germany)

Bradford Assay Rothiquant (Roth, Karlsuhe, Germany)

Qiagen kit (Qiagen, Hilden, Germany)

DNA purification kit Easy pure (Biozym Diagnostik, Oldendorf, Germany)

5.5 Used apparatus

Nucleofector from Amaxa (Köln, Germany)

Elisa-*Reader* (EL_X 800, Bio-Tek Instruments, Bad Friedrichshall, Germany)

Z2 Coulter Counter (Beckman Coulter, Krefeld, Germany)

Confocal laserscanning system Leica TCS

Equipped with a DM IRBE inverted microscope (lens: PlanApo 63 × / 1.32 oil) and an argon/krypton laser; connected to a Märzhäuser computerised stage control SCAN 100 × 100

Tank-blot system ‚Mini Trans-Blot' (Bio-Rad, Munich, Germany)

SDS-PAGE system ‚Mini-Protean II' (Bio-Rad, Munich, Germany)

SN4 dosimeter (PTW Freiburg, Germany)

X-ray generator Isovolt DS1, type IV320-13 (Seifert, Germany)

6 SUPPLEMENT

6.1 To Sect. 2.2.1 Kinetics of p21/PCNA foci formation

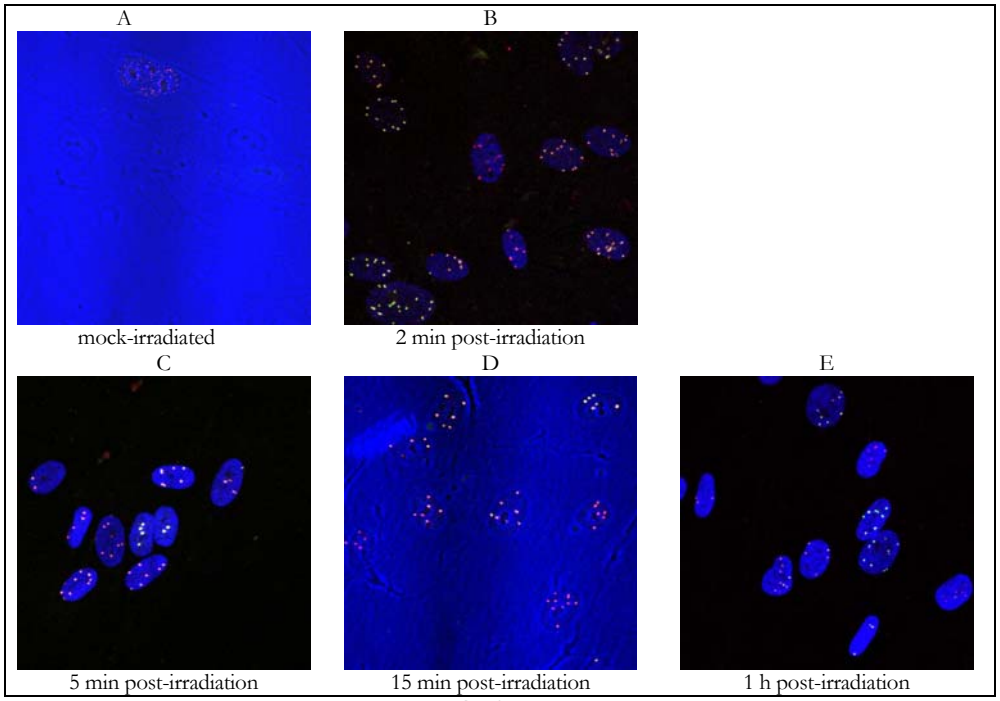

Fig. 71 **Early time course for p21 and PCNA accumulations in human fibroblasts after exposure to uranium ions.** A: mock-irradiated; B–F: after irradiation with uranium ions. p21 (green) and PCNA (red), DNA (blue). Unfortunately, the ToPro3 signal (blue) was hardly detectable in various samples, as in A and D. At all time-points, clear foci of both p21 and PCNA are detectable in the irradiated samples.

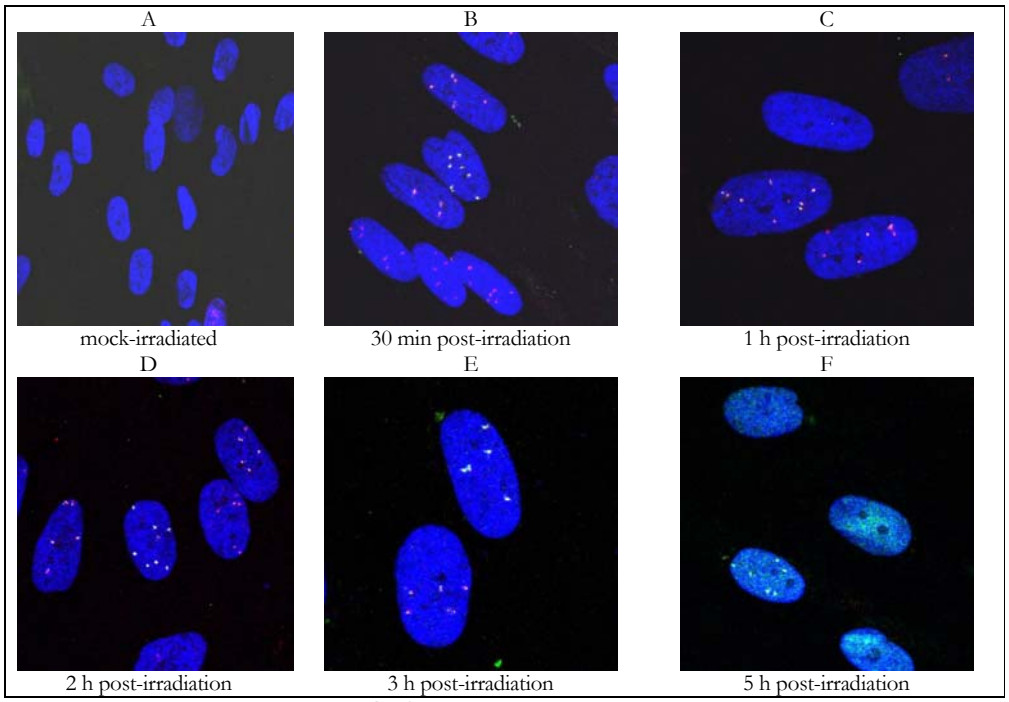

Fig. 72 **Resolution of p21 and PCNA foci in human fibroblasts after irradiation with nickel ions.** p21 (green) and PCNA (red) accumulate to foci at all taken time-points. The mock-irradiated cells do not show any protein accumulations (A). An induction of the p21 level 5 h post-irradiation is seen by the elevated green dispersed fluorescence in F. DNA visualized by ToPro3 (blue).

Human fibroblasts irradiated with Ni ions and fixed 30 min, 1, 2, 3 or 5 h post-irradiation showed accumulations of p21 as well as PCNA (Fig. 72 B–F). Analysis showed, that within this chosen time frame, a maximum of cells showing p21 foci occurred 3 h post-irradiation (75%, n = 28). However, 5 hours after irradiation, still many nuclei showed visible p21 foci (60%, n = 10), with less nuclei displaying PCNA foci (40%, n = 10). It must be noted that here the p21 level was quite high compared to the earlier taken time-points due to an induction of the p21 protein level and PCNA was hardly visible, making me only analyze 10 nuclei making it only being a preliminary result.

6.2 To Sect. 2.2.4 Recombinant p21T145D no longer interacts with PCNA

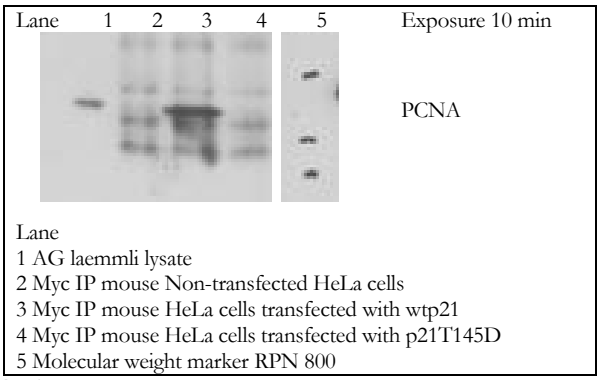

Fig. 73 **PCNA is not co-immunoprecipitated by anti-myc immunoprecipitation of p21T145D.** Westernblot analysis of the anti-myc complexes from HeLa cells, non-transfected (lane 2), transfected with the wtp21 plasmid (lane 3) or with the p21T145D plasmid (lane 4). Lane 1: Crude lysate from AG cells. Lane 5: Molecularweightmarker.

6.3 To 2.7.1 Ectopical expression of a GFPp21 Fusion protein

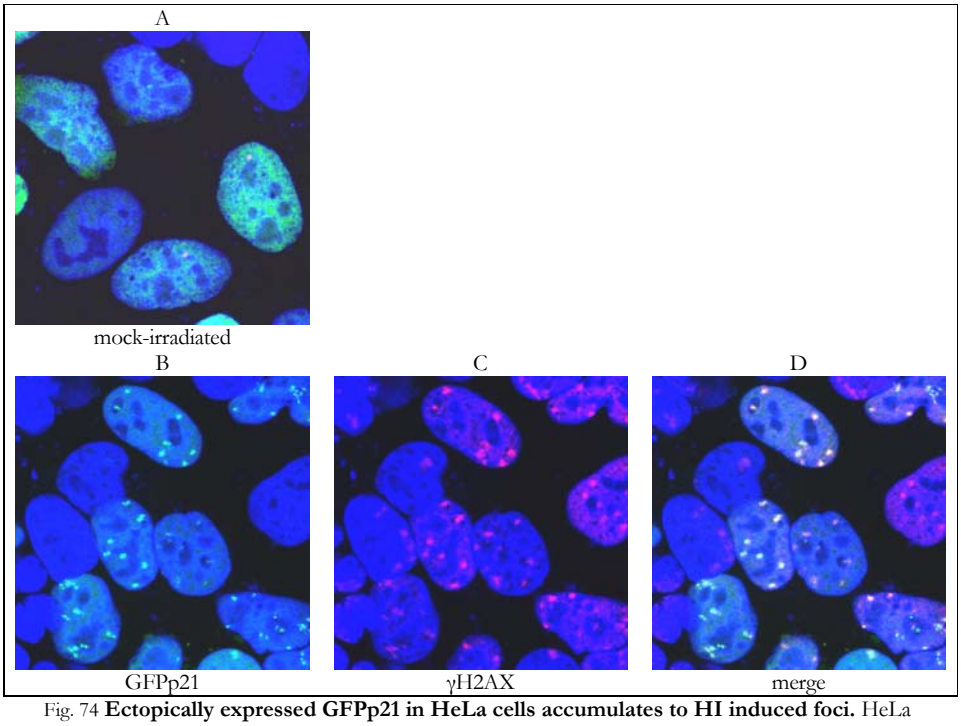

Fig. 74 **Ectopically expressed GFPp21 in HeLa cells accumulates to HI induced foci.** HeLa cells transfected with GFPp21 fusion protein and irradiated with Sm ions (3×10^6 p/cm^2; 11.4 MeV/u; 10290 V/µm) 24 h after transfection show clear GFPp21 foci 30 min post irradiation (B–D). Fixed without extraction and stained for γH2AX (red). A: mock-irradiated. GFPp21: green. DNA: blue.

HeLa cells transfected with the p21GFP construct and exposed to Sm ions (3×10^6 p/cm^2; 11.4 MeV/u; 10290 V/µm) also showed clear irradiation-induced p21GFP foci as displayed in Fig. 74 B. Mock-irradiated cells show a heterogeneous expression level of the p21GFP protein (Fig. 74 A). Non-transfected HeLa cells do not give any detectable green fluorescence signal (data not shown).

6.4 To Sect. 4.8.1 Establishment of a method to immunoprecipitate a p21 complex

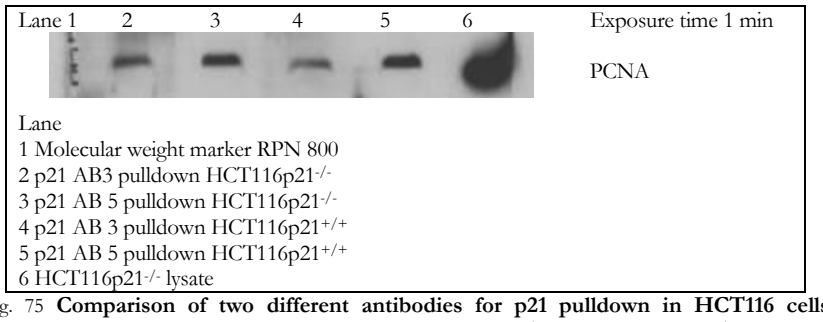

Fig. 75 **Comparison of two different antibodies for p21 pulldown in HCT116 cells.** Western Blot analysis of p21 pulldown in HCT116p21$^{+/+}$ and HCT116p21$^{-/-}$ cells. The pulldown was done either with a polyclonal rabbit or monoclonal mouse antibody against human p21 followed by Western Blot detection with PCNA mouse or rabbit, respectively.

Fig. 75 displays the WB analysis of the p21 pulldown in both HCT116 cell lines using two different p21 antibodies. A slight difference between the used antibody was seen, as the detectable PCNA band is elevated with the use of the p21 polyclonal rabbit antibody (AB5) compared to the IP's done with the p21 monoclonal mouse antibody (AB3) (Fig. 75 lane 3 and 5 versus lane 2 and 4). However, both cell lines gave a comparable PCNA signal with the same antibody used for the pulldown (Fig. 75; lane 2 versus 4 and lane 3 versus 5). As the AB5 p21 antibody gave the best and clearest detectable PCNA band after WB analysis, this antibody was used for the further made IP's. The next approach was to check the non-specific binding of PCNA to the used IgG's, Western Blot analysis is shown in Fig. 76.

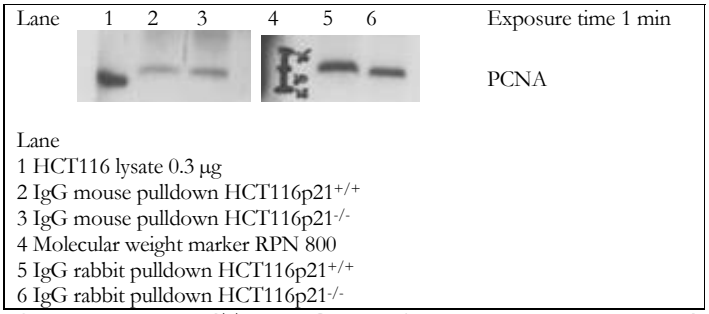

Fig. 76 **IgG pulldown from HCT116 cell Dignam A lysates gives a detectable PCNA signal by Western Blot analysis.** Western Blot analysis of IgG rabbit and mouse pulldown in HCT116 cells.

The pulldown with IgG mouse antibody in Dignam A buffer gave a detectable PCNA signal in both HCT116 cell lines as seen in Fig. 76, lane 2 and 3. Also with the IgG rabbit pulldown, a

clear PCNA band was detected, Fig. 76 lane 5 and 6. It is seen, that with the used IgG's a non-specific binding of a PCNA complex is reached. Before the specific p21 precipitation however, the lysates are precleared with the appropriate IgG antibody. This means that the shown PCNA band in Fig. 76 should be cleared out of the sample before the specific p21 pulldown is carried out. Therefore, I assume that the detectable PCNA band after p21 pulldown in the HCT116p21$^{-/-}$ cells is not a result of the unspecific binding of a PCNA complex to the used IgG's, but maybe caused by binding of a p21-like protein. If it is the case, possibly the binding affinity differ from the specific binding of p21. This made me try various protocols using different harsh buffers. It must be mentioned however, that the immunofluorescence analysis and WB analysis of HCT116p21$^{-/-}$ whole cell lysate did not give any positive p21 signal with the here used p21 antibodies.

I compared the results of IP's in RIPA and Dignam A buffer (RIPA contains a detergent, Dignam A not) and changed the waschbuffer from 0.1% SDS Babco buffer to 0.5% SDS Babco buffer. The WB analysis is shown below in Fig. 77.

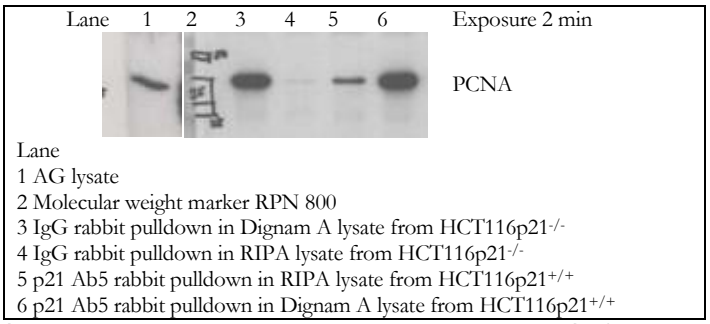

Fig. 77 **Changed IP conditions clear out the former observed PCNA signal after IgG pulldown in HCT116p21$^{-/-}$cell lysate.**

The change of the buffer in which the IP was carried out from Dignam A to Ripa buffer made a severe difference in the unspecific IgG pulldown from the HCT116p21$^{-/-}$ cells. The IP in Dignam A buffer with the IgG rabbit from the HCT116p21$^{-/-}$ cell lysate resulted in a clear PCNA band after WB analysis (Fig. 77 lane 3). However, if the RIPA buffer was used during this IP, a hardly detectable PCNA signal was observed (Fig. 77 lane 4). Also, the p21 pulldown with the p21 Ab5 antibody in HCT116p21$^{+/+}$ cells showed a difference in the PCNA signal, depending on the used buffer. The detectable PCNA is clearly reduced by the usage of the RIPA buffer in stead of Dignam A buffer throughout the IP (Fig. 77 lane 5 versus 6).

BIBLIOGRAPHY

Adimoolam,S., C.X.Lin, and J.M.Ford. 2001. "The p53-regulated cyclin-dependent kinase inhibitor, p21 (cip1, waf1, sdi1), is not required for global genomic and transcription-coupled nucleotide excision repair of UV-induced DNA photoproducts." *J.Biol.Chem.* 276:25813-25822.

Agell,N., M.Jaumot, A.Rodriguez-Vilarrupla, S.Brun, N.Abella, N.Canela, J.M.Estanyol, O.Bachs. 2006. "The diverging roles of calmodulin and PKC in the regulation of p21 intracellular localization." *Cell cycle.* Jan. 5(1):3-6

Ahnesorg,P., P.Smith, and S.P.Jackson. 2006. "XLF interacts with the XRCC4-DNA ligase IV complex to promote DNA nonhomologous end-joining." *Cell.* 124:301-313.

Ame,J.C., C.Spenlehauer, and M.G.De. 2004. "The PARP superfamily." *Bioessays.* 26:882-893.

Ando,T., T.Kawabe, H.Ohara, B.Ducommun, M.Itoh, and T.Okamoto. 2001. "Involvement of the interaction between p21 and proliferating cell nuclear antigen for the maintenance of G2/M arrest after DNA damage." *J.Biol.Chem.* 276:42971-42977.

Appella,E. and C.W.Anderson. 2000. "Signaling to p53: breaking the posttranslational modification code." *Pathol.Biol.(Paris)* . 48:227-245.

Asada,M., T.Yamada, H.Ichijo, D.Delia, K.Miyazono, K.Fukumuro, and S.Mizutani. 1999. "Apoptosis inhibitory activity of cytoplasmic p21(Cip1/WAF1) in monocytic differentiation." *EMBO J.* 18:1223-1234.

Audebert,M., B.Salles, and P.Calsou. 2004. "Involvement of poly(ADP-ribose) polymerase-1 and XRCC1/DNA ligase III in an alternative route for DNA double-strand breaks rejoining." *J.Biol.Chem.* 279:55117-55126.

Avkin,S., Z.Sevilya, L.Toube, N.Geacintov, S.G.Chaney, M.Oren, and Z.Livneh. 2006. "p53 and p21 regulate error-prone DNA repair to yield a lower mutation load." *Mol.Cell.* 22:407-413.

Bakkenist,C.J. and M.B.Kastan. 2003. "DNA damage activates ATM through intermolecular autophosphorylation and dimer dissociation." *Nature.* 421:499-506.

Balajee,A.S. and C.R.Geard. 2001. "Chromatin-bound PCNA complex formation triggered by DNA damage occurs independent of the ATM gene product in human cells." *Nucleic Acids Res.* 29:1341-1351.

Barrows,L.R., J.A.Holden, M.Anderson, and P.D'Arpa. 1998. "The CHO XRCC1 mutant, EM9, deficient in DNA ligase III activity, exhibits hypersensitivity to camptothecin independent of DNA replication." *Mutat.Res.* 408:103-110.

Bassing,C.H. and F.W.Alt. 2004. "The cellular response to general and programmed DNA double strand breaks." *DNA Repair (Amst).* 3:781-796.

Beard,W.A. and S.H.Wilson. 2000. "Structural design of a eukaryotic DNA repair polymerase: DNA

polymerase beta." *Mutat.Res.* 460:231-244.

Bendjennat,M., J.Boulaire, T.Jascur, H.Brickner, V.Barbier, A.Sarasin, A.Fotedar, and R.Fotedar. 2003. "UV irradiation triggers ubiquitin-dependent degradation of p21(WAF1) to promote DNA repair." *Cell.* 114:599-610.

Blagosklonny, M.V. 2002. "Are p27 and p21 cytoplasmatic oncoproteins?" *Cell cycle.* Nov-Dec 1(6):391-3

Bohr,V.A., C.A.Smith, D.S.Okumoto, and P.C.Hanawalt. 1985. "DNA repair in an active gene: removal of pyrimidine dimers from the DHFR gene of CHO cells is much more efficient than in the genome overall." *Cell.* 40:359-369.

Bradford,M.M. 1976. "A rapid and sensitive method for the quantitation of microgram quantities of protein utilizing the principle of protein-dye binding." *Anal.Biochem.* 72:248-254.

Bragg,W., R.Kleemann. 1905. "On the α-particles of radium and their loss of range in passing through various atoms and molecules." *Phil.Mag.* 10:318–340

Brem,R. and J.Hall. 2005. "XRCC1 is required for DNA single-strand break repair in human cells." *Nucleic Acids Res.* 33:2512-2520.

Brugarolas,J., C.Chandrasekaran, J.I.Gordon, D.Beach, T.Jacks, and G.J.Hannon. 1995. "Radiation-induced cell cycle arrest compromised by p21 deficiency." *Nature.* 377:552-557.

Brugarolas,J., K.Moberg, S.D.Boyd, Y.Taya, T.Jacks, and J.A.Lees. 1999. "Inhibition of cyclin-dependent kinase 2 by p21 is necessary for retinoblastoma protein-mediated G1 arrest after gamma-irradiation." *Proc.Natl.Acad.Sci.U.S.A.* 96:1002-1007.

Bunz,F., A.Dutriaux, C.Lengauer, T.Waldman, S.Zhou, J.P.Brown, J.M.Sedivy, K.W.Kinzler, and B.Vogelstein. 1998. "Requirement for p53 and p21 to sustain G2 arrest after DNA damage." *Science.* 282:1497-1501.

Cai,K. and B.D.Dynlacht. 1998. "Activity and nature of p21(WAF1) complexes during the cell cycle." *Proc.Natl.Acad.Sci.U.S.A.* 95:12254-12259.

Caldecott,K. and P.Jeggo. 1991. "Cross-sensitivity of gamma-ray-sensitive hamster mutants to cross-linking agents." *Mutat.Res.* 255:111-121.

Caldecott,K.W., J.D.Tucker, L.H.Stanker, and L.H.Thompson. 1995. "Characterization of the XRCC1-DNA ligase III complex in vitro and its absence from mutant hamster cells." *Nucleic Acids Res.* 23:4836-4843.

Caldecott,K.W., S.Aoufouchi, P.Johnson, and S.Shall. 1996. "XRCC1 polypeptide interacts with DNA polymerase beta and possibly poly (ADP-ribose) polymerase, and DNA ligase III is a novel molecular 'nick-sensor' in vitro." *Nucleic Acids Res.* 24:4387-4394.

Caldecott,K.W. 2001. "Mammalian DNA single-strand break repair: an X-ra(y)ted affair." *Bioessays.* 23:447-455.

Cantoni,O., D.Murray, and R.E.Meyn. 1987. "Induction and repair of DNA single-strand breaks in EM9 mutant

CHO cells treated with hydrogen peroxide." *Chem.Biol.Interact.* 63:29-38.

Cazzalini,O., P.Perucca, F.Riva, L.A.Stivala, L.Bianchi, V.Vannini, B.Ducommun, and E.Prosperi. 2003. "p21CDKN1A does not interfere with loading of PCNA at DNA replication sites, but inhibits subsequent binding of DNA polymerase delta at the G1/S phase transition." *Cell Cycle.* 2:596-603.

Chen,I.T., M.Akamatsu, M.L.Smith, F.D.Lung, D.Duba, P.P.Roller, A.J.Fornace, Jr., and P.M.O'Connor. 1996. "Characterization of p21Cip1/Waf1 peptide domains required for cyclin E/Cdk2 and PCNA interaction." *Oncogene.* 12:595-607.

Chen,J., P.K.Jackson, M.W.Kirschner, and A.Dutta. 1995. "Separate domains of p21 involved in the inhibition of Cdk kinase and PCNA." *Nature.* 374:386-388.

Chen,J., P.Saha, S.Kornbluth, B.D.Dynlacht, and A.Dutta. 1996. "Cyclin-binding motifs are essential for the function of p21CIP1." *Mol.Cell Biol.* 16:4673-4682.

Child,E.S. and D.J.Mann. 2006. "The intricacies of p21 phosphorylation: protein/protein interactions, subcellular localization and stability." *Cell Cycle.* 5:1313-1319.

Chuang,L.S., H.I.Ian, T.W.Koh, H.H.Ng, G.Xu, and B.F.Li. 1997. "Human DNA-(cytosine-5) methyltransferase-PCNA complex as a target for p21WAF1." *Science.* 277:1996-2000.

Cooper,M.P., A.S.Balajee, and V.A.Bohr. 1999. "The C-terminal domain of p21 inhibits nucleotide excision repair In vitro and In vivo." *Mol.Biol.Cell.* 10:2119-2129.

Coqueret,O. 2003. "New roles for p21 and p27 cell-cycle inhibitors: a function for each cell compartment?" *Trends Cell Biol.* 13:65-70.

Costa,R.M., V.Chigancas, R. da S.Galhardo, H.Carvalho, C.F.Menck. 2003. "The eukaryotic nucleotide excision repair pathway." *Biochemie.* Nov. 85(11):1083-99.

Costes,S.V., A.Ponomarev, J.L.Chen, D.Nguyen, F.A.Cucinotta, and M.H.Barcellos-Hoff. 2007. "Image-Based Modeling Reveals Dynamic Redistribution of DNA Damage into Nuclear Sub-Domains." *PLoS.Comput.Biol.* 3:e155.

Covey,J.M., C.Jaxel, K.W.Kohn, and Y.Pommier. 1989. "Protein-linked DNA strand breaks induced in mammalian cells by camptothecin, an inhibitor of topoisomerase I." *Cancer Res.* 49:5016-5022.

Critchlow,S.E. and S.P.Jackson. 1998. "DNA end-joining: from yeast to man." *Trends Biochem.Sci.* 23:394-398.

Dantzer,F., H.P.Nasheuer, J.L.Vonesch, M.G.De, and M.J.Menissier-De. 1998. "Functional association of poly(ADP-ribose) polymerase with DNA polymerase alpha-primase complex: a link between DNA strand break detection and DNA replication." *Nucleic Acids Res.* 26:1891-1898.

de Murcia,J.M., C.Niedergang, C.Trucco, M.Ricoul, B.Dutrillaux, M.Mark, F.J.Oliver, M.Masson, A.Dierich, M.LeMeur, C.Walztinger, P.Chambon, and M.G.De. 1997. "Requirement of poly(ADP-ribose)

polymerase in recovery from DNA damage in mice and in cells." *Proc.Natl.Acad.Sci.U.S.A.* 94:7303-7307.

Demple,B., T.Herman, and D.S.Chen. 1991. "Cloning and expression of APE, the cDNA encoding the major human apurinic endonuclease: definition of a family of DNA repair enzymes." *Proc.Natl.Acad.Sci.U.S.A.* 88:11450-11454.

Deng,C., P.Zhang, J.W.Harper, S.J.Elledge, and P.Leder. 1995. "Mice lacking p21CIP1/WAF1 undergo normal development, but are defective in G1 checkpoint control." *Cell.* 82:675-684.

Dianova,I.I., V.A.Bohr, and G.L.Dianov. 2001. "Interaction of human AP endonuclease 1 with flap endonuclease 1 and proliferating cell nuclear antigen involved in long-patch base excision repair." *Biochemistry.* 40:12639-12644.

Dong,Y., S.L.Chi, A.D.Borowsky, Y.Fan, and R.H.Weiss. 2004. "Cytosolic p21Waf1/Cip1 increases cell cycle transit in vascular smooth muscle cells." *Cell Signal.* 16:263-269.

Dotto,G.P. 2000. "p21(WAF1/Cip1): more than a break to the cell cycle?" *Biochim.Biophys.Acta.* 1471:M43-M56.

Dulic,V., W.K.Kaufmann, S.J.Wilson, T.D.Tlsty, E.Lees, J.W.Harper, S.J.Elledge, and S.I.Reed. 1994. "p53-dependent inhibition of cyclin-dependent kinase activities in human fibroblasts during radiation-induced G1 arrest." *Cell.* 76:1013-1023.

Dupont,J., M.Karas, and D.LeRoith. 2003. "The cyclin-dependent kinase inhibitor p21CIP/WAF is a positive regulator of insulin-like growth factor I-induced cell proliferation in MCF-7 human breast cancer cells." *J.Biol.Chem.* 278:37256-37264.

Durocher,D. and S.P.Jackson. 2001. "DNA-PK, ATM and ATR as sensors of DNA damage: variations on a theme?" *Curr.Opin.Cell Biol.* 13:225-231.

Eguchi-Kasai,K., M.Murakami, H.Itsukaichi, K.Fukutsu, T.Kanai, Y.Furusawa, K.Sato, H.Ohara, and F.Yatagai. 1996. "The role of DNA repair on cell killing by charged particles." *Adv.Space Res.* 18:109-118.

El-Deiry,W.S., T.Tokino, V.E.Velculescu, D.B.Levy, R.Parsons, J.M.Trent, D.Lin, W.E.Mercer, K.W.Kinzler, and B.Vogelstein. 1993. "WAF1, a potential mediator of p53 tumor suppression." *Cell.* 75:817-825.

El-Khamisy,S.F., M.Masutani, H.Suzuki, and K.W.Caldecott. 2003. "A requirement for PARP-1 for the assembly or stability of XRCC1 nuclear foci at sites of oxidative DNA damage." *Nucleic Acids Res.* 31:5526-5533.

Falck,J., J.Coates, and S.P.Jackson. 2005. "Conserved modes of recruitment of ATM, ATR and DNA-PKcs to sites of DNA damage." *Nature.* 434:605-611.

Fan,J., M.Otterlei, H.K.Wong, A.E.Tomkinson, and D.M.Wilson, III. 2004. "XRCC1 co-localizes and physically interacts with PCNA." *Nucleic Acids Res.* 32:2193-2201.

Fernandez-Capetillo,O., A.Lee, M.Nussenzweig, and A.Nussenzweig. 2004. "H2AX: the histone guardian of the genome." *DNA Repair (Amst).* 3:959-967.

Fernet,M., V.Ponette, E.iaud-Alexandre, M.J.Menissier-De, M.G.De, N.Giocanti, F.Megnin-Chanet, and V.Favaudon. 2000. "Poly(ADP-ribose) polymerase, a major determinant of early cell response to ionizing radiation." *Int.J.Radiat.Biol.* 76:1621-1629.

Fournier,C., C.Wiese, and G.Taucher-Scholz. 2004. "Accumulation of the cell cycle regulators TP53 and CDKN1A (p21) in human fibroblasts after exposure to low- and high-LET radiation." *Radiat.Res.* 161:675-684.

Fournier,C., D.Becker, M.Winter, P.Barberet, M.Heiss, B.Fischer, J.Topsch, and G.Taucher-Scholz. 2007. "Cell cycle-related bystander responses are not increased with LET after heavy-ion irradiation." *Radiat.Res.* 167:194-206.

Fricke,H., E.J.Hart. 1966. "Chemical dosimetry." *Radiation Dosimetry.* Vol. II:167-239

Friedberg,E.C., G.G.Walker and W.Siede. 1995. "DNA repair and mutagenesis." *AM Press, Washington DC.*

Frosina,G., P.Fortini, O.Rossi, F.Carrozzino, G.Raspaglio, L.S.Cox, D.P.Lane, A.Abbondandolo, and E.Dogliotti. 1996. "Two pathways for base excision repair in mammalian cells." *J.Biol.Chem.* 271:9573-9578.

Frouin,I., G.Maga, M.Denegri, F.Riva, M.Savio, S.Spadari, E.Prosperi, and A.I.Scovassi. 2003. "Human proliferating cell nuclear antigen, poly(ADP-ribose) polymerase-1, and p21waf1/cip1. A dynamic exchange of partners." *J.Biol.Chem.* 278:39265-39268.

Furuta,T., H.Takemura, Z.Y.Liao, G.J.Aune, C.Redon, O.A.Sedelnikova, D.R.Pilch, E.P.Rogakou, A.Celeste, H.T.Chen, A.Nussenzweig, M.I.Aladjem, W.M.Bonner, and Y.Pommier. 2003. "Phosphorylation of histone H2AX and activation of Mre11, Rad50, and Nbs1 in response to replication-dependent DNA double-strand breaks induced by mammalian DNA topoisomerase I cleavage complexes." *J.Biol.Chem.* 278:20303-20312.

Gartel,A.L., M.S.Serfas, and A.L.Tyner. 1996. "p21--negative regulator of the cell cycle." *Proc.Soc.Exp.Biol.Med.* 213:138-149.

Gartel,A.L. and A.L.Tyner. 2002. "The role of the cyclin-dependent kinase inhibitor p21 in apoptosis." *Mol.Cancer Ther.* 1:639-649.

Goodhead,D.T. 1994. "Initial events in the cellular effects of ionizing radiations: clustered damage in DNA." *Int.J.Radiat.Biol.* 65:7-17.

Gu,Y., C.W.Turck, and D.O.Morgan. 1993. "Inhibition of CDK2 activity in vivo by an associated 20K regulatory subunit." *Nature.* 366:707-710.

Gueven,N., O.J.Becherel, A.W.Kijas, P.Chen, O.Howe, J.H.Rudolph, R.Gatti, H.Date, O.Onodera, G.Taucher-Scholz, and M.F.Lavin. 2004. "Aprataxin, a novel protein that protects against genotoxic stress." *Hum.Mol.Genet.* 13:1081-1093.

Gulbis,J.M., Z.Kelman, J.Hurwitz, M.O'Donnell, and J.Kuriyan. 1996. "Structure of the C-terminal region of p21(WAF1/CIP1) complexed with human PCNA." *Cell.* 87:297-306.

Haberer T., W.Becher, D.Schardt, G.Kraft (1993) Magnetic scanning system for heavy ion therapy. *Nucl.Instr.Meth.* 330:296-305

Halicka,H.D., X.Huang, F.Traganos, M.A.King, W.Dai, and Z.Darzynkiewicz. 2005. "Histone H2AX phosphorylation after cell irradiation with UV-B: relationship to cell cycle phase and induction of apoptosis." *Cell Cycle.* 4:339-345.

Harper,J.W., G.R.Adami, N.Wei, K.Keyomarsi, and S.J.Elledge. 1993. "The p21 Cdk-interacting protein Cip1 is a potent inhibitor of G1 cyclin-dependent kinases." *Cell.* 75:805-816.

Heilmann,J., G.Taucher-Scholz, and G.Kraft. 1995. "Induction of DNA double-strand breaks in CHO-K1 cells by carbon ions." *Int.J.Radiat.Biol.* 68:153-162.

Heilmann,J., G.Taucher-Scholz, T.Haberer, M.Scholz, and G.Kraft. 1996. "Measurement of intracellular dna double-strand break induction and rejoining along the track of carbon and neon particle beams in water." *Int.J.Radiat.Oncol.Biol.Phys.* 34:599-608.

Hinz,J.M., N.A.Yamada, E.P.Salazar, R.S.Tebbs, and L.H.Thompson. 2005. "Influence of double-strand-break repair pathways on radiosensitivity throughout the cell cycle in CHO cells." *DNA Repair (Amst).* 4:782-792.

hm-Daphi,J., C.Sass, and W.Alberti. 2000. "Comparison of biological effects of DNA damage induced by ionizing radiation and hydrogen peroxide in CHO cells." *Int.J.Radiat.Biol.* 76:67-75.

Hoeijmakers,J.H. 2001. "DNA repair mechanisms." *Maturitas.* 38:17-22.

Hopfner,K.P., C.D.Putnam, and J.A.Tainer. 2002. "DNA double-strand break repair from head to tail." *Curr.Opin.Struct.Biol.* 12:115-122.

ICRU. 1970. "Linear Energy Transfer." Tech. Rep. 16. International Commission on Radiation Units and Measurements.

Ismail,I., S.Nyström, J.Nygren, O.Hammersten. 2005. "Activation of Ataxia Telangiectasia Mutated by DNA srand break-inducing agents correlates closely with the number of DNA double strandbreaks." J.Biol.Chem. Vol. 280(6):4649-4655

Izumi,T., L.R.Wiederhold, G.Roy, R.Roy, A.Jaiswal, K.K.Bhakat, S.Mitra, and T.K.Hazra. 2003. "Mammalian DNA base excision repair proteins: their interactions and role in repair of oxidative DNA damage." *Toxicology.* 193:43-65.

Jackson,S.P. 2002. "Sensing and repairing DNA double-strand breaks." *Carcinogenesis.* 23:687-696.

Jaiswal,A.S., L.B.Bloom, and S.Narayan. 2002. "Long-patch base excision repair of apurinic/apyrimidinic site DNA is decreased in mouse embryonic fibroblast cell lines treated with plumbagin: involvement of cyclin-dependent kinase inhibitor p21Waf-1/Cip-1." *Oncogene.* 21:5912-5922.

Jakob,B., M.Scholz, and G.Taucher-Scholz. 2000. "Immediate localized CDKN1A (p21) radiation response after damage produced by heavy-ion tracks." *Radiat.Res.* 154:398-405.

Jakob,B., M.Scholz, and G.Taucher-Scholz. 2002. "Characterization of CDKN1A (p21) binding to sites of heavy-ion-induced damage: colocalization with proteins involved in DNA repair." *Int.J.Radiat.Biol.* 78:75-88.

Jakob,B., M.Scholz, and G.Taucher-Scholz. 2003. "Biological imaging of heavy charged-particle tracks." *Radiat.Res.* 159:676-684.

Jakob,B., J.H.Rudolph, N.Gueven, M.F.Lavin, and G.Taucher-Scholz. 2005. "Live cell imaging of heavy-ion-induced radiation responses by beamline microscopy." *Radiat.Res.* 163:681-690.

Janicke,R.U., D.Sohn, F.Essmann, and K.Schulze-Osthoff. 2007. "The multiple battles fought by anti-apoptotic p21." *Cell Cycle.* 6:407-413.

Jeggo,P.A. 1998. "DNA breakage and repair." *Adv.Genet.* 38:185-218.

Johnson,R.D. and M.Jasin. 2000. "Sister chromatid gene conversion is a prominent double-strand break repair pathway in mammalian cells." *EMBO J.* 19:3398-3407.

Kanaar,R., J.H.Hoeijmakers, and G.van. 1998. "Molecular mechanisms of DNA double strand break repair." *Trends Cell Biol.* 8:483-489.

Karran,P. 2000. "DNA double strand break repair in mammalian cells." *Curr.Opin.Genet.Dev.* 10:144-150.

Kelman,Z. and J.Hurwitz. 1998. "Protein-PCNA interactions: a DNA-scanning mechanism?" *Trends Biochem.Sci.* 23:236-238.

Kim,J.A., M.Kruhlak, F.Dotiwala, A.Nussenzweig, and J.E.Haber. 2007. "Heterochromatin is refractory to gamma-H2AX modification in yeast and mammals." *J.Cell Biol.* 178:209-218.

Kobayashi,J., A.Antoccia, H.Tauchi, S.Matsuura, and K.Komatsu. 2004. "NBS1 and its functional role in the DNA damage response." *DNA Repair (Amst).* 3:855-861.

Kohn,K.W. 1999. "Molecular interaction map of the mammalian cell cycle control and DNA repair systems." *Mol.Biol.Cell.* 10:2703-2734.

Kraft,G., H.Dautes, B.Fischer., U.Kopf, H.Liebold, D.Quis, H.Stelzer. 1980. "Irradiation chamber and sample changer for biological samples." *Nucl.Instr.Meth.* 169: 175-179

Kraft,G. 1997. "Radiobiology of heavy charged particles". *Advances in Hardrontherapy. Excerpta Medica.* Int. Congr. Series 1144:385–404

Kraft,G. 2000. "Tumor therapy with heavy charged particles". *Prog.Part.Nucl.Phys.* 45 (suppl. 2), 473-544

Kraft,G. 2002. "Radiobiological effects of highly charged ions." The physics of highly and multiple charged ions. *Curell Kluwer Academic Publischer.*

Krokan,H.E., R.Standal, and G.Slupphaug. 1997. "DNA glycosylases in the base excision repair of DNA." *Biochem.J.* 325 (Pt 1):1-16.

Kruhlak,M.J., A.Celeste, G.Dellaire, O.Fernandez-Capetillo, W.G.Muller, J.G.McNally, D.P.Bazett-Jones, and A.Nussenzweig. 2006. "Changes in chromatin structure and mobility in living cells at sites of DNA double-strand breaks." *J.Cell Biol.* 172:823-834.

Kurz,E.U. and S.P.Lees-Miller. 2004. "DNA damage-induced activation of ATM and ATM-dependent signaling pathways." *DNA Repair (Amst).* 3:889-900.

LaBaer,J., M.D.Garrett, L.F.Stevenson, J.M.Slingerland, C.Sandhu, H.S.Chou, A.Fattaey, and E.Harlow. 1997. "New functional activities for the p21 family of CDK inhibitors." *Genes Dev.* 11:847-862.

Leammli,U.K. 1970. "Cleavage of structural proteins during the assembly of the head of bacteriophage T4." *Nature.* 227 (259): 680-5

Lan,L., S.Nakajima, Y.Oohata, M.Takao, S.Okano, M.Masutani, S.H.Wilson, and A.Yasui. 2004. "In situ analysis of repair processes for oxidative DNA damage in mammalian cells." *Proc.Natl.Acad.Sci.U.S.A.* 101:13738-13743.

Lee,H., J.M.Larner, and J.L.Hamlin. 1997. "A p53-independent damage-sensing mechanism that functions as a checkpoint at the G1/S transition in Chinese hamster ovary cells." *Proc.Natl.Acad.Sci.U.S.A.* 94:526-531.

Lee,J.H. and T.T.Paull. 2005. "ATM activation by DNA double-strand breaks through the Mre11-Rad50-Nbs1 complex." *Science.* 308:551-554.

Levy,N., A.Martz, A.Bresson, C.Spenlehauer, M.G.De, and M.J.Menissier-De. 2006. "XRCC1 is phosphorylated by DNA-dependent protein kinase in response to DNA damage." *Nucleic Acids Res.* 34:32-41.

Li,R., S.Waga, G.J.Hannon, D.Beach, and B.Stillman. 1994. "Differential effects by the p21 CDK inhibitor on PCNA-dependent DNA replication and repair." *Nature.* 371:534-537.

Li,X., J.Li, J.Harrington, M.R.Lieber, and P.M.Burgers. 1995. "Lagging strand DNA synthesis at the eukaryotic replication fork involves binding and stimulation of FEN-1 by proliferating cell nuclear antigen." *J.Biol.Chem.* 270:22109-22112.

Lieber,M.R., Y.Ma, U.Pannicke, and K.Schwarz. 2003. "Mechanism and regulation of human non-homologous DNA end-joining." *Nat.Rev.Mol.Cell Biol.* 4:712-720.

Lin,J., C.Reichner, X.Wu, and A.J.Levine. 1996. "Analysis of wild-type and mutant p21WAF-1 gene activities." *Mol.Cell Biol.* 16:1786-1793.

Livneh,Z. 2006. "Keeping mammalian mutation load in check: regulation of the activity of error-prone DNA polymerases by p53 and p21." *Cell Cycle.* 5:1918-1922.

Lobrich,M., P.K.Cooper, and B.Rydberg. 1996. "Non-random distribution of DNA double-strand breaks induced by particle irradiation." *Int.J.Radiat.Biol.* 70:493-503.

Lobrich,M., P.K.Cooper, and B.Rydberg. 1998. "Joining of correct and incorrect DNA ends at double-strand breaks produced by high-linear energy transfer radiation in human fibroblasts." *Radiat.Res.* 150:619-626.

Lobrich,M. and P.A.Jeggo. 2005. "Harmonising the response to DSBs: a new string in the ATM bow." *DNA Repair (Amst).* 4:749-759.

LOWRY,O.H., N.J.ROSEBROUGH, A.L.FARR, and R.J.RANDALL. 1951. "Protein measurement with the

Folin phenol reagent." *J.Biol.Chem.* 193:265-275.

Luo,Y., J.Hurwitz, and J.Massague. 1995. "Cell-cycle inhibition by independent CDK and PCNA binding domains in p21Cip1." *Nature.* 375:159-161.

Maga,G. and U.Hubscher. 2003. "Proliferating cell nuclear antigen (PCNA): a dancer with many partners." *J.Cell Sci.* 116:3051-3060.

Martin,R.M., H.Leonhardt, and M.C.Cardoso. 2005. "DNA labeling in living cells." *Cytometry A.* 67:45-52.

Masson,M., C.Niedergang, V.Schreiber, S.Muller, M.J.Menissier-De, and M.G.De. 1998. "XRCC1 is specifically associated with poly(ADP-ribose) polymerase and negatively regulates its activity following DNA damage." *Mol.Cell Biol.* 18:3563-3571.

Matsumoto,Y. and K.Kim. 1995. "Excision of deoxyribose phosphate residues by DNA polymerase beta during DNA repair." *Science* . 269:699-702.

Matsuura,K., T.Balmukhanov, H.Tauchi, C.Weemaes, D.Smeets, K.Chrzanowska, S.Endou, S.Matsuura, and K.Komatsu. 1998. "Radiation induction of p53 in cells from Nijmegen breakage syndrome is defective but not similar to ataxia-telangiectasia." *Biochem.Biophys.Res.Commun.* 242:602-607.

McDonald,E.R., III, G.S.Wu, T.Waldman, and W.S.El-Deiry. 1996. "Repair Defect in p21 WAF1/CIP1 -/- human cancer cells." *Cancer Res.* 56:2250-2255.

Mellon,I., G.Spivak, and P.C.Hanawalt. 1987. "Selective removal of transcription-blocking DNA damage from the transcribed strand of the mammalian DHFR gene." *Cell.* 51:241-249.

Mirzayans,R., S.Pollock, A.Scott, L.Enns, B.Andrais, and D.Murray. 2004. "Relationship between the radiosensitizing effect of wortmannin, DNA double-strand break rejoining, and p21WAF1 induction in human normal and tumor-derived cells." *Mol.Carcinog.* 39:164-172.

Mirzoeva,O.K. and J.H.Petrini. 2001. "DNA damage-dependent nuclear dynamics of the Mre11 complex." *Mol.Cell Biol.* 21:281-288.

Moggs,J.G. and G.Almouzni. 1999. "Chromatin rearrangements during nucleotide excision repair." *Biochimie.* 81:45-52.

Munro,T.R. 1970. "The relative radiosensitivity of the nucleus and cytoplasm of Chinese hamster fibroblasts." *Radiat.Res.* 42:451-470.

Nakanishi,M., R.S.Robetorye, G.R.Adami, O.M.Pereira-Smith, and J.R.Smith. 1995. "Identification of the active region of the DNA synthesis inhibitory gene p21Sdi1/CIP1/WAF1." *EMBO J.* 14:555-563.

Nash,H.M., S.D.Bruner, O.D.Scharer, T.Kawate, T.A.Addona, E.Spooner, W.S.Lane, and G.L.Verdine. 1996. "Cloning of a yeast 8-oxoguanine DNA glycosylase reveals the existence of a base-excision DNA-repair protein superfamily." *Curr.Biol.* 6:968-980.

Newman,H.C., K.M.Prise, and B.D.Michael. 2000. "The role of higher-order chromatin structure in the yield and distribution of DNA double-strand breaks in cells irradiated with X-rays or alpha-particles." *Int.J.Radiat.Biol.* 76:1085-1093.

Nichols,A.F. and A.Sancar. 1992. "Purification of PCNA as a nucleotide excision repair protein." *Nucleic Acids Res.* 20:2441-2446.

Niculescu,A.B., III, X.Chen, M.Smeets, L.Hengst, C.Prives, and S.I.Reed. 1998. "Effects of p21(Cip1/Waf1) at both the G1/S and the G2/M cell cycle transitions: pRb is a critical determinant in blocking DNA replication and in preventing endoreduplication." *Mol.Cell Biol.* 18:629-643.

O'Reilly,M.A., P.F.Vitiello, S.C.Gehen, and R.J.Staversky. 2005. "p21(Cip1/WAF1/Sdi1) does not affect expression of base excision DNA repair enzymes during chronic oxidative stress." *Antioxid.Redox.Signal.* 7:719-725.

Ogryzko,V.V., P.Wong, and B.H.Howard. 1997. "WAF1 retards S-phase progression primarily by inhibition of cyclin-dependent kinases." *Mol.Cell Biol.* 17:4877-4882.

Ogryzko,V.V., P.Wong, and B.H.Howard. 1997. "WAF1 retards S-phase progression primarily by inhibition of cyclin-dependent kinases." *Mol.Cell Biol.* 17:4877-4882.

Okano,S., L.Lan, K.W.Caldecott, T.Mori, and A.Yasui. 2003. "Spatial and temporal cellular responses to single-strand breaks in human cells." *Mol.Cell Biol.* 23:3974-3981.

Okayasu,R., M.Okada, A.Okabe, M.Noguchi, K.Takakura, and S.Takahashi. 2006. "Repair of DNA damage induced by accelerated heavy ions in mammalian cells proficient and deficient in the non-homologous end-joining pathway." *Radiat.Res.* 165:59-67.

Pan,Z.Q., J.T.Reardon, L.Li, H.Flores-Rozas, R.Legerski, A.Sancar, and J.Hurwitz. 1995. "Inhibition of nucleotide excision repair by the cyclin-dependent kinase inhibitor p21." *J.Biol.Chem.* 270:22008-22016.

Pearl,L.H. 2000. "Structure and function in the uracil-DNA glycosylase superfamily." *Mutat.Res.* 460:165-181.

Perkins,N.D. 2002. "Not just a CDK inhibitor: regulation of transcription by p21(WAF1/CIP1/SDI1)." *Cell Cycle.* 1:39-41.

Perucca,P., O.Cazzalini, O.Mortusewicz, D.Necchi, M.Savio, T.Nardo, L.A.Stivala, H.Leonhardt, M.C.Cardoso, and E.Prosperi. 2006. "Spatiotemporal dynamics of p21CDKN1A protein recruitment to DNA-damage sites and interaction with proliferating cell nuclear antigen." *J.Cell Sci.* 119:1517-1527.

Podust,V.N., L.M.Podust, F.Goubin, B.Ducommun, and U.Hubscher. 1995. "Mechanism of inhibition of proliferating cell nuclear antigen-dependent DNA synthesis by the cyclin-dependent kinase inhibitor p21." *Biochemistry.* 34:8869-8875.

Poon,R.Y. and T.Hunter. 1998. "Expression of a novel form of p21Cip1/Waf1 in UV-irradiated and transformed cells." *Oncogene.* 16:1333-1343.

Prasad,R., G.L.Dianov, V.A.Bohr, and S.H.Wilson. 2000. "FEN1

stimulation of DNA polymerase beta mediates an excision step in mammalian long patch base excision repair." *J.Biol.Chem.* 275:4460-4466.

Prosperi,E. 2006. "The fellowship of the rings: distinct pools of proliferating cell nuclear antigen trimer at work." *FASEB J.* 20:833-837.

Raderschall,E., A.Bazarov, J.Cao, R.Lurz, A.Smith, W.Mann, H.H.Ropers, J.M.Sedivy, E.I.Golub, E.Fritz, and T.Haaf. 2002. "Formation of higher-order nuclear Rad51 structures is functionally linked to p21 expression and protection from DNA damage-induced apoptosis." *J.Cell Sci.* 115:153-164.

Radhakrishnan,S.K., C.S.Feliciano, F.Najmabadi, A.Haegebarth, E.S.Kandel, A.L.Tyner, and A.L.Gartel. 2004. "Constitutive expression of E2F-1 leads to p21-dependent cell cycle arrest in S phase of the cell cycle." *Oncogene.* 23:4173-4176.

Rappold,I., K.Iwabuchi, T.Date, and J.Chen. 2001. "Tumor suppressor p53 binding protein 1 (53BP1) is involved in DNA damage-signaling pathways." *J.Cell Biol.* 153:613-620.

Rossig,L., A.S.Jadidi, C.Urbich, C.Badorff, A.M.Zeiher, and S.Dimmeler. 2001. "Akt-dependent phosphorylation of p21(Cip1) regulates PCNA binding and proliferation of endothelial cells." *Mol.Cell Biol.* 21:5644-5657.

Rothkamm,K., I.Kruger, L.H.Thompson, and M.Lobrich. 2003. "Pathways of DNA double-strand break repair during the mammalian cell cycle." *Mol.Cell Biol.* 23:5706-5715.

Russo,A.A., P.D.Jeffrey, and N.P.Pavletich. 1996. "Structural basis of cyclin-dependent kinase activation by phosphorylation." *Nat.Struct.Biol.* 3:696-700.

Rydberg,B., M.Lobrich, and P.K.Cooper. 1994. "DNA double-strand breaks induced by high-energy neon and iron ions in human fibroblasts. I. Pulsed-field gel electrophoresis method." *Radiat.Res.* 139:133-141.

Saha,P., Q.Eichbaum, E.D.Silberman, B.J.Mayer, and A.Dutta. 1997. "p21CIP1 and Cdc25A: competition between an inhibitor and an activator of cyclin-dependent kinases." *Mol.Cell Biol.* 17:4338-4345.

Sancar,A., L.A.Lindsey-Boltz, K.Unsal-Kacmaz, and S.Linn. 2004. "Molecular mechanisms of mammalian DNA repair and the DNA damage checkpoints." *Annu.Rev.Biochem.* 73:39-85.

Savio,M., L.A.Stivala, A.I.Scovassi, L.Bianchi, and E.Prosperi. 1996. "p21waf1/cip1 protein associates with the detergent-insoluble form of PCNA concomitantly with disassembly of PCNA at nucleotide excision repair sites." *Oncogene.* 13:1591-1598.

Scholz,M., B.Jakob, and G.Taucher-Scholz. 2001. "Direct evidence for the spatial correlation between individual particle traversals and localized CDKN1A (p21) response induced by high-LET radiation." *Radiat.Res.* 156:558-563.

Schreiber,V., J.C.Ame, P.Dolle, I.Schultz, B.Rinaldi, V.Fraulob, M.J.Menissier-De, and M.G.De. 2002. "Poly(ADP-ribose) polymerase-2 (PARP-2) is required for efficient base excision DNA repair in association with

PARP-1 and XRCC1." *J.Biol.Chem.* 277:23028-23036.

Scott,M.T., N.Morrice, and K.L.Ball. 2000. "Reversible phosphorylation at the C-terminal regulatory domain of p21(Waf1/Cip1) modulates proliferating cell nuclear antigen binding." *J.Biol.Chem.* 275:11529-11537.

Sengupta,S., A.I.Robles, S.P.Linke, N.I.Sinogeeva, R.Zhang, R.Pedeux, I.M.Ward, A.Celeste, A.Nussenzweig, J.Chen, T.D.Halazonetis, and C.C.Harris. 2004. "Functional interaction between BLM helicase and 53BP1 in a Chk1-mediated pathway during S-phase arrest." *J.Cell Biol.* 166:801-813.

Shall,S. and M.G.De. 2000. "Poly(ADP-ribose) polymerase-1: what have we learned from the deficient mouse model?" *Mutat.Res.* 460:1-15.

Sheikh,M.S., Y.Q.Chen, M.L.Smith, and A.J.Fornace, Jr. 1997. "Role of p21Waf1/Cip1/Sdi1 in cell death and DNA repair as studied using a tetracycline-inducible system in p53-deficient cells." *Oncogene.* 14:1875-1882.

Sherr,C.J. and J.M.Roberts. 1995. "Inhibitors of mammalian G1 cyclin-dependent kinases." *Genes Dev.* 9:1149-1163.

Sherr,C.J. and J.M.Roberts. 1999. "CDK inhibitors: positive and negative regulators of G1-phase progression." *Genes Dev.* 13:1501-1512.

Shiloh,Y. 2003. "ATM and related protein kinases: safeguarding genome integrity." *Nat.Rev.Cancer.* 3:155-168.

Shiloh,Y. 2006. "The ATM-mediated DNA-damage response: taking shape." *Trends Biochem.Sci.* 31:402-410.

Shivji,K.K., M.K.Kenny, and R.D.Wood. 1992. "Proliferating cell nuclear antigen is required for DNA excision repair." *Cell.* 69:367-374.

Shivji,M.K., S.J.Grey, U.P.Strausfeld, R.D.Wood, and J.J.Blow. 1994. "Cip1 inhibits DNA replication but not PCNA-dependent nucleotide excision-repair." *Curr.Biol.* 4:1062-1068.

Shivji,M.K., V.N.Podust, U.Hubscher, and R.D.Wood. 1995. "Nucleotide excision repair DNA synthesis by DNA polymerase epsilon in the presence of PCNA, RFC, and RPA." *Biochemistry.* 34:5011-5017.

Shivji,M.K., E.Ferrari, K.Ball, U.Hubscher, and R.D.Wood. 1998. "Resistance of human nucleotide excision repair synthesis in vitro to p21Cdn1." *Oncogene.* 17:2827-2838.

Shiyanov,P., S.Bagchi, G.Adami, J.Kokontis, N.Hay, M.Arroyo, A.Morozov, and P.Raychaudhuri. 1996. "p21 Disrupts the interaction between cdk2 and the E2F-p130 complex." *Mol.Cell Biol.* 16:737-744.

Shroff,R., A.rbel-Eden, D.Pilch, G.Ira, W.M.Bonner, J.H.Petrini, J.E.Haber, and M.Lichten. 2004. "Distribution and dynamics of chromatin modification induced by a defined DNA double-strand break." *Curr.Biol.* 14:1703-1711.

Siegal,G., J.J.Turchi, T.W.Myers, and R.A.Bambara. 1992. "A 5' to 3' exonuclease functionally interacts with calf DNA polymerase epsilon."

Proc.Natl.Acad.Sci.U.S.A. 89:9377-9381.

Singhal,R.K., R.Prasad, and S.H.Wilson. 1995. "DNA polymerase beta conducts the gap-filling step in uracil-initiated base excision repair in a bovine testis nuclear extract." *J.Biol.Chem.* 270:949-957.

Smith,M.L., J.M.Ford, M.C.Hollander, R.A.Bortnick, S.A.Amundson, Y.R.Seo, C.X.Deng, P.C.Hanawalt, and A.J.Fornace, Jr. 2000. "p53-mediated DNA repair responses to UV radiation: studies of mouse cells lacking p53, p21, and/or gadd45 genes." *Mol.Cell Biol.* 20:3705-3714.

Sobol,R.W., R.Prasad, A.Evenski, A.Baker, X.P.Yang, J.K.Horton, and S.H.Wilson. 2000. "The lyase activity of the DNA repair protein beta-polymerase protects from DNA-damage-induced cytotoxicity." *Nature.* 405:807-810.

Stivala,L.A., F.Riva, O.Cazzalini, M.Savio, and E.Prosperi. 2001. "p21(waf1/cip1)-null human fibroblasts are deficient in nucleotide excision repair downstream the recruitment of PCNA to DNA repair sites." *Oncogene.* 20:563-570.

Stivala,L.A., E.Prosperi. 2004. "Analysis of p21CDKN1A recruitment to DNA excision repair foci in the UV-induced DNA damage response." *Meth. Mol. Biol.* 281:73-89

Takata,M., M.S.Sasaki, E.Sonoda, C.Morrison, M.Hashimoto, H.Utsumi, Y.Yamaguchi-Iwai, A.Shinohara, and S.Takeda. 1998. "Homologous recombination and non-homologous end-joining pathways of DNA double-strand break repair have overlapping roles in the maintenance of chromosomal integrity in vertebrate cells." *EMBO J.* 17:5497-5508.

Tanaka,H., T.Yamashita, M.Asada, S.Mizutani, H.Yoshikawa, and M.Tohyama. 2002. "Cytoplasmic p21(Cip1/WAF1) regulates neurite remodeling by inhibiting Rho-kinase activity." *J.Cell Biol.* 158:321-329.

Taucher-Scholz,G., J.Heilmann, and G.Kraft. 1996. "Induction and rejoining of DNA double-strand breaks in CHO cells after heavy ion irradiation." *Adv.Space Res.* 18:83-92.

Taucher-Scholz,G. and G.Kraft. 1999. "Influence of radiation quality on the yield of DNA strand breaks in SV40 DNA irradiated in solution." *Radiat.Res.* 151:595-604.

Thompson,L.H., K.W.Brookman, L.E.Dillehay, A.V.Carrano, J.A.Mazrimas, C.L.Mooney, and J.L.Minkler. 1982. "A CHO-cell strain having hypersensitivity to mutagens, a defect in DNA strand-break repair, and an extraordinary baseline frequency of sister-chromatid exchange." *Mutat.Res.* 95:427-440.

Thompson,L.H. and D.Schild. 2001. "Homologous recombinational repair of DNA ensures mammalian chromosome stability." *Mutat.Res.* 477:131-153.

Tom,S., L.A.Henricksen, and R.A.Bambara. 2000. "Mechanism whereby proliferating cell nuclear antigen stimulates flap endonuclease 1." *J.Biol.Chem.* 275:10498-10505.

Tom,S., L.A.Henricksen, M.S.Park, and R.A.Bambara. 2001. "DNA ligase I and proliferating cell nuclear antigen

form a functional complex." *J.Biol.Chem.* 276:24817-24825.

Tom,S., T.A.Ranalli, V.N.Podust, and R.A.Bambara. 2001. "Regulatory roles of p21 and apurinic/apyrimidinic endonuclease 1 in base excision repair." *J.Biol.Chem.* 276:48781-48789.

Tomkinson,A.E. and Z.B.Mackey. 1998. "Structure and function of mammalian DNA ligases." *Mutat.Res.* 407:1-9.

Tornaletti,S. and P.C.Hanawalt. 1999. "Effect of DNA lesions on transcription elongation." *Biochimie.* 81:139-146.

Tsurimoto,T. 1999. "PCNA binding proteins." *Front Biosci.* 4:D849-D858.

van,G., J.H.Hoeijmakers, and R.Kanaar. 2001. "Chromosomal stability and the DNA double-stranded break connection." *Nat.Rev.Genet.* 2:196-206.

Vermeulen,W., B.J.de, E.Citterio, A.J.van Gool, G.T.van der Horst, N.G.Jaspers, W.L.de Laat, A.M.Sijbers, P.J.van der Spek, K.Sugasawa, G.Weeda, G.S.Winkler, D.Bootsma, J.M.Egly, and J.H.Hoeijmakers. 1997. "Mammalian nucleotide excision repair and syndromes." *Biochem.Soc.Trans.* 25:309-315.

Vidal,A.E., S.Boiteux, I.D.Hickson, and J.P.Radicella. 2001. "XRCC1 coordinates the initial and late stages of DNA abasic site repair through protein-protein interactions." *EMBO J.* 20:6530-6539.

Vogelstein,B., D.Lane, and A.J.Levine. 2000. "Surfing the p53 network." *Nature.* 408:307-310.

Volker,M., M.J.Mone, P.Karmakar, H.A.van, W.Schul, W.Vermeulen, J.H.Hoeijmakers, D.R.van, A.A.van Zeeland, and L.H.Mullenders. 2001. "Sequential assembly of the nucleotide excision repair factors in vivo." *Mol.Cell.* 8:213-224.

Waga,S., G.J.Hannon, D.Beach, and B.Stillman. 1994. "The p21 inhibitor of cyclin-dependent kinases controls DNA replication by interaction with PCNA." *Nature.* 369:574-578.

Waldman,T., K.W.Kinzler, and B.Vogelstein. 1995. "p21 is necessary for the p53-mediated G1 arrest in human cancer cells." *Cancer Res.* 55:5187-5190.

Walker,J.R., R.A.Corpina, and J.Goldberg. 2001. "Structure of the Ku heterodimer bound to DNA and its implications for double-strand break repair." *Nature.* 412:607-614.

Wani,M.A., G.Wani, J.Yao, Q.Zhu, and A.A.Wani. 2002. "Human cells deficient in p53 regulated p21(waf1/cip1) expression exhibit normal nucleotide excision repair of UV-induced DNA damage." *Carcinogenesis.* 23:403-410.

Warbrick,E., D.P.Lane, D.M.Glover, and L.S.Cox. 1997. "Homologous regions of Fen1 and p21Cip1 compete for binding to the same site on PCNA: a potential mechanism to co-ordinate DNA replication and repair." *Oncogene.* 14:2313-2321.

Warbrick,E. 2000. "The puzzle of PCNA's many partners." *Bioessays.* 22:997-1006.

Ward,I.M. and J.Chen. 2001. "Histone H2AX is phosphorylated in an ATR-dependent manner in response to

replicational stress." *J.Biol.Chem.* 276:47759-47762.

Ward,J.F., W.F.Blakely, and E.I.Joner. 1985. "Mammalian cells are not killed by DNA single-strand breaks caused by hydroxyl radicals from hydrogen peroxide." *Radiat.Res.* 103:383-392.

Ward,J.F. 1988. "DNA damage produced by ionizing radiation in mammalian cells: identities, mechanisms of formation, and reparability." *Prog.Nucleic Acid Res.Mol.Biol.* 35:95-125.

Ward,J.F. 1994. "The complexity of DNA damage: relevance to biological consequences." *Int.J.Radiat.Biol.* 66:427-432.

Ward,J.F. 1995. "Radiation mutagenesis: the initial DNA lesions responsible." *Radiat.Res.* 142:362-368.

Weiss,R.H., A.Joo, and C.Randour. 2000. "p21(Waf1/Cip1) is an assembly factor required for platelet-derived growth factor-induced vascular smooth muscle cell proliferation." *J.Biol.Chem.* 275:10285-10290.

Weyrather,W.K., S.Ritter, M.Scholz, and G.Kraft. 1999. "RBE for carbon track-segment irradiation in cell lines of differing repair capacity." *Int.J.Radiat.Biol.* 75:1357-1364.

Wilson,D.M., III and V.A.Bohr. 2007. "The mechanics of base excision repair, and its relationship to aging and disease." *DNA Repair (Amst).* 6:544-559.

Wilson,S.H. 1998. "Mammalian base excision repair and DNA polymerase beta." *Mutat.Res.* 407:203-215.

Wood,R.D. 1996. "DNA repair in eukaryotes." *Annu.Rev.Biochem.* 65:135-167.

Wu,X., J.Li, X.Li, C.L.Hsieh, P.M.Burgers, and M.R.Lieber. 1996. "Processing of branched DNA intermediates by a complex of human FEN-1 and PCNA." *Nucleic Acids Res.* 24:2036-2043.

Xiong,Y., G.J.Hannon, H.Zhang, D.Casso, R.Kobayashi, and D.Beach. 1993. "p21 is a universal inhibitor of cyclin kinases." *Nature.* 366:701-704.

Xu,X. and D.F.Stern. 2003. "NFBD1/KIAA0170 is a chromatin-associated protein involved in DNA damage signaling pathways." *J.Biol.Chem.* 278:8795-8803.

Zhang,H., G.J.Hannon, and D.Beach. 1994. "p21-containing cyclin kinases exist in both active and inactive states." *Genes Dev.* 8:1750-1758.

Zhang,Y., N.Fujita, and T.Tsuruo. 1999. "Caspase-mediated cleavage of p21Waf1/Cip1 converts cancer cells from growth arrest to undergoing apoptosis." *Oncogene.* 18:1131-1138.

Zhou,B.P., Y.Liao, W.Xia, B.Spohn, M.H.Lee, and M.C.Hung. 2001. "Cytoplasmic localization of p21Cip1/WAF1 by Akt-induced phosphorylation in HER-2/neu-overexpressing cells." *Nat.Cell Biol.* 3:245-252.

CURRICULUM VITAE

PERSONAL INFORMATION

Name	**RUDOLPH, JEANETTE HEEDE**
Nationality	DANISH
Date of birth	19. 03. 1973
Place of birth	DARMSTADT, GERMANY
Resident 1973–1977	MÜHLTAL-TRAISA, GERMANY
Resident 1977–1994	NOORDWIJKERHOUT AND LEIDEN, HOLLAND
Resident 1994–	MÜHLTAL-TRAISA, GERMANY
Mother tongue	DANISH
Other languages	DUTCH, ENGLISH AND GERMAN
Reading skills	EXCELLENT
Writing skills	GOOD
Verbal skills	EXCELLENT

Married with Andreas Rudolph since 1999; son Mark from 19.09.2005 (maternity leave: 01.09.2005 –01.10.2006).

WORK EXPERIENCE

• Dates (from – to)	2002 –2007
• Name and address of employer	GESELLSCHAFT FÜR SCHWERIONENFORSCHUNG PLANCKSTRASSE 1, D-64291 DARMSTADT, GERMANY
• Type of business or sector	BIOPHYSICS
• Occupation or position held	PH.D. STUDENT

• Dates (from – to)	2001 – 2002
• Name and address of employer	GESELLSCHAFT FÜR SCHWERIONENFORSCHUNG PLANCKSTRASSE 1, D-64291 DARMSTADT, GERMANY
• Type of business or sector	BIOPHYSICS
• Occupation or position held	DIPLOMA THESIS

• Dates (from – to)	1999 – 2001
• Name and address of employer	GESELLSCHAFT FÜR SCHWERIONENFORSCHUNG PLANCKSTRASSE 1, D-64291 DARMSTADT, GERMANY
• Type of business or sector	BIOPHYSICS
• Occupation or position held	PART-TIME LABORATORY ASSISTANT

EDUCATION AND TRAINING

• Dates (from – to)	10.1995 – 08.2002
• Name and type of organization providing education and training	TECHNISCHE UNIVERSITÄT DARMSTADT, GERMANY
• Principal subjects	MOLECULAR BIOLOGY, GENETICS, PHYSIOLOGY
• Title of qualification awarded	DIPL. BIOL (MS)
• Dates (from – to)	– 07.1994
• Name and type of organization providing education and training	BOERHAVE COLLEGE LEIDEN, HOLLAND
• Principal subjects	PHYSICS, MATHEMATICS, CHEMISTRY, BIOLOGY, ENGLISH, DUTCH
• Title of qualification awarded	VWO (GRADUATION)

PUBLICATIONS

B. Jakob, J.H. Rudolph, N. Geuven, M.F. Lavin and G. Taucher-Scholz
Live Cell Imaging of Heavy-Ion-Induced Radiation Responses by Beamline Microscopy.
Radiation Research 168, 681 – 690 (2005)

N. Geuven, O.J. Becherel, A.W. Kijas, P. Chen, O. Howe, J.H. Rudolph, G. Taucher-Scholz, R. Gatti, H. Date, O. Onodera and M.F. Lavin
Aprataxin, a Novel Protein that Protects Against Genotoxic Stress.
Human Molecular Genetics 13, 1081 – 1093 (2004)

J. Rudolph, B. Jakob, C.Fourniert, G. Taucher-Scholz, C. Wiese. GSI Report 2002: 158
Analysis of p21 Accumulation at Complex DNA Lesions.

Y. Schweinfurth, B. Jakob, J. Rudolph, G. Taucher-Scholz. GSI Report 2003: 157
TP53 Foci Formation at Sites of Radiation-Induced DNA Damage.

B. Jakob, J.H. Rudolph, N. Gueven, M.F. Lavin and G. Taucher-Scholz. GSI Report 2004
Live Cell Imaging of Heavy Ion Induced Radiation Responses- A Novel Microscope Setup at the UNILAC.

Y. Schweinfurth, B. Jakob, J. Rudolph, D. Fink and G. Taucher-Scholz. GSI Report 2004.
Quantification of DNA Double Strand Breaks in Cancer Therapy-related Experiments with Carbon Ions.

J. Rudolph, B. Jakob, Y. Schweinfurth, K. Kratz, C. Wiese. G. Taucher-Scholz. GSI Report 2004
PCNA Dependent Accumulation of p21 at Heavy Ion-induced DNA-lesions.

D. Fink, J.H. Rudolph, B. Jakob, K. Knoop, G. Taucher-Scholz. GSI Report 2005: 368
Charactersiation of p21 Foci at Heavy Ion-induced DNA Lesions.

D. Fink, J.H. Rudolph, K. Knoop, J. Topsch, B. Jakob, G. Taucher Scholz. GSI Report 2006
Effect of UV-C and Ion-irradiation on PCNA and p21 Foci Formation.

J. Rudolph, D. Fink, C.Wiese, G. Taucher-Scholz, GSI Report 2006
PCNA and p21 both accumulate very fast at Heavy Ion-induced DNA Damage and become Chromatin-associated after X-ray Irradiation.

CONTRIBUTIONS TO CONFERECNCES

12th International Congress of Radiation Research, 2003. Brisbane, Australia.
Poster: Analysis of p21 accumulation at complex DNA lesions.
J. H. Rudolph, B. Jakob, C. Wiese and G. Taucher-Scholz

7te Jahrestagung der Gesellschaft für Biologische Strahlenforschung, 2004. Darmstadt, Germany.
Induktions-unabhängige Relokalisierung des Proteins p21 an Ionen-induzierten DNA-Schäden.
J. H. Rudolph, B. Jakob, Y.Schweinfurth, C. Wiese. G. Taucher-Scholz

8th International Wolfsberg Meeting on Molecular Radiation Biology/Oncology, 2004. Ermatingen, Switzerland.
Poster: Involvment of p21 in the Early DNA Damage Response.
J. H. Rudolph, B. Jakob. Y.Schweinfurth, C. Wiese, G. Taucher-Scholz,

8te Jahrestagung der Gesellschaft für Biologische Strahlenforschung, 2005. Buxtehude, Germany.
PCNA- abhängige Akkumulation des p21 Proteins an Schwerionen-induzierten DNA-Schäden
J. H. Rudolph, C. Wiese, G. Taucher-Scholz

AWARDS

Travel Award for the 'International Congress of Radiation Research 2003' (Brisbane, Australia) from the Radiation Research Society.

Member of the Helmholtz-Gemeinschaft delegation for the '53rd Meeting of Nobel Laureates in Lindau'. Germany. 2003.

EIDESSTATTLICHE ERKLÄRUNG

Hierdurch erkläre ich an Eides Statt, daß ich bisher noch keinen Promotionsversuch unternommen habe.

Datum (Unterschrift)